APPLICATIONS OF THE DIFFERENTIAL EVOLUTION OPTIMIZATION ALGORITHM IN POWER SYSTEMS PLANNING, OPERATION AND CONTROL

By

Alfredo Antonio Cuello Reyna

A thesis submitted in partial fulfillment of the requirements for the degree of

MASTER OF SCIENCE
in
ELECTRICAL ENGINEERING
(Power Systems)

UNIVERSITY OF PUERTO RICO
MAYAGUEZ CAMPUS
2006

Approved by:

_____	_____
Agustín A. Irizarry Rivera, Ph.D. Member, Graduate Committee	Date
_____	_____
Efraín O'Neill Carrillo, Ph.D. Member, Graduate Committee	Date
_____	_____
José R. Cedeño Maldonado, Ph.D. Chairperson, Graduate Committee	Date
_____	_____
Pedro Vásquez Urbano, Ph.D. Representative of Graduate School	Date
_____	_____
Isidoro Couvertier, Ph.D. Chairperson of the Department	Date

TABLE OF CONTENTS

ABSTRACT

This research work presents the application of the Differential Evolution Optimization Algorithm for solving various complex power systems problems: Reactive Power Planning, Congestion Management in Restructured Power Systems, State Estimation with Phasor Measurement Units and with Equality and Inequality Constraints, and Intelligent Power Routers Based Controlled Islanding Scheme.

Due to their non-continuous, non-differentiable and highly nonlinear nature; these problems are difficult or impossible to solve using the main classical optimization techniques. In order to show the flexibility and applicability of the Differential Evolution algorithm for solving these complex problems, the proposed solution methodologies were tested and validated through standard test systems with satisfactory results. The solutions obtained were compared with those obtained by means of other traditional and evolutionary optimization techniques available in the literature reviewed.

Finally, we provide specific recommendations regarding to the correct adjustment of the Differential Evolution control parameters, which may lead to very successful results in complex and large scale optimization problems, in a reasonable computational time.

RESUMEN

Este trabajo de investigación presenta la aplicación del Algoritmo de Optimización Evolución Diferencial (“Differential Evolution”) para resolver varios problemas complejos de sistemas de potencia: Planeación Optima de la Potencia Reactiva, Manejo de la Congestión en Sistemas de Potencia Desregulados, Estimación de Estados utilizando Medición de Fasores Sincronizados y con Restricciones de Igualdad y Desigualdad, y el Desarrollo de Esquemas de Islas Controladas basados en los Enrutadores Inteligentes de Potencia (“Intelligent Power Routers”).

Debido a su naturaleza no-continua, no-diferenciable y altamente no lineal; estos problemas son difíciles o imposible de resolver usando las técnicas de optimización convencionales. Con el objetivo de mostrar la aplicabilidad y flexibilidad del algoritmo de Evolución Diferencial para resolver estos problemas complejos, los esquemas de solución propuestos fueron probados y validados a través de sistemas de prueba estándar con muy buenos resultados. Las soluciones obtenidas se compararon con aquellas obtenidas mediante otras técnicas de optimización tradicionales y evolutivas.

Finalmente, proveemos recomendaciones específicas sobre el ajuste correcto de los parámetros de control del algoritmo de Evolución Diferencial, los cuales podrían influir en la obtención de resultados satisfactorios en problemas de optimización complejos y de gran escala, en un tiempo computacional razonable.

ACKNOWLEDGEMENTS

I am deeply indebted to Dr. José R. Cedeño Maldonado, president of my graduate committee, for his support and guidance through the master program and especially in this research. Thanks Dr. Cedeño for your time and patience and for giving me the opportunity of being one of your graduate students.

I also want to express my gratitude to Dr. Agustín Irizarry Rivera and Dr. Efraín O'Neill Carrillo for serving as member of my graduate committee and for their valuable advice during the course of the master program. I would also express my gratitude to Dr. Pedro Vásquez Urbano who greatly enriched my knowledge with his exceptional insights into optimization.

I want to thank the graduate students of the Electrical and Computer Department, for their sincere friendship and for their constant encouragement and support. I would also want to express my gratitude to the members of the EPNES Project at UPRM, especially to the professors Agustín Irizarry, Manuel Rodríguez, Bienvenido Vélez, Miguel Vélez and the graduate students Janeth Gómez, Christian Feliciano, Marianela Santiago, Carlos Torres and Idálides Vergara.

Finally, but certainly not least, I would like to thank God for giving me the opportunity of being the person that I am and for giving me the strength of developing personal and spiritually.

This work was supported in part by the National Science Foundation (NSF) thru award number 0224743 as well as by the University of Puerto Rico-Mayagüez.

DEDICATION

This thesis is dedicated to my parents Yolanda and Antonio; my sister, Claudia; and my brothers Ignacio and Guillermo for their endless support in every one of my endeavors. The enrollment and pursuance of graduate studies would have been impossible without their continuous encouragement and motivation throughout the years. Thanks for supporting me in this journey….

LIST OF TABLES

LIST OF FIGURES

LIST OF SYMBOLS

CHAPTER 2

N_P : population size

C_R : crossover constant

F : scaling factor

D : parameter vector dimension

G : generation

$\mathbf{P}^{(\mathbf{G})}$: population of generation **G**

$\mathbf{X}_i$: i^{th} individual

$X_j^{\min}$: lower bound of the j^{th} decision parameter

$X_j^{\max}$: upper bound of the j^{th} decision parameter

η_j : uniformly distributed random number within [0, 1]

$\mathbf{X}_i'$: mutant vector

$\mathbf{X}_i''$: trial vector

η_j' : uniformly distributed random number within [0, 1]

ω : equality penalty factor

μ : inequality penalty factor

Y : k dimensional vector of continuous parameters

Z : vector of ($D-k$) discrete parameters

CHAPTER 3

N_l : number of load level durations

N_E : the set of branch numbers

N_C : the buses candidates for installing new reactive power sources

h : per unit energy cost ($/p.u. MWh) with $S_B = 100$ MVA

d_l : duration of load level (h)

g_{ij} : conductance of the branch i,j (p.u.)

V_i : Voltage magnitude at the bus i (p.u.)

θ_{ij} : Voltage angle difference between bus i and bus j (rad)

e_i : fixed reactive power source installation cost at bus i ($)

C_{ci} : reactive power source purchase cost at bus i ($/MVAR)

Q_{ci} : reactive power source installation at bus i (MVAR)

N_i : set of buses adjacent to bus i, including the bus i

N_{PQ} : number of PQ-buses, which are buses with constant P and Q injections

N_G : number of generator buses

N_T : number of tap-setting transformer branches

N_B : number of buses of the system

N_{B-1} : number of buses of the system, excluding the slack bus

P_i, Q_i : real and reactive power powers, respectively, injected to the network at the bus I (p.u)

G_{ij}, B_{ij} : transference conductance and susceptance, respectively, between buses *i* and *j* (p.u)

G_{ii}, B_{ii} : self conductance and susceptance, respectively, of bus *i* (p.u)

P_{gi}, Q_{gi} : real and reactive power generation at bus *i* (p.u), respectively

T_k : transformer tap setting of branch *k* (p.u.)

δ : weight factor

κ : scaling factor

CHAPTER 4

u : set of control variables, i.e., active power at generator and load buses

x : set of dependent variables

$\mathbf{u}^0$: desired value of **u**

A : constant matrix reflecting curtailment strategies used by market participants

W : diagonal matrix whose elements are the "willingness to pay" charges to avoid curtailment

g, **h** : set of systems operation constraints, including system power flow equations, line flow limits and power balance constraints

P_i : active power injected at bus *i*

D_j : active power extracted at bus *j*

P_{Pi} : pool power injected at bus *i*

D_{Pj} : pool power extracted at bus *j*

$C_i(P_{Pi})$: pool generation cost at bus *i*

$B_j(D_{Pj})$: bid price of pool demand at bus *j*

N_G, N_D : set of generators and loads, respectively

a_{Gi}, b_{Gi}, c_{Gi} : quadratic, linear and non load cost coefficients of a pool generator bid price at bus *i.*

a_{Dj}, b_{Dj}, c_{Dj} : quadratic, linear and non load cost coefficients of a pool demand bid price at bus *j*.

$P_{T_K i}$: power injected at bus *i* under transaction T_K

$D_{T_K j}$: power extracted at bus *j* under transaction T_K

P_{Lossi} : power loss compensation at bus *i*

T_k : k^{th} bilateral/multilateral transaction

N_G : set of generator buses

N_D : set of load buses

K : total number of bilateral/multilateral transactions

w_{PLj} : willingness to pay factor to avoid curtailment for the pool contract

$D_{Pj}^{\ 0}$: preferred schedule for pool demand at bus *j*

w_{Bij} : willingness to pay factor to avoid curtailment of an individual contract $\{P_{Bij}, D_{Bji}\}$

P_{Bij}^0 : desired value of P_{Bij}

w_{Mik} : willingness to pay factor to avoid curtailment of k^{th} multilateral contract

P_{Mik}^0 : desired value of P_{Mik}

w_{Mik} : willingness to pay factor to avoid curtailment of injected power block P_{Mik}

CHAPTER 5

$\mathbf{x}$: vector of unknown values to be estimated

m : number of independent measurements

σ_i^2 : variance of the i^{th} measurement

z_i : i^{th} measurement value

$h_i(\mathbf{x})$: function used to calculate the estimated value of the i^{th} measurement

$V_i,\ \delta_i$: voltage magnitude and phase angle at bus i

δ_{ij} : phase angle difference between buses i and j

$G_{ij} + jB_{ij}$: ij^{th} element of the complex bus admittance matrix

$g_{ij} + jb_{ij}$: admittance of the series branch connecting buses i and j

$g_{ij} + jb_{ij}$: admittance of the shunt branch connected at bus i

N_B : total number of buses of the system being studied

P_{ij}, Q_{ij} : real and reactive power flow through the ij^{th} branch

P_i, Q_i : real and reactive power injected at the i^{th} bus

V_i : voltage magnitude at the bus i

δ_i : direct angle measure with PMU at the bus i

δ_{ref} : reference measurement

z_i : i^{th} unconstrained measurement

$\mathbf{z}_e$: vector of equality constrained measurements

$\mathbf{z}_l, \mathbf{z}_u$: vector of lower and upper limits, respectively, of inequality constrained measurements

g(x) : nonlinear function vector corresponding to equality constrained measures

f(x) : nonlinear function vector corresponding to inequality constrained measures

N_V : number of voltage measurements

N_P : number of angle measurements

$N_{P_{inj}}$, $N_{Q_{inj}}$: number of real and reactive power injection measurements

$N_{P_{flow}}$, $N_{Q_{flow}}$: number of real and reactive power flow measurements

$meas, est$: measured and estimated value for the i^{th} measurement data

M_i : i^{th} measured value

T_i : i^{th} true value

σ_i : standard deviation corresponding to the i^{th} measured value

v_i : random number normally distributed with zero mean and standard deviation one

E_i : i^{th} estimated value

T_i : i^{th} true value

N_m : number of measures

CHAPTER 6

δ_i : rotor angle of the i^{th} machine in radians

ω_i : angular velocity of the i^{th} machine in radians/sec

ω_0 : reference speed in radians/sec ($\omega_0 = 377$ rad/sec)

H : inertia constant in MW.s/MVA

P_{m_i} : mechanical power input of the i^{th} machine, in p.u.

P_{e_i} : electric power output of the i^{th} machine, in p.u.

D_i : damping factor of the i^{th} machine proportional to the speed deviation, in p.u./rad/sec.

V_i : constant voltage behind the direct axis transient reactance in p.u.

G_{ij}, B_{ij} : ij^{th} real and imaginary entries of the Y_{BUS} matrix

δ_i : $\delta_i - \delta_j$

$P^i_{G_n}$: power generated by the n^{th} generator that belong to the i^{th} group

$P^i_{D_k}$: power demanded by the k^{th} load that belong to the i^{th} group

R : residual matrix which represents the link between the generators and loads of the i^{th} group

m,n : subscripts used for generating buses

k : subscript used for load buses

$\mathbf{L}^i$: set of load buses that belong to the i^{th} group

$\mathbf{G}^i$: set of generating buses that belong to the i^{th} group

$\mathbf{A}^i$: set of load and generating buses that belong to the i^{th} group

Z_{app} : measured apparent impedance

P_{ij}, Q_{ij} : real and reactive power flow through the ij^{th} branch

V_i : voltage magnitude at bus i

$a_1 - a_6$: coefficients of the polynomial load model

CHAPTER 1

INTRODUCTION

Power engineering, the oldest and most traditional of the various areas within electrical engineering, is currently undergoing the more dramatic revolution in both technology and industry restructuring. One of the most impressive areas of technical improvement over the past twenty years has been the advent of powerful and practical numerical optimization methods for power system engineering and operation, methods that ensure optimal power systems performance in both operation and economics, providing electricity to the costumers in a reliable, secure and economic way.

However, as a consequence of the structural changes in the electric power industry, the incorporation of optimization methods in the decision-making process has become inevitable. Moreover, the industry restructuring introduces a wide range of new optimization tasks characterized by their complexity and the amount of variables involved in the optimization process. In some instances, the solution of these multidimensional problems by means of classical optimization techniques is difficult or even impossible. To deal with these types of optimization problems, a special class of searching algorithm, the evolutionary algorithms (EAs), have received increased attention regarding to their potential as optimization techniques to solve complex problems.

Evolutionary Algorithms (EAs) are stochastic optimization techniques based on the principles of evolutionary theory. The field of investigation that covers these algorithms is known as Evolutionary Computation (EC). These algorithms simulate the evolution of individual structures in order to find optimal solutions.

All Evolutionary Algorithms have certain points in common: a randomly initialized population of individuals (points of the search space) evolves based on the Darwinian principle of the survival of the fittest. At every generation, new individuals are created using genetics operations such as mutation and crossover. The probability of survival of the new solutions generated depends on their fitness (how well they perform in the objective function of the optimization problem at hand): the best individuals survive and the worst are rapidly discarded. Some of the most popular evolutionary computation techniques currently being used are: genetic algorithms, evolutionary programming, evolution strategies, tabu search and ant colony optimization.

Evolutionary algorithms have been applied successfully to many complex problems in the field of industrial and operational engineering. In power systems, well known applications include thermal unit commitment, hydrothermal coordination, economic dispatch, load forecasting, reliability studies and various resources allocation problems.

Differential Evolution (DE) is a simple and extremely powerful evolutionary computation technique that solves real-valued problems based on the principles of natural evolution. DE uses a population of floating point encoded individuals and the operators of mutation, crossover and selection to explore the solution space in search of global optima. Each individual, or candidate solution, is a vector that contains as many parameters as the problem dimension.

As a robust optimization tool we propose to use this novel technique for solving various complex power systems problems including: reactive power planning, congestion management in restructured power systems, state estimation and controlled islanding.

1.1 TOPIC OF THE THESIS

The topic of this thesis is “Applications of the Differential Evolution Optimization Algorithm in Power Systems Planning, Operation and Control.” This research covers four different problems of three different areas of power systems: planning, operation and control. Table 1.1 presents a brief description of the problems covered in this work as well as the main classical approach used for solving them traditionally.

1.2 OBJECTIVES AND CONTRIBUTION

The objective of the present research is to use the Differential Evolution algorithm to solve various complex power systems optimization problems. Due to their non-continuous, non-differentiable and highly nonlinear nature; these problems are difficult or impossible to solve using the main classical optimization techniques.

To show the effectiveness, flexibility, and applicability of the DE algorithm solving these power systems problems, the results obtained will be compared with results obtained by means of other traditional and evolutionary optimization techniques reported in the literature. Based on the result obtained in the case studies, the optimal selection of the control parameters of the algorithm will be proposed.

The specific objectives of this work are:

1. To analyze and solve complex power systems optimization problems with different objective functions and constraints which involves discontinuities and increase the degree of difficulty for obtaining optimal solutions.
2. To develop a solution methodology for solving these complex problems by using the Differential Evolution optimization algorithm.

3. To compare the results obtained using DE with those obtained by means of other classical and evolutionary optimization algorithms.
4. To estimate the potential of the DE algorithm for obtaining optimal solutions in the case studies in terms of the variability of the solutions, convergence rate of the algorithm and computational requirements.
5. To evaluate the tradeoff associated with the adjustment of the control parameters of the algorithm.
6. To organize the system data and the results obtained in order to facilitate future research in the evolutionary computation field.
7. To present specific recommendations regarding to the performance and the adjustment of the control parameter of the algorithm.

The main contribution of this thesis is the application of modern optimization techniques for solving complex power systems problems that had not previously being addressed with the Differential Evolution optimization algorithm.

TABLE 1.1
POWER SYSTEMS PROBLEMS TO BE ADDRESSED IN THIS WORK

Applications of the Differential Evolution Optimization Algorithm in Power Systems Planning, Operation and Control			
Power System Planning			
Problem	*Control Variables Types*	*Objective*	*Main Classical Approach*
A. Reactive Power Planning	Mixed-Integer	Minimize the real power losses as well as the allocation costs of new reactive power sources	Interior Point methods, Newton and Quasi Newton based methods.
Power System Operation			
Problem	*Control Variables Types*	*Objective*	*Main Classical Approach*
B. Congestion Management in Restructured Power Systems	Continuous	Minimize the amount of transaction rescheduled by the Independent System Operator in deregulated power systems.	Quadratric Programming, Newton and Quasi Newton based methods.
C.1 State Estimation with Phasor Measurement Units	Continuous	Perform a reliable estimation of the current operating state of the system.	Weighted Least Squares method using Gradient and Newton based methods.
C.2 Contrained WLS State Estimation			Penalty, Barrier and Augmented Lagrangian methods.
Power System Control			
Problem	*Control Variables Types*	*Objective*	*Main Classical Approach*
D. Controlled System Separation	Integer	Develop the best strategy to divide a power system into several “small islands”, minimizing the real power imbalance within the islands.	OBDD*, BFS Graph Theory, Spectral Methods, Minimal Cutsets Graphs.

* Ordered Binary Decision Diagrams

1.3 THESIS OUTLINE

The present work is organized as follows: An introduction of the thesis is provided in Chapter 1, in conjunction with the research objectives and scope. Chapter 2 presents an overview of the Differential Evolution algorithm, as well as its implementation for the solution of different problems. Chapters 3-6 describe the application of DE for the solution of the problems addressed in this work. Those chapters also provide: a general description of the problems, their mathematical formulation, the DE model used for solve them, the results of the different case studies, as well as the discussion of the results obtained. Finally, Chapter 7 presents the general conclusions and recommendations for future work.

CHAPTER 2

DIFFERENTIAL EVOLUTION

2.1 EVOLUTIONARY COMPUTATION TECHNIQUES

In many engineering disciplines a large spectrum of optimization problems has grown in size and complexity. In some instances, the solution to complex multidimensional problems by using classical optimization techniques is sometimes difficult and/or computationally expensive. This realization has led to an increased interest in a special class of searching algorithms: the evolutionary algorithms (EAs).

In general, these are referred to as “stochastic” optimization techniques and their foundations lie in the evolutionary patterns observed in living things. The field of investigation that concerns all evolutionary algorithms is known as evolutionary computation. An evolutionary algorithm searches for the solution based in a population of individuals that evolve over a number of generations motivated in the Darwinian principle of survival of the fittest. Through cooperation and competition among the population, population based optimization approaches often can find very good solutions efficiently and effectively [1]. In this area of research there exist several primary branches:

1. Genetics Algorithms (GA)
2. Evolutionary Programming (EP)
3. Evolution Strategies (ES)

Most of these methods have in common certain properties [2]. One of these similarities is that they work with a population of solutions, instead of one solution in

each iteration. By starting with a random set of solutions, an EA modifies the current population to a different population in each iteration. This feature provides to the EA the ability to capture multiple optimal solutions in one single simulation run.

Another common property is that they all simulate evolution by one or more of these three processes: Selection, Mutation, and Recombination (also known as Crossover). The selection process is applied in order to determine which individuals are kept for the next generation according to their fitness. The mutation operator allows for some attributes to be changed occasionally. The recombination or crossover process takes the attributes of two or more individuals and combines them in order to create a new individual. The type of genetic operator and the way these operators are implemented can be different, depending on the evolutionary computation technique which is used.

An important feature of the EAs is that they do not use any gradient information performing the above operations. This property makes EAs flexible enough to be used in a wide variety of problems domains as: highly nonlinear, mixed-integer and non-continuous spaces. As they operators use stochastic principles, the EAs do not assume any particular structure of a problem to be solved.

There are some advantages to using evolutionary algorithms [3]:

- As explained previously, the EAs have the ability to handle non-differentiable, non linear and multimodal functions because they do not use gradient information in the optimization process.
- They are well adapted to distributed or parallel implementations. This is important for computationally demanding optimizations where, for example, one evaluation of the objective function might take from minutes to hours.

- Ease of use, i.e. few control parameters to steer minimization. These variables should also be robust and easy to choose.
- Good convergence properties, i.e. consistent convergence to the global minimum in consecutive independent trials.

Evolutionary computation techniques have been used for several applications in power systems. Generation planning, network planning, unit commitment, and economic dispatch among others are just some of these applications [4]-[6].

2.2 DIFFERENTIAL EVOLUTION

Differential Evolution (DE) is an extremely powerful optimization algorithm that solves real-valued problems based on the principles of natural evolution. As other evolutionary computation techniques, DE uses a population of floating point encoded individuals and mutation, crossover and selection operators to explore the solution space in search of global optima [3].

The general scheme of the DE method is quite similar to others evolutionary algorithms. At every generation *G*, DE maintains a population $\mathbf{P}^{(G)}$ of N_p vectors of candidate solutions to the problem, which evolve throughout the optimization process to find global solutions:

$$\mathbf{P}^{(G)} = \left[\mathbf{X}_1^{(G)}, ..., \mathbf{X}_{N_p}^{(G)} \right] \tag{2.1}$$

The population size, N_p, does not change during the optimization process.

The dimension of each vector of candidate solutions correspond to the number of the decision parameters, D, to be optimized. Therefore,

$$\mathbf{X}_i^{(G)} = \left[X_{1,i}^{(G)}, ..., X_{D,i}^{(G)} \right]^{\mathrm{T}}, \quad i = 1, ..., N_p \tag{2.2}$$

The optimization process is conducted by means of three main operations: mutation, crossover and selection. Once every generation, each parameter vector of the current population becomes a target vector. For each target vector, the mutation operation produces a new parameter vector (called mutant vector), by adding the weighted difference between two randomly chosen vectors to a third (also randomly chosen) vector. The crossover operation generates a new vector (the trial vector), by mixing the parameters of the mutant vector with those of the target vector. If the trial vector obtains a better fitness value than the target vector, then the trial vector replaces the target vector in the following generation.

2.2.1 General Optimization Process of the Differential Evolution Algorithm

The Differential Evolution optimization process is conducted by means of the following operations:

2.2.1 A: Initialization

In order to establish a starting point for the optimization process, an initial population must be created. Typically, each decision parameter in every vector of the initial population is assigned a randomly chosen value from within its corresponding feasible bounds:

$$X_{j,i}^{(0)} = X_j^{\min} + \eta_j \left(X_j^{\max} - X_j^{\min} \right), \quad i = 1, ..., N_p, \quad j = 1, ..., D \tag{2.3}$$

where η_j denotes a uniformly distributed random number between a range [0,1], generated anew for each decision parameter. $X_j^{\max}$ and $X_j^{\min}$ are the upper and lower bound for the j^{th} decision parameter, respectively.

After that the initial population is created, it evolves through the operation of mutation, crossover and selection.

2.2.1 B: Mutation

Mutation generally refers to an operation that adds a zero-mean random variable to one or more vector parameters. Unlike other EAs, Differential Evolution does not use a predefined probability density functions (i.e., Gaussian, Cauchy) to generate perturbing fluctuations. Instead, DE relies upon the population itself to supply increments of the appropriate magnitude and orientation. The purpose is to introduce supply increments for each population member of the appropriate magnitude and orientation [7].

At every generation *G*, each vector in the population has to serve once a target vector. For each target vector $\mathbf{X}_i^{(G)}$, a mutant vector $\mathbf{X}_i^{\prime(G)} = \left[X_{1,i}^{\prime(G)}, ..., X_{D,i}^{\prime(G)} \right]^{\mathrm{T}}$ is generated according to:

$$\mathbf{X}_i^{\prime(G)} = \mathbf{X}_a^{(G)} + F\left(\mathbf{X}_b^{(G)} - \mathbf{X}_c^{(G)}\right) \tag{2.4}$$

where $\mathbf{X}_a^{(G)}$, $\mathbf{X}_b^{(G)}$ and $\mathbf{X}_c^{(G)}$ are randomly chosen vectors from the set $\{1, ..., N_p\}$, mutually different and different to the target vector. It is interesting to note that the indexes *a*, *b*, *c* must be generated anew for each individual of the population. *F* is a user-defined constant (also known mutation scaling factor), which is typically chosen from the range (0,2] [3]. Figure 2.1 shows a two dimensional example which plays a part in the

generation of the mutant vector $\mathbf{X}_i^{'(G)}$. If the mutation process causes a parameter to violate it feasible bounds, the value of the parameter is generated anew using (2.3).

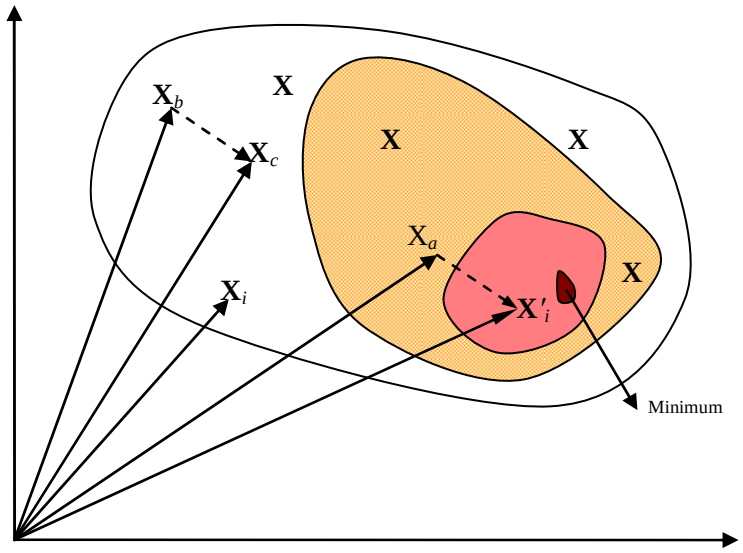

Figure 2.1: Example of Two-Dimensional Cost Function and the Process of Generating $\mathbf{X}_i^{'(G)}$

2.2.1 C: Crossover

In order to increase the diversity of the perturbed parameter vectors, the crossover operation is introduced. To the end, the trial vector $\mathbf{X}_i^{''(G)} = \left[X_{1,i}^{''(G)}, ..., X_{D,i}^{''(G)} \right]^{\mathrm{T}}$ is created by mixing the parameter of the parent vector $\mathbf{X}_i^{(G)}$ and the mutant vector $\mathbf{X}_i^{'(G)}$ by means of a series of D-1 binomial experiments in the form:

$$\mathbf{X}_{j,i}^{''(G)} = \begin{cases} \mathbf{X}_{j,i}^{'(G)} & \text{if} \quad \eta_j^{'} \le C_R \quad \text{or} \quad j = q \\ \mathbf{X}_{j,i}^{(G)} & \text{otherwise} \end{cases}, \quad i = 1, ...N_p, \quad j = 1, ..., D \qquad (2.5)$$

where $\eta_j^{'}$ is an uniformly distributed random number within the range [0,1), generated anew for each value j. C_R is known as a crossover rate constant and is a user-defined

parameter within the range [0,1]. The index q is randomly chosen from the set $\{1,...,D\}$, which is used to ensure that $\mathbf{X}_i^{''(G)}$ get a least one parameter from $\mathbf{X}_i^{'(G)}$. Figure 2.2 gives an example of the crossover mechanism for 7-dimensional vector.

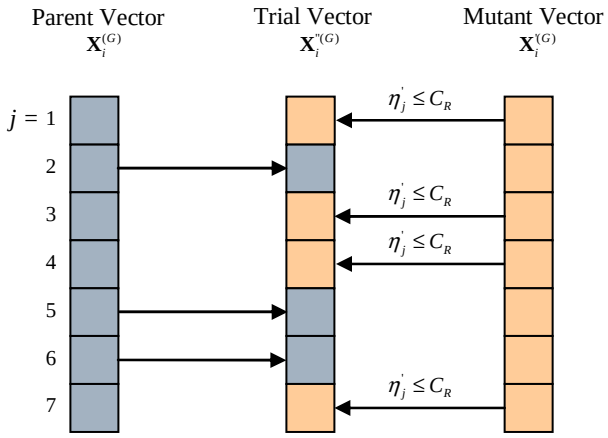

Figure 2.2: Crossover Process for a 7-Dimensional Vector.

2.2.1 D: Selection

To decide whether or not it should become a member of the next generation, the trial vector $\mathbf{X}_i^{''(G)}$ is compared to the target vector $\mathbf{X}_i^{(G)}$ using a greedy criterion. The best individual is allowed to advance to the next generation. That is,

$$\mathbf{X}_i^{(G+1)} = \begin{cases} \mathbf{X}_i^{''(G)} & \text{if} \quad f(\mathbf{X}_i^{''(G)}) \le f(\mathbf{X}_i^{(G)}) \\ \mathbf{X}_i^{(G)} & \text{otherwise} \end{cases}, \quad i = 1,...,N_p \tag{2.6}$$

By using this selection procedure, all individuals of the next generation are as good as or better than the individuals of the current population.

2.2.2 General DE Algorithm

Initialize the population $\mathbf{P}^{(0)} = \left[\mathbf{X}_i^{(0)}, ..., \mathbf{X}_{N_p}^{(0)} \right]$ using:

$$X_{j,i}^{(0)} = X_j^{\min} + \eta_j \left(X_j^{\max} - X_j^{\min} \right), \quad i = 1, ..., N_p, \quad j = 1, ..., D$$

Repeat until a stop criteria is satisfied

A. Mutation Step:

$$\mathbf{X}_i^{\prime(G)} = \mathbf{X}_a^{(G)} + F\left(\mathbf{X}_b^{(G)} - \mathbf{X}_c^{(G)} \right) \text{ where } a, b, c, i \in \left\{ 1, ..., N_p \right\} \quad \text{and} \quad a \neq b \neq c \neq i$$

B. Crossover Step:

$$\mathbf{X}_{j,i}^{\prime\prime(G)} = \begin{cases} \mathbf{X}_{j,i}^{\prime(G)} & \text{if} \quad \eta_j^{'} \leq C_R \quad \text{or} \quad j = q \\ \mathbf{X}_{j,i}^{(G)} & \text{otherwise} \end{cases}, \quad i = 1, ...N_p, \quad j = 1, ..., D$$

C. Selection Step:

$$\mathbf{X}_i^{(G+1)} = \begin{cases} \mathbf{X}_i^{\prime\prime(G)} & \text{if} \quad f(\mathbf{X}_i^{\prime\prime(G)}) \leq f(\mathbf{X}_i^{(G)}) \\ \mathbf{X}_i^{(G)} & \text{otherwise} \end{cases}, \quad i = 1, ..., N_p$$

Increase the iteration count

End Repeat

2.2.3 Other Variants of the DE Algorithm

The previous scheme is not the only variant of the DE algorithm which has proven useful. In order to classify the different variants, the notation *DE/x/y/z* is introduced, where:

x specifies the vector to be mutated which currently can be “rand” (a randomly chose population vector) or “best” (the vector with better performance in the objective function).

y is the number of different vector used.

z denotes de crossover scheme, which could be “bin” for binomial experiments or “exp” for higher order exponential experiments.

Using this notation, the basic DE-strategy described previously is DE/rand/1/bin. Nevertheless, one highly beneficial method that deserves special mention is the DE/best/2/bin, where:

$$\mathbf{X}_i^{(G)} = \mathbf{X}_{best}^{(G)} + F\left(\mathbf{X}_a^{(G)} + \mathbf{X}_b^{(G)} - \mathbf{X}_c^{(G)} - \mathbf{X}_d^{(G)}\right) \tag{2.7}$$

and all of these vector are mutually different. This strategy dramatically improves the convergence rate of the algorithm. However, in multimodal problems, this strategy could lead to premature convergence of the algorithm.

2.2.4 Constraint Handling Techniques

In the canonical form, Differential Evolution, as other evolutionary algorithms, was conceived to solve unconstrained optimization problems only. However, almost all problems in engineering (and in the real life) are constrained ones. To solve this dilemma a wide variety of constraint handling methods have been proposed in the field of the evolutionary computation techniques.

Michalewicz and Schoenauer [8] have classified the constraint handling methods applied with evolutionary algorithms into four categories:

1. Methods based on preserving feasibility of solutions.
2. Methods based on penalty functions.
3. Methods which make a clear distinction between feasible and unfeasible solutions.
4. Hybrids methods.

In general, the first two categories are undoubtedly the most widely applied with all types of nonlinear optimization algorithms, while the remaining two categories include a wide variety of less frequently applied approaches. The methods to be addressed in this work uses two main approaches depending of the type of constraints involved: boundary operator for boundary constraints and penalty functions applied to equality and inequality constraints.

2.2.4 A: Boundary Constraints

In boundary constrained problems, it is essential to ensure that parameter values lies inside their allowed ranges after the mutation operation. A simple way to guarantee this is to replace parameter values that violate boundary constraints with random values generated within the feasible range:

$$X_{j,i}^{(G)} = \begin{cases} X_j^{\min} + \eta_j \left(X_j^{\max} - X_j^{\min} \right), & \text{if} \quad X_{j,i}^{(G)} < X_j^{\min} \quad \text{or} \quad X_{j,i}^{(G)} > X_j^{\max} \\ X_{j,i}^{(G)} & \text{otherwise} \end{cases} \tag{2.8}$$

where $i = 1, ..., N_p, \quad j = 1, ..., D$

Another method for keeping trial vectors within their bounds is to adjust the parameter that exceeds a feasible bound to the corresponding violated bound. However, the deterministic approach of this method contrasts with the stochastic nature of the EAs. Also some alternative approaches for handling boundary constraints can be found in literature [9].

2.2.4 B: Penalty Functions

A general constrained optimization problem can be defined as:

$$\begin{aligned} &\min \quad f(\mathbf{x}) \\ &\text{s.t.} \quad g_i(\mathbf{x}) = 0 \qquad \forall i \in \{1,...,m\} \\ &\qquad h_j(\mathbf{x}) \le 0 \qquad \forall j \in \{1,...,r\} \\ &\qquad x_k^{\min} \le x_k \le x_k^{\max} \quad \forall k \in \{1,...,D\} \end{aligned} \tag{2.9}$$

This problem could be modified adding penalty functions to the original formulation. The function that has to be optimized is the fitness function $f'(\mathbf{x})$, instead the objective function $f(\mathbf{x})$. Then, the fitness function is the sum of the original objective function with the equality and inequality penalty functions:

$$f'(\mathbf{x}) = f(\mathbf{x}) + G(\mathbf{x}) + H(\mathbf{x}) \tag{2.10}$$

$G(\mathbf{x})$ and $H(\mathbf{x})$ are the equality and inequality penalty functions which could be modeled using the equations (2.11) and (2.12), as shown as follows:

$$G(\mathbf{x}) = \omega \sum_{j=1}^{m} \left(g_i(\mathbf{x}) \right)^2 \tag{2.11}$$

$$H(\mathbf{x}) = \mu \sum_{j=1}^{r} \left(h_j^-(\mathbf{x}) \right)^2 \tag{2.12}$$

$h_j^-(\mathbf{x})$ is the magnitude of the j^{th} inequality constraint which could be expressed as:

$$h_j^-(\mathbf{x}) = \max\{0, h_j(\mathbf{x})\} \tag{2.13}$$

The scaling parameters ω and μ are new control parameters that have to be set by the user and remain fixed during the optimization process.

2.2.5 Discrete Variables Handling

In its canonical form, the Differential Evolution algorithm is only capable of handling continuous variables. Extending it to solve mixed integer optimization problems, however, is quite simple. Only a couple of simple modifications are required [10]-[11]. This is achieved with an operator that rounds the variable to nearest integer value, when it lies between two integer values. The rounding operator is performed after the initialization and mutation process.

$$\mathbf{X}_{1,\ldots,D} = \left[\mathbf{Y}_{1,\ldots,k}, \text{round}\left(\mathbf{Z}_{k+1,\ldots,D}\right)\right]^{\text{T}} \tag{2.13}$$

where **X**, is a *D* dimensional vector with continuous and discrete variables, **Y** is *k* dimensional vector of continuous parameters and **Z** is the *(D – k)* dimensional vector of integer parameters.

Discrete parameters whit fixed step sizes Δ can be converted from integer values to discrete values using:

$$Z_i = Z_i^{\min} + n \times \Delta, \quad i = 1,\ldots,\left(D-k\right) \tag{2.14}$$

where n is a integer in the range of $\left[0,\ldots,n^{\max}\right]$.

2.2.6 Differential Evolution Example

With the objective of demonstrating the DE optimization process in continuous spaces, a simple example is analyzed.

Objective Function: $f(\mathbf{X}) = 1 - \cos(x_1) \times \cos(x_2) \times e^{-\frac{\sqrt{x_1^2 + x_2^2}}{4}}$

$$|x_1| \leq 5, \ |x_2| \leq 5$$

1. Select the control parameters of the algorithm

Control Parameters of DE		
Decision Variables	*D*	2
Population Size	*NP*	20
Scaling Mutation Factor	*F*	0.6
Crossover Rate Constant	*CR*	0.9

2. Initialize the population according to (2.3):

	Individual 1	Individual 2	Individual 3	Individual 4	…	Individual 17	Individual 18	Individual 19	Individual 20
Parameter 1	1.3672	-3.3851	-0.88877	-4.0671	…	1.9752	1.3373	-1.7956	0.82337
Parameter 2	4.3502	-2.0982	1.0022	-4.1138	…	3.8331	0.8126	4.0478	0.61102

3. Select the target vector from current population:

$\mathbf{X}_i$	1

4. Select randomly three indices a, b and c from the current population. These indices mut be mutually different and different to the index of the target vector:

a	3
b	17
c	2

5. Apply the mutation operation to generate the mutant vector according to (2.4).

	X_3	X_{17}	X_2	X_{17}-X_2	F*(X_{17}-X_2)	X_3+F*(X_{17}-X_2)
Parameter 1	-0.89	1.98	-3.39	5.37	3.22	2.33
Parameter 2	1.00	3.83	-2.10	5.93	3.56	4.56
Fitness	**0.76**	**0.90**	**0.82**	-	-	**0.97**

6. Create the trial vector by means of the crossover operation according to (2.5):

	Target Vector	**Mutant Vector**	**Random #**	**Trial Vector**
Parameter 1	1.37	2.33	0.13	2.33
Parameter 2	4.35	0.67	0.86	0.67
Fitness	**1.02**	**0.97**	-	**0.97**

7. Select the individual that will advance to the next generation according to (2.6):

	Individual 1	**Individual 2**	**Individual 3**	**…**	**Individual 18**	**Individual 19**	**Individual 20**
Parameter 1	2.33			…			
Parameter 2	0.67			…			
Fitness	**0.97**			…			

In this case the trial vector is selected because of it have the better performance in the objective function.

8. Return to step 3 and repeat these task for all individual within the current population.
9. This procedure is executed for several generations until a convergence criterion is satisfied.

Figure 2.3 shows the distribution of four generations in the objective function. It is interesting to note how all individuals are moving toward the local minimums of the function. In the end all individuals are practically over the global minimum. It is also interesting to note that in the 20^{th} generation all the points are nearby the global optimum; however it is necessary to run 100 iterations more to reach the global optimum.

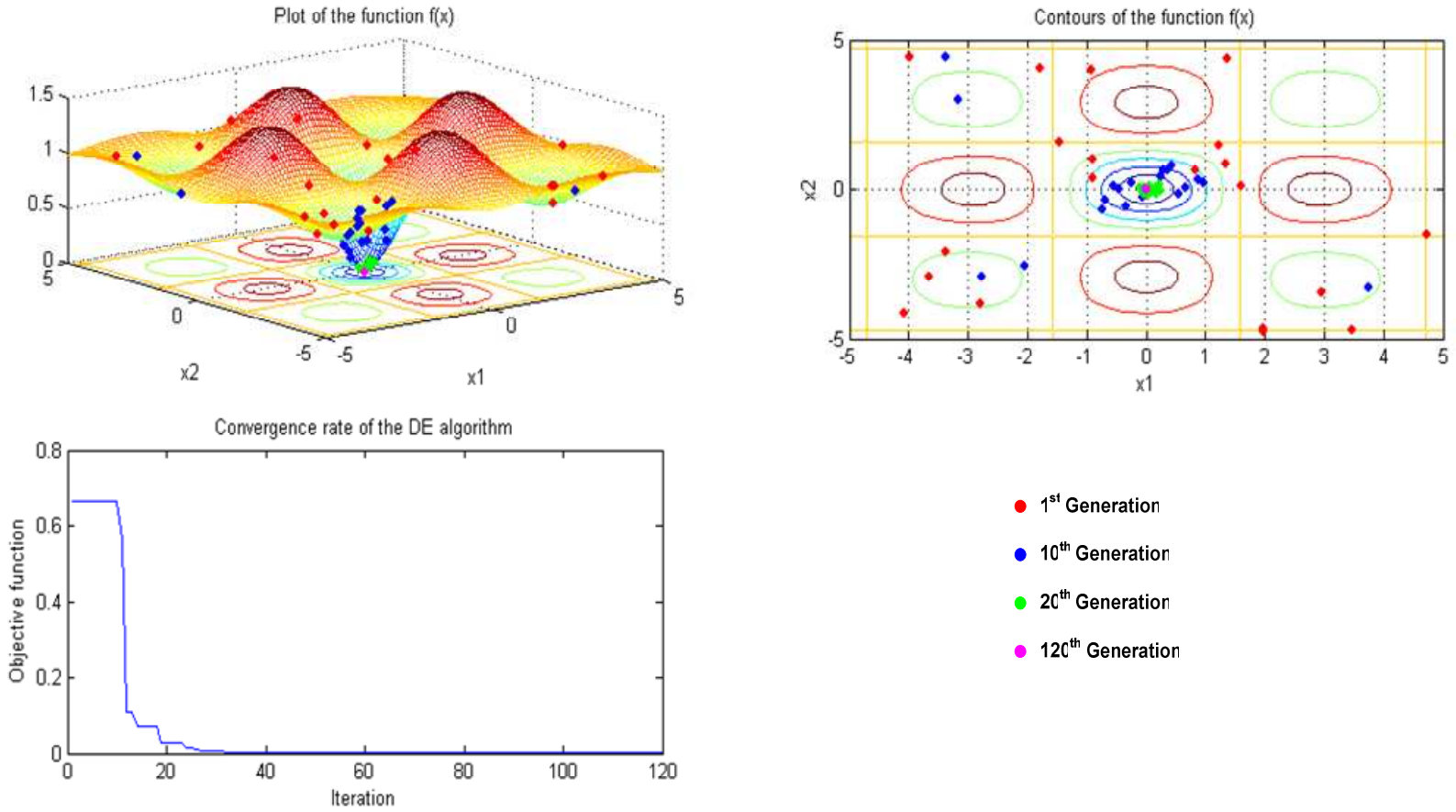

Figure 2.3: Plot of Four Generations of the DE Algorithm in the function $f(\mathbf{X}) = 1 - \cos(x_1) \times \cos(x_2) \times e^{-\frac{\sqrt{x_1^2 + x_2^2}}{4}}$

CHAPTER 3

REACTIVE POWER PLANNING

3.1 INTRODUCTION

During the last decade there has been a growing concern in the electric utility industry about reactive power issues at the operation planning and capacity expansion levels. Among other reasons, this interest is derived from the fact that in many power systems there is a trend towards operating them closer to their operational limits. Therefore, issues such as voltage control, voltage instability, reactive power security dispatch and reactive power planning have attracted much attention [12].

The objective of reactive power planning is the determination of the new reactive power sources (in terms of type, size and location in the network) that will result in an adequate voltage control capability by achieving a correct balance between security and economic concerns. Reactive power planning typically has a time horizon of one to three years, and it is performed in coordination with transmission capacity studies, that have a longer time horizon and a higher priority.

In reactive power planning it is sought to find the right tradeoff between the investment cost of the new VAR sources and the benefits in system operation derived from the presence of these additional sources of reactive compensation.

The reactive power planning (RPP) problem could be formulated mathematically as a nonlinear, non-smooth, mixed-integer, multi-objective optimization problem. One of the objectives deals with the minimization of the real power losses that result in a reduction of the operational costs and improving the voltage profile across the system. The other

objective minimizes the allocation of additional reactive power sources throughout the system.

Various traditional optimization techniques, based in successive approximations of the objective function to linear or quadratic functions, have been used to solve this complex problem [12]-[18]. However, in most cases, these approximations lead the problem to local minimum solutions.

More recently, new methods, based on artificial intelligence techniques, have been applied to the reactive power planning optimization problem in order to avoid stagnation in local minima and uncertainties. Genetic Algorithms, Evolution Strategies, Evolutionary Programming, Simulated Annealing and Neural Networks are some of these new optimization methods that have been applied to solve the reactive power planning problem [19]-[28].

In this thesis work, we use the Differential Evolution algorithm to properly estimate the amount of reactive power sources that have to be installed over the system. Because of the stochastic nature of the Differential Evolution algorithm, it could explore the solution space more effectively, providing better solutions than traditional optimization techniques.

3.2 REACTIVE POWER PLANNING PROBLEM FORMULATION

3.2.1 Single-objective Formulation

Reactive planning is one of the most complex problems in electric power systems. It requires adjustments in voltage controllers such as reactor and capacitor banks, static VAR compensators, excitation of synchronous generators and synchronous compensators, etc. The adjustments result in a prespecified voltage profile to meet

security constraints and power quality requirements. When the reactive reserves present in the existing power system are unable to meet the imposed constraints, optimal reactive source expansion (minimum costs) can be considered, taking into account the physical characteristics and the operating conditions of the system [25].

The reactive power planning problem is to determine the optimal investment of reactive power sources over a planning horizon. The cost function to be minimized is the sum of the operation costs and the investment costs [19]-[23]. In our approach, the operation costs refer to the annual cost of energy loss. The investment cost is the cost to install new shunt reactive power compensation devices through the system.

The mathematical formulation of the reactive power planning problem is:

$$\text{Min } f_C = W_C + I_C \tag{3.1}$$

The first term represents the total cost of energy loss as follows:

$$\begin{aligned} W_C &= h \sum_{l \in N_l} d_l P_{loss}^l \\ &= h \sum_{l \in N_l} d_l \left[\sum_{i,j \in N_E} g_{ij} \left(V_i^2 + V_j^2 - 2 V_i V_j \cos\theta_{ij} \right) \right]^l \end{aligned} \tag{3.2}$$

The second term represents the cost of reactive power source installation which also has two components:

$$I_C = \sum_{i \in N_C} \left(e_i + C_{ci} \left| Q_{ci} \right| \right) \tag{3.3}$$

where:

N_l : number of load level durations

N_E : the set of branch numbers

h : per unit energy cost ($/p.u. MWh) with $S_B = 100$ MVA

d_l : duration of load level (h)

g_{ij} : conductance of the branch i,j (p.u.)

V_i : Voltage magnitude at the bus i (p.u.)

θ_{ij} : Voltage angle difference between bus i and bus j (rad)

e_i : fixed reactive power source installation cost at bus i ($)

C_{ci} : reactive power source purchase cost at bus i ($/MVAR)

Q_{ci} : reactive power source installation at bus i (MVAR)

P_{loss}^{l} : network real power losses during the period of load level l.

The problem is subjected to several equality and inequality constraints. The power flow equations are used as equality constraints, as shown:

$$\begin{aligned} P_i - V_i \sum_{j \in N_i} V_j \left(G_{ij} \cos \theta ij + B_{ij} \sin \theta_{ij} \right) = 0 \quad i \in N_{B-1} \\ Q_i - V_i \sum_{j \in N_i} V_j \left(G_{ij} \sin \theta ij - B_{ij} \cos \theta_{ij} \right) = 0 \quad i \in N_{PQ} \end{aligned} \tag{3.4}$$

Reactive power source installation restrictions, real and reactive power generation restrictions, transformer tap setting restrictions, as well as bus voltages restrictions are used as inequality constraints for the problem:

$$\begin{aligned} Q_{ci}^{\min} \le Q_{ci} \le Q_{ci}^{\max} \quad i \in N_C \\ P_{gi}^{\min} \le P_{gi} \le P_{gi}^{\max} \quad i \in N_G \\ Q_{gi}^{\min} \le Q_{gi} \le Q_{gi}^{\max} \quad i \in N_G \\ T_k^{\min} \le T_k \le T_k^{\max} \quad i \in N_T \\ V_i^{\min} \le V_i \le V_i^{\max} \quad i \in N_B \end{aligned} \tag{3.5}$$

where:

N_i : set of buses adjacent to bus *i*, including the bus *i*

N_{PQ} : number of PQ-buses, which are buses with constant *P* and *Q* injections

N_G : number of generator buses

N_T : number of tap-setting transformer branches

N_B : number of buses of the system

N_{B-1} : number of buses of the system, excluding the slack bus

P_i, Q_i : real and reactive power powers, respectively, injected to the network at the bus *I* (p.u)

G_{ij}, B_{ij} : transference conductance and susceptance, respectively, between buses *i* and *j* (p.u)

G_{ii}, B_{ii} : self conductance and susceptance, respectively, of bus *i* (p.u)

P_{gi}, Q_{gi} : real and reactive power generation at bus *i* (p.u), respectively

T_k : transformer tap setting of branch *k* (p.u.)

The control variables for the problem are: the voltage magnitudes at PV buses, the transformers tap settings T_k and the adjustment of the reactive power sources proposed Q_{ci}.

A major concern in the reactive power planning problem is the nature of the variables being optimized. In practical systems, almost all transformers must have taps changing on primary windings (usually high-voltage windings) to adjust the ratio of transformation for improving the voltage profile on secondary windings (low-voltage windings). Some of these tap changing transformers could perform these adjustment under load conditions for

maintaining quasi-constant voltage on secondary windings. In addition, some shunt capacitors could adjust their capacity by adding/removing capacitors within a certain region of operation. These capacitor banks, have fixed increments/decrements between consecutive stages that depends on the combination of capacitors in service.

Therefore, the shunt capacitors as well as the transformer tap settings could be modeled as discrete variables, which imply that the optimization process requires special mixed-integer programming techniques.

3.2.2 Multi-objective Formulation

Multi-objective optimization simultaneously intends to optimize several parameters, turning most traditional constraints into new objective functions. This seems more natural for real world problems where choosing a threshold may seem arbitrary. As a result, a wide set of optimal solutions (known as Pareto set) may be found. Therefore, a whole set of optimal alternatives is obtained before deciding which solution is the best compromise of different (and sometimes contradictory) features [29]-[30].

In the case of the reactive power planning problem, the multi-objective formulation comprises two main objective functions: the annual costs of energy loss and the investment costs, as shown in (3.6):

$$\begin{aligned} &\text{Min } h\sum_{l\in N_l} d_l P_{loss}^{l} \\ &\text{Min } \sum_{i\in N_C} \left(e_i + C_{ci}\left|Q_{ci}\right|\right) \end{aligned} \tag{3.6}$$

where

$$P_{loss} = \sum_{i,\, j \in N_E} g_{ij} \left(V_i^2 + V_j^2 - 2 V_i V_j \cos \theta_{ij} \right) \tag{3.7}$$

As in the single-objective formulation, the problem is subjected to several equality and inequality constraints. The power flow equations (3.4) are used as equality constraints, while the inequality constraints (3.5) refer to reactive power source installation restrictions, real and reactive power generation restrictions, transformer tap setting restrictions and bus voltages restrictions.

Several techniques have been proposed to solve these complex optimization problems. The Weighted Sum of Objectives Functions (WSOF), Vector Evaluated Genetic Algorithms (VEGA), Non-dominated Sorting Genetic Algorithm (NSGA), Niched Pareto-Genetic Algorithm, among others are some of the most widely applied traditional and evolutionary optimization techniques applied to these complex problems. Reference [31] offers a widely discussion of these methods.

In our case, the problem is solved using the Weighted Sum of Objective Functions (WSOF) method, which, as the name suggests, scales a set of objectives into a single-objective by premultiplying each objective with a user supplied weight, using an appropriate scaling factor. Therefore, the multi-objective problem is transformed to the following single-objective optimization problem:

$$\text{Min } \delta \times h \sum_{l \in N_l} d_l P_{loss}^l + (1 - \delta) \times \kappa \sum_{i \in N_C} \left(e_i + C_{ci} \left| Q_{ci} \right| \right) \tag{3.8}$$

Where δ (the weight factor) is a constant number within the range [0, 1]. κ is an appropriate scaling factor.

Varying the corresponding weight factor δ, the true Pareto-optimal front could be found. The Pareto-front is a set of "best compromise" solutions that cannot be dominated (no objective can be improved without making some other objective worse) [31].

3.3 DE MODEL FOR REACTIVE POWER PLANNING

As a robust optimization technique, we use Differential Evolution to properly estimate the amount of reactive power sources that have to be installed in the system.

Control Variables: The set of control variables used in the optimization process are:

1. The voltage magnitudes at PV buses, which are modeled as continuous variables
2. The transformers tap settings T_k, modeled as discrete variables.
3. The adjustment of the reactive power sources proposed Q_{ci}, modeled as discrete variables.

Initialization: All the control variables are initialized randomly within their feasible bounds by means of (2.3). If during the evolution process, any of these settings become unfeasible, they were adjusted using the boundary operator (2.8).

Objective Function: Minimize the total energy loss costs, as well the investment costs of new reactive power sources:

$$F'(\mathbf{X}) = h\sum_{l\in N_l} d_l \left[\sum_{i,\, j\in N_E} g_{ij}\left(V_i^2 + V_j^2 - 2V_iV_j\cos\theta_{ij}\right)\right]^l + \sum_{i\in N_C}\left(e_i + C_{ci}\left|Q_{ci}\right|\right) \qquad (3.9)$$

Penalty Functions: The objective function could be modified adding penalty factors, when equality and inequality constraints are not satisfied. The equality constraints (3.4) are the power flow equations. The inequality constraints (3.5) include: real and reactive power generation limits, as well as voltage constraints through the system.

a. *Equality Penalty Function*: The equality constraints are satisfied when the power flow subroutine converges, therefore no penalty function were added to the fitness function.

b. *Inequality Penalty Functions*: Generators real power limits, generators reactive power limits and bus voltages limits, were modeled as inequality penalty functions for the case studies, as shown in equations (3.10), (3.11) and (3.12).

$$H_1(\mathbf{X}) = \mu_1 \sum_{i=1}^{N_G} \max\left[0,\ P_i - P_i^{\max},\ P_i^{\min} - P_i\right] \tag{3.10}$$

$$H_2(\mathbf{X}) = \mu_2 \sum_{i=1}^{N_G} \max\left[0,\ Q_i - Q_i^{\max},\ Q_i^{\min} - Q_i\right] \tag{3.11}$$

$$H_3(\mathbf{X}) = \mu_3 \sum_{i=1}^{N_B} \max\left[0,\ V_i - V_i^{\max},\ V_i^{\min} - V_i\right] \tag{3.12}$$

Where μ is the inequality penalty factor.

Fitness Function: The fitness function used in the optimization process was a combination of the original objective function with the inequality penalty functions, as shown in (3.13):

$$F''(\mathbf{X}) = F'(\mathbf{X}) + H_1(\mathbf{X}) + H_2(\mathbf{X}) + H_3(\mathbf{X}) \tag{3.13}$$

3.4 CASE STUDIES AND RESULTS

3.4.1 Single-objective Formulation

The proposed approach has been tested in the modified IEEE 30-bus test system with satisfactory results. In the case studies, buses 6, 17, 18 and 27 were selected for VAR compensation. Tables 3.1-3.5 show the system data used in the analysis.

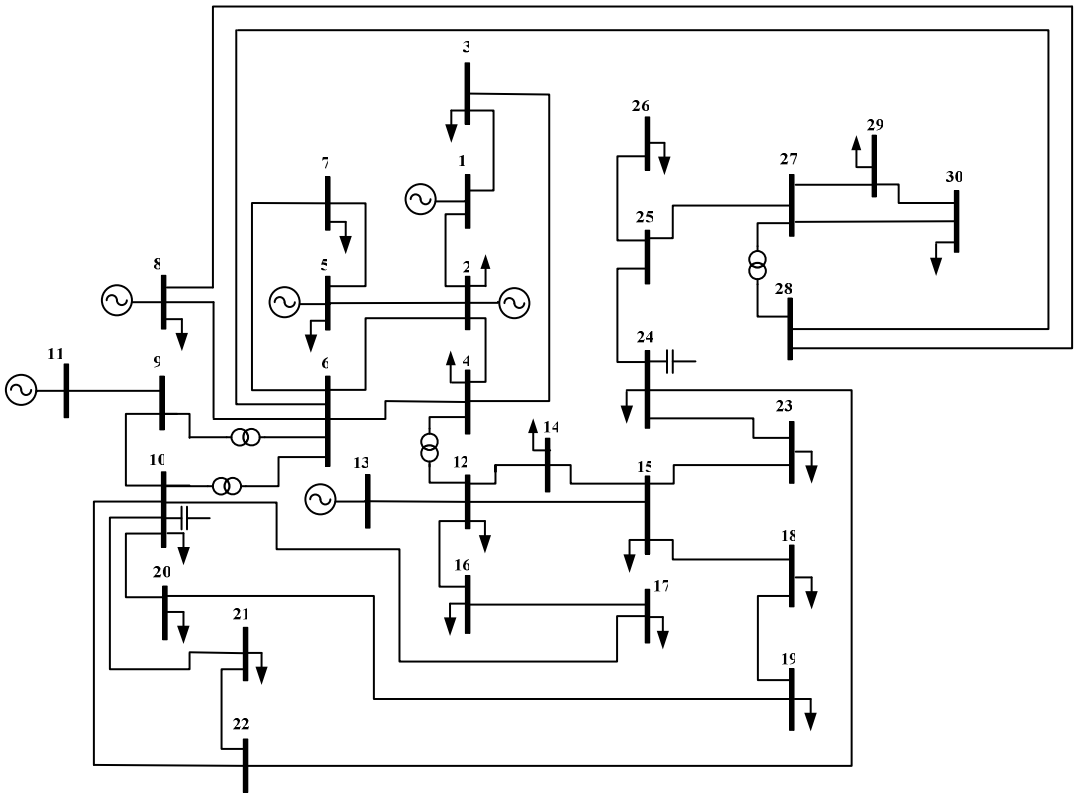

Figure 3.1: IEEE 30–Bus Test System

TABLE 3.1
BUS DATA

Bus	Type	MW	MVAR	Bus	Type	MW	MVAR
1	Slack	0	0	16	PQ	3.5	1.8
2	PV	21.7	12.7	17	PQ	9	5.8
3	PQ	2.4	1.2	18	PQ	3.2	0.9
4	PQ	7.6	1.6	19	PQ	9.5	3.4
5	PV	94.2	19	20	PQ	2.2	0.7
6	PQ	0	0	21	PQ	17.5	11.2
7	PQ	22.8	10.9	22	PQ	0	0
8	PV	30	30	23	PQ	3.2	1.6
9	PQ	0	0	24	PQ	8.7	6.7
10	PQ	5.8	2	25	PQ	0	0
11	PV	0	0	26	PQ	3.5	2.3
12	PQ	11.2	7.5	27	PQ	0	0
13	PV	0	0	28	PQ	0	0
14	PQ	6.2	1.6	29	PQ	2.4	0.9
15	PQ	8.2	2.5	30	PQ	10.6	1.9

TABLE 3.2
TRANSFORMER TAP SETTINGS DATA

Transformer	From Bus	To Bus	Minimum Tap	Maximum Tap
$T_{6\text{-}9}$	6	9	0.9	1.1
$T_{6\text{-}10}$	6	10	0.9	1.1
$T_{4\text{-}12}$	4	12	0.9	1.1
$T_{28\text{-}27}$	28	27	0.9	1.1

TABLE 3.3
INSTALLED SHUNT CAPACITOR BANKS

Capacitor	At Bus	Size (MVAR)
Qc_{10}	10	19
Qc_{24}	24	4.3

TABLE 3.4
PROPOSED SHUNT CAPACITOR BANKS

Capacitor	At Bus	Minimum Size (MVAR)	Maximum Size (MVAR)
Qc_6	6	0	30
Qc_{17}	17	0	30
Qc_{18}	18	0	30
Qc_{27}	27	0	30

TABLE 3.5
BRANCH DATA

Branch		R (pu)	X (pu)	B (pu)	Rating (MVA)	Branch		R (pu)	X (pu)	B (pu)	Rating (MVA)
From	To					From	To				
1	2	0.0192	0.0575	0.0264	130	18	19	0.0639	0.1292	0.0000	16
1	3	0.0452	0.1852	0.0204	130	19	20	0.0340	0.0680	0.0000	32
2	4	0.0570	0.1737	0.0184	65	10	20	0.0936	0.2090	0.0000	32
3	4	0.0132	0.0379	0.0042	130	10	17	0.0324	0.0845	0.0000	32
2	5	0.0472	0.1983	0.0209	130	10	21	0.0348	0.0749	0.0000	32
2	6	0.0581	0.1763	0.0187	65	10	22	0.0727	0.1499	0.0000	32
4	6	0.0119	0.0414	0.0045	90	21	22	0.0116	0.0236	0.0000	32
5	7	0.0460	0.1160	0.0102	70	15	23	0.1000	0.2020	0.0000	16
6	7	0.0267	0.0820	0.0085	130	22	24	0.1150	0.1790	0.0000	16
6	8	0.0120	0.0420	0.0045	50	23	24	0.1320	0.2700	0.0000	16
9	11	0.0000	0.2080	0.0000	90	24	25	0.1885	0.3292	0.0000	16
9	10	0.0000	0.1100	0.0000	90	25	26	0.2544	0.3800	0.0000	16
12	13	0.0000	0.1400	0.0000	100	25	27	0.1093	0.2087	0.0000	16
12	14	0.1231	0.2559	0.0000	32	27	29	0.2198	0.4153	0.0000	16
12	15	0.0662	0.1304	0.0000	32	27	30	0.3202	0.6027	0.0000	16
12	16	0.0945	0.1987	0.0000	32	29	30	0.2399	0.4533	0.0000	16
14	15	0.2210	0.1997	0.0000	16	8	28	0.0636	0.2000	0.0214	32
16	17	0.0824	0.1923	0.0000	16	6	28	0.0169	0.0599	0.0065	32
15	18	0.1073	0.2185	0.0000	16						

Branch		R (pu)	X (pu)	Transformer Tap Ratio	Rating (MVA)	Branch		R (pu)	X (pu)	Transformer Tap Ratio	Rating (MVA)
From	To					From	To				
6	9	0.0000	0.2080	1.0	65	4	12	0.0000	0.2560	1.0	65
6	10	0.0000	0.5560	1.0	32	28	27	0.0000	0.3960	1.0	65

In our approach, the generator output voltages, the transformer tap settings and the capacity of the shunt capacitor banks are adjusted simultaneously to optimize the reactive power allocation. To test the capability of the algorithm for solving mixed discrete optimization problems, the transformers taps and shunt capacitor banks were modeled as discrete variables. The transformers taps steps were set to 0.25 p.u., with 4 steps over and 4 steps under 1.0 p.u. Capacitor banks steps were chosen to be of 0.3 MVAR from 0 to 30 MVAR. The powerflow algorithm used was the Full Newton-Raphson from Matpower 3.0. The limits of the control variables are given in Table 3.6.

TABLE 3.6
CONTROL VARIABLES LIMITS (P.U.)

Bus	1	2	5	8	11	13
$Q_G^{\max}$	0.596	0.48	0.60	0.53	0.15	0.155
$Q_G^{\min}$	-0.298	-0.24	-0.30	-0.265	-0.075	-0.078
$V^{\max}$	$V^{\min}$	$T^{\max}$	$T^{\min}$	$Q_C^{\max}$	$Q_C^{\min}$	
1.05	0.95	1.1	0.9	0.3	0.0	

Four cases were analyzed using the proposed approach. The first case is of light loads, whose loads and initial real power generations, except for the generation at slack bus, are the same as those in [32]. In the second case, the loads and initial real power generation are 150% higher than the original case. The third case is of heavy loads, whose loads and initial real power generation are twice as those of Case 1. The fourth case has two level load periods, one light load period having the same loads as those in the original case, and one heavy load period having the same loads as those in Case 3.

The initial generator bus voltages and transformer taps were set to 1.0 p.u. The total load, initial generation and power losses for the case studies are given in Table 3.7. The limit-violating quantities for these cases are given in Table 3.8. In Case 2 and 3, because

of heavy loads, almost all reactive power generations and bus voltages violate their limits.

TABLE 3.7
INITIAL GENERATION AND POWER LOSSES (P.U.)

	P_{load}	Q_{load}	P_G	Q_G	P_{loss}	Q_{loss}
Case 1	2.834	1.262	2.8940	1.1381	0.0600	0.2597
Case 2	4.251	1.893	4.3954	2.1593	0.1444	0.6329
Case 3	5.668	2.524	5.9466	3.4119	0.2786	1.2354

TABLE 3.8
LIMIT – VIOLATING VARIABLES (P.U.)

Case 1							
Bus	24	26	29	30	Bus	8	
V_i	0.94997	0.93155	0.93889	0.92658	Q_{G_i}	61.47	
Case 2							
Bus	10	14	15	16	17	18	19
V_i	0.94551	0.93725	0.92965	0.94206	0.93613	0.91457	0.91101
Bus	20	21	22	23	24	25	26
V_i	0.91827	0.92438	0.92517	0.91256	0.90408	0.90766	0.87741
Bus	27	29	30				
V_i	0.92481	0.89028	0.87037				
Bus	1	5	8	11	13		
Q_{G_i}	-31.963	68.813	104.63	16.777	27.875		
Case 3							
Bus	10	12	14	15	16	17	18
V_i	0.90803	0.9396	0.90364	0.89153	0.9083	0.89651	0.86806
Bus	19	20	21	22	23	24	25
V_i	0.86177	0.87135	0.87802	0.87905	0.86436	0.84836	0.85357
Bus	26	27	29	30			
V_i	0.80979	0.87849	0.82729	0.7978			
Bus	1	2	5	8	11	13	
Q_{G_i}	-37.621	54.174	97.655	154.27	28.378	44.333	

Differential Evolution solves this highly nonlinear, mixed-integer, multi-objective optimization problem. For each approach, 50 independent runs were made using the best suited control parameters. These control parameters (scaling factor, crossover constant and population size) were determined via parameter tuning. All runs were limited to a maximum of 2000 iterations. The DE strategy used in all cases was DE/rand/1/bin.

TABLE 3.9
CONTROL PARAMETERS OF THE DE ALGORITHM

Control Parameters	Case 1	Case 2	Case 3	Case 4A	Case 4B
F	0.6	0.6	0.6	0.6	0.6
C_R	0.9	0.9	0.9	0.9	0.9
N_P	40	40	40	40	40
μ_1	1×10^5	1×10^5	1×10^5	1×10^5	1×10^5
μ_2	1×10^6	1×10^6	1×10^6	1×10^6	1×10^6
μ_3	1×10^6	1×10^6	1×10^6	1×10^6	1×10^6

The optimal results are given in Table 3.10. All state variables are regulated back into their limits. In Case 4, two sets of control variables are obtained, one for each load level period. The DE algorithm subroutine has to run twice for finding two different set of control parameters, incrementing the computational time spent in the case.

Due to the installation costs is only accounted in the heavy load period, the reactive power sources used in the light load period do not induce any costs. Therefore, in the light load period, there are some reactive power generations from reactive power sources that are previously installed for the heavy load periods. As a direct consequence of that, the real power loss in this period is lower than the corresponding value in Case 1.

TABLE 3.10
OPTIMAL RESULTS FOR THE CASE STUDIES

Generator Bus Voltages, p.u.						
Bus	1	2	5	8	11	13
Case 1	1.05	1.04384	1.02293	1.02496	1.05	1.05
Case 2	1.05	1.03518	1.01015	0.98257	1.04895	1.05
Case 3	1.05	1.02182	0.97230	0.96159	1.04548	1.05
Case 4A	1.05	1.04449	1.02439	1.02617	1.05	1.05
Case 4B	1.05	1.02181	0.97228	0.96154	1.04543	1.05
Transformers tap-settings, p.u.						
Branch	(6,9)	(6,10)	(4,12)	(28,27)		
Case 1	1.050	0.900	0.975	0.950		
Case 2	0.975	0.900	0.925	0.900		
Case 3	0.975	0.900	0.925	0.950		
Case 4A	1.075	0.900	0.975	0.975		
Case 4B	0.975	0.900	0.925	0.950		
Reactive power source installations, p.u.						
Bus	6	17	18	27		
Case 1	0.000	0.000	0.000	0.000		
Case 2	0.000	0.000	0.000	0.000		
Case 3	0.069	0.297	0.150	0.297		
Case 4A	0.060	0.075	0.060	0.060		
Case 4B	0.072	0.300	0.147	0.294		
Power generation and losses, p.u.						
	P_G	Q_G	P_{loss}	Q_{loss}		
Case 1	2.8857	1.0972	0.0517	0.2583		
Case 2	4.3796	2.0521	0.1286	0.5645		
Case 3	5.9004	2.2500	0.2324	0.9889		
Case 4A	2.8848	0.8231	0.0508	0.2636		
Case 4B	5.9004	2.2513	0.2324	0.9889		
Optimization results						
Case 1	Case 2	Case 3	Case 4A	Case 4B		
2,714,769.16	6,758,334.56	14,656,565.57	1,333,991.06	8,550,327.47		

The results obtained by means of the Differential Evolution approach were compared with those obtained by means of another evolutionary computation technique, Evolutionary Programming [20]. As shown in Table 3.11, similar results were obtained by both approaches for the Case 1. DE adjusted the voltages magnitudes of all PV buses and transformers tap settings such that the total losses decreased from 6.0 MW to 5.171 MW achieving a reduction of 0.829 MW, which traduces in an annual energy costs savings of $435,722.4.

In Case 2, because of the adjustment of the voltage magnitudes in the PV buses and the transformers, the total system losses are reduced in 1.58 MW, from 14.44 MW to 12.86 MW, which corresponds to an annual energy costs savings of $830,448.0

In Case 3, the Differential Evolution approach adjusted the voltages magnitudes of all PV buses, transformers taps settings and adjustable shunt capacitor banks such that the total losses decrease from 27.86 MW to 23.24 MW, achieving a reduction of 4.64 MW, which corresponds to an annual energy costs savings of $2,438,784.0. Due to the solution obtained by [20] become unfeasible (the solution may produce violations on the bus voltage magnitude at bus 7 and on the reactive power generated by the machines connected to buses 2, 5 and 8), no proper comparison could be made for this case.

In Case 4B, the reduction in system losses obtained was similar to the obtained in Case 3. However, in Case 4A, due to the allocation of the reactive power sources accomplished in Case 4B, the real power losses in this period are lower than the corresponding value in Case 1. The annual energy costs savings achieved in this case was of $1,461,168.0.

TABLE 3.11
COMPARISON OF RESULTS

	Case 1		Case 3	
Variables	EP [20]	DE	EP [20]	DE
V_1	1.050	1.050	1.050	1.050
V_2	1.044	1.044	1.022	1.022
V_5	1.023	1.023	0.973	0.972
V_8	1.025	1.025	0.959	0.962
V_{11}	1.050	1.050	1.050	1.045
V_{13}	1.050	1.050	1.050	1.050
T_{6-9}	1.050	1.050	0.950	0.975
T_{6-10}	0.900	0.900	0.900	0.900
T_{4-12}	0.975	0.975	0.900	0.925

T_{28-27}	0.950	0.950	0.900	0.950
Q_{c_6}	0.000	0.000	0.198	0.069
$Q_{c_{17}}$	0.000	0.000	0.229	0.297
$Q_{c_{18}}$	0.000	0.000	0.133	0.150
$Q_{c_{27}}$	0.000	0.000	0.196	0.297
P_G	2.886	2.886	5.901	5.900
Q_G	0.926	1.097	2.204	2.250
P_{loss}	0.052	0.052	0.233	0.232
Q_{loss}	-0.336	0.258	0.436	0.989
Objective Function	2,714,769.16	2,714,769.16	14,507,217.71	14,656,565.57

3.4.2 Multi-objective Formulation

The proposed approach could be adapted to solve efficiently the multi-objective formulation of the Reactive Power Planning Problem. As mentioned before, the method used in the analysis was the Weighted Sum of Objectives Functions (WSOF). For determining the Pareto-optimal front for the case studies, the weight factor (δ) was varied conveniently and the corresponding objective function (3.8) was optimized using Differential Evolution.

Tables 3.12 and 3.13 show the tradeoff-values for cases 1 and 2. In case 3, due to heavy load conditions, variations on the weight factor (δ) hardly affect the optimization results, so for this case it is not possible to determine the corresponding tradeoff-values.

TABLE 3.12
INSTALLATION/ENERGY LOSS COSTS TRADEOFF VALUES FOR CASE 1

Case 1					
	Installation Costs ($)	Energy Loss Costs ($)		Installation Costs ($)	Energy Loss Costs ($)
1	1,048,000.00	2,667,900.00	16	73,000.00	2,700,900.00
2	634,000.00	2,668,600.00	17	64,000.00	2,702,300.00
3	552,000.00	2,669,600.00	18	55,000.00	2,703,800.00
4	525,000.00	2,670,300.00	19	46,000.00	2,705,400.00
5	444,000.00	2,673,500.00	20	37,000.00	2,707,100.00
6	399,000.00	2,675,800.00	21	28,000.00	2,708,900.00
7	300,000.00	2,679,800.00	22	19,000.00	2,710,700.00
8	273,000.00	2,681,900.00	23	0.00	2,714,800.00
9	227,000.00	2,684,400.00	24	0.00	2,714,800.00
10	200,000.00	2,686,900.00	25	0.00	2,714,800.00
11	173,000.00	2,689,500.00	26	0.00	2,714,800.00
12	109,000.00	2,696,200.00	27	0.00	2,714,800.00
13	100,000.00	2,697,200.00	28	0.00	2,714,800.00
14	91,000.00	2,698,400.00	29	0.00	2,714,800.00
15	82,000.00	2,699,600.00	30	0.00	2,714,800.00

TABLE 3.13
INSTALLATION/ENERGY LOSS COSTS TRADEOFF VALUES FOR CASE 2

Case 2					
	Installation Costs ($)	Energy Loss Costs ($)		Installation Costs ($)	Energy Loss Costs ($)
1	2,056,000.00	6,265,146.39	16	498,000.00	6,477,081.92
2	2,011,000.00	6,265,625.14	17	480,000.00	6,484,188.40
3	1,588,000.00	6,278,974.90	18	444,000.00	6,498,968.39
4	1,435,000.00	6,287,864.24	19	426,000.00	6,506,774.68
5	1,282,000.00	6,300,323.53	20	345,000.00	6,554,199.97
6	1,120,000.00	6,317,323.40	21	290,000.00	6,581,827.33
7	1,030,000.00	6,328,714.36	22	335,000.00	6,548,573.97
8	975,000.00	6,337,079.35	23	227,000.00	6,616,623.98
9	948,000.00	6,341,980.74	24	181,000.00	6,642,911.48
10	930,000.00	6,345,483.11	25	163,000.00	6,653,989.68
11	921,000.00	6,347,475.15	26	28,000.00	6,739,565.72
12	840,000.00	6,373,929.97	27	0.00	6,758,334.55
13	615,000.00	6,438,663.04	28	0.00	6,758,334.55
14	525,000.00	6,467,676.24	29	0.00	6,758,334.55
15	516,000.00	6,470,662.11	30	0.00	6,758,334.55

The corresponding Pareto-optimal front for cases 1 and 2 are presented in Figure 3.2 and 3.3. In those cases, non-dominated solutions were found (no objective could be improved without making some other objective worse).

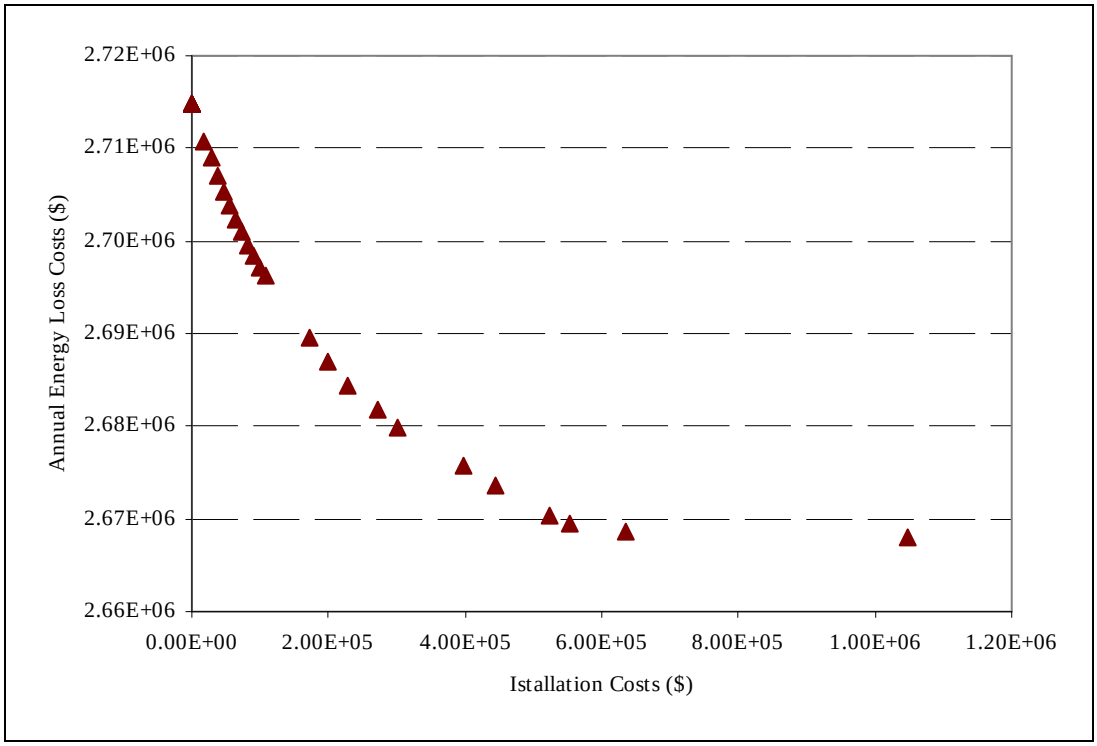

Figure 3.2: Installation/Annual Energy Loss Costs Tradeoff Curve for Case 1

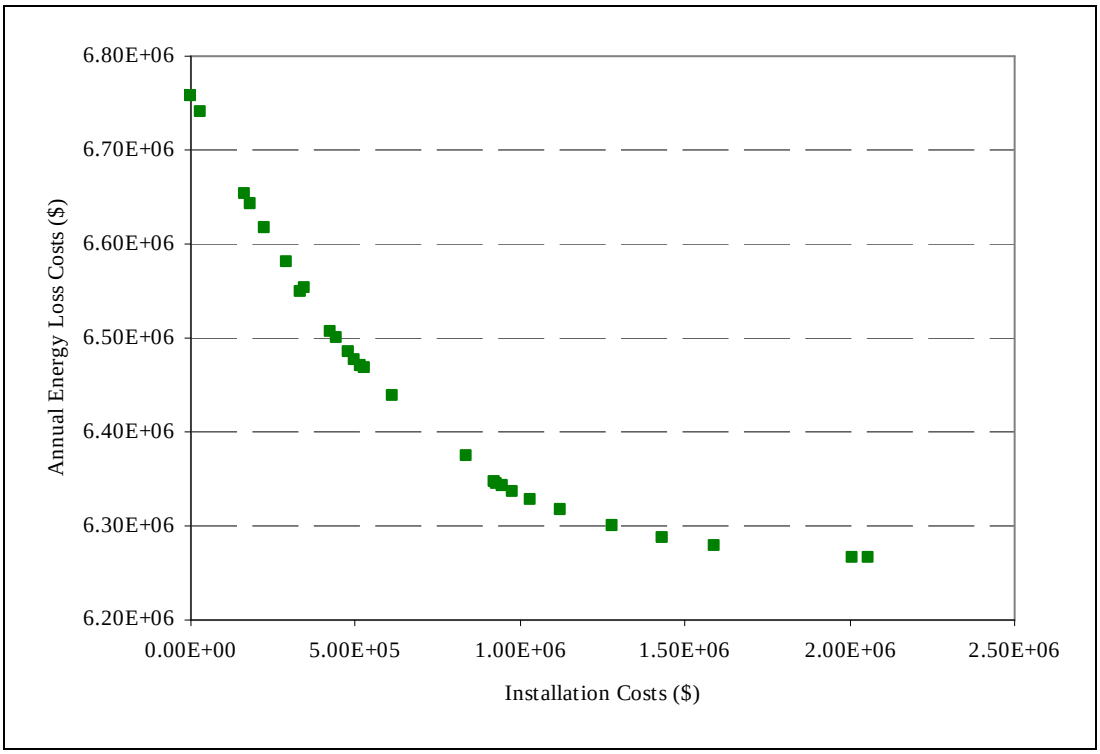

Figure 3.3: Installation/Annual Energy Loss Costs Tradeoff Curve for Case 2

3.4.3 Rate of Convergence of the Proposed Framework and Statistical Results

Table 3.14 provides the statistical results for the case studies based on 50 independent runs of the DE algorithm. In this table *BSF* and *WSF* refer to best solution and worst solution found, respectively. Is interesting to note that, in the cases that involve light load periods, the variability of the results obtained by DE are minimal. However, in cases that involve heavy load periods, such as Case 3 and Case 4B, the results vary slightly from one run to another, reducing the successful rate of the algorithm for obtaining the best solution.

TABLE 3.14
STATISTICAL RESULTS BASED ON 50 INDEPENDENT RUNS

	Case 1	Case 2	Case 3	Case 4A	Case 4B
Average	2,714,769.16	6,758,334.56	14,670,892.05	1,333,991.06	8,571,692.70
Median	2,714,769.16	6,758,334.56	14,668,268.00	1,333,991.06	8,570,852.63
Mode	2,714,769.16	6,758,334.56	14,658,907.60	1,333,991.06	8,570,852.63
Standard Deviation	6.46E-09	1.02E-06	12,395.00	3.16E-09	12,527.59
SR	100%	100%	43%	100%	63%
BSF	2,714,769.16	6,758,334.56	14,656,565.57	1,333,991.06	8,550,327.47
WSF	2,714,769.16	6,758,334.56	14,693,990.91	1,333,991.06	8,602,388.99

Figure 3.4 shows the convergence rate of the algorithm for the best values founded in all case studies. Note that the objective function is improved rapidly in a few iterations. Further improvements in the objective function, requires a large number of iterations, which implies a considerable drop in the rate of convergence of the DE algorithm.

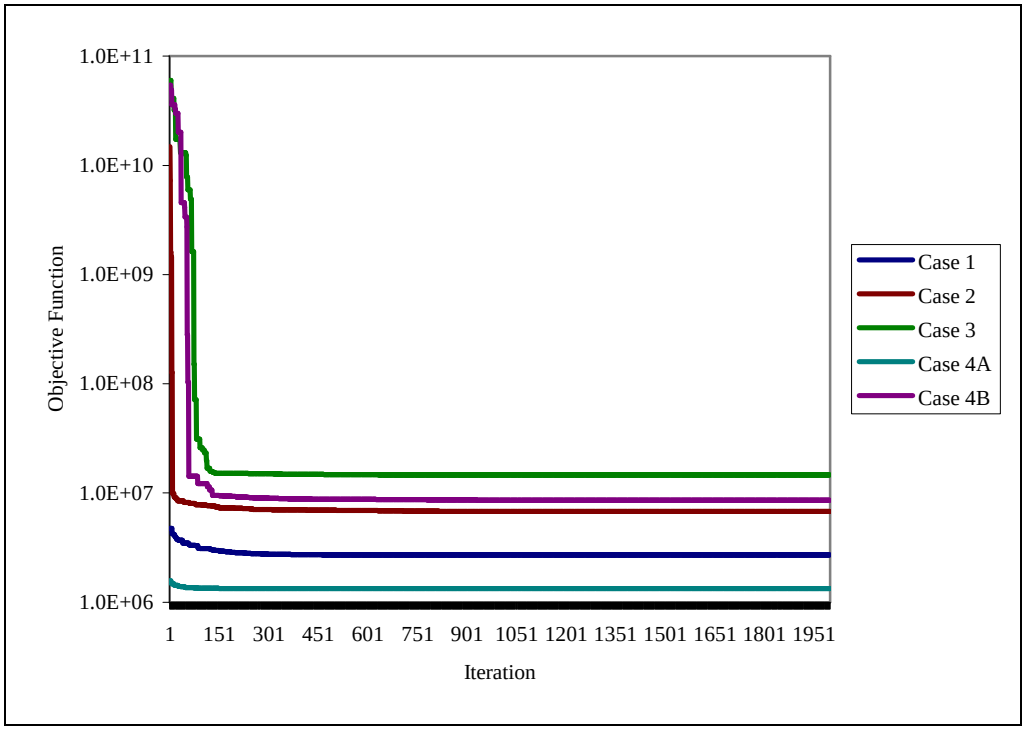

Figure 3.4: Rate of Convergence of the DE Algorithm for the Case Studies

3.5 CONCLUSION

In this chapter we used the Differential Evolution algorithm to solve the reactive power planning problem (RPP), which intends to properly allocate reactive power sources in order to maintain a secure voltage profile across the system, while other operational constraints are satisfied simultaneously.

The allocation of the reactive power (sizing process) is inherently a mixed discrete optimization problem when transformer taps and capacitor banks are modeled as discrete variables. DE was capable of solving the RPP problem successfully for the case studies, providing a considerable reduction in the system losses and an improvement on the voltage profile over the system. The results obtained proved that the DE algorithm is appropriate for solving highly nonlinear mixed-integer optimization problems.

CHAPTER 4

CONGESTION MANAGEMENT IN RESTRUCTURED POWER SYSTEMS

4.1 INTRODUCTION

When producers and consumers of electric energy desire to produce and consume in amounts that would cause the transmission system to operate at or beyond one or more transfer limits, the system is said to be congested [33].

In the past, congestion was discussed in terms of steady state security, and the basic objective was to control generator outputs so that the system remained secure (no limit violations) at the lowest cost. The optimal power flow routine was the most significant tool for obtaining minimum cost of generation with existing transmission and operational constraints. In this case, traditional optimization techniques such as sequential, quadratic, linear, integer and dynamic programming, interior point methods, and Newton-based methods, have been proposed by researches for solving this problem [34]-[41].

In deregulated power systems, with open transmission access, congestion management is one of the most challenging operational problems. With the trend of an increasing number of bilateral and multilateral contracts submitted for electricity market trades, the possibility of insufficient resources in the transmission system may be unavoidable [42]. An optimal power flow function, with the objective of minimizing the amount of the transactions rescheduled, could be developed to solve the congestion problem.

Under this new scenario, the role of the transmission system operator is to create a set of rules that ensure sufficient control over producers and consumers to maintain an acceptable level of power system security and reliability in the short and long term operation.

In this work we use Differential Evolution as a robust optimization technique, for solving various congested scenarios that include pool, bilateral and multilateral transactions, and to estimate the way that the economic valuation of those transactions affects the optimization process.

4.2 CONGESTION MANAGEMENT IN OPEN ACCESS TRANSMISSION SYSTEMS

Open access transmission systems have led to an evolution in the power markets organizational structures. This approach implies opening to competition those tasks that are, in vertically integrated structures, coordinated jointly with the objective of minimizing the total cost of operation of the utility [33].

In these traditional structures, control functions such as automatic generation control (AGC), state estimation, generation dispatch, unit commitment, are carried out by an Energy Management System (EMS). In these vertically integrated structures, congestion management was discussed in terms of steady state security and the basic objective was to control generators output so that the systems remained secure (no limits violations) at the lowest cost [42].

In competitive markets scenarios, transactions among participants, i.e., generation companies (GENCOS), distribution companies (DISCOS) and third parties, with no intervention of the Independent System Operator (ISO), comprise the main system decision variables.

In these scenarios various types of transactions are involved [33]:

- Single auction power pools, where wholesale sellers (competitive generators) bid to supply power into a single pool. Load serving entities (LSEs) buy wholesale power form that pool at a regulated price and resell it to the retail loads.
- Double auction power pools, where the sellers put their bids in a single pool and the buyers compete, with their offers, to buy wholesale power from the pool for resell it to the retail loads.
- Bilateral contracts between the wholesale generators and load serving entities without third party intervention.
- Multilateral contracts, i.e., purchase and sale agreements between several sellers and buyers, with or without intervention of third parties such as forward contractors and brokers.

In the new deregulated environment, whenever there are overloaded transmission branches, the system is considered to have a congestion problem, and hence operational and price signals are generated to ensure operational feasibility for the transaction proposed [43]. These price signals (increased marginal price of electricity) can be used to reschedule the generation or for planning purposes [44]-[45].

In this statement, the role for the transmission system operator is to create a set of rules that ensure sufficient control over producers and consumers to maintain an acceptable level of power system security and reliability in the short term and long term operation.

4.2.1 Congestion Management Methodologies

There are two paradigms that may be employed for congestion management. These are the *cost-free* means and the *non-cost- free* means. Reference [46] offers a simple and straightforward discussion about these topics.

The cost-free means include actions like: tripping congested lines; adjustment of transformer taps settings, phase shifter or FACTS devices; etc.

The non-cost-free means include:

- Rescheduling generation. This leads to generation operation at an equilibrium point different to the optimal economic dispatch. Mathematical models of pricing tools may be incorporated in the dispatch framework and the corresponding price signals could be obtained. These price signals could be used for congestion pricing and as indicator to the market participants to rearrange their power injections/extractions such that congestion is avoided [45].
- Priorization and curtailment of transactions, in where a *willingness to pay to avoid curtailment factor* [47]-[50] could be an effective instrument in setting the transaction curtailment strategies, which may be incorporated in the optimal power flow framework.

4.3 DISPATCH METHODOLOGIES FOR OPEN ACCESS TRANSMISSION SYSTEMS

Open transmission access modifies the traditional operational and system control strategies in the emerging electricity market structures. The fundamental entity in all emerging structure is the Independent System Operator (ISO), whose role is to maintain equity and transparency in the charges imposed on users of transmission facilities and to ensure fair and impartial treatment if restrictions have to be imposed on users during periods of transmission overloading [48]. Thus, successful trading requires that the ISO match the power bids from the supply side (GENCOS) with the offers from the demand side (DISCOS).

The contractual scheme between selling and buyers may impose differences in the ISO operational strategies. For that purpose in convenient to analyze the three principal contractual models widely used in deregulated environments: pool, bilateral and multilateral contracts.

4.3.1 Pool Dispatch Formulation

When several GENCOS and DISCOS decide to interchange power, a pool structure is created. In this scheme an economic dispatch only can be performed if all GENCOS and DISCOS exchange relevant operational information, i.e., cost curves, generators capability curves, commitment status, among others [33].

The basic purpose of this arrangement is to minimize the operational cost and to develop market power in the competitive scenario. The optimal operation point is in which the cost of the system are minimal, i.e., the social benefit of the participants are maximum, but the coexistence of the pool market with short-term electricity spot market

introduce some complications regarding to the electricity price elasticity and the variation of the spot price with the purchaser's location on the grid [51]-[53].

Neglecting the effect of zonal price elasticity, the dispatch formulation could be stated as follows:

$$\underset{P_{Pi},D_{Pj}}{\text{Min}} \sum_{\substack{i=1 \\ i\neq skack}}^{N_G} C_i(P_{Pi}) - \sum_{j=1}^{N_D} B_j(D_{Pj}) \tag{4.1}$$

subject to

$$\begin{aligned} \mathbf{g}(\mathbf{x},\mathbf{u}) &= 0 \\ \mathbf{h}(\mathbf{x},\mathbf{u}) &\leq 0 \end{aligned} \tag{4.2}$$

where

P_{Pi} : pool generation at bus *i*

D_{Pj} : pool demand at bus *j*

$C_i(P_{Pi})$: pool generation cost at bus *i*

$B_j(D_{Pj})$: bid price of pool demand at bus *j*

N_G, N_D : set of generators and loads, respectively

g, **h** : set of systems operation constraints, including system power flow equations, line flow limits and power balance constraints

u : set of control variables, i.e., active power at generator and load buses

x : set of dependent variables

The pool generation costs and demand bid prices are described by simple quadratic cost functions. Thus,

$$C_i(P_{Pi}) = a_{Gi}P_{Pi}^{\ 2} + b_{Gi}P_{Pi} + c_{Gi}, \quad \forall i \in N_G \tag{4.3}$$

$$B_j(D_{Pj}) = a_{Dj}D_{Pj}^{\ 2} + b_{Dj}D_{Pj} + c_{Dj}, \quad \forall j \in N_D \tag{4.4}$$

where

a_{Gi}, b_{Gi}, c_{Gi} : quadratic, linear and non load cost coefficients of a pool generator bid price at bus *i.*

a_{Dj}, b_{Dj}, c_{Dj} : quadratic, linear and non load cost coefficients of a pool demand bid price at bus *j*.

4.3.2 Bilateral/Multilateral Dispatch Formulation

The conceptual model of bilateral market structures is that sellers and buyers could perform transactions in where the quantities traded and the prices are settled without intervention of the ISO. These transactions are submitted to the ISO who, in absence of any congestion in the system, simply dispatches all transaction requested, making an impartial charge for the service.

Multilateral transactions are, in effect, an extension of bilateral transactions. This type of transactions is simply a trade that is arranged by energy brokers, and involves more than two parties. In some situations, in order to reduce the risk of the business, GENCOS and DISCOS may prefer to make the contracts through brokers rather than directly find buyers or sellers themselves.

In bilateral/multilateral markets structures the purpose of transmission dispatch problem in an open access environment is to minimize the deviations from the transactions requested by participants. The ideal of open access transmission system is to make possible all transaction without curtailment arising from physical and operational constraints [48]. One of the most logical ways of rescheduling the transactions is to do it on the basis of rationing of transmission access, which could be modeled as extra charges paid by the participants to avoid curtailment of the transactions requested.

The mathematical formulation of the bilateral/multilateral dispatch problem can be expressed as [49]:

$$\text{Min } f(\mathbf{u},\mathbf{x}) = [(\mathbf{u}-\mathbf{u}^0)^T\ \mathbf{A}]\ \mathbf{W}\ [(\mathbf{u}-\mathbf{u}^0)^T\ \mathbf{A}]^T \tag{4.5}$$

subject to

$$\begin{aligned} \mathbf{g}(\mathbf{x},\mathbf{u}) &= 0 \\ \mathbf{h}(\mathbf{x},\mathbf{u}) &\le 0 \end{aligned} \tag{4.6}$$

where

u : set of control variables, i.e., active power at generator and load buses

x : set of dependent variables

$\mathbf{u}^0$: desired value of **u**

A : constant matrix reflecting curtailment strategies used by market participants

W : diagonal matrix whose elements are the "willingness to pay" charges to avoid curtailment

g, **h** : set of systems operation constraints, including system power flow equations, line flow limits and power balance constraints

4.3.3 Power Balance Constraints

In general the power injected/extracted at a specific bus consists of power sold by the pool, injections for bilateral and multilateral contracts, and injections for loss compensation:

$$P_i = P_{Pi} + \sum_{k\in K} P_{T_K i} + P_{Lossi}, \quad \forall i \in N_G \tag{4.7}$$

$$D_j = D_{Pj} + \sum_{k\in K} D_{T_K j}, \quad \forall j \in N_D \tag{4.8}$$

where:

P_i : active power injected at bus *i*

D_j : active power extracted at bus *j*

P_{Pi} : pool power injected at bus *i*

D_{Pj} : pool power extracted at bus *j*

$P_{T_K i}$: power injected at bus *i* under transaction T_K

$D_{T_K j}$: power extracted at bus *j* under transaction T_K

P_{Lossi} : power loss compensation at bus *i*

T_k : k^{th} bilateral/multilateral transaction

N_G : set of generator buses

N_D : set of load buses

K : total number of bilateral/multilateral transactions

The power balance equation for bilateral contracts is:

$$P_{Bij} = D_{Bij}, \quad \forall i \in N_G \text{ and } \forall j \in N_D \tag{4.9}$$

For multilateral contracts the power balance constraint could be stated as follows:

$$\sum P_{Mik} = \sum D_{Mik}, \quad \forall k \in K \tag{4.10}$$

In this optimal power flow problem the control variables can be either P_{Bij} or D_{Bji} for bilateral contracts, and a certain number of variables from the set $\{ P_{Mik}, D_{Mjk} \}$.

Some schemes are developed for loss compensation, but in this work we assume that the ISO is required to provide all loss compensation services without cost to the participants. Other schemes of loss compensation based on participation factors are addressed in [50].

4.4 CURTAILMENT STRATEGIES

As proposed in [49] and [54], four basic types of strategies implemented by the ISO in collaboration with market participants are the basis of the proposed transmission dispatch model.

4.4.1 Pool Curtailment

In congested scenarios, a third term is added to the pool objective function. The purpose is to minimize the deviation of the transactions from the desired values. The curtailment strategy for pool transactions can be stated as follows:

$$\text{Min } f_1(\mathbf{u},\mathbf{x}) = \sum_{j=1}^{N_D} w_{PLj}(D_{Pj} - D_{Pj}^0)^2 \tag{4.11}$$

where

w_{PLj} : willingness to pay factor to avoid curtailment for the pool contract

$D_{Pj}^{\ 0}$: preferred schedule for pool demand at bus *j*

4.4.2 Point to Point Curtailment

This strategy concerns to bilateral contracts. As we suggested before, in an individual contract the curtailment of P_{Bij} must be the same of the curtailment of D_{Bji}. The objective function of the optimal dispatch model is:

$$\text{Min } f_2(\mathbf{u},\mathbf{x}) = \sum_{\substack{i=1 \\ i=slack}}^{m} \sum_{j=m+1}^{n} [w_{Bij} \ (P_{Bij} - P_{Bij}^0)^2] \tag{4.12}$$

where

w_{Bij} : willingness to pay factor to avoid curtailment of an individual contract { P_{Bij}, D_{Bji} }

P_{Bij}^0 : desired value of P_{Bij}

4.4.3 Group Curtailment

This is one of the two basic strategies of curtailment for multilateral (group based) transfers. The concern is to make possible a group transfer without curtailment, even if an individual generator within the group or utility has to be rescheduled. The objective function of the optimal dispatch model is:

$$\text{Min } f_3(\mathbf{u},\mathbf{x}) = \sum_{k=1}^{K} [w_{Mik} \ (\sum_{\substack{i=1 \\ i\neq slack}}^{n} P_{Mik} - \sum_{\substack{i=1 \\ i\neq slack}}^{n} P_{Mik}^0)^2] \tag{4.13}$$

where

w_{Mik} : willingness to pay factor to avoid curtailment of k^{th} multilateral contract

P_{Mik}^0 : desired value of P_{Mik}

K : number of multilateral contracts

4.4.4 Separate Curtailment

The objective of this strategy is to minimize the change of the real power injected or extracted at a specific bus of a multilateral contract. The objective function of the optimal dispatch model is:

$$\text{Min } f_4(\mathbf{u},\mathbf{x}) = \sum_{k=1}^{K} \sum_{\substack{i=1 \\ i \neq slack}}^{m} [w_{Mik}(P_{Mik} - P_{Mik}^0)^2] \tag{4.14}$$

where

w_{Mik} : willingness to pay factor to avoid curtailment of injected power block P_{Mik}

4.5 POOL, BILATERAL AND MULTILATERAL DISPATCH PROCEDURE

In this optimal transmission dispatch problem all power transfers are required to be as close as possible to the initial desired power transfers and curtailment decisions are based on markets participants' willingness to pay to avoid curtailment factor, their preferred curtailment strategies and on system security constraints [49]. The transmission dispatch procedure could be stated as follows:

Step 1: Pool, bilateral and multilateral structures submit their desired transactions to the ISO.

Step 2: If all equality and inequality constraints are satisfied go to step 4. Otherwise go to the next step.

Step 3: Use the optimal dispatch procedure model to curtail the requested power transfer. The process continues until all equality and inequality constraints are satisfied.

Step 4: When all constraints are satisfied, the generation at slack bus (loss

compensation) must be spread among all participants.

Step 5: Stop.

4.6 DE MODEL FOR CONGESTION MANAGEMENT IN RESTRUCTURED POWER SYSTEMS.

As an optimization tool, the DE algorithm can be used for solving various congested scenarios, including pool, bilateral and multilateral contracts.

Control Variables: Depending on the type of transactions involved in the studied scenario, the set of control variables could be:

1. P_{Pi} and D_{Pj} for pool transactions.
2. P_{Bij} or D_{Bji} for bilateral contracts (one of them).
3. A certain number of variables from the set $\{ P_{Mik}, D_{Mjk} \}$.

Initialization: Restrictions in the minimum power generated/demanded at a certain seller/buyer and the preferred values of transactions could be used as boundary constraints for the case. The population size is selected depending on the number of control variables of the problem.

Objective Function: The objective function for this optimization problem could be the equation (4.1), (4.11), (4.12), (4.13) or (4.14) or a combination of them, depends on the case:

$$F'(\mathbf{X}) = \left\{ \sum_{\substack{i=1 \\ i \neq skack}}^{N_G} C_i(P_{Pi}) - \sum_{j=1}^{N_D} B_j(D_{Pj}) + \sum_{j=1}^{N_D} w_{PLj}(D_{Pj} - D_{Pj}^0)^2 \right.$$
$$+ \sum_{\substack{i=1 \\ i \neq slack}}^{m} \sum_{j=m+1}^{n} [w_{Bij} \ (P_{Bij} - P_{Bij}^0)^2] + \sum_{k=1}^{K} [w_{Mik} \ (\sum_{\substack{i=1 \\ i \neq slack}}^{n} P_{Mik} - \sum_{\substack{i=1 \\ i \neq slack}}^{n} P_{Mik}^0)^2] \quad (4.15)$$
$$\left. + \sum_{k=1}^{K} \sum_{\substack{i=1 \\ i \neq slack}}^{m} [w_{Mik}(P_{Mik} - P_{Mik}^0)^2] \right\}$$

<u>*Penalty Functions*</u>: The objective function could be modified adding penalties factors, when equality and inequality constraints are not satisfied. The equality constraints include the power balance constraints, represented by equations (4.7) and (4.8), as well as the power flow equations. The inequality constraints include: real and reactive power flows between buses, limits on active and reactive power generation, as well as voltage constraints through the system.

a. Equality Penalty Function: An equality penalty function was added to the original objective function to ensure that the power balance constraint within the groups are satisfied:

$$G(\mathbf{X}) = \omega_1 \sum_{i=1}^{I} \left| P_G^i - P_D^i \right| \quad (4.16)$$

where :

ω : equality penalty factor

P_G^i : active power generated by the i^{th} group

P_D^i : active power demanded by the i^{th} group

I : set of groups

b. Inequality Penalty Functions: Maximum apparent power flows, generators reactive power limits and bus voltages limits, were modeled as inequality penalty functions for the case studies, as shown in equations (4.17), (4.18) and (4.19)

$$H_1(\mathbf{X}) = \mu_1 \sum_{i=1}^{N_{Br}} \max\left[0,\ S_i - S_i^{\max}\right] \tag{4.17}$$

$$H_2(\mathbf{X}) = \mu_2 \sum_{i=1}^{N_G} \max\left[0,\ Q_i - Q_i^{\max},\ Q_i^{\min} - Q_i\right] \tag{4.18}$$

$$H_3(\mathbf{X}) = \mu_3 \sum_{i=1}^{N_B} \max\left[0,\ V_i - V_i^{\max},\ V_i^{\min} - V_i\right] \tag{4.19}$$

where :

μ : inequality penalty factor

N_B : set of buses

N_{Br} : set of branches

<u>*Fitness Function*</u>: The fitness function used in the optimization process was a combination of the original objective function with the equality and inequality penalty functions, as stated in (4.20):

$$F''(\mathbf{X}) = F'(\mathbf{X}) + G(\mathbf{X}) + H_1(\mathbf{X}) + H_2(\mathbf{X}) + H_3(\mathbf{X}) \tag{4.20}$$

4.7 CASE STUDIES AND RESULTS

The proposed framework is applied to a 6-bus test system, to a modified IEEE 14-bus system and to a modified IEEE 30-bus system.

4.7.1 Six–Bus System

A six - bus system [54], shown in Figure 4.1, is used to demonstrate the effectiveness of the algorithm solving congested scenarios. In this system three types of transactions (pool, bilateral and multilateral) were considered.

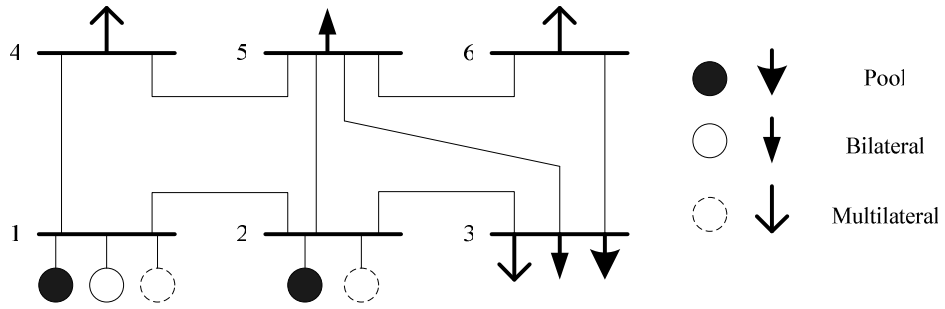

Figure 4.1: Six–Bus Test System

Tables 4.1–4.4 provide the system data and the pool, bilateral and multilateral transactions data and its preferred schedules, respectively. In those tables G, D, Min, Max, a, b, Prefer and W refer to: generation, load, minimum value, maximum value, quadratic and linear coefficient of the pool cost/bid curves, preferred values of transactions and willingness to pay to avoid curtailment factor for all transactions. Table 4.5 presents the curtailment weights for the multilateral contract at each bus. Table 4.6 shows the voltage limits. In this case, separate curtailment strategy was selected to curtail the load, if is necessary, in the multilateral contract. The bus 1 is selected as slack bus.

TABLE 4.1
SYSTEM DATA

Line	From bus	To bus	R	X	Rating (MW)
1	1	2	0.030	0.10	100
2	1	4	0.025	0.06	120
3	2	3	0.025	0.08	140
4	2	5	0.020	0.05	130
5	3	5	0.020	0.10	100
6	3	6	0.020	0.10	100
7	4	5	0.020	0.08	100
8	5	6	0.010	0.05	100

TABLE 4.2
POOL DATA

Bus	Type	Min	Max	a	b	Pref	W
1	G	0.0	200.0	0.06	6.00	-	-
2	G	0.0	200.0	0.03	3.00	-	-
3	D	0.0	100.0	0.00	9.00	100.0	20.0
5	D	0.0	80.0	0.00	10.00	80.0	20.0

TABLE 4.3
BILATERAL CONTRACT DATA

Bus	Type	Min	Max	Pref	W
1	G	0	100	100.0	-
3	D	0	100	100.0	15.0

TABLE 4.4
MULTILATERAL CONTRACT DATA

Bus	Type	Min	Max	Pref	W
1	G	0.0	100.0	100.0	-
2	G	0.0	100.0	100.0	-
3	D	0.0	50.0	50.0	15.0
4	D	0.0	100.0	100.0	15.0
6	D	0.0	50.0	50.0	20.0

TABLE 4.5
MULTILATERAL CURTAILMENT WEIGHTS

Bus	Type	Transaction	Weight
3	D	Multilateral	0.25
4	D	Multilateral	0.50
6	D	Multilateral	0.25

TABLE 4.6
BUS VOLTAGE LIMITS

Bus	V_{min}	V_{max}
1	1.02	1.02
2	1.04	1.04
3	0.95	1.05
4	0.95	1.05
5	0.95	1.05
6	0.95	1.05

If initial schedules submitted by the three types of transactions are honored by the ISO, they would cause congestion in lines 2, 3 and 4, as shown in Table 4.7.

TABLE 4.7
LINE FLOWS OF INITIAL SCHEDULES

Line	From bus	To bus	P_{ij}	P_{ji}	Rating (MW)
2	1	4	158.91	-152.84	120
3	2	3	177.77	-170.27	140
4	2	5	164.08	-158.86	130

Based on the proposed DE framework for this optimization problem, the congestion could be effectively solved. Table 4.8 shows the control parameters used in the optimization process for the case studies. The results obtained are shown in Tables 4.9 and 4.10. These results are compared with the results obtained by means of a traditional optimization technique [54].

TABLE 4.8
CONTROL PARAMETERS OF THE DE ALGORITHM

Control Parameters	6-Bus Test System	IEEE 14-Bus Test System	IEEE 30-Bus Test System
F	0.6	0.6	0.6
C_R	0.9	0.9	0.9
N_P	70	30-50	50-80
ω_1	1×10^5	1×10^5	1×10^5
μ_1	1×10^5	1×10^5	1×10^5
μ_2	1×10^3	1×10^3	1×10^3
μ_3	1×10^5	1×10^5	1×10^5

TABLE 4.9
OPTIMIZATION RESULTS: GENERATION VALUES

Bus	Type	Transaction	Min	Max	Pref	Traditional	DE
1	G	Pool	0.0	200.0	100.0	33.59	37.27
2	G	Pool	0.0	200.0	80.0	129.50	125.50
1	G	Bilateral	0.0	100.0	100.0	77.50	78.06
1	G	Multilateral	0.0	100.0	100.0	50.06	50.10
2	G	Multilateral	0.0	100.0	100.0	100.00	99.98

TABLE 4.10
OPTIMIZATION RESULTS: LOAD VALUES

Bus	Type	Transaction	Min	Max	Pref	Traditional	DE
3	D	Pool	0.0	100.0	100.0	80.58	83.51
5	D	Pool	0.0	80.0	80.0	66.70	65.80
3	D	Bilateral	0.0	100.0	100.0	77.55	78.06
3	D	Multilateral	0.0	50.0	50.0	37.51	37.52
4	D	Multilateral	0.0	100.0	100.0	75.03	75.04
6	D	Multilateral	0.0	50.0	50.0	37.51	37.52

TABLE 4.11
OPTIMIZATION RESULTS: OBJECTIVE FUNCTION

Traditional	DE
$ 33,221.71	$ 31,231.44

As shown in Table 4.11, Differential Evolution improves the solution obtained by means of a traditional optimization technique.

4.7.2 Modified IEEE 14-Bus Test System

The proposed framework is also applied to the modified IEEE 14–bus test system shown in Figure 4.2. In this work we consider only bilateral and multilateral transactions, since those are the most common transaction types in deregulated environments. Tables 4.12 – 4.13 provide the system data used for this case.

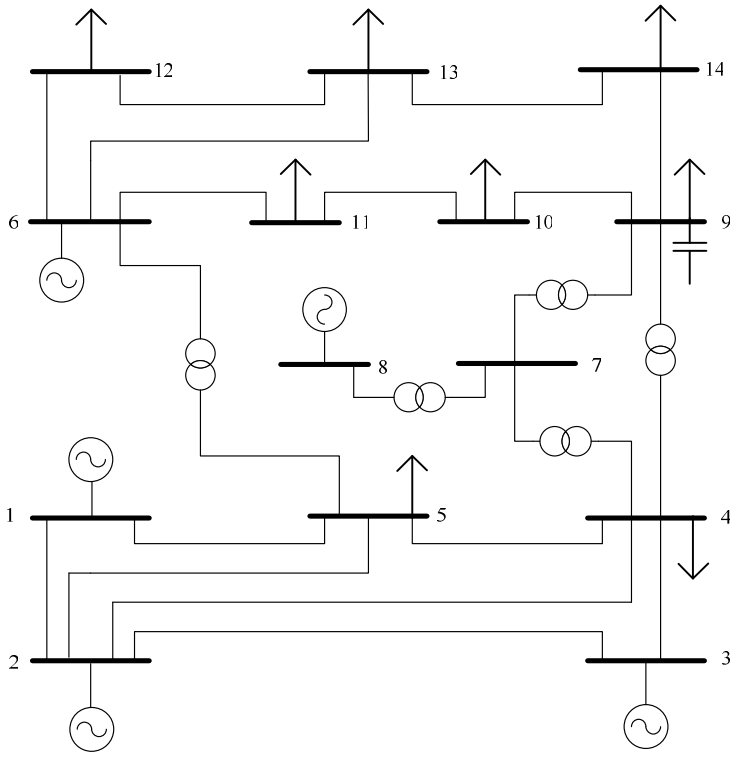

Figure 4.2: Modified IEEE 14–Bus Test System

Two multilateral groups sell and buy energy in this market. The group 1 makes transfers from generators at buses 2 and 6 to loads at buses 4, 9, 11, 12 y 14 and the group 2 makes transfers from generator at bus 1 to loads at buses 5, 10 and 13. For

simplicity we assume that the generator at bus 3 was designated by the ISO for loss compensation, hence this bus was selected as slack bus. The generator at bus 8 works as synchronous capacitor.

TABLE 4.12
BUS DATA

Bus No.	V (pu)	*Qd* (MVAR)	*Qc* (MVAR)	Bus No.	V (pu)	*Qd* (MVAR)	*Qc* (MVAR)
1	1.08	-	-	8	1.09	-	-
2	1.08	-	-	9	0.97-1.10	16.8	19.0
3	1.08	-	-	10	0.97-1.10	5.8	-
4	0.97-1.10	54.9	-	11	0.97-1.10	7.8	-
5	0.97-1.10	31.6	-	12	0.97-1.10	6.6	-
6	1.08	-	-	13	0.97-1.10	5.8	-
7	0.97-1.10	-	-	14	0.97-1.10	10.0	-

TABLE 4.13
BRANCH DATA

Branch		R (pu)	X (pu)	B (pu)	Rating (MVA)	Branch		R (pu)	X (pu)	B (pu)	Rating (MVA)
From	To					From	To				
1	2	0.0194	0.0592	0.0528	220	6	12	0.1229	0.2558	0.0000	55
1	5	0.0540	0.2230	0.0492	110	6	13	0.0662	0.1303	0.0000	55
2	3	0.0470	0.1980	0.0438	110	9	10	0.0318	0.0845	0.0000	55
2	4	0.0581	0.1763	0.0374	110	9	14	0.1271	0.2704	0.0000	55
2	5	0.0570	0.1739	0.0340	110	10	11	0.0821	0.1921	0.0000	55
3	4	0.0670	0.1710	0.0346	110	12	13	0.2209	0.1999	0.0000	55
4	5	0.0134	0.0421	0.0128	110	13	14	0.1709	0.3480	0.0000	55
6	11	0.0950	0.1989	0.0000	55						

Branch		R (pu)	X (pu)	Transformer Tap Ratio	Rating (MVA)	Branch		R (pu)	X (pu)	Transformer Tap Ratio	Rating (MVA)
From	To					From	To				
4	7	0.0000	0.2091	0.978	70	7	8	0.0000	0.1762	1.000	55
4	9	0.0000	0.5562	0.969	40	7	9	0.0000	0.1100	1.000	70
5	6	0.0000	0.2520	0.932	70						

If initial schedules submitted by the both groups are dispatched by the ISO, they would cause congestion in lines 1-5, 2-4, 2-5 and 6-11, as shown in Table 4.14.

TABLE 4.14
LINE FLOWS OF INITIAL SCHEDULES

Branch From	Branch To	S_{ij}	S_{ji}	Rating (MVA)
1	5	114.28	104.92	110
2	4	113.72	104.13	110
2	5	112.52	103.20	110
6	11	62.21	57.99	55

Some curtailment strategies were considered:

a) The group curtailment strategy (4.13) is employed by both groups. The willingness to pay to avoid curtailment factor for both groups is $5\$/MW^2$.

b) The willingness to pay to avoid curtailment factor of group 2 is increased to $15\$/MW^2$, but the other information remains as case a).

c) Group 1 selects the separate curtailment strategy (4.14). The willingness to pay to avoid curtailment factor for generator at bus 2 is set at $15\$/MW^2$, while the value at bus 6 remains at $5\$/MW^2$.

d) Group 2 abandons the group curtailment strategy (4.13) and adopts the point-to-point curtailment strategy (4.12) for the three individual contracts (1-5, 1-10 and 1-13). The willingness to pay to avoid curtailment factor of each individual contract is $5\$/MW^2$ and the group 1 maintains the group curtailment strategy as case a).

e) The willingness to pay to avoid curtailment factor for the individual contract 1–10 is increased to $15\$/MW^2$, while the willingness to pay to avoid curtailment factor of the contracts 1-5 and 1-13 remain at $5\$/MW^2$. The other information is the same as case d).

The results of the optimization process for all cases treated are shown in Table 4.15. The optimal dispatch procedure results in uncongested system solutions for all cases.

TABLE 4.15
ORIGINAL AND CURTAILED GENERATION AND LOAD DATA FOR THE IEEE 14-BUS TEST SYSTEM

Bus	Type	Desired (MW)	Curtailed Data				
			Case 2A	Case 2B	Case 2C	Case 2D	Case 2E
			Loss Compensation				
3	G	35.05	28.03	27.77	27.87	27.82	27.77
			Group 1				
2	G	157.70	157.70	150.13	153.16	155.65	155.14
6	G	98.00	78.08	81.71	80.26	80.75	78.79
4	D	102.90	94.88	93.30	93.93	95.14	94.14
9	D	57.80	53.30	52.41	52.76	53.44	52.88
11	D	53.50	49.33	48.51	48.84	49.46	48.95
12	D	16.10	14.85	14.60	14.70	14.89	14.73
14	D	25.40	23.42	23.03	23.19	23.48	23.24
			Group 2				
1	G	214.10	202.45	206.70	205.00	203.39	203.68
5	D	167.80	158.67	162.00	160.67	164.11	163.19
10	D	19.00	17.97	18.34	18.19	15.43	17.51
13	D	27.30	25.82	26.36	26.14	23.85	22.99

In the Case 2A (base case), when both groups have the same curtailment strategy and the same willingness to pay to avoid curtailment factor, the generation and load of group 1 was curtailed most severely than the generation and load of group 2. This is because of the congested lines 2-4 and 2-5 serve the heaviest loads of the group 1, while for the group 2 the main restriction is on line 1-5 which serves the load at bus 5.

The Case 2B shows a very modest increase in generation and demand of group 2, when the willingness to pay to avoid curtailment factor for the group was increased to $15\,\$/MW^2$.

In Case 2C when group 1 becomes more selective, the results show a slightly increment in generation at bus 2, when compared with the Case 2B.

In Case 2D, when the group 2 shifts to a point to point curtailment strategy, the load at bus 10 is considerably reduced in comparison with the base case, while the load at buses 5 and 13 increases, respectively. The nominal load is partially restored in case 2E, when the willingness to pay to avoid curtailment factor for this contract is increased to $15 \$/MW^2$.

4.7.3 Modified IEEE 30-Bus Test System

The last case analyzed was the modified IEEE-30 bus test system. As in case 2, we consider only bilateral and multilateral transactions, because those are the most common transaction in deregulated environments. Tables 4.16 – 4.18 provide the system data used in this case. All bus voltages must lie between 0.95 – 1.05 p.u. The system is shown in Figure 4.3.

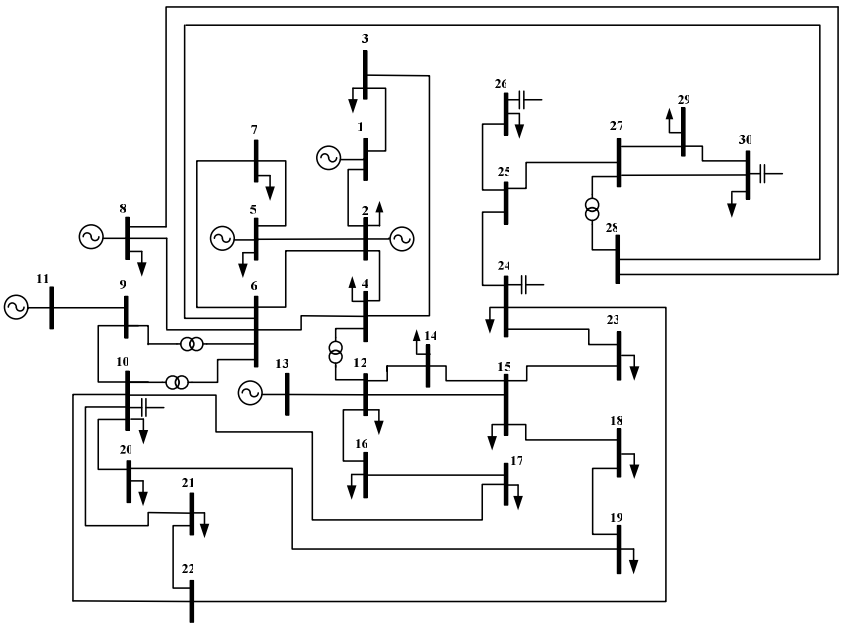

Figure 4.3: Modified IEEE 30–Bus Test System

TABLE 4.16
BUS DATA

Bus	P_D (MW)	Q_D (MVAR)	Q_C (MVAR)	Bus	P_D (MW)	Q_D (MVAR)	Q_C (MVAR)
2	21.7	12.7	0.0	17	18.0	11.6	0.0
3	4.8	2.4	0.0	18	6.4	1.8	0.0
4	15.2	3.2	0.0	19	19.0	6.8	0.0
5	94.2	19.0	0.0	20	4.4	1.4	0.0
7	45.6	21.8	0.0	21	35.0	22.4	0.0
8	30.0	30.0	0.0	23	6.4	3.2	0.0
10	11.6	4.0	19.0	24	17.4	13.4	4.3
12	22.4	30.0	0.0	26	7.0	4.6	5.0
14	12.4	1.6	0.0	29	4.8	1.8	0.0
15	16.4	5.0	0.0	30	21.2	3.8	4.0
16	7.0	3.6	0.0				

TABLE 4.17
GENERATORS DATA

Bus	V_G (pu)	P_G (MW)	Q_{min} (MVAR)	Q_{max} (MVAR)	Bus	V_G (pu)	P_G (MW)	Q_{min} (MVAR)	Q_{max} (MVAR)
1	1.08	0.0	-40.0	100.0	8	1.08	79.4	-30.0	80.0
2	1.08	54.1	-40.0	100.0	11	1.08	79.6	-12.0	48.0
5	1.08	106.6	-40.0	80.0	13	1.07	101.2	-12.0	48.0

TABLE 4.18
BRANCH DATA

Branch From	Branch To	R (pu)	X (pu)	B (pu)	Rating (MVA)	Branch From	Branch To	R (pu)	X (pu)	B (pu)	Rating (MVA)
1	2	0.0192	0.0575	0.0528	130	18	19	0.0639	0.1292	0.0000	16
1	3	0.0452	0.1852	0.0408	130	19	20	0.0340	0.0680	0.0000	32
2	4	0.0570	0.1737	0.0368	65	10	20	0.0936	0.2090	0.0000	32
3	4	0.0132	0.0379	0.0084	130	10	17	0.0324	0.0845	0.0000	32
2	5	0.0472	0.1983	0.0418	130	10	21	0.0348	0.0749	0.0000	32
2	6	0.0581	0.1763	0.0374	65	10	22	0.0727	0.1499	0.0000	32
4	6	0.0119	0.0414	0.0090	90	21	22	0.0116	0.0236	0.0000	32
5	7	0.0460	0.1160	0.0204	70	15	23	0.1000	0.2020	0.0000	16
6	7	0.0267	0.0820	0.0170	130	22	24	0.1150	0.1790	0.0000	16
6	8	0.0120	0.0420	0.0090	50	23	24	0.1320	0.2700	0.0000	16
9	11	0.0000	0.2080	0.0000	90	24	25	0.1885	0.3292	0.0000	16
9	10	0.0000	0.1100	0.0000	90	25	26	0.2544	0.3800	0.0000	16
12	13	0.0000	0.1400	0.0000	100	25	27	0.1093	0.2087	0.0000	16
12	14	0.1231	0.2559	0.0000	32	27	29	0.2198	0.4153	0.0000	16
12	15	0.0662	0.1304	0.0000	32	27	30	0.3202	0.6027	0.0000	16
12	16	0.0945	0.1987	0.0000	32	29	30	0.2399	0.4533	0.0000	16
14	15	0.2210	0.1997	0.0000	16	8	28	0.0636	0.2000	0.0428	32
16	17	0.0824	0.1923	0.0000	16	6	28	0.0169	0.0599	0.1300	32
15	18	0.1073	0.2185	0.0000	16						

Branch From	Branch To	R (pu)	X (pu)	Transformer Tap Ratio	Rating (MVA)	Branch From	Branch To	R (pu)	X (pu)	Transformer Tap Ratio	Rating (MVA)
6	9	0.0000	0.2080	0.978	65	4	12	0.0000	0.2560	0.932	65
6	10	0.0000	0.5560	0.969	32	28	27	0.0000	0.3960	0.968	65

Three multilateral groups sell and buy energy in this market. The group 1 makes transfers from generators at buses 2 and 8 to loads at buses 2, 8, 15, 16, 19, 23, 26, 29 and 30. The group 2 makes transfers from generators at buses 11 and 13 to loads at buses 3, 4, 7, 10, 12, 17, 20 and 24. The group 3 is formed for generator at bus 5 and loads at buses 5, 14, 18 and 21.

If initial schedules submitted by the three groups are dispatched by the ISO, they would cause congestion in the branches 6-8, 12-15 and 10-21, as shown in Table 4.19. Therefore ISO has to curtail the initial power transfers in order to maintain the system within the specified limits.

TABLE 4.19
LINE FLOWS OF INITIAL SCHEDULES

Branch From	Branch To	S_{ij}	S_{ji}	Rating (MVA)
6	8	53.83	54.06	50
12	15	36.84	35.57	32
10	21	38.04	37.15	32

As case 2, some curtailment strategies were considered:

a) The group curtailment strategy (4.13) is employed by the three groups and the willingness to pay to avoid curtailment factor for the groups is $5\$/MW^2$

b) The willingness to pay to avoid curtailment factor of group 1 is increased to $15\$/MW^2$, but other information remains as case a).

c) Group 1 selects the separate curtailment strategy (4.14). The willingness to pay to avoid curtailment factor for generator at bus 2 is set at $15\$/MW^2$ while value at bus 8 remains at $5\$/MW^2$.

d) The Group 3 abandons the group curtailment strategy (4.13) and adopts the point-to-point curtailment strategy (4.12) for the four individual contracts (5-5, 5-14, 5-18 and 5-21). The willingness to pay to avoid curtailment factor of each individual contract is $5\$/MW^2$ and the groups 1 and 2 maintain the group curtailment strategy as case a).

e) The willingness to pay to avoid curtailment factor for the individual contract 5-18 is increased to $15\$/MW^2$ while willingness to pay to avoid curtailment factor of the contracts 5-5, 5-14 and 5-21 remain at $5\$/MW^2$. Other information is the same as case d).

The results of the optimization process for all case treated are shown in Table 4.20. The optimal dispatch procedure results in uncongested system solutions for all case studies.

TABLE 4.20
ORIGINAL AND CURTAILED GENERATION AND LOAD DATA FOR THE IEEE 30-BUS TEST SYSTEM

Bus	Type	Desired (MW)	Curtailed Data				
			Case 3A	Case 3B	Case 3C	Case 3D	Case 3E
			Loss Compensation				
1	G	6.55	4.77	5.13	4.76	5.26	5.20
			Group 1				
2	G	54.10	39.43	50.01	48.20	53.68	51.52
8	G	79.40	74.18	75.45	62.38	76.65	76.18
2	D	21.70	18.47	20.39	17.98	21.18	20.76
8	D	30.00	25.53	28.19	24.85	29.29	28.70
15	D	16.40	13.96	15.41	13.59	16.01	15.69
16	D	7.00	5.96	6.58	5.80	6.83	6.70
19	D	19.00	16.17	17.86	15.74	18.55	18.17
23	D	6.40	5.45	6.01	5.30	6.25	6.12
26	D	7.00	5.96	6.58	5.80	6.83	6.70
29	D	4.80	4.08	4.51	3.98	4.69	4.59
30	D	21.20	18.04	19.92	17.56	20.70	20.28
			Group 2				
11	G	79.60	68.45	73.99	67.26	79.60	79.60
13	G	59.80	58.61	50.79	59.80	57.03	53.99
3	D	4.80	4.37	4.30	4.38	4.70	4.60
4	D	15.20	13.85	13.61	13.85	14.90	14.57
7	D	45.60	41.56	40.82	41.56	44.69	43.70
10	D	11.60	10.57	10.38	10.57	11.37	11.12
12	D	22.40	20.42	20.05	20.42	21.96	21.47
17	D	18.00	16.41	16.11	16.41	17.64	17.25
20	D	4.40	4.01	3.94	4.01	4.31	4.22
24	D	17.40	15.86	15.58	15.86	17.05	16.68
			Group 3				
5	G	148.00	113.64	107.50	115.10	128.42	129.54
5	D	94.20	72.33	68.42	73.26	94.19	94.19
14	D	12.40	9.52	9.01	9.64	9.48	6.85
18	D	6.40	4.91	4.65	4.98	0.43	3.78
21	D	35.00	26.87	25.42	27.22	24.32	24.71

In Case 3A, the three groups use the same curtailment strategies with identical willingness-to-pay factors, and this results in all power transactions getting curtailed in varying degrees.

In Case 3B, the willingness to pay of group 1 is increased. The result is a proportionate increase in the power transferred not only by the group 1, but also by the group 2; and a considerable reduction in the transactions requested by the group 3.

In Case 3C, the separate curtailment strategy of group 1 provide a considerable increase in power injected by generator 2 and a considerable reduction in power injected by the generator 8. The others groups were not affected practically for this strategy.

In Case 3D the use of different curtailment strategy for the group 3 seems to affect some transactions more than others. For instance, the transaction between buses 5 and 18 gets relatively heavily curtailed. This is remedied in Case 3E where the willingness to pay factor for this transaction is increased to $15\,\$/MW^2$.

4.7.4 Rate of Convergence of the Proposed Framework and Statistical Results

Table 4.21 provides the statistical results for the case studies based on 50 independent runs of the DE algorithm. In this table *BSF* and *WSF* refer to best solution and worst solution found, respectively. Figure 4.4 shows the convergence rate of the algorithm for the Case 2. Note that the DE algorithm obtains very good solutions in a few iterations for all case studies.

TABLE 4.21
STATISTICAL RESULT BASED ON 50 INDEPENDENT RUNS

	Case 1A	Case 2D	Case 3D
Average	31,231.45	212.19	1,192.10
Median	31,231.45	212.19	1,192.10
Mode	31,231.45	212.19	1,192.10
Standard Deviation	0.006334	0.000000	0.002092
BSF	31,231.44	212.19	1,192.10
WSF	31,231.46	212.19	1,192.11

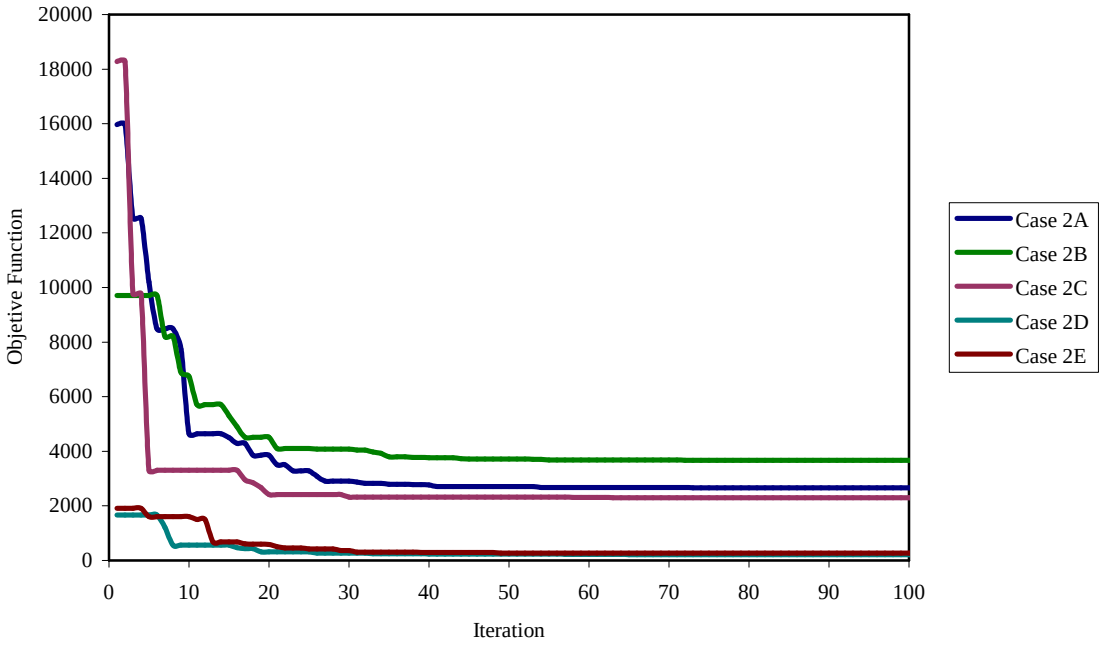

Figure 4.4: Rate of Convergence of the DE Algorithm for the IEEE 14-Bus Test System Case Study

4.8 CONCLUSION

In deregulated power systems, with open transmission access, congestion management is one of the most challenging operational problems. With the trend of an increasing number of bilateral and multilateral contracts submitted for electricity market trades, the possibility of insufficient resources in the transmission system may be unavoidable.

In this statement, the role for the transmission system operator is to create a set of rules that ensure sufficient control over producers and consumers to maintain an acceptable level of power system security and reliability in the short term and long term operation. An optimal power flow, with two simultaneous objectives: cost minimization and minimization of transaction deviations, can be developed to solve the congestion problem.

The results obtained show that the willingness to pay and the curtailment strategy selected by market participants are two factors that will significantly affect the constrained dispatch. Obviously, while higher the willingness to pay, less the curtailment of the transaction requested, but the complex interactions among market participants underline the need for careful design of the dispatch strategies.

CHAPTER 5

POWER SYSTEMS STATE ESTIMATION

5.1 INTRODUCTION

Through the years, interconnected power systems have become much more complex and the task of securely operating the systems has become more difficult. To help avoiding major system failures and regional power blackouts, electric utilities have installed more extensive supervisory control and data acquisition (SCADA) systems throughout the network, which support computer-based systems at the energy control center. The database created serves in supporting a wide range of applications, some to ensure the economic operation and others to assess the security of the system if transmission line outages or other equipment failures should occur.

Before executing any security assessment program or taking any control action in the system, a reliable estimate of the existing state of the system must be determined. The state estimation program provides an estimate of the system state and a quantitative measure of how good that estimate is, before it is used for real time power flow calculations or for on-line security purposes [55].

Besides some of the inputs typically required for conventional power flow calculations, additional measurements should be provided in order to counteract the effect of inaccurate (or missing) data due to instrument failures. A good state estimation will smooth out small random errors in measurements, detect and identify large measurement errors, and compensate for missing data [56]. Thus, gross errors detected in the course of state estimation are automatically filtered out, improving the reliability of the estimation.

Since state estimation provides the platform for advanced security monitoring applications in control centers, this is perhaps the most important application of the Phasor Measurement Units (PMUs) in power systems. PMUs improve the monitoring and control functions of power systems through accurate, synchronized, and direct measurement of the system state. The greatest benefit comes from their unique capability to provide real time synchronized measurements. With PMUs the security indicators produced by these advance applications are representative of the true real time status of the power system. The challenge therefore is to incorporate the information provided by the PMUs in the conventional state estimator to improve the assessment of the current state of the system [57].

On the other hand, the operational constraints can be utilized effectively in enhancing the reliability of the state estimators. These constraints may represent the zero injections at the switching substations, or the bounds imposed on the reactive power injections at the generator buses, or the upper and lower limits on the tie-line power flows at the area boundaries, etc. Estimates of the system states will become more reliable, if these constraints are incorporated into the estimation formulation [58].

In this chapter we propose to use the Differential Evolution algorithm for solving the Weighted Least Squares State Estimation problem, incorporating the information of the PMUs to the original formulation. Besides, we propose to analyze the effect of equality and inequality constraints and how the solution is improved (or degraded) when these constraints are included in the original formulation.

5.2 STATE ESTIMATION PROBLEM FORMULATION

5.2.1 Weighted Least Squares (WLS) State Estimation Problem Formulation

In the least-squares formulation, the objective is to minimize the sum of the squares of the difference between the measured value and the estimated value, weighted by the variance of their corresponding meter error. The mathematical formulation of the problem is [55], [56], [59]-[62]:

$$\text{Min } J(\mathbf{x}) = \sum_{i=1}^{m} \frac{1}{\sigma_i^2} \left[z_i - h_i(\mathbf{x}) \right]^2 \tag{5.1}$$

where

$\mathbf{x}$: vector of unknown values to be estimated

m : number of independent measurements

σ_i^2 : variance of the i^{th} measurement

z_i : i^{th} measurement value

$h_i(\mathbf{x})$: function used to calculate the estimated value of the i^{th} measurement

The standard deviation σ_i of each measurement provides a way to reflect the expected accuracy of the corresponding meter used. For instance, if the standard deviation is large, the measurement is relatively inaccurate, while a small standard deviation value indicates a small error range.

In the WLS formulation, the vector of state variables ($\mathbf{x}$) usually includes the following states:

1) Complex nodal voltages:

- Voltage magnitudes (V_i).
- Phase angles (δ_i).

2) Transformers turns ratio:

- Turns ratio magnitudes (T_{ij}).
- Phase shift angles (φ_{ij}).

When using only the complex voltages for a system of *N* buses, the state vector will have (*2N-1*) elements, *N* bus voltage magnitudes and (*N-1*) phase angles, since the phase angle of the reference bus is set to an arbitrary value, (typically 0°). The state vector (**x**) will have the following form, assuming bus 1 is chosen as the reference bus.

$$\mathbf{x} = \begin{bmatrix} \delta_2 & \delta_3 & \cdots & \delta_n & V_1 & V_2 & \cdots & V_n \end{bmatrix}^{\mathrm{T}} \tag{5.2}$$

*5.2.2 The Measurement Function, h(**x**)*

The most commonly used measurements in state estimation are the line power flows, bus power injections, bus voltages magnitudes, and line current magnitudes. The $h_i(\mathbf{x})$ functions will be nonlinear functions, except for the voltage measurements, in which the $h_i(\mathbf{x})$ function is simply the voltage magnitude being measured. Thus, the corresponding measurement functions for each of the above types of measurements are stated as [61]-[62]:

- Real and reactive power injections

$$P_i = V_i \sum_{j=1}^{N_B} V_j \left(G_{ij} \cos \delta_{ij} + B_{ij} \sin \delta_{ij} \right) \tag{5.3}$$

$$Q_i = V_i \sum_{j=1}^{N_B} V_j \left(G_{ij} \sin \delta_{ij} - B_{ij} \cos \delta_{ij} \right) \tag{5.4}$$

- Real and reactive power flow from bus *i* to bus *j*:

$$P_{ij} = V_i^2 \left(g_{si} + g_{ij} \right) - V_i V_j \left(g_{ij} \cos \delta_{ij} + b_{ij} \sin \delta_{ij} \right) \tag{5.5}$$

$$Q_{ij} = -V_i^2 \left(b_{si} + b_{ij} \right) - V_i V_j \left(g_{ij} \sin \delta_{ij} - b_{ij} \cos \delta_{ij} \right) \tag{5.6}$$

- Line current flow magnitude from bus *i* to bus *j*:

$$I_{ij} = \frac{\sqrt{P_{ij}^2 + Q_{ij}^2}}{V_i} \tag{5.7}$$

Or ignoring the shunt admittance $\left(g_{si} + jb_{si} \right)$

$$I_{ij} = \sqrt{\left(g_{ij}^2 + b_{ij}^2 \right) \left(V_i^2 + V_j^2 - 2V_i V_j \cos \delta_{ij} \right)} \tag{5.8}$$

where:

V_i, δ_i : voltage magnitude and phase angle at bus *i*

δ_{ij} : phase angle difference between buses *i* and *j*

$G_{ij} + jB_{ij}$: ij^{th} element of the complex bus admittance matrix

$g_{ij} + jb_{ij}$: admittance of the series branch connecting buses *i* and *j*

$g_{si} + jb_{si}$: admittance of the shunt branch connected at bus *i*

N_B : total number of buses of the system being studied

5.2.3 Weighted Least Squares (WLS) State Estimation Formulation with Phasor Measurement Units (PMUs)

Phasor Measurement Units (PMUs) are among the most interesting developments in the field of real-time monitoring of power systems. PMUs provide real time measurement of positive sequence voltages and currents at power system substations. Synchronicity among phasor measurement units (PMUs) is achieved by same-time sampling of voltage and current waveforms using a common synchronizing signal from a global positioning satellite (GPS). Data from substations are collected at suitable sites, and by aligning the time stamps of the measurements, a coherent picture of the state of the system is created [63]. Many applications of these measurements have been described in the literature. State estimation, stability prediction, and adaptive relaying are some of these applications in power systems [64]-[66].

Since state estimation provides the platform for advanced security monitoring applications in control centers, this is perhaps the most important application of the phasor measurement units (PMUs). Their impact in the solution of the traditional state estimation algorithms, observability analysis and bad data identification, has been reported in the literature [67]-[72].

Several methods have been proposed to integrate phasor measurements to the classical WLS algorithm. Basically, the methods involve accommodating the direct angle measurements to the classical measurement set, which results in a balanced set of measurement equations, as shown in (5.9) and (5.10). Since PMUs measurements have much smaller error variances than all the other conventional meters, the addition of these

phase angle measurements to a conventional state estimator could greatly increase the accuracy of the solution obtained.

$$\mathbf{z} = \begin{bmatrix} \mathbf{z}_A & \mathbf{z}_R \end{bmatrix}^{\mathrm{T}} \tag{5.9}$$

where

$$\mathbf{z}_A = \begin{bmatrix} P_{ij} \\ P_i \\ \delta_i \end{bmatrix} \quad \mathbf{z}_R = \begin{bmatrix} Q_{ij} \\ Q_i \\ V_i \end{bmatrix} \tag{5.10}$$

direct angle measurement with PMUs

P_{ij}, Q_{ij} are the real and reactive power flows through the ij^{th} branch of the system; P_i, Q_i are the real and reactive power injected at the i^{th} bus of the system; V_i is the voltage magnitude at bus *i*, δ_i is the direct angle measured with the PMU at bus *i*.

On the other hand, selection of reference bus becomes more complicated in the presence of phasor measurements. For a given set of measurements, the choice of angle reference (zero or non-zero) establishes the angle profile in the solved network. At the same time, phase angles are measured with respect to some other reference that has no power system significance. For phasor measurements to be properly used in estimator solution, the reference bus must chosen among buses with phasor measurements and values of all remaining phasor measurements must be corrected by the value of the reference measurement, as shown in (5.11)

$$\overline{\delta}_i = \delta_i - \delta_{ref} \tag{5.11}$$

Where δ_i and $\overline{\delta}_i$ are the estimated and corrected value for the phasor measurement at bus *i*, and δ_{ref} is the reference measurement. To avoid further complications, in our approach

δ_{ref} is selected to be the same as the state estimation reference, so it is not necessary to correct the phasor measurement estimated in the process.

5.2.4 Weighted Least Squares (WLS) State Estimation with Equality and Inequality Constraints

The constrained WLS estate estimation problem is formulated so that the operational constraints on the various measurements may be accounted during the estimation process. Estimates of the system states, becomes more reliable, if these constraints are incorporated into the estimation formulation.

Equality constraints are introduced in the WLS state estimation formulation for modeling very accurate virtual measurements such as zero injections or net injections at a particular bus of a power system that are previously specified to a fixed value. To avoid the use of high weights in the traditional WLS state estimation formulation, these measurements are modeled as explicit constraints for the problem [73]-[76].

The use of inequality constraints is justified if they are needed to make an unobservable system observable. Limits, such as minimum and maximum real and reactive power injections/flows, transformers and phase shifters, could also be used to improve the representation of unobservable parts of the network. Furthermore, the inequality constraints are useful for external system state estimation with insufficient local redundancy. These constraints take the form of boundary constraints of the measurements and help to reject bad data measurement placed in the external subsystem [75]-[78].

The constrained WLS state estimation could be formulated as follows:

$$\text{Min } J(\mathbf{x}) = \sum_{i=1}^{m} \frac{1}{\sigma_i^2} \left[z_i - h_i(\mathbf{x}) \right]^2 \tag{5.12}$$

subject to

$$\begin{aligned} \mathbf{g(x)} &= \mathbf{z}_e \\ \mathbf{z}_l \le \mathbf{f(x)} &\le \mathbf{z}_u \end{aligned} \tag{5.13}$$

where

z_i : i^{th} unconstrained measurement

$\mathbf{z}_e$: vector of equality constrained measurements

$\mathbf{z}_l, \mathbf{z}_u$: vector of lower and upper limits, respectively, of inequality constrained measurements

g(x) : nonlinear function vector corresponding to equality constrained measures

f(x) : nonlinear function vector corresponding to inequality constrained measures

Several methods such as, penalty, barriers, lagrangian relaxation, interior points, have been proposed in the literature to solve the constrained WLS state estimation problem [73]-[79]. In our thesis work, we propose to use the Differential Evolution optimization algorithm to solve both, the WLS State Estimation with Phasor Measurement Units (PMUs) and the Constrained WLS State Estimation.

5.3 DE MODEL FOR POWER SYSTEMS STATE ESTIMATION

As described before, in the WLS state estimation formulation the objective is to minimize the sum of squares of the difference between the measured value and the estimated value, weighted by the variance of their corresponding meter error.

Control Variables: The set of control variables used in the optimization process were:

- Bus voltages magnitudes, V_i
- Phase angles, δ_i

Since the phase angle of the reference bus is set to an arbitrary value, such as 0, the state vector (**x**) will have the following form.

$$\mathbf{x} = \left[\delta_2 \quad \delta_3 \quad \cdots \quad \delta_n \quad V_1 \quad V_2 \quad \cdots \quad V_n\right]^{\mathrm{T}} \tag{5.14}$$

Initialization: All the control variables are initialized randomly within their feasible bounds by means of (2.3). If during the evolution process, any of these settings become unfeasible, they were adjusted using the boundary operator (2.8).

Objective Function: Minimize the weighted sum of the squares of the errors, with weights chosen equal to the reciprocal of the corresponding error variances:

$$F'(\mathbf{X}) = \begin{cases} \displaystyle\sum_{i=1}^{N_B} \frac{\left(V_i^{meas} - V_i^{est}\right)^2}{\sigma_{V_i}^2} + \sum_{i=1}^{N_{P_{inj}}} \frac{\left(P_i^{meas} - P_i^{est}\right)^2}{\sigma_{P_i}^2} + \sum_{i=1}^{N_{Q_{inj}}} \frac{\left(Q_i^{meas} - Q_i^{est}\right)^2}{\sigma_{Q_i}^2} \\ + \displaystyle\sum_{i=1}^{N_{P_{flow}}} \frac{\left(P_{flow_i}^{meas} - P_{flow_i}^{est}\right)^2}{\sigma_{P_{flow_i}}^2} + \sum_{i=1}^{N_{Q_{flow}}} \frac{\left(Q_{flow_i}^{meas} - Q_{flow_i}^{est}\right)^2}{\sigma_{Q_{flow_i}}^2} \end{cases} \tag{5.15}$$

When considering phasor measurement units (PMUs) in the WLS state estimation formulation, the objective function is transformed to:

$$F'(\mathbf{X}) = \begin{cases} \sum_{i=1}^{N_V} \frac{\left(V_i^{meas} - V_i^{est}\right)^2}{\sigma_{V_i}^2} + \sum_{\substack{i=1 \\ i \neq slack}}^{N_P} \frac{\left(\delta_i^{meas} - \delta_i^{est}\right)^2}{\sigma_{\delta_i}^2} + \sum_{i=1}^{N_{P_{inj}}} \frac{\left(P_i^{meas} - P_i^{est}\right)^2}{\sigma_{P_i}^2} \\ + \sum_{i=1}^{N_{Q_{inj}}} \frac{\left(Q_i^{meas} - Q_i^{est}\right)^2}{\sigma_{Q_i}^2} + \sum_{i=1}^{N_{P_{flow}}} \frac{\left(P_{flow_i}^{meas} - P_{flow_i}^{est}\right)^2}{\sigma_{P_{flow_i}}^2} + \sum_{i=1}^{N_{Q_{flow}}} \frac{\left(Q_{flow_i}^{meas} - Q_{flow_i}^{est}\right)^2}{\sigma_{Q_{flow_i}}^2} \end{cases} \quad (5.16)$$

where the variables are defined as follows

N_V : number of voltage measurements

N_P : number of angle measurements

$N_{P_{inj}}$, $N_{Q_{inj}}$: number of real and reactive power injection measurements

$N_{P_{flow}}$, $N_{Q_{flow}}$: number of real and reactive power flow measurements

meas, *est* : measured and estimated value for the i^{th} measurement data

Penalty Functions: In the constrained WLS state estimation formulation, the objective function could be modified adding penalty factors, when equality and inequality constraints are not satisfied. The equality constraints are modeled as real and reactive power injections at specific buses of the system. The inequality constraints include real and reactive power flow constraints, used to model the interaction with external systems with insufficient local redundancy.

c. Equality Penalty Function: Real and reactive power injections measurements in specific buses were modeled through equality penalty functions:

$$G_1(\mathbf{X}) = \omega_1 \sum_{i=1}^{N_E} \left| P_i - V_i \sum_{j=1}^{N_B} V_j \left(G_{ij} \cos \delta_{ij} + B_{ij} \sin \delta_{ij} \right) \right| \tag{5.17}$$

$$G_2(\mathbf{X}) = \omega_2 \sum_{i=1}^{N_E} \left| Q_i - V_i \sum_{j=1}^{N_B} V_j \left(G_{ij} \sin \delta_{ij} - B_{ij} \cos \delta_{ij} \right) \right| \tag{5.18}$$

Where ω_i is the i^{th} equality penalty factor and N_E is the set of equality constraints.

d. Inequality Penalty Functions: Real and reactive power flow limits were modeled as inequality penalty functions for the case studies:

$$H_1(\mathbf{X}) = \mu_1 \sum_{i=1}^{N_I} \max\left[0,\ P_{ij} - P_{ij}^{\max},\ P_{ij}^{\min} - P_{ij} \right] \tag{5.19}$$

$$H_2(\mathbf{X}) = \mu_2 \sum_{i=1}^{N_I} \max\left[0,\ Q_{ij} - Q_{ij}^{\max},\ Q_{ij}^{\min} - Q_{ij} \right] \tag{5.20}$$

Where μ_i is the i^{th} inequality penalty factor and N_I is the set of inequality constraints.

Fitness Function: The fitness function used in the optimization process was a combination of the original objective function with the equality and inequality penalty functions, as shown in (5.21):

$$F''(\mathbf{X}) = F'(\mathbf{X}) + G_1(\mathbf{X}) + G_2(\mathbf{X}) + H_1(\mathbf{X}) + H_2(\mathbf{X}) \tag{5.21}$$

5.4 WEIGHTED LEAST SQUARES (WLS) STATE ESTIMATION WITH PHASOR MEASUREMENT UNITS CASE STUDIES AND RESULTS

In order to demonstrate the effectiveness of the phasor measurement units improving the reliability of the estimation process, various cases were analyzed.

5.4.1 Case 1: Six-Bus Test System

A simple six bus test system [59], shown in Figure 5.1, is used to demonstrate the effectiveness of the proposed approach improving the reliability of the estimators. The system and measurement data for the base case are shown in Tables 5.1 and 5.2.

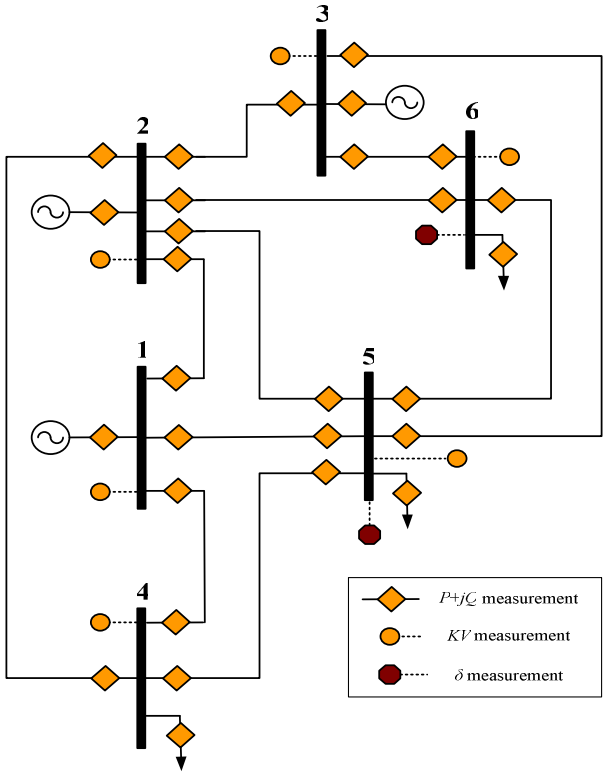

Figure 5.1: Six-Bus Test System with Measurements Location

TABLE 5.1
SYSTEM DATA

Branch		R (pu)	X (pu)	B (pu)
From Bus	To Bus			
1	2	0.10	0.20	0.04
1	4	0.05	0.20	0.04
1	5	0.08	0.30	0.06
2	3	0.05	0.25	0.06
2	4	0.05	0.10	0.02
2	5	0.10	0.30	0.04
2	6	0.07	0.20	0.05
3	5	0.12	0.26	0.05
3	6	0.02	0.10	0.02
4	5	0.20	0.40	0.08
5	6	0.10	0.30	0.06

TABLE 5.2
MEASUREMENT DATA

Voltage and Power Injection Measurements

Bus	KV	MW	MVAR	Bus	KV	MW	MVAR
1	238.4	113.1	20.2	4	225.7	-71.8	-71.9
2	237.8	48.4	71.9	5	225.2	-72	-67.7
3	250.7	55.1	90.6	6	228.9	-72.3	-60.9

Power Flow Measurements

From Bus	To Bus	MW	MVAR	From Bus	To Bus	MW	MVAR
1	2	31.5	-13.2	2	1	-34.9	9.7
1	4	38.9	21.2	4	1	-40.1	-14.3
1	5	35.7	9.4	5	1	-36.6	-17.5
2	3	8.6	-11.9	3	2	-2.1	10.2
2	4	32.8	38.3	4	2	-29.8	-44.3
2	5	17.4	22	5	2	-11.7	-22.2
2	6	22.3	15	6	2	-19.6	-22.3
3	5	17.7	23.9	5	3	-25.1	-29.9
3	6	43.3	58.3	6	3	-46.8	-51.1
4	5	0.7	-17.4	5	4	-2.1	-1.5
5	6	-2.1	-0.8	6	5	1.0	2.9

Meter Precisions

Measurement	Standard Deviation (σ)
Voltage Magnitude, *V*	3.83 KV
Real Power, *P*	5 MW
Reactive Power, *Q*	5 MVAR

To test the capability of the Differential Evolution algorithm solving the WLS State Estimation problem, two cases were analyzed. In the first case (Case 1A) the measurement data used was the same as the showed in Table 5.2. In Case 1B, instead of the measurements of real and reactive power injections at bus 5, phasor measurement units with standard deviation (σ) of 0.1 degrees were added in buses 5 and 6, as shown in Table 5.3.

TABLE 5.3
ANGLE MEASUREMENTS

Angle Measurements			
Bus	Degrees	Bus	Degrees
5	-5.3193	6	-6.1136

These angle measurements were obtained by adding random errors to the true angles magnitudes. The errors were selected from the set of numbers having a normal probability density function with zero mean and standard deviation specified for each measurement type, as shown as follows:

$$M_i = T_i + (\nu_i \times \sigma_i) \tag{5.22}$$

where:

M_i : i^{th} measured value

T_i : i^{th} true value

σ_i : standard deviation corresponding to the i^{th} measured value

ν_i : random number normally distributed with zero mean and standard deviation one

Table 5.4 shows the control parameters of the DE algorithm used in the proposed approach. These control parameters (scaling factor, crossover constant and population size) were determined via parameter tuning. All runs were limited to a maximum of 1000 iterations. The DE strategy used in all cases was DE/rand/1/bin. Table 5.5 presents a comparison of the solutions obtained by both cases and the Gradient Newton based method (GNSE) used in [59].

TABLE 5.4
CONTROL PARAMETERS OF THE DE ALGORITHM

Control Parameters	Case 1A	Case 1B
F	0.6	0.6
C_R	0.9	0.9
N_P	50	50

As shown in Table 5.5, the solutions obtained by both approaches are pretty similar to those obtained by the main classical approach. However, in order to demonstrate which solution is closest to the true values, the Mean Square Error (MSE) analysis was performed. The MSE is defined as follows [80]:

$$MSE = \frac{1}{N_m}\sum_{i=1}^{N_m}\left(E_i - T_i\right)^2 \tag{5.23}$$

where

E_i : i^{th} estimated value

T_i : i^{th} true value

N_m : number of measures

TABLE 5.5
COMPARISON OF ESTIMATED VALUES

Voltage and Power Injection Measurements

Bus	KV			MW			MVAR		
	GNSE	Case 1A	Case 1B	GNSE	Case 1A	Case 1B	GNSE	Case 1A	Case 1B
1	240.6	240.9	241.2	111.9	110.2	110.1	18.7	19.3	19.8
2	239.9	240.1	240.3	47.5	47.3	47.2	70.3	70.1	70.6
3	244.7	244.9	245.1	59.5	60.1	59.9	87.4	87.3	87.8
4	226.1	226.3	226.6	-70.2	-70.4	-70.6	-70.2	-70.0	-69.5
5	225.3	225.5	225.4	-71.8	-71.8	-	-69.4	-69.6	-
6	230.1	230.2	230.5	-68.9	-67.6	-67.8	-65.8	-66.5	-65.9

Power Flow Measurements

From Bus	To Bus	MW			MVAR		
		GNSE	Case 1A	Case 1B	GNSE	Case 1A	Case 1B
1	2	30.4	29.7	29.7	-14.4	-14.0	-14.0
1	4	44.8	44.3	44.4	21.2	21.4	21.3
1	5	36.8	36.2	36.0	11.8	12.0	12.5
2	3	3.0	2.5	2.5	-12.6	-12.5	-12.4
2	4	32.4	32.8	32.8	45.3	45.0	44.9
2	5	15.6	15.6	15.4	14.8	14.9	15.4
2	6	25.9	25.2	25.2	10.8	11.2	11.2
3	5	19.2	19.5	19.4	22.9	22.8	23.4
3	6	43.3	43.0	43.0	58.3	58.5	58.4
4	5	4.3	4.1	4.1	-5.1	-5.0	-4.6
5	6	1.3	0.9	1.1	-10.1	-9.9	-10.5
2	1	-29.4	-28.7	-28.8	11.9	11.5	11.5
4	1	-43.6	-43.2	-43.2	-20.7	-20.9	-20.9
5	1	-35.6	-35.1	-34.9	-13.6	-13.9	-14.5
3	2	-3.0	-2.4	-2.5	6.2	6.0	6.0
4	2	-30.9	-31.4	-31.4	-44.4	-44.1	-44.1
5	2	-15.1	-15.1	-14.9	-17.4	-17.5	-18.0
6	2	-25.4	-24.6	-24.7	-14.5	-14.9	-14.9
5	3	-18.1	-18.4	-18.2	-25.8	-25.6	-26.2
6	3	-42.3	-42.1	-42.1	-55.7	-55.9	-55.8
5	4	-4.2	-4.1	-4.0	-2.5	-2.7	-3.1
6	5	-1.2	-0.8	-1.1	4.4	4.2	4.8

Angle Measurements

Bus	Degrees		Bus	Degrees		
	GNSE	Case 1A	Case 1B		GNSE	Case 1A	Case 1B
5	-	-	-5.3212	6	-	-	-5.9588

The MSE provides an average error for all estimated values such that smaller values of MSE indicate a more accurate estimation procedure. Table 5.7 summarizes the results of the MSE analysis. The true values used in the MSE analysis are shown in Table 5.6.

TABLE 5.6
TRUE STATE VALUES

Voltages and Power Injections							
Bus	KV	MW	MVAR	Bus	KV	MW	MVAR
1	241.5	107.9	16	4	227.6	-70	-70
2	241.5	50	74.4	5	226.7	-70	-70
3	246.1	60	89.6	6	231	-70	-70
Power Flows							
From Bus	To Bus	MW	MVAR	From Bus	To Bus	MW	MVAR
1	2	28.7	-15.4	2	1	-27.8	12.8
1	4	43.6	20.1	4	1	-42.5	-19.9
1	5	35.6	11.3	5	1	-34.5	-13.5
2	3	2.9	-12.3	3	2	-2.9	5.7
2	4	33.1	46.1	4	2	-31.6	-45.1
2	5	15.5	15.4	5	2	-15	-18
2	6	26.2	12.4	6	2	-25.7	-16
3	5	19.1	23.2	5	3	-18	-26.1
3	6	43.8	60.7	6	3	-42.8	-57.9
4	5	4.1	-4.9	5	4	-4	-2.8
5	6	1.6	-9.7	6	5	-1.6	3.9
Angles							
Bus	Degrees			Bus	Degrees		
5	-5.276			6	-5.947		

TABLE 5.7
MEAN SQUARE ERROR ANALYSIS RESULTS

Measurements		GNSE	Case 1A	Case 1B
Voltages		1.7250	1.2621	0.9010
Angles		-	-	0.0011
Power Injections	Real	4.4983	3.6388	3.5436
	Reactive	7.8300	7.8822	9.7352
Power Flows	Real	0.6327	0.3996	0.3440
	Reactive	1.0109	1.0021	1.1233
All Values		1.9432	1.7345	1.6788

The MSE results demonstrate that the Differential Evolution state estimation approach (Case 1A) is more accurate than the traditional Gradient Newton state estimation procedure. When incorporating phasor measurement units in the state estimation formulation (Case 1B), this accuracy is improved even further, providing a better estimate of the system state than the obtained via the main classical approach.

5.4.2 Case 2: Modified IEEE 14-Bus Test System

The proposed approach was also applied to a modified IEEE 14-bus test system, shown in Figure 5.2. The system and measurement data used in the analysis are shown in Tables 5.8 and 5.9.

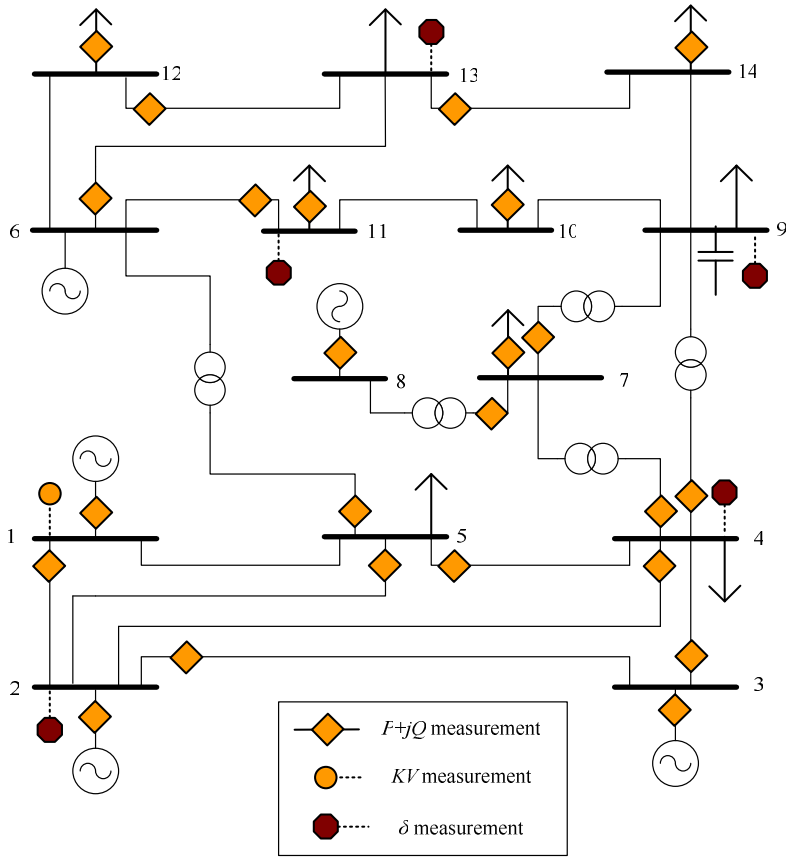

Figure 5.2: Modified IEEE 14-Bus Test System with Measurements Location

TABLE 5.8
SYSTEM DATA

Branch From	Branch To	R (pu)	X (pu)	B (pu)	Branch From	Branch To	R (pu)	X (pu)	B (pu)
1	2	0.0194	0.0592	0.0528	6	12	0.1229	0.2558	0.0000
1	5	0.0540	0.2230	0.0492	6	13	0.0662	0.1303	0.0000
2	3	0.0470	0.1980	0.0438	9	10	0.0318	0.0845	0.0000
2	4	0.0581	0.1763	0.0374	9	14	0.1271	0.2704	0.0000
2	5	0.0570	0.1739	0.0340	10	11	0.0821	0.1921	0.0000
3	4	0.0670	0.1710	0.0346	12	13	0.2209	0.1999	0.0000
4	5	0.0134	0.0421	0.0128	13	14	0.1709	0.3480	0.0000
6	11	0.0950	0.1989	0.0000					

Branch From	Branch To	R (pu)	X (pu)	Transformer Tap Ratio	Branch From	Branch To	R (pu)	X (pu)	Transformer Tap Ratio
4	7	0.0000	0.2091	0.978	7	8	0.0000	0.1762	1.000
4	9	0.0000	0.5562	0.969	7	9	0.0000	0.1100	1.000
5	6	0.0000	0.2520	0.932					

TABLE 5.9
MEASUREMENT DATA

Voltage and Power Injection Measurements

Bus	KV	MW	MVAR	Bus	KV	MW	MVAR
1	242.81	229.51	-18.90	10	-	-11.41	-4.57
2	-	19.44	32.87	11	-	-3.54	-0.78
3	-	-95.00	2.99	12	-	-6.41	1.78
7	-	2.58	-4.34	14	-	-14.39	-6.29
8	-	1.34	17.94				

Power Flow Measurements

From Bus	To Bus	MW	MVAR	From Bus	To Bus	MW	MVAR
1	2	157.60	-18.83	7	9	29.14	4.50
2	3	73.16	1.92	12	13	-1.32	-1.63
3	4	-23.96	-1.39	13	14	5.24	1.91
4	7	24.25	-10.07	4	2	-55.15	5.09
4	9	16.89	0.69	5	4	63.48	-17.38
5	6	46.01	13.20	11	6	-9.38	-6.46
6	13	17.87	5.52	5	2	-39.38	-1.50
7	8	1.35	-18.33				

Meter Precisions

Measurement	Standard Deviation (σ)
Voltage Magnitude, *V*	1 KV
Real Power, *P*	2 MW
Reactive Power, *Q*	2 MVAR

In order to analyze the improvement in the estimation process by means of the use of phasor measurement units, three cases were addressed. In the first case (Case 2A) the state estimation were conducted using the measurement data given in Table 5.9. In the second case (Case 2B) phasor measurement units with standard deviation (σ) of 0.1 degrees were installed in buses 2, 4, 9, 11 and 13. To maintain a comparable set of measurements, the following measures were eliminated for the state estimation process:

- Real power injection at bus 8.
- Reactive power injection at bus 3.
- Real power flow between buses 4 and 9.
- Reactive power flow between buses 7 and 9.

In the third case (Case 2C) the standard deviation of the phasor measurement units considered in the analysis was 5 degrees. The other information remains as in Case 2B. The angle measurements data for both cases are given in Table 5.10.

TABLE 5.10
ANGLE MEASUREMENTS

Angle Measurements (Degrees)					
Bus	Case 2B	Case 2C	Bus	Case 2B	Case 2C
2	-4.970	-4.412	11	-14.869	-18.259
4	-10.312	-10.022	13	-15.048	-8.904
9	-14.864	-11.364			

Table 5.11 shows the control variables used in the proposed approach. These control parameters (scaling factor, crossover constant and population size) were determined via parameter tuning. All runs were limited to a maximum of 4000 iterations. The DE strategy used in all cases was DE/rand/1/bin. Table 5.12 presents a comparison of the

solutions obtained by the traditional state estimation formulation with those in which phasor measurement units were considered.

TABLE 5.11
CONTROL PARAMETERS OF THE DE ALGORITHM

Control Parameters	Case 2A	Case 2B	Case 2C
F	0.6	0.6	0.6
C_R	0.9	0.9	0.9
N_P	80	80	80

TABLE 5.12
COMPARISON OF ESTIMATED VALUES

Voltage and Power Injection Measurements									
Bus	KV			MW			MVAR		
	Case 2A	Case 2B	Case 2C	Case 2A	Case 2B	Case 2C	Case 2A	Case 2B	Case 2C
1	242.61	243.46	242.99	230.76	230.52	230.71	-18.24	-18.21	-18.23
2	-	-	-	19.03	18.83	18.96	31.21	31.36	31.36
3	-	-	-	-94.93	-94.92	-94.88	2.09	-	-
7	-	-	-	3.12	3.34	3.45	-3.82	-3.73	-3.75
8	-	-	-	0.26	-	-	18.63	18.68	18.67
10	-	-	-	-11.70	-11.73	-11.72	-4.99	-4.99	-4.97
11	-	-	-	-4.55	-4.60	-4.62	-2.11	-2.04	-2.06
12	-	-	-	-7.30	-7.19	-7.29	0.18	0.12	0.17
14	-	-	-	-14.49	-14.20	-14.51	-5.76	-5.85	-5.73

Power Flow Measurements								
From Bus	To Bus	MW			MVAR		
		Case 2A	Case 2B	Case 2C	Case 2A	Case 2B	Case 2C
1	2	155.88	155.73	155.81	-21.37	-21.24	-21.25
2	3	73.43	73.28	73.30	4.62	5.31	5.30
3	4	-23.87	-23.98	-23.93	1.33	0.43	0.40
4	7	25.77	26.37	25.58	-8.29	-8.15	-8.27
4	9	15.45	-	-	-0.15	-0.04	-0.12
5	6	45.51	44.42	45.35	12.14	12.11	12.16
6	13	17.39	16.34	17.31	4.97	5.50	5.01
7	8	-0.26	0.59	0.48	-18.11	-18.16	-18.15
7	9	29.15	29.13	28.55	4.58	-	-
12	13	1.02	0.83	1.01	1.19	1.34	1.20
13	14	4.97	5.62	4.93	3.11	2.90	3.18
4	2	-54.50	-54.45	-54.51	4.01	4.06	4.15
5	4	63.97	64.07	63.98	-17.53	-17.52	-17.53
11	6	-7.55	-8.33	-7.49	-4.18	-3.95	-4.25
5	2	-40.10	-40.03	-40.12	-1.61	-1.55	-1.47

Angle Measurements							
Bus	Degrees			Bus	Degrees		
	Case 2A	Case 2B	Case 2C		Case 2A	Case 2B	Case 2C
2	-	-4.967	-4.989	11	-	-14.848	-14.937
4	-	-10.332	-10.384	13	-	-15.095	-15.365
9	-	-14.839	-14.788				

As shown in Table 5.12 similar results were obtained by the three approaches, however, as in previous case, the Mean Square Error analysis were conducted, in order to determine the closest solution to the real (true) state values. These true state values are given in Table 5.12. The results of the Mean Square Error analysis are shown in Table 5.13.

TABLE 5.12
TRUE STATE VALUES

Voltages and Power Injections							
Bus	KV	MW	MVAR	Bus	KV	MW	MVAR
1	243.8	232.39	-16.78	10	-	-9.00	-5.80
2	-	18.30	30.04	11	-	-3.50	-1.80
3	-	-94.20	4.60	12	-	-6.10	-1.60
7	-	0.00	0.00	14	-	-14.90	-5.00
8	-	0.00	18.06				
Power Flows							
From Bus	To Bus	MW	MVAR	From Bus	To Bus	MW	MVAR
1	2	156.84	-20.40	7	9	28.00	6.88
2	3	73.20	3.56	12	13	1.63	0.80
3	4	-23.32	3.01	13	14	5.70	1.99
4	7	28.00	-9.03	4	2	-54.44	3.19
4	9	16.03	0.04	5	4	61.59	-15.05
5	6	44.22	12.73	11	6	-7.36	-3.83
6	13	17.79	7.42	5	2	-40.63	-1.76
7	8	0.00	-17.58				
Angles							
Bus	Degrees			Bus	Degrees		
2	-4.981			11	-14.800		
4	-10.318			13	-15.174		
9	-14.935						

TABLE 5.13
MEAN SQUARE ERROR ANALYSIS RESULTS

Measurements		Case 2A	Case 2B	Case 2C
Voltages		1.4225	0.1175	0.6514
Angles		-	0.0037	0.0163
Power Injections	Real	2.6160	3.2291	3.2366
	Reactive	3.2484	2.8132	2.8360
Power Flows	Real	1.1110	1.1559	1.1663
	Reactive	1.7181	1.6934	1.8989
All Values		1.9722	1.7673	1.8445

The MSE results show that the inclusion of phasor measurements units in the state estimation procedure improves the accuracy of the solution obtained, even if the error variance of the equipments is poor (Case 2C).

5.4.3 Case 3: Modified IEEE 30-Bus Test System

In order to test and validate the proposed approach in larger systems, the modified IEEE 30-bus test system was used as test case system. The system and measurement data used in the analysis are shown in Tables 5.14 and 5.15, respectively. The measurements location is shown in Figure 5.3

TABLE 5.14
SYSTEM DATA

Branch		R (pu)	X (pu)	B (pu)	Branch		R (pu)	X (pu)	B (pu)
From	To				From	To			
1	2	0.0192	0.0575	0.0528	18	19	0.0639	0.1292	0.0000
1	3	0.0452	0.1852	0.0408	19	20	0.0340	0.0680	0.0000
2	4	0.0570	0.1737	0.0368	10	20	0.0936	0.2090	0.0000
3	4	0.0132	0.0379	0.0084	10	17	0.0324	0.0845	0.0000
2	5	0.0472	0.1983	0.0418	10	21	0.0348	0.0749	0.0000
2	6	0.0581	0.1763	0.0374	10	22	0.0727	0.1499	0.0000
4	6	0.0119	0.0414	0.0090	21	22	0.0116	0.0236	0.0000
5	7	0.0460	0.1160	0.0204	15	23	0.1000	0.2020	0.0000
6	7	0.0267	0.0820	0.0170	22	24	0.1150	0.1790	0.0000
6	8	0.0120	0.0420	0.0090	23	24	0.1320	0.2700	0.0000
9	11	0.0000	0.2080	0.0000	24	25	0.1885	0.3292	0.0000
9	10	0.0000	0.1100	0.0000	25	26	0.2544	0.3800	0.0000
12	13	0.0000	0.1400	0.0000	25	27	0.1093	0.2087	0.0000

12	14	0.1231	0.2559	0.0000	27	29	0.2198	0.4153	0.0000
12	15	0.0662	0.1304	0.0000	27	30	0.3202	0.6027	0.0000
12	16	0.0945	0.1987	0.0000	29	30	0.2399	0.4533	0.0000
14	15	0.2210	0.1997	0.0000	8	28	0.0636	0.2000	0.0428
16	17	0.0824	0.1923	0.0000	6	28	0.0169	0.0599	0.1300
15	18	0.1073	0.2185	0.0000					

Branch		R (pu)	X (pu)	Transformer Tap Ratio	Branch		R (pu)	X (pu)	Transformer Tap Ratio
From	To				From	To			
6	9	0.0000	0.2080	0.978	4	12	0.0000	0.2560	0.932
6	10	0.0000	0.5560	0.969	28	27	0.0000	0.3960	0.968

TABLE 5.15
MEASUREMENT DATA

Voltage and Power Injection Measurements

Bus	KV	MW	MVAR	Bus	KV	MW	MVAR
1	242.88	261.77	-16.86	15		-7.55	-1.92
2		18.48	37.16	16		-3.03	1.16
3		-3.67	-3.54	21		-19.87	-11.86
8		-28.86	1.95	23		-0.26	-0.60
10		-6.33	15.71	24		-8.59	0.58
13		1.97	8.13	26		-3.58	-3.99
14		-7.24	1.08				

Power Flow Measurements

From Bus	To Bus	MW	MVAR	From Bus	To Bus	MW	MVAR
1	2	177.07	-20.73	16	12	-4.51	-1.08
1	3	81.34	8.94	16	17	3.11	-3.39
2	5	82.18	1.02	18	19	6.29	2.77
6	2	-59.85	5.20	21	10	-16.96	-11.10
9	11	0.63	-19.40	23	24	4.12	4.27
12	13	-1.10	-10.97	24	22	-6.31	-0.71
12	14	8.36	3.33	24	23	-2.75	-2.64
12	16	6.02	5.64	25	26	4.62	4.82
14	12	-6.15	-0.89	27	25	2.96	0.26
14	15	5.84	-0.61	27	28	-15.57	-3.29
15	18	3.17	-0.83	28	6	-17.13	-6.02
15	23	4.71	0.85	30	29	-4.67	-2.60

Meters Precision

Measurement	Standard Deviation
Voltage Magnitude, *V*	1 KV
Real Power, *P*	2 MW
Reactive Power, *Q*	2 MVAR

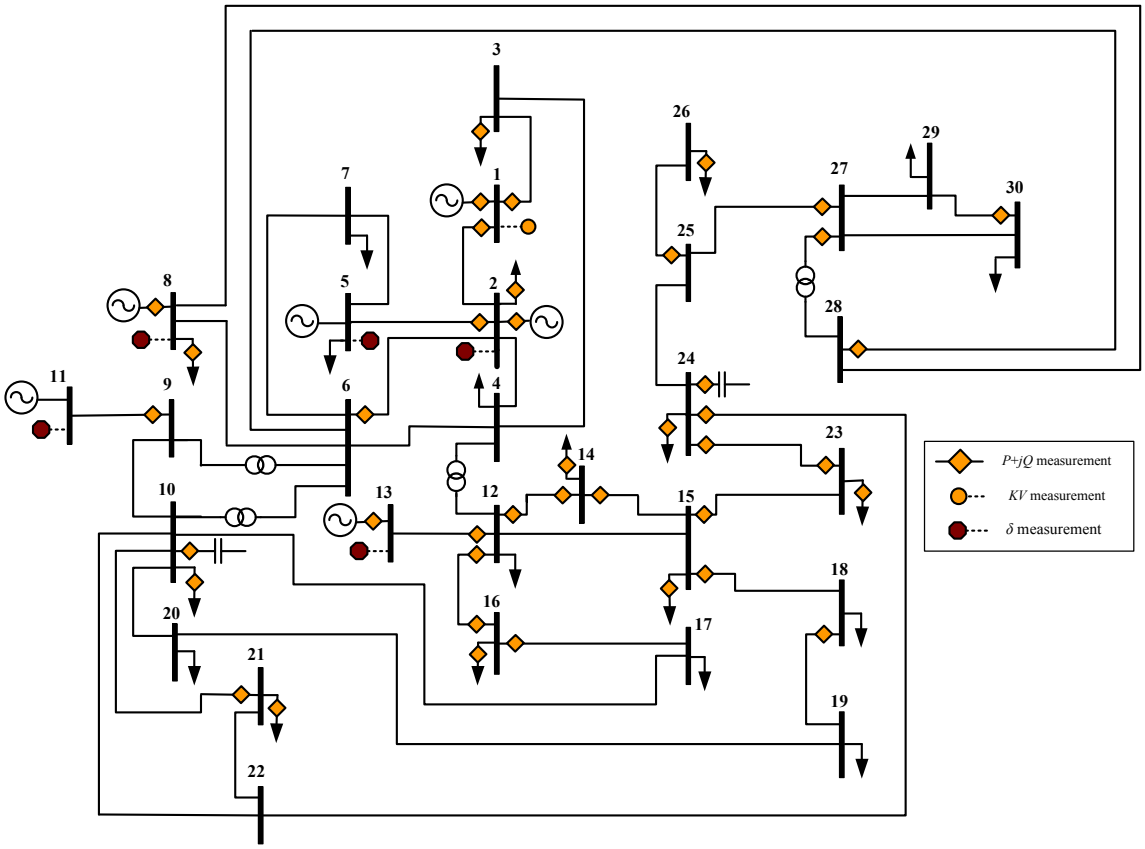

Figure 5.3: Modified IEEE 30-Bus Test System with Measurements Location

To demonstrate the ability of the proposed approach providing better estimates than the traditional state estimation routine, three cases were conducted. In the first case (Case 3A) the state estimation were conducted using the measurement data given in Table 5.14. In the second case (Case 3B) phasor measurement units with standard deviation (σ) of 0.1 degrees were installed in buses 2, 5, 8, 11 and 13. To maintain a comparable set of measurements, the following measures were eliminated for the state estimation process:

- Real and reactive power injection at bus 14.
- Real and reactive power flow between buses 2 and 5.
- Real and reactive power flow between buses 15 and 18.

In the third case (Case 3C) the standard deviation of the phasor measurement units considered in the analysis was 5 degrees. The other information remains as in Case 3.B. The angle measurements data for both cases are given in Table 5.16.

TABLE 5.16
ANGLE MEASUREMENTS

Angle Measurements (Degrees)					
Bus	Case 3B	Case 3C	Bus	Case 3B	Case 3C
2	-5.528	-7.086	11	-14.381	-11.594
5	-14.337	-12.239	13	-15.330	-17.180
8	-12.056	-9.225			

Table 5.17 shows the control variables used in the proposed approach. These control parameters (scaling factor, crossover constant and population size) were determined via parameter tuning. All runs were limited to a maximum of 4000 iterations. The DE strategy used in all cases was DE/rand/1/bin. Table 5.17 presents a comparison of the solutions obtained by the traditional state estimation formulation with those in which phasor measurement units were considered. The estimated values by using the three approaches proposed are shown in Table 5.18.

TABLE 5.17
CONTROL PARAMETERS OF THE DE ALGORITHM

Control Parameters	Case 3A	Case 3B	Case 3C
F	0.6	0.6	0.6
C_R	0.9	0.9	0.9
N_P	100	100	100

TABLE 5.18 A
COMPARISON OF ESTIMATED VALUES: VOLTAGES AND POWER MEASUREMENTS

Voltage and Power Injection Measurements

Bus	KV			MW			MVAR		
	Case 3A	Case 3B	Case 3C	Case 3A	Case 3B	Case 3C	Case 3A	Case 3B	Case 3C
1	244.95	244.63	244.38	260.36	261.70	261.16	-15.07	-15.41	-16.21
2	-	-	-	17.61	18.32	18.35	36.90	37.11	37.10
3	-	-	-	-3.53	-3.95	-3.58	-3.67	-3.67	-4.60
8	-	-	-	-29.50	-28.70	-29.35	1.86	2.37	2.58
10	-	-	-	-6.46	-6.43	-5.68	15.74	15.89	15.02
13	-	-	-	1.70	0.63	1.04	9.23	9.60	9.94
14	-	-	-	-5.86	-	-	-0.52	-	-
15	-	-	-	-8.40	-7.69	-8.36	-2.22	-1.77	-1.66
16	-	-	-	-2.75	-3.63	-2.84	-1.99	-2.11	-1.16
21	-	-	-	-19.48	-19.49	-20.61	-11.93	-11.32	-11.54
23	-	-	-	-1.19	-1.74	-1.06	0.24	0.47	0.24
24	-	-	-	-9.98	-9.14	-9.20	-0.42	0.12	-1.69
26	-	-	-	-4.02	-3.41	-2.79	-4.35	-4.22	-3.58

Power Flow Measurements

From Bus	To Bus	MW			MVAR		
		Case 3A	Case 3B	Case 3C	Case 3A	Case 3B	Case 3C
1	2	178.00	178.34	179.85	-22.37	-22.52	-22.74
1	3	82.36	83.36	81.31	7.30	7.11	6.53
2	5	82.38	-	-	0.92	-	-
6	2	-60.91	-60.04	-60.42	4.22	4.06	3.96
9	11	0.42	-0.18	0.88	-19.23	-19.52	-19.38
12	13	-1.70	-0.63	-1.04	-9.13	-9.48	-9.81
12	14	7.11	7.76	7.56	1.12	2.36	1.96
12	16	5.45	7.21	6.14	1.76	1.99	1.61
14	12	-7.06	-7.69	-7.50	-1.00	-2.21	-1.82
14	15	1.20	1.89	2.08	0.48	-0.08	0.80
15	18	4.66	-	-	-0.04	-	-
15	23	3.76	3.99	3.56	1.69	1.63	2.05
16	12	-5.42	-7.16	-6.10	-1.70	-1.90	-1.54
16	17	2.67	3.53	3.26	-0.29	-0.22	0.38
18	19	6.91	2.74	3.05	3.05	3.21	3.09
21	10	-16.93	-15.23	-14.16	-11.16	-11.49	-11.93
23	24	2.55	2.23	2.49	1.90	2.07	2.25
24	22	-5.60	-4.74	-6.36	-0.25	-0.69	-0.78
24	23	-2.54	-2.22	-2.48	-1.88	-2.05	-2.22
25	26	4.11	3.49	2.84	4.49	4.33	3.66
27	25	3.21	4.58	4.92	0.46	0.50	0.65
27	28	-16.09	-18.06	-17.72	-4.17	-3.88	-3.50
28	6	-17.10	-18.66	-18.65	-5.99	-6.37	-5.93
30	29	-4.67	-3.87	-2.27	-2.60	-2.35	-2.04

TABLE 5.18 B
COMPARISON OF ESTIMATED VALUES: ANGLE MEASUREMENTS

Angle Measurements							
Bus	Degrees			Bus	Degrees		
	Case 3A	Case 3B	Case 3C		Case 3A	Case 3B	Case 3C
2	-	-5.4785	-5.5375	11	-	-14.379	-14.580
5	-	-14.337	-14.863	13	-	-15.325	-15.016
8	-	-12.06	-12.185		-		

As in the earlier cases, in order to make a direct comparison between the estimated values resulting from the proposed approaches, the Mean Square Error Analysis was performed. The true state values used in the analysis are shown in Table 5.19.

TABLE 5.19
TRUE STATE VALUES

Voltages and Power Injections							
Bus	KV	MW	MVAR	Bus	KV	MW	MVAR
1	243.8	260.99	-17.12	15	-	-8.20	-2.50
2	-	18.30	35.85	16	-	-3.50	-1.80
3	-	-2.40	-1.20	21	-	-17.50	-11.20
8	-	-30.00	0.08	23	-	-3.20	-1.60
10	-	-5.80	17.00	24	-	-8.70	-2.40
13	-	0.00	10.11	26	-	-3.50	-2.30
14	-	-6.20	-1.60				
Power Flows							
From Bus	To Bus	MW	MVAR	From Bus	To Bus	MW	MVAR
1	2	177.77	-22.15	16	12	-7.13	-3.06
1	3	83.23	5.03	16	17	3.63	1.26
2	5	82.98	1.70	18	19	2.75	0.66
6	2	-59.87	3.37	21	10	-15.65	-9.69
9	11	0.00	-17.21	23	24	1.76	1.22
12	13	0.00	-9.98	24	22	-5.65	-2.86
12	14	7.84	2.41	24	23	-1.75	-1.21
12	16	7.18	3.17	25	26	3.54	2.37
14	12	-7.77	-2.25	27	25	4.88	0.76
14	15	1.57	0.65	27	28	-18.16	-4.09
15	18	5.99	1.63	28	6	-18.74	-3.51
15	23	4.99	2.89	30	29	-3.67	-0.54
Angles							
Bus	Degrees			Bus	Degrees		
2	-5.497			11	-14.438		
5	-14.380			13	-15.292		
8	-12.114						

The results of the MSE analysis are shown in Table 5.20

TABLE 5.20
MEAN SQUARE ERROR ANALYSIS RESULTS

Measurements		Case 3A	Case 3B	Case 3C
Voltages		1.3269	0.6947	0.3366
Angles			0.0019	0.0674
Power Injections	Real	1.2518	0.9975	1.5375
	Reactive	2.3284	2.6918	2.5765
Power Flows	Real	1.9921	0.1599	0.9727
	Reactive	2.3194	2.2210	1.8989
All Values		2.0179	1.3156	1.5300

It is clear from the results that the angle measurements could improve the performance of the Weighted Least Squares (WLS) estate estimation algorithm. However, these measurements can degrade the performance if they are not accurate enough. For the WLS algorithm, active/reactive injection and power flow measurements, with enough local redundancy, are the most important feature for obtaining a good estimate of the system states. The angle measurements should only complement (not replace) other measurements, while an exclusive use of voltage angle and magnitude measurements does result in a simplified formulation of the state estimation problem, the remaining non-phasor measurements are not any less important and must not be ignored.

5.4.4 Rate of Convergence of the Proposed Framework and Statistical Results

Table 5.21 provides the statistical results for 50 independent runs of the Differential Evolution algorithm. Figure 5.4 shows the rate of convergence for the modified IEEE 14-bus (Case 2) and 30-bus (Case 3) test systems. It is interesting to note that, due to the large number of state variables used in the optimization process in the Case 3, a large number of iterations were necessary for finding optimal solutions.

TABLE 5.21
STATISTICAL RESULT BASED ON 50 INDEPENDENT RUNS

	Case 1A	Case 1B	Case 2A	Case 2B	Case 2C	Case 3A	Case 3B	Case 3C
Average	40.7553	42.7965	19.4081	19.4478	20.3665	32.5242	19.9224	25.9960
Median	40.7553	42.7965	19.4081	19.4478	20.3665	32.1312	19.7528	26.1345
Mode	40.7553	42.7965	19.4081	19.4478	20.3665	31.9318	19.7865	26.1841
Standard Deviation	7.03E-14	1.05E-13	4.17E-05	1.25E-10	1.66E-04	2.5371	1.1920	3.0282
BSF	40.7553	42.7965	19.4081	19.4478	20.3664	29.2529	18.2123	21.5324
WSF	40.7553	42.7965	19.4083	19.4478	20.3671	41.8486	22.1575	33.6205

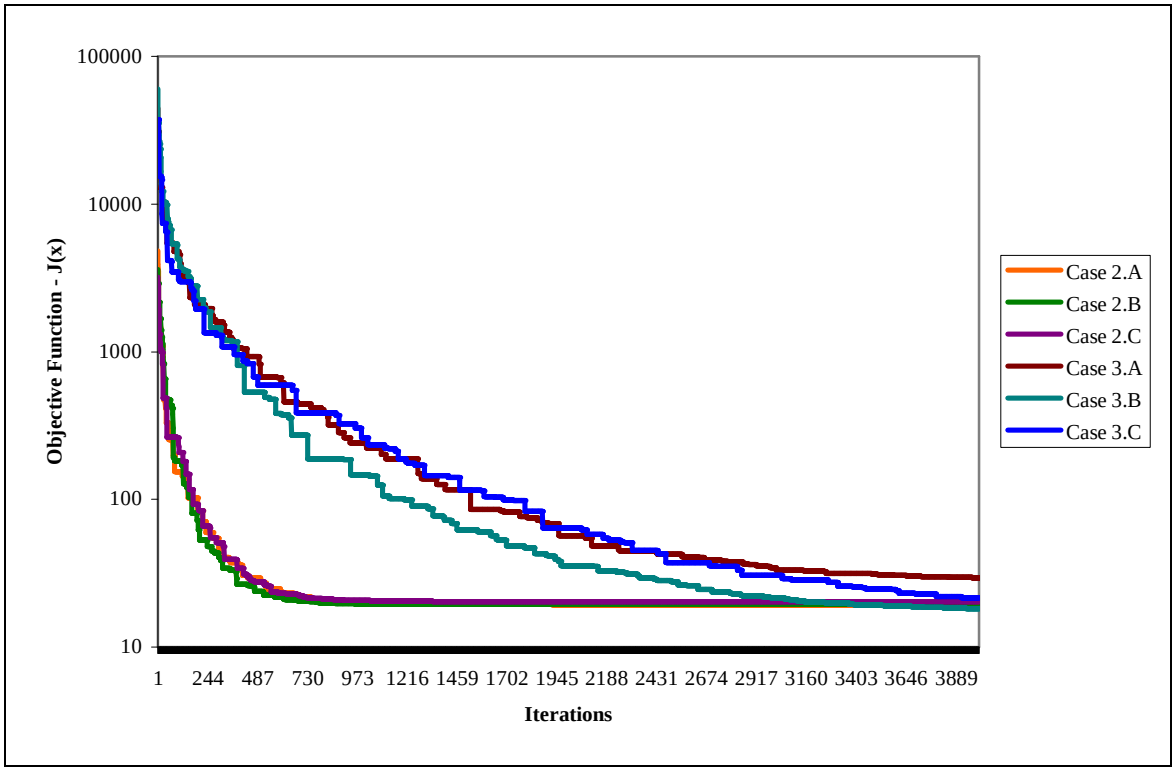

Figure 5.4: Rate of Convergence of the DE Algorithm for the Case Studies

5.5 CONSTRAINED WEIGHTED LEAST SQUARES (WLS) STATE ESTIMATION CASE STDUDIES AND RESULTS

The constrained WLS estimator is tested using the IEEE 14-bus and 30-bus test systems. In both cases, a set of equality and inequality constraints were considered.

5.5.1 Case 1: Modified IEEE 14-Bus Test System

To illustrate the effectiveness of the constrained WLS estimation, the IEEE 14-bus system is used as test case. The system data used in the analysis is the same as presented in the Section 5.4.2 (Table 5.8).

In this case, the IEEE 14-bus test system is partitioned into internal and external subsystems, as shown in Figure 5.5. The internal system, with highly redundant measurement set, is connected to the external subsystem, through the tie lines 5-6, 9-10 and 9-14. The external system contains only bus injections measurements which represent the forecasted (predicted) bus loads, and a few others voltage and power flow measurements.

For the case, the real and reactive power injections at buses 1, 2, 3, 4, 5, 7 and 8 were considered as equality constraints. The real and reactive power flows through the tie-lines was specified to be bounded within certain limits, and were modeled as inequality constraints.

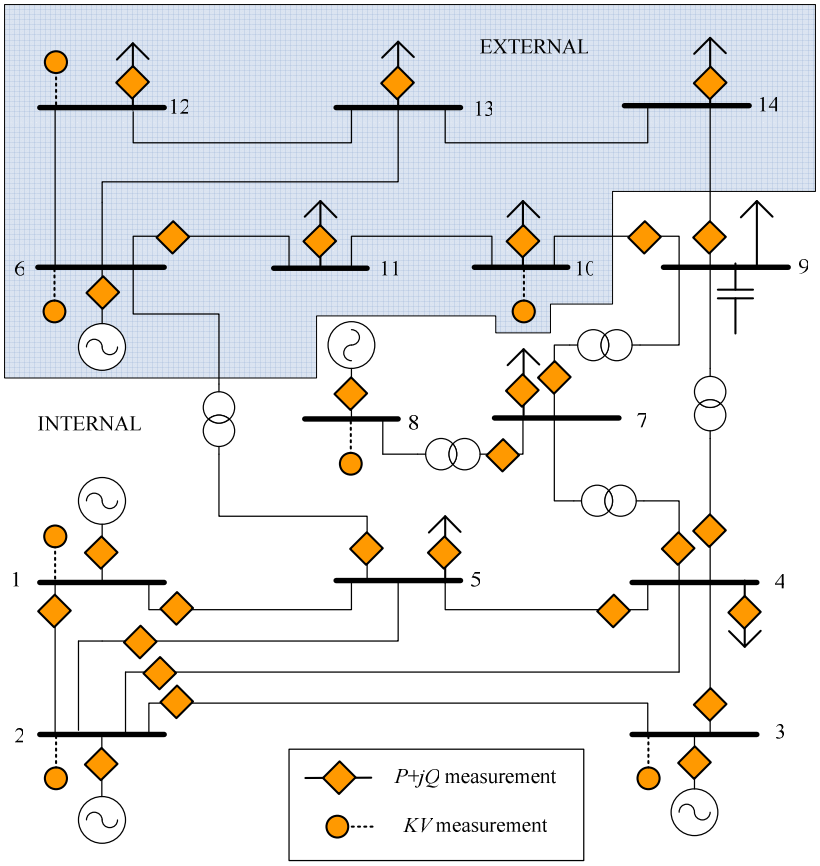

Figure 5.5: Modified IEEE 14-Bus Test System and Measurements Configuration

To test the capability of the constrained WLS estimator, two cases were developed. The first case is where the external injections do not contain any bad data. The measurement and constraints data used in the case is shown in Table 5.22.

The second case, the real and reactive power injection measurement at bus 14 is replaced by 4.7 MW and 13.9 MVAR, respectively and the other information remains as Case 1.

TABLE 5.22
MEASUREMENT AND CONSTRAINTS DATA

Voltage and Power Injection Measurements							
Bus	KV	MW	MVAR	Bus	KV	MW	MVAR
1	242.81	-	-	10	241.78	-11.41	-4.57
2	236.52	-	-	11	-	-3.54	-0.78
3	232.59	-	-	12	244.33	-6.41	1.78
6	248.84	-9.78	3.80	13	-	-16.71	-4.62
8	250.61	-	-	14	-	-14.39	-6.29

Power Flow Measurements							
From Bus	To Bus	MW	MVAR	From Bus	To Bus	MW	MVAR
1	2	157.60	-18.83	4	5	-58.89	17.31
1	5	73.53	4.75	4	7	24.25	-10.07
2	3	73.16	1.92	4	9	16.89	0.69
2	4	56.02	-2.61	6	11	8.88	3.99
2	5	41.53	-1.48	7	8	1.35	-18.33
3	4	-23.96	-1.39	7	9	29.14	4.50

Equality Constraints					
Bus	MW	MVAR	Bus	MW	MVAR
1	232.39	-16.78	5	-7.60	-1.60
2	18.30	30.04	7	0.00	0.00
3	-94.20	4.60	8	0.00	18.06
4	-47.80	3.90			

Inequality Constraints					
From Bus	To Bus	P_{min} MW	Q_{min} MVAR	P_{max} MW	Q_{max} MVAR
5	6	30.0	10.0	82.0	30.0
9	10	5.0	2.0	30.0	12.0
9	14	9.0	3.0	30.0	15.0

Measurement Precisions	
Measurement	Standard Deviation (σ)
Voltage Magnitude, *V*	1 KV
Real Power, *P*	2 MW
Reactive Power, *Q*	2 MVAR

Table 5.23 shows the control parameters (scaling factor, crossover constant and population size) used in the proposed approach. All runs were limited to a maximum of 6500 iterations. The DE strategy used in all cases was DE/rand/1/bin. Table 5.24 presents a comparison of the solutions obtained by both cases.

TABLE 5.23
CONTROL PARAMETERS OF THE DE ALGORITHM

Control Parameters	Case 1A	Case 1B
F	0.6	0.6
C_R	0.9	0.9
N_P	80	80

TABLE 5.24
COMPARISON OF ESTIMATED VALUES

Voltage and Power Injection Measurements						
Bus	KV		MW		MVAR	
	Case 1A	Case 1B	Case 1A	Case 1B	Case 1A	Case 1B
1	243.4	243.8	-	-	-	-
2	239.9	240.3	-	-	-	-
3	231.9	232.3	-	-	-	-
6	245.6	245.2	-10.36	-11.23	3.01	2.46
8	250.4	251.2	-	-	-	-
10	241.1	241.9	-11.53	-11.62	-4.55	-4.80
11	-	-	-3.56	-4.27	-1.29	-1.58
12	242.9	241.8	-6.80	-6.30	1.45	-0.74
13	-	-	-17.17	-18.58	-4.97	-7.50
14	-	-	-14.60	-11.31	-6.42	-3.32
Power Flow Measurements						
From Bus	To Bus	MW		MVAR		
		Case 1A	Case 1B	Case 1A	Case 1B	
1	2	156.76	156.78	-20.41	-20.51	
1	5	75.63	75.60	3.63	3.73	
2	3	73.12	73.14	3.56	3.47	
2	4	55.97	56.00	-2.15	-2.28	
2	5	41.66	41.64	0.89	1.07	
3	4	-23.40	-23.39	2.98	2.93	
4	5	-59.91	-60.05	15.50	16.77	
4	7	27.11	27.22	-9.21	-10.11	
4	9	15.52	15.59	-0.08	-0.60	
6	11	6.63	6.54	6.63	6.54	
7	8	0.00	0.00	-17.57	-17.57	
7	9	27.12	27.23	6.77	5.82	

In the first case, in absence of any bad data, all flows in the tie lines remain within their feasible bounds and therefore, there are no active constraints at the solution point. In the second case, the algorithm enforces the estimation of the real and reactive power flow on line 9-14 to its feasible (lower) bound, as shown in Table 5.25. Hence, the estimator could reject this bad data to obtain a very good solution for both, the internal and external subsystems.

TABLE 5.25
ESTIMATED TIE LINE FLOWS WITH BAD DATA AT BUS 14

From bus	To bus	P_{ij} (MW)	Q_{ij} (MVAR)
5	6	45.41	14.44
9	11	9.44	3.90
9	14	9.00	3.00

As in the earlier cases, in order to make a direct comparison between the estimated values resulting from the proposed approaches, the Mean Square Error Analysis was performed. The true state values used in the MSE analysis are shown in Table 5.26.

The results of the Mean Square Error analysis, given in Table 5.27, reveal that the constrained WLS estimator, even in the presence of bad data in the external subsystem, could perform a reliable estimation of the real state of the system. This feature makes the constrained estimator an attractive alternative for today's Energy Management System (EMS).

TABLE 5.26
TRUE STATE VALUES

Voltage and Power Injections							
Bus	KV	MW	MVAR	Bus	KV	MW	MVAR
1	243.80	-	-	10	241.37	-9.00	-5.80
2	240.35	-	-	11	-	-3.50	-1.80
3	232.30	-	-	12	242.66	-6.10	-1.60
6	246.10	-11.20	5.64	13	-	-13.50	-5.80
8	250.70	-	-	14	-	-14.90	-5.00
Power Flows							
From Bus	To Bus	MW	MVAR	From Bus	To Bus	MW	MVAR
1	2	156.84	-20.40	4	5	-61.08	15.33
1	5	75.55	3.61	4	7	28.00	-9.03
2	3	73.20	3.56	4	9	16.03	0.04
2	4	56.12	-2.08	6	11	7.42	3.95
2	5	41.53	0.89	7	8	0.00	-17.58
3	4	-23.32	3.01	7	9	28.00	6.88

TABLE 5.27
MEAN SQUARE ERROR ANALYSIS RESULTS

Measurements		Case 1A	Case 1B
Voltages		0.1419	0.3012
Power Injections	Real	3.5292	6.6612
	Reactive	3.4671	2.9655
Power Flows	Real	0.3238	0.2743
	Reactive	0.6068	0.9619
All Values		1.2590	1.5872

5.5.2 Case 2: Modified IEEE 30-Bus Test System

The proposed approach was also applied to the modified IEEE 30-bus system. The system data used in the analysis is the same as presented in the Section 5.4.3 (Table 5.14).

As the previous case, the IEEE 30-bus test system is partitioned into internal and external subsystems, as shown in Figure 5.6. The internal system, with highly redundant measurement set, is connected to the external subsystem, through the tie lines 22-24, 23-24, 8-28 and 6-28.

For the case, the real and reactive power injections at buses 1, 2, 8, 10 and 11 were considered as equality constraints. The real and reactive power flows through the tie-lines, which are bounded within certain limits, were modeled as inequality constraints.

To demonstrate the capability of the constrained WLS estimator improving the reliability of the estimation, even in the presence of bad measurements in the external subsystem, two cases were analyzed. The first case (Case 2A) is where the external injections do not contain any bad data. The measurement data used in the case is shown in Table 5.28. The constraints and meter precision data is given in Table 5.29.

In the second case, the real and reactive power injection measurement at bus 24 is replaced by -30.14 MW and 5.7 MVAR, respectively and the other information remains as Case 2A.

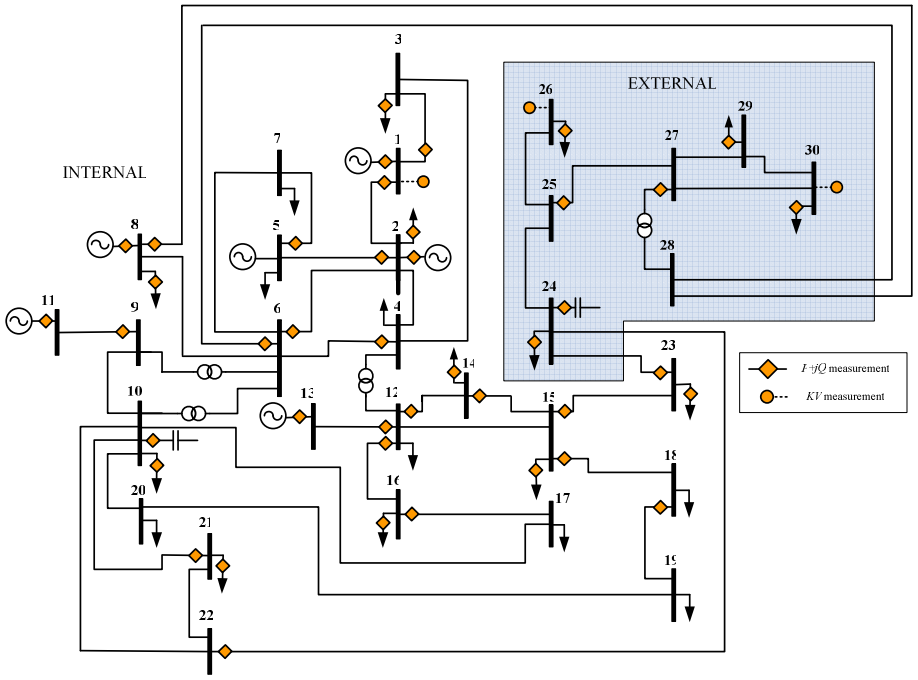

Figure 5.6: Modified IEEE 30-Bus Test System and Measurements Configuration

TABLE 5.28
MEASUREMENT DATA

Voltage and Power Injection Measurements							
Bus	KV	MW	MVAR	Bus	KV	MW	MVAR
1	242.88			15		-7.55	-1.92
2				16		-3.03	1.16
3		-3.67	-3.54	21		-19.87	-11.86
8				23		-0.26	-0.60
10				24		-8.59	0.58
11				26	228.97	-3.58	-3.99
13		1.97	8.13	29		-2.92	-2.61
14		-7.24	1.08	30	228.75	-8.69	-4.30
Power Flow Measurements							
From Bus	To Bus	MW	MVAR	From Bus	To Bus	MW	MVAR
1	2	177.07	-20.73	14	15	5.84	-0.61
1	3	81.34	8.94	16	17	3.11	-3.39
2	5	82.18	1.02	15	18	3.17	-0.83
4	6	69.96	-18.08	18	19	6.29	2.77
5	7	-12.09	12.75	15	23	4.71	0.85
9	11	0.63	-19.40	25	27	-6.28	-2.10
12	13	-1.10	-10.97	6	2	-59.85	5.20
12	14	8.36	3.33	21	10	-16.96	-11.10
12	16	6.02	5.64	27	28	-15.57	-3.29

TABLE 5.29
CONSTRAINTS AND METERS PRECISION DATA

Equality Constraints					
Bus	MW	MVAR	Bus	MW	MVAR
1	260.99	-17.12	10	-5.80	17.00
2	18.30	35.85	11	0.00	17.76
8	-30.00	0.08			

Inequality Constraints					
From Bus	To Bus	P_{min} MW	Q_{min} MVAR	P_{max} MW	Q_{max} MVAR
22	24	3.0	1.0	12.0	6.0
23	24	1.0	0.0	4.0	3.0
8	28	-1.0	-5.0	1.0	-1.0
6	28	9.0	-20.0	40.0	-5.0

Meters Precision	
Measurement	Standard Deviation
Voltage Magnitude, V	1 KV
Real Power, P	2 MW
Reactive Power, Q	2 MVAR

Table 5.30 shows the control parameters (scaling factor, crossover constant and population size) used in the proposed approach. All runs were limited to a maximum of 7000 iterations. The DE strategy used in all cases was DE/rand/1/bin. Table 5.31 presents a comparison of the estimated values by both cases.

TABLE 5.30
CONTROL PARAMETERS OF THE DE ALGORITHM

Control Parameters	Case 2A	Case 2B
F	0.6	0.6
C_R	0.9	0.9
N_P	100	100

TABLE 5.31
COMPARISON OF ESTIMATED VALUES

Voltage and Power Injection Measurements

Bus	KV		MW		MVAR	
	Case 2A	Case 2B	Case 2A	Case 2B	Case 2A	Case 2B
1	243.37	242.99	-	-	-	-
2	-	-	-	-	-	-
3	-	-	-4.22	-3.79	-3.46	-4.13
8	-	-	-	-	-	-
10	-	-	-	-	-	-
11	-	-	-	-	-	-
13	-	-	1.87	1.56	9.40	9.37
14	-	-	-6.27	-5.90	-0.28	-0.97
15	-	-	-8.88	-8.49	-2.74	-2.43
16	-	-	-3.21	-2.92	-1.98	-2.18
21	-	-	-20.25	-19.01	-12.08	-11.91
23	-	-	-1.46	-1.43	-0.56	-0.83
24	-	-	-9.18	-26.51	-0.15	0.27
26	228.96	229.91	-3.49	-4.12	-3.65	-4.15
29	-	-	-3.33	-3.46	-2.97	-3.32
30	227.88	228.91	-9.23	-9.79	-3.74	-3.51

Power Flow Measurements

From Bus	To Bus	MW		MVAR	
		Case 2A	Case 2B	Case 2A	Case 2B
1	2	177.20	177.25	-22.00	-22.09
1	3	83.17	83.18	5.80	5.80
2	5	81.95	82.28	0.76	1.55
4	6	70.43	70.97	-18.58	-18.20
5	7	-11.95	-12.24	12.57	13.13
9	11	0.16	0.38	-17.82	-18.09
12	13	-1.87	-1.56	-9.29	-9.25
12	14	7.50	7.49	0.96	1.47
12	16	6.32	5.82	2.24	1.73
14	15	1.17	1.52	0.55	0.37
16	17	3.07	2.86	0.18	-0.52
15	18	3.90	4.62	-0.35	-0.31
18	19	5.97	5.99	2.56	2.68
15	23	4.62	5.44	1.32	2.29
25	27	-6.92	-4.62	-2.15	-2.31
6	2	-59.82	-60.02	3.28	3.38
21	10	-17.27	-17.77	-10.84	-10.78
27	28	-15.52	-14.12	-3.10	-2.55

As in the previous cases, in absence of any bad data in the external subsystem, the real and reactive power flows through the tie-lines remain within their specified limits. In the second case, the algorithm enforces the estimation of the real and reactive power flow on lines 22-24, 23-24 and 8-28 to their feasible bounds, obtaining very good estimates for both, the internal and external subsystems, except for the estimated value of the real power injection at bus 24.

TABLE 5.32
ESTIMATED TIE LINE FLOWS WITH BAD DATA AT BUS 24

From bus	To bus	P_{ij} (MW)	Q_{ij} (MVAR)
22	24	12.0	1.9
23	24	4.0	1.4
8	28	-1.0	-4.7
6	28	17.5	-19.2

Table 5.33 summarizes the results of the MSE analysis. The true values used in the MSE analysis are shown in Table 5.34. It is evident that the results obtained for the original case (without bad data placed in the external subsystem) are pretty much accurate than the obtained in the case containing bad data in the estimation. However, both results demonstrate that the operational constraints, when incorporated to the WLS state estimation, could enhance the reliability of the estimation process, by obtaining very good estimates, even in the presence of bad data in parts of the system.

TABLE 5.33
MEAN SQUARE ERROR ANALYSIS RESULTS

Measurements		Case 2A	Case 2B
Voltages		1.1203	0.3136
Power Injections	Real	1.9042	1.2448
	Reactive	2.1686	2.7065
Power Flows	Real	2.2324	2.4313
	Reactive	1.4747	1.6879
All Values		1.8835	1.9551

TABLE 5.34
TRUE STATE VALUES

Voltage and Power Injections							
Bus	KV	MW	MVAR	Bus	KV	MW	MVAR
1	243.80	-	-	15	-	-8.20	-2.50
2	-	-	-	16	-	-3.50	-1.80
3	-	-2.40	-1.20	21	-	-17.50	-11.20
8	-	-	-	23	-	-3.20	-1.60
10	-	-	-	24	-	-8.70	-2.40
11	-	-	-	26	230.45	-3.50	-2.30
13	-	0.00	10.11	29	-	-2.40	-0.90
14	-	-6.20	-1.60	30	228.86	-10.60	-1.90
Power Flows							
From Bus	To Bus	MW	MVAR	From Bus	To Bus	MW	MVAR
1	2	177.77	-22.15	14	15	1.57	0.65
1	3	83.23	5.03	16	17	3.63	1.26
2	5	82.98	1.70	15	18	5.99	1.63
4	6	70.19	-17.66	18	19	2.75	0.66
5	7	-14.22	10.37	15	23	4.99	2.89
9	11	0.00	-17.21	25	27	-4.85	-0.71
12	13	0.00	-9.98	6	2	-59.87	3.37
12	14	7.84	2.41	21	10	-15.65	-9.69
12	16	7.18	3.17	27	28	-18.16	-4.09

5.5.3 Rate of Convergence of the Proposed Approach and Statistical Results.

Table 5.35 provides the statistical results for the case studies based on 50 independent runs of the DE algorithm. Is interesting to note that, in the Case 1, the best solution was found with consistency and very low data dispersion was obtained. In the Case 2, due to

the large number of state variables involved in the optimization process, the data dispersion increases and the successful rate of the algorithm decreases considerably.

Figure 5.7 shows the rate of convergence of the DE algorithm for the best solution found in all case studies. As in the previous approach, a large number of iterations were necessary to achieve optimal solutions.

TABLE 5.35
STATISTICAL RESULT BASED ON 50 INDEPENDENT RUNS

	Case 1A	Case 1B	Case 2A	Case 2B
Average	24.8240	168.4475	28.4196	33.9140
Median	24.5910	168.4369	28.1486	33.8648
Mode	24.4324	168.4351	28.1486	34.5895
Standard Deviation	0.5969	0.0301	2.4558	1.9596
BSF	24.2684	168.4323	25.6037	31.3687
WSF	25.9541	168.5445	33.3386	37.5615

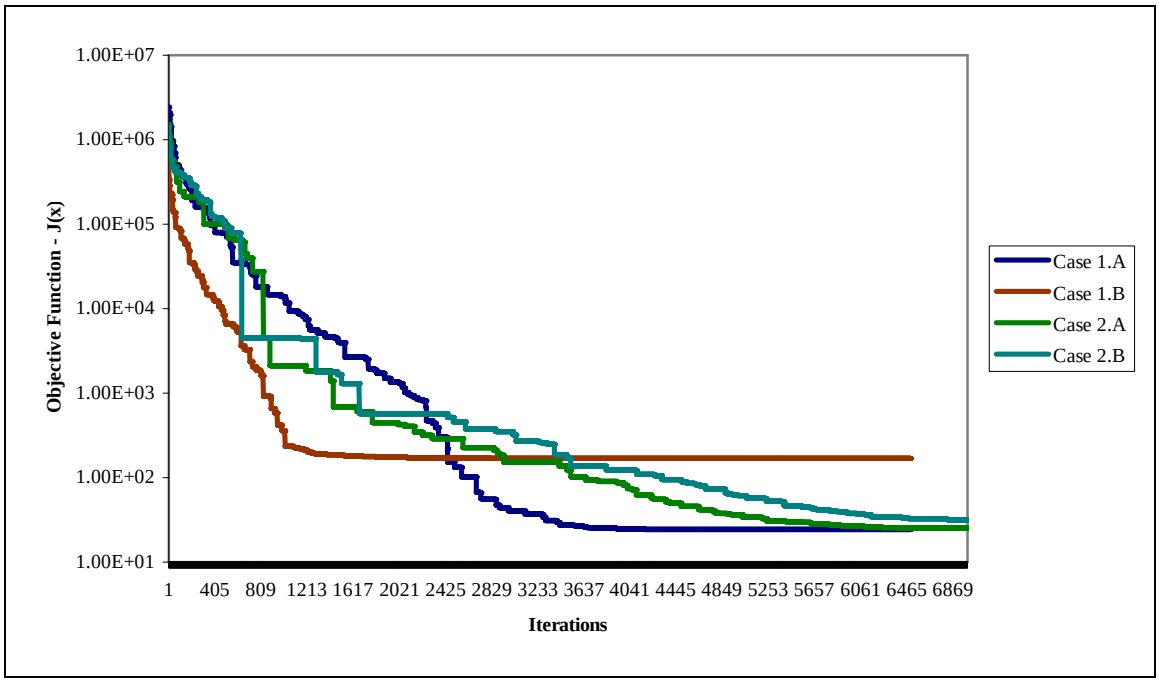

Figure 5.7: Rate of Convergence of the DE Algorithm for the Case Studies

5.6 CONCLUSIONS

State estimators provide a platform for selective monitoring and real-time control of electric power systems. By collecting analog measurements and the status data of the circuit breakers from remotely monitored and controlled substations, state estimators can provide an estimate for all metered and un-metered electrical quantities and network parameters of the power system, detect and filter out gross errors in the measurement set and detect the topology errors in the network configuration.

There are several topics in state estimation being studied to improve the accuracy and reliability of the state estimators in power systems. The integration of the new technology of phasor measurement units (PMUs), the incorporation of operational constraints to the traditional state estimation formulation, and the way that these features could be used to improve the estimation of the real state of the system in the new emerging electricity markets, have been analyzed in this thesis work.

The results obtained in this research work show that the angle measurements could effectively enhance the performance of the WLS state estimation algorithm. However, these measurements could degrade the performance of the estimator if they are not accurate enough. Since modern satellite clock synchronization technology is expected to provide phasor metering accuracy better than 0.l°, the incorporation of PMUs in the state estimators would have a real impact in the improvement of the confidence level obtained by means of the estimation process.

On the other hand, the operational constraints could be utilized effectively in enhancing the reliability of the state estimators. The results obtained through the case studies demonstrated that the constrained WLS estimator, even in the presence of bad data in parts of the system, could perform a reliable estimation of the real state of the system. This feature makes the constrained estimator an attractive alternative for today's Energy Management System (EMS).

CHAPTER 6

INTELLIGENT POWER ROUTERS BASED CONTROLLED ISLANDING SCHEME

6.1 INTRODUCTION

As modern society has become increasingly dependent on electricity, not only it is important to prevent power system disturbances, but it is also imperative to limit the extent and duration of such events. Power system disturbances can occur due to numerous reasons, most of which fall into one of the following categories: weather (e.g., lightning, ice storms, wind storms, hurricanes, tornadoes), protection system failures and misoperations, equipment failures, solar magnetic storms, personnel error, fires, excessive customer demand, insufficient generation, and sabotage.

Whenever one of the previously mentioned initiating events occur, power system components may be left operating beyond their permissible feasible limits, and may be switched out of service by automatic protection devices. Under certain conditions, this initial event may be followed by a series of further automatic actions that switch other power system components out of service. If this process of cascading failures continues, the entire system or large parts of it may completely collapse, resulting in what is commonly known as a power system blackout.

For this reason, emergency control actions must be taken in order to minimize (or mitigate) the effects of these disturbances over the system. Examples of these control actions could be: line tripping, capacitor switching, load shedding, controlled islanding and other special protection schemes.

Traditionally, power systems have been operated and controlled in a centralized way, with a considerable amount of human intervention. Under such circumstances, cascading outages may result extremely difficult to prevent or control. It is therefore necessary to design new mechanisms that can react promptly and automatically to unpredicted (and potentially catastrophic) system disturbances.

Researchers of the University of Puerto Rico at Mayagüez have proposed a distributed and "intelligent" control scheme, the so-called Intelligent Power Routers (IPRs), aimed at minimizing the potential damaging effects that a major disturbance may cause on a power system. One of the potential applications of these intelligent controls is to support a controlled islanding scheme to prevent cascade failures in power systems.

The main objective of the controlled islanding scheme (also known as "system splitting") is to properly separate the system into several subsystems ("islands") of reduced capacity to avoid passive collapse or blackout over the entire system [81]-[86]. The basis for forming the islands is to minimize the load–generation imbalance in each island, thereby facilitating the restoration process.

Because power system emergencies may strike the system within minute or even seconds, it is necessary to guarantee both speediness and correctness in determining the splitting strategy to avoid more serious and catastrophic faults in time. To solve the controlled islanding problem in real-time, at least two challenges must be faced [84]. First, the islanding strategy needs to correspond to an acceptable steady state operating point after splitting, such that the system can avoid collapse. Second, it has to be assured that the system can securely reach that steady state operating point. It is therefore necessary to bring each of the islands individually to stable condition after system

separation. In order to guarantee this condition, the following constraints must be satisfied:

1. Asynchronous groups of generators must be separated into different islands and generators in each island must be synchronous.
2. In each island, power must be balanced.
3. Transmission lines and other transmission services must not be loaded above their transmission capacity limits.

The main objective of this chapter is to develop an intelligent and adaptive controlled islanding scheme, based on the IPRs. The proposed scheme was tested and validated through dynamic simulations on the New England 39 bus – 10 generators and the WSCC 179 bus – 29 generators test systems.

This chapter is organized as follows: First of all, we introduce the coherency recognition algorithm and its implementation for finding coherent groups of generators. After that we present the mathematical formulation of the system splitting problem and its implementation using the Differential Evolution algorithm. A brief discussion of the conventional as well as other special protection schemes and their interaction with the IPRs is introduced afterward. Finally, several case studies on the New England and the WSCC test systems are analyzed.

6.2 SLOW COHERENCY GENERATORS GROUPING

The coherency recognition technique is based on the fact that, after the occurrence of a disturbance, some generators have the tendency to swing together. Several methods of coherency recognition were developed by researchers [87]-[90]. However, two approaches are the most commonly used:

- Dynamic simulations
- Slow coherency

The slow coherency method for determining coherent groups of generators is an application of the singular perturbation method in power systems. This method requires the calculation of the slow eigenbasis matrix of the electromechanical modes of the power system [87].

Two assumptions simplify considerably the process of determining coherent groups of generators [81]:

1. The coherency identification is independent of the size of the disturbance; therefore the linearized model of the power system could be used in this process.
2. The coherent groups of generators are independent of the level of detail used in modeling the generators units, which implies that the classical generator model could be used in this approach.

The first assumption is based on the observation that the coherency behavior of a generator is not significantly changed as the clearing time of a specific fault is increased. Although the amount of detail of the generator model can affect the simulated swing curve, it does not radically change the basic network characteristics such as inter-area modes. This forms the basis of the second assumption.

6.2.1 Coherency Grouping Algorithm

As mentioned in previous section, it has been observed that, in multi-machine transient after a disturbance, some generators have the tendency to “swing together”. A coherency grouping approach requires the machine states to be coherent with respect to a selected modes φ of the system. This approach allows coherency to be examined in terms

of the row of an eigenvector matrix **U** which can be used to find coherent groups of states.

Most grouping criteria result in coherent states that are disturbance-dependent because they simultaneously treat the following two tasks [91]:

- Select the modes which are excited by a given disturbance o set of disturbances.
- Find the states with the same degree of disturbed modes.

The slow coherency based approach, thus, implies the calculation of the coherent states for a given set of the *r* slowest modes. Since the classical swing equation model generally preserves the frequencies and mode shapes sufficiently well for coherency studies, it was appropriate for used in this work [87]-[88], [91].

For a multi-machine power system, the classical model is defined as follows [92]-[93]:

$$\frac{d\delta_i}{dt} = \omega_i - \omega_0 \tag{6.1}$$

$$\frac{2H_i}{\omega_0}\frac{d^2\delta_i}{dt^2} = P_{m_i} - P_{e_i} - D_i\left(\omega_i - \omega_0\right) \tag{6.2}$$

Where

δ_i : rotor angle of the i^{th} machine in radians

ω_i : angular velocity of the i^{th} machine in radians/sec

ω_0 : reference speed in radians/sec ($\omega_0 = 377$ rad/sec)

H : inertia constant in MW.s/MVA

P_{m_i} : mechanical power input of the i^{th} machine, in p.u.

P_{e_i} : electric power output of the i^{th} machine, in p.u.

D_i : damping factor of the i^{th} machine proportional to the speed deviation, in p.u./rad/sec.

In the classical model, the mechanical power input P_{m_i} is assumed to be constant. The electrical power output is determined as follows

$$P_{e_i} = V_i^2 G_{ii} + \sum_{\substack{j=1 \\ j \neq i}}^{N_B} V_i V_j \left(G_{ij} \cos \delta_{ij} + B_{ij} \sin \delta_{ij} \right) \tag{6.3}$$

Where:

V_i : constant voltage behind the direct axis transient reactance in p.u.

G_{ij}, B_{ij} : ij^{th} real and imaginary entries of the Y_{BUS} matrix

δ_i : $\delta_i - \delta_j$

Linearizing equations (6.1) and (6.2) about the equilibrium operating point, we obtain:

$$\frac{d\left(\Delta \delta_i\right)}{dt} = \Delta \omega_i \tag{6.4}$$

$$\frac{d\left(\Delta \omega_i\right)}{dt} = \frac{\omega_0}{2H_i} \left(\Delta P_{m_i} - \Delta P_{e_i} - k_D \left(\Delta \omega_i \right) \right) \tag{6.5}$$

The linearized value of the electric power output ΔP_{e_i} is calculates as follows

$$\Delta P_{e_i} = V_i V_j \left(B_{ij} \cos \delta_{ij0} - G_{ij} \sin \delta_{ij0} \right) \times \Delta \delta_{ij} \tag{6.6}$$

The linearized equation of the electric power output for a given machine is also known as synchronized power coefficient (k_{Si}).

Thus, the second order dynamic model for a given machine can be obtained as follows:

$$\frac{d}{dt}\begin{bmatrix}\Delta\delta_i\\ \Delta\omega_i\end{bmatrix}=\begin{bmatrix}0 & 1\\ \left(\frac{-k_{Si}\omega_0}{2H_i}\right) & \left(\frac{-k_{Di}\omega_0}{2H_i}\right)\end{bmatrix}\begin{bmatrix}\Delta\delta_i\\ \Delta\omega_i\end{bmatrix}+\begin{bmatrix}0\\ \left(\frac{\omega_0}{2H_i}\right)\end{bmatrix}\Delta P_{m_i} \tag{6.7}$$

Neglecting the damping constant which not significantly changes the mode shape and rewriting the previous equation in matrix form, we obtain:

$$\begin{bmatrix}\dot{\mathbf{x}}_1\\ \dot{\mathbf{x}}_2\end{bmatrix}=\begin{bmatrix}0 & \mathbf{I}\\ \mathbf{N} & 0\end{bmatrix}\begin{bmatrix}\mathbf{x}_1\\ \mathbf{x}_2\end{bmatrix}+\mathbf{B}\times\Delta\mathbf{u} \tag{6.8}$$

Where **I** is the identity matrix and the matrix **N** is calculated as follows:

$$\mathbf{N}=\begin{bmatrix}\frac{\omega_0}{2H_1} & 0 & \cdots & 0\\ 0 & \frac{\omega_0}{2H_2} & \cdots & 0\\ \vdots & \vdots & \ddots & \vdots\\ 0 & 0 & \cdots & \frac{\omega_0}{2H_n}\end{bmatrix}\begin{bmatrix}k_{S_{11}} & k_{S_{12}} & \cdots & k_{S_{1n}}\\ k_{S_{21}} & k_{S_{22}} & \cdots & k_{S_{2n}}\\ \vdots & \vdots & \ddots & \vdots\\ k_{S_{n1}} & k_{S_{n2}} & \cdots & k_{S_{nn}}\end{bmatrix} \tag{6.9}$$

The matrix $\begin{bmatrix}0 & \mathbf{I}\\ \mathbf{N} & 0\end{bmatrix}$ is also known as system state matrix or matrix **A.**

From the definition, two machines are coherent if the eigenvectors associated to changes in rotor angles for both machines are identical. This implies that, to examine the coherency of the second order system, the eigenbasis matrix of **A** is required.

Usually in real dynamic networks, the coherency definition may not be exactly satisfied. As a result, an approach for finding near-coherent groups will be presented such that the total number of near-coherent groups is equal to the number of the selected modes of **A**. Thus, the procedure used for finding the near-coherent groups of generators for a specific contingency is [87]-[88]:

- Calculate the **A** matrix of the linearized model of the power system and compute its eigenvalues.
- Choose the number of areas (groups) *r*.
- Compute the right eigenvector matrix **U** for the *r* smallest eigenvalues.
- Apply Gaussian elimination with complete pivoting to obtain *r* reference machines.
- Calculate the direction cosines of the rows of the eigenvectors corresponding to the generator angles as follows:

$$dcv = \frac{\sum_{i=1}^{n} v_{1_i} v_{2_i}}{\sqrt{\sum_{i=1}^{n} v_{1_i}^2 \sum_{i=1}^{n} v_{2_i}^2}} \tag{6.10}$$

The EPRI's Dynamic Reduction Program (DYNRED) in conjunction with the Power System Toolbox (PST) was used to find the coherent groups of generators for a predetermined set of contingencies.

The coherency recognition algorithm also allows identifying those buses that have voltage phase angles that are coherent with the angles of a set of coherent generators. This divides the system into sets of coherent buses and generators equal in number to the

number of interarea modes. The tie lines between one coherent group and another are the weak connections that are the root cause of the inter-area oscillations. We propose monitoring these weak connections in order to deploy the controlled islanding mechanism [88].

6.2.2 Coherency Grouping Example: 9 Bus – 3 Generator Test System

The 9 bus – 3 generators test system is chosen to illustrate the coherency based grouping algorithm. The system data and other information regarding this case are provided on pages 37-45 of [92].

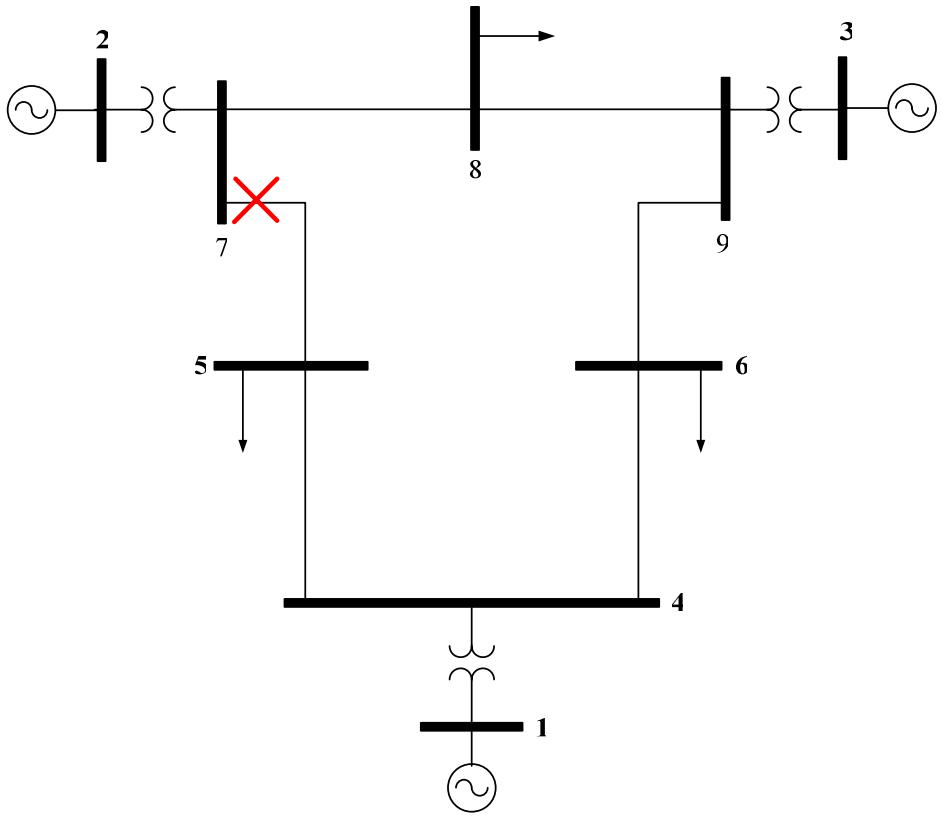

Figure 6.1: 9 Bus – 3 Generators Test System with Fault on Line 5-7

For a fault on bus 7, which is cleared by removing the line 5-7, the eigenvalues associated to the angular displacement are:

$$\mathbf{\Lambda} = \begin{bmatrix} 0 \\ -0.0974 - j8.689 \\ -0.0858 - j13.36 \end{bmatrix}$$

By selecting the first two eigenvalues for forming two coherent groups, the corresponding right eigenvectors are:

$$\mathbf{\Phi} = \begin{bmatrix} 0.5735 & -0.3825 \\ 0.5735 & 1 \\ 0.5735 & 0.5729 \end{bmatrix}$$

The direction cosines of the rows of the selected eigenvectors are:

$$\mathbf{DCV} = \begin{bmatrix} 1.0000 & 0.0615 & 0.2027 \\ 0.0615 & 1.0000 & 0.9649 \\ 0.2027 & 0.9649 & 1.0000 \end{bmatrix}$$

Since directional cosines corresponding to the machines 2 and 3 are close to the unity, it can be concluded that those machines must be added to the same coherent-group. On the other hand, the machine 1 itself is another coherent-group.

The previous statement could be validated through the results of the dynamic simulation for this case, as shown in Figures 6.2 A and B.

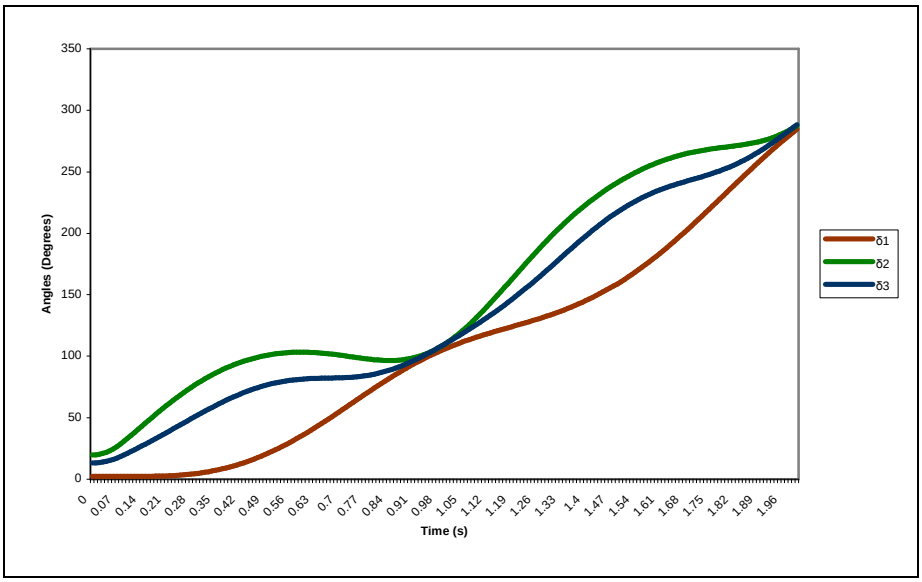

Figure 6.2 A: Generators Absolute Angles

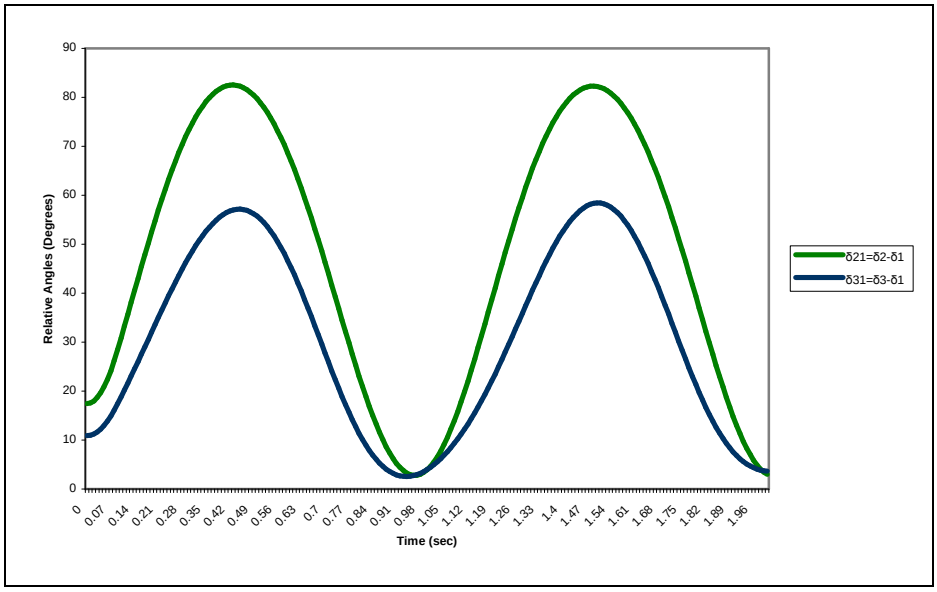

Figure 6.2 B: Generators Relative Angles

As shown in Figure 6.2 A and 6.2 B the rotor angles of generators 2 and 3 practically oscillate in counter phase with the rotor angle of generator 1, for the given conditions. Hence generators 2 and 3 form one of the coherent-groups, while the other is formed by the generator 1 itself.

6.3 SYSTEM SPLITTING PROBLEM

As mentioned before, the objective of the controlled islanding strategy is to separate an interconnected transmission network into islands of loads with matched generation at proper splitting points by opening selected transmission lines. Applied together with load shedding and perhaps generator tripping, the load and generation of each island would theoretically remain in balance, thus avoiding cascading instability or even blackout of the entire system [84].

After separating the generators into different groups by the coherency recognition procedure, it is necessary to assign the load buses to these groups for forming the islands. This task is conducted via a complex optimization problem, the System Splitting Problem (SSP).

The objective of the System Splitting Problem is to minimize the load-generation imbalance within the groups, after forming the islands. In our approach we consider only real power imbalance, because of the local nature of the reactive power.

For determining the physical boundaries of each island, a set of criteria must be satisfied, as shown [81]:

1) Consideration of Generation-Load Imbalance: The reduction of generation load imbalance in each island reduces the amount of under-frequency load shedding to be done once the islands are formed. It also makes it easier for each island to be capable of matching the generation and loads within the prescribed frequency limit and is beneficial during restoration.

2) Topological Requirement: In order to form the islands and specifically isolate one island from the other, all the lines connecting the islands need to be determined and disconnected.

The System Splitting Problem is a special application of the minimum spanning trees problems which intend to find the smallest total cost of its constituent arcs, measured as the sum of costs of the arcs in the spanning tree. In this case, the essential issue is to partition a set of data into “natural groups”, or clusters, in which the data points within a particular group of data should be more “closely related” to each other than the data points not in that cluster [94].

A popular method for solving this type of problems is by using of the Kruskal’s algorithm [94], which allows obtaining *n* partitions of a network with minimum spanning trees by deleting a determined number of arcs within the network. Figure 6.3 illustrate the latter approach.

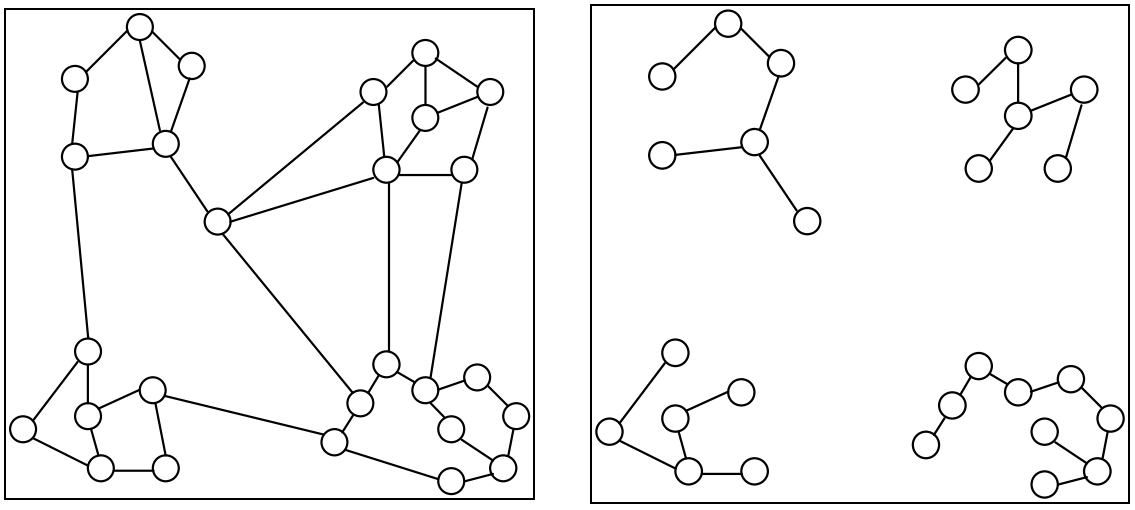

Figure 6.3: Partitions of a Network with Minimum Spanning Trees

For the system splitting problem, the costs are related to the real power injected or demanded by the groups formed, instead than the cost of the arcs of the traditional minimum spanning tree problem. Furthermore, in this approach, it is not necessary to delete the arcs that connect data points within the groups or clusters, but the arcs that connect the groups or clusters. Hence, small subnetworks are formed, instead the spanning trees, as shown in Figure 6.4.

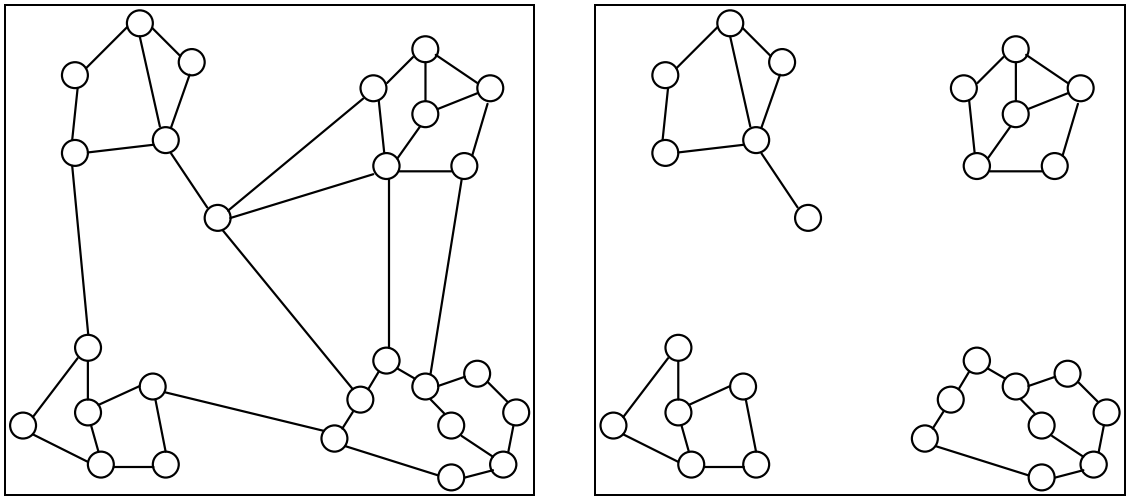

Figure 6.4: Partitions of a Network into Small Subnetworks

As a special type of minimum spanning tree problem, the system splitting problem (SSP) is a complex combinatorial optimization problem. Besides the Kruskal's algorithm and others traditional methods, several advanced techniques have been proposed to solve this problem, such as Minimal Cutsets algorithms [83], Ordered Binary Decision Diagrams (OBDD) [84]-[86], Breath First Search (BFS) algorithms [95], etc. We propose to use an evolutionary computation technique, Differential Evolution, as optimization tool to solve this complex problem.

6.3.1 Mathematical Formulation of the System Splitting Problem

The System Splitting Problem (SSP) could be formulated mathematically as follows:

$$\text{Min} \quad \sum_{i=1}^{r} \left\| \sum P_{G_n}^{i} - \sum P_{D_k}^{i} \right\| \quad \forall n,k \in \mathbf{A}^{i} \tag{6.11}$$

In order to avoid unexpected islands formation, two constraints must be satisfied:

- There is a physical path between all generating buses that belong to a group.
- The load buses must be connected to at least one generator bus.

$$\begin{aligned} R_{m,n} &\neq 0 \ \forall m,n \in \mathbf{G}^{i} \\ R_{k,n} &\neq 0 \ \forall k \in \mathbf{L}^{i}, n \in \mathbf{G}^{i} \end{aligned} \tag{6.12}$$

where

$P_{G_n}^{i}$: power generated by the n^{th} generator that belong to the i^{th} group

$P_{D_k}^{i}$: power demanded by the k^{th} load that belong to the i^{th} group

R : residual matrix which represents the link between the generators and loads of the i^{th} group

m,n : subscripts used for generating buses

k : subscript used for load buses

$\mathbf{L}^{i}$: set of load buses that belong to the i^{th} group

$\mathbf{G}^{i}$: set of generating buses that belong to the i^{th} group

$\mathbf{A}^{i}$: set of load and generating buses that belong to the i^{th} group

The residual matrix **R** is an *N* by *N* matrix that contains the connectivity information for each group, where *N* is the number of buses of the system. The procedure for forming the **R** matrix for each group is:

1. Create the **H** matrix by eliminating the columns of the $\mathbf{Y_{BUS}}$ matrix for the buses that do not belong to the group.
2. If both $m,n \in \mathbf{A}^i$, then $H_{m,n} = Y_{m,n}$. Otherwise $H_{m,n} = 0$
3. Calculate the gain matrix **G** as follows: $\mathbf{G} = \mathbf{H}^T \times \mathbf{H}$.
4. Calculate the residual matrix **R** as follows: $\mathbf{R} = \mathbf{H} \times \mathbf{G}^{-1} \times \mathbf{H}^T$.

6.3.2 Simplifications of the Original Network

The complexity of the SSP problem highly depends on the size of the system being analyzed, especially the number of load buses, which are also equal to the number of decision variables used in the optimization problem. Therefore, in some instances, it was necessary to simplify the original network, by removing those nodes which do not modify the objective function and/or do not explicitly affect the connectivity of the system. The reductions performed include:

a) The generators and their corresponding step up transformers are considered to be connected into a single node.

b) Two transmission nodes (with no loads) connected directly are merged into a single transmission node.

c) Radial nodes are eliminated from the decision variables. The load information of these nodes is added at the point of connection in the network.

d) When a load bus is connected directly between two generating buses that belong to the same group, this load bus is automatically assigned to the same group and thus eliminated from the set of decision variables.

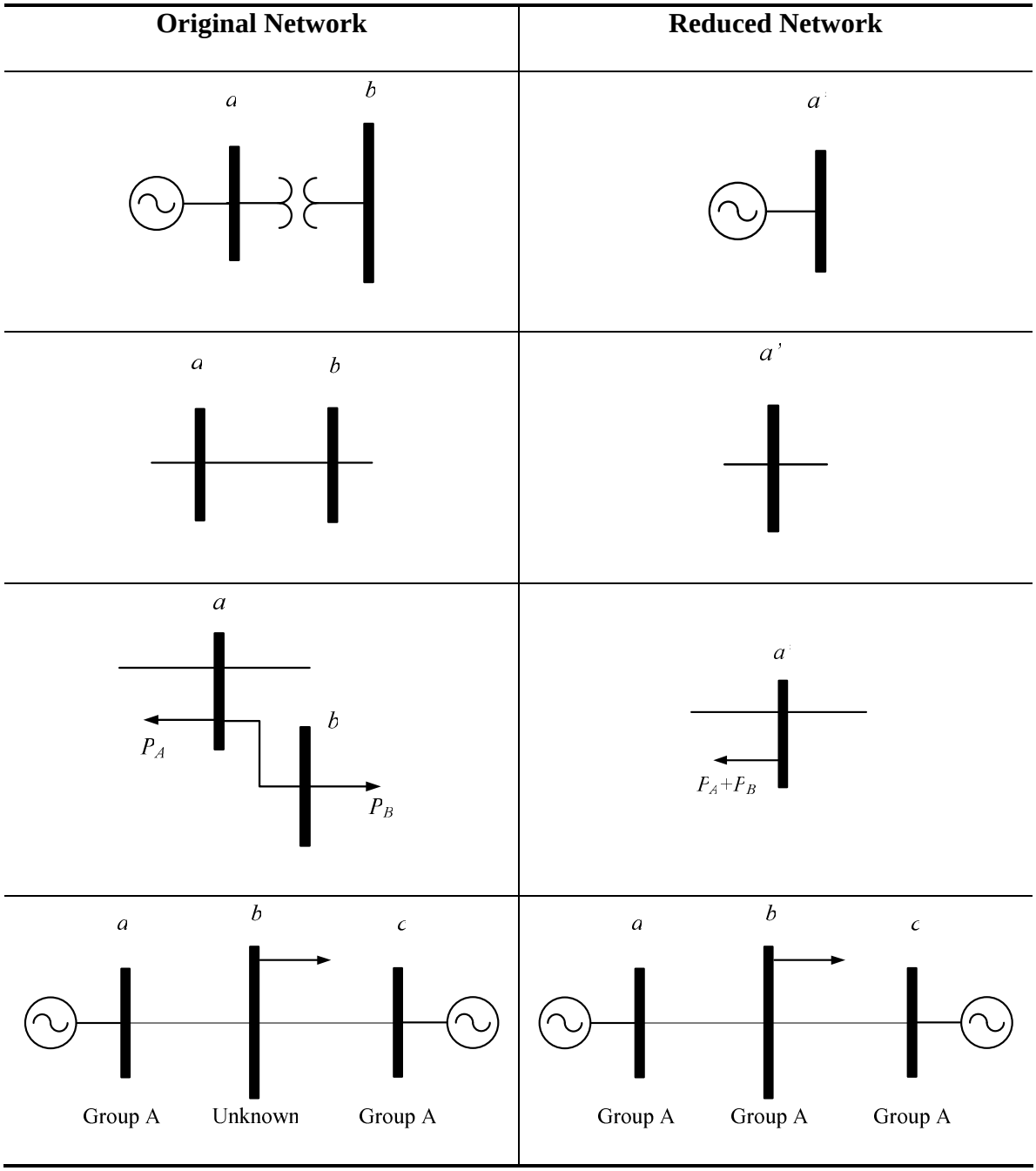

Figure 6.5: Simplifications of the Original Network

6.3.3 DE Model for the System Splitting Problem (DESPS)

As a robust optimization technique, we use Differential Evolution to solve effectively the system splitting problem, as shown as follows.

Control Variables: The set of control variables used in the optimization process are the set of load buses resulting of the simplifications made to the original network.

Initialization: DE assigns, randomly, an integer between 1 and *r* to each load buses, where *r* is the number of groups selected. If during the evolution process, any of these settings become unfeasible, they were adjusted using the boundary operator (2.8).

Objective Function: Minimize the real power imbalance within the groups, after forming the islands:

$$F'(\mathbf{X}) = \sum_{i=1}^{r} \left\| \sum P_{G_n}^i - \sum P_{D_k}^i \right\| \quad \forall n, k \in \mathbf{A}^i \tag{6.13}$$

Penalty Functions: The objective function could be modified adding penalty factors, when the constraints are not satisfied. These constraints are associated to the connectivity information within the groups.

e. Static Penalty Functions: The penalty functions used in this particular case are related with the number of constraints violations, instead of the distance-based penalty functions. Thus, the penalty functions used in the analysis were:

$$G_1(\mathbf{X}) = \omega_1 \sum_{i=1}^{r} \sum_{j=1}^{N_G^i} \max\left[0,\ \Upsilon_1\right] \tag{6.14}$$

$$G_2(\mathbf{X}) = \omega_2 \sum_{i=1}^{r} \sum_{j=1}^{N_L^i} \max\left[0,\ \Upsilon_2\right] \tag{6.15}$$

Where ω is the static penalty factor, N_G^i is the number of generating buses that belong to the i^{th} group and N_L^i is the number of load buses that belong to the i^{th} group. Υ_1 and Υ_2 are functions that reflect the connectivity information within the groups, as shown as follows:

$$\Upsilon_1 = \begin{cases} 0 & \text{if} \quad |Y_{m,n}| \neq 0 \\ 1 & \text{if} \quad |Y_{m,n}| = 0 \end{cases} \tag{6.16}$$

$$\Upsilon_2 = \begin{cases} 0 & \text{if} \quad |Y_{k,n}| \neq 0 \\ 1 & \text{if} \quad |Y_{k,n}| = 0 \end{cases} \tag{6.17}$$

Fitness Function: The fitness function used in the optimization process was a combination of the original objective function with the static penalty functions, as shown in (6.18):

$$F''(\mathbf{X}) = F'(\mathbf{X}) + G_1(\mathbf{X}) + G_2(\mathbf{X}) \tag{6.18}$$

6.3.4 System Splitting Problem Example: 9 Bus – 3 Generator Test System

Having separated the generators into coherent groups in Section 6.2.2, the next step is to assign the loads for forming the islands. In this case, there are 6 load buses; hence the problem may have 6 control variables. Performing the reduction proposed in the previous section, the number of control variables is reduced to 2 (load buses 5 and 6), as shown in Figure 6.6. The buses 1 and 4 form the group 1, and buses 2, 3, 7, 8 and 9 belong to the group 2.

Suppose that, for one individual of the population, the vector of control variables is:

$$\mathbf{X} = [2 \quad 2]$$

Bus 5 Bus 6

Hence, the groups are formed by:

$$\mathbf{A}_1 = [1 \quad 4]$$

$$\mathbf{A}_2 = [2 \quad 3 \quad 5 \quad 6 \quad 7 \quad 8 \quad 9]$$

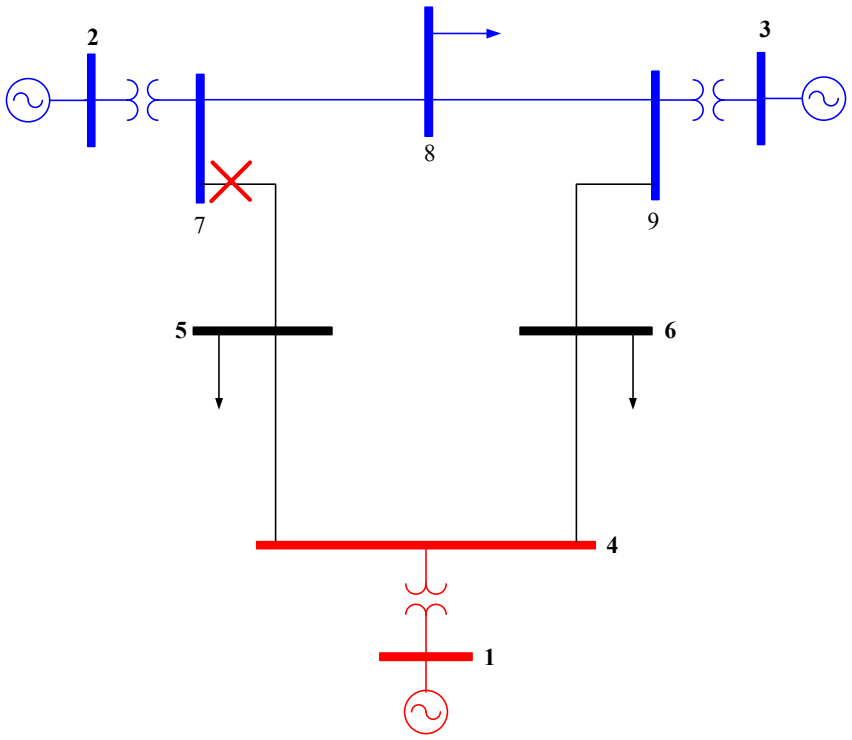

Figure 6.6: 9 Bus – 3 Generators Test System with Reductions

By following the procedure for creating the residual matrices (see Section 6.3.1) it is necessary to:

1. Create the matrices **H** for both groups by eliminating the columns of the $\mathbf{Y}_{\mathbf{BUS}}$ matrix for the buses that do not belong to the group.
2. If both $m,n \in \mathbf{A}^i$, then $H_{m,n} = Y_{m,n}$. Otherwise $H_{m,n} = 0$. Hence the corresponding **H** matrices are:

$$\mathbf{H_1} = \begin{bmatrix} -j8.4459 & j8.4459 \\ 0 & 0 \\ 0 & 0 \\ j8.4459 & 3.3074 - j30.394 \\ 0 & 0 \\ 0 & 0 \\ 0 & 0 \\ 0 & 0 \\ 0 & 0 \end{bmatrix}$$

$$\mathbf{H_2} = \begin{bmatrix} 0 & 0 & 0 & 0 & 0 & 0 & 0 \\ -j5.4855 & 0 & 0 & 0 & j5.4855 & 0 & 0 \\ 0 & -j4.1684 & 0 & 0 & 0 & 0 & j4.1684 \\ 0 & 0 & 0 & 0 & 0 & 0 & 0 \\ 0 & 0 & 3.8138 - j17.843 & 0 & 0 & 0 & 0 \\ 0 & 0 & 0 & 4.1019 - j16.134 & 0 & 0 & -1.282 + j5.5882 \\ j5.4844 & 0 & 0 & 0 & 2.8047 - j24.931 & -1.6171 + j13.698 & 0 \\ 0 & 0 & 0 & 0 & -1.6171 + j13.698 & 3.7414 - j23.642 & -1.1551 + j9.7843 \\ 0 & j4.1684 & 0 & -1.282 + j5.5882 & 0 & -1.1551 + j9.7843 & 2.4371 - j19.257 \end{bmatrix}$$

3. Calculate the gain matrices **G** for both groups as follows: $\mathbf{G} = \mathbf{H}^{\mathrm{T}} \times \mathbf{H}$.

$$\mathbf{G_1} = \begin{bmatrix} -1.43 & 3.28 + j0.28 \\ 3.28 + j0.28 & -9.84 - j2.01 \end{bmatrix} \times 10^{-7}$$

$$\mathbf{G_2} = \begin{bmatrix} -6.08 & 0 & 0 & 0 & 16.69 - j1.54 & -7.51 - j0.89 & 0 \\ 0 & -3.48 & 0 & -2.33 - j0.534 & 0 & -4.08 - j0.48 & 9.76 + j1.02 \\ 0 & 0 & -30.38 - j13.61 & 0 & 0 & 0 & 0 \\ 0 & -2.33 - j0.534 & 0 & -27.31 - j14.67 & 0 & -5.32 - j1.90 & 18.94 + j8.19 \\ 16.69 - j1.54 & 0 & 0 & 0 & -82.88 - j18.42 & 65.48 + j16.82 & -13.21 - j3.16 \\ -7.51 - j0.89 & -4.08 - j0.48 & 0 & -5.32 - j1.90 & 65.48 + j16.82 & -82.44 - j24.38 & 42.61 + 11.0 \\ 0 & 9.76 + j1.02 & 0 & 18.94 + j8.19 & -13.21 - j3.16 & 42.61 + 11.0 & -50.63 - j13.08 \end{bmatrix} \times 10^{-8}$$

As expected, both gain matrices are symmetric. Since the rank of $\mathbf{G_1}$ is 2 and the rank of $\mathbf{G_2}$ is 7, both matrices are also invertible.

4. The residual matrices **R,** which are calculated by means of $\mathbf{R} = \mathbf{H} \times \mathbf{G}^{-1} \times \mathbf{H}^{T}$, give the following information:

$$\mathbf{R_1} = \begin{bmatrix} \times & 0 & 0 & \times & 0 & 0 & 0 & 0 & 0 \\ 0 & 0 & 0 & 0 & 0 & 0 & 0 & 0 & 0 \\ 0 & 0 & 0 & 0 & 0 & 0 & 0 & 0 & 0 \\ \times & 0 & 0 & \times & 0 & 0 & 0 & 0 & 0 \\ 0 & 0 & 0 & 0 & 0 & 0 & 0 & 0 & 0 \\ 0 & 0 & 0 & 0 & 0 & 0 & 0 & 0 & 0 \\ 0 & 0 & 0 & 0 & 0 & 0 & 0 & 0 & 0 \\ 0 & 0 & 0 & 0 & 0 & 0 & 0 & 0 & 0 \\ 0 & 0 & 0 & 0 & 0 & 0 & 0 & 0 & 0 \end{bmatrix} \qquad \mathbf{R}_2 = \begin{bmatrix} 0 & 0 & 0 & 0 & 0 & 0 & 0 & 0 & 0 \\ 0 & \times & \times & 0 & 0 & \times & \times & \times & \times \\ 0 & \times & \times & 0 & 0 & \times & \times & \times & \times \\ 0 & 0 & 0 & 0 & 0 & 0 & 0 & 0 & 0 \\ 0 & 0 & 0 & 0 & \times & 0 & 0 & 0 & 0 \\ 0 & \times & \times & 0 & 0 & \times & \times & \times & \times \\ 0 & \times & \times & 0 & 0 & \times & \times & \times & \times \\ 0 & \times & \times & 0 & 0 & \times & \times & \times & \times \\ 0 & \times & \times & 0 & 0 & \times & \times & \times & \times \end{bmatrix}$$

In those matrices, x represents a non-zero entry. By analyzing the residual matrices, it could be concluded that:

- In the first group there exists a physical connection between the generating buses (bus 1) and load buses (bus 4), since $\mathbf{R_1}(1,4)$ or $\mathbf{R_1}(4,1)$ have a non-zero entries.
- In the second group, a physical path exists between the generators connected at buses 2 and 3, which could be verified by means of the entries of the residual matrix $\mathbf{R_2}$.
- In the group 2, all load buses, except the bus 5, are connected at least to one generator that belongs to the group. The bus 5 is isolated of the rest of the group; hence a penalty term is added to the objective function to reflect a constraint violation.

The optimal solution is obtained when the load at bus 5 is added to the first group, and the load at bus 6 is added to the second group. The islands, thus, are formed by removing the line 4-6, as shown in Figure 6.7 (it is assumed that faulted line 5-7 was previously removed in order to clear the fault).

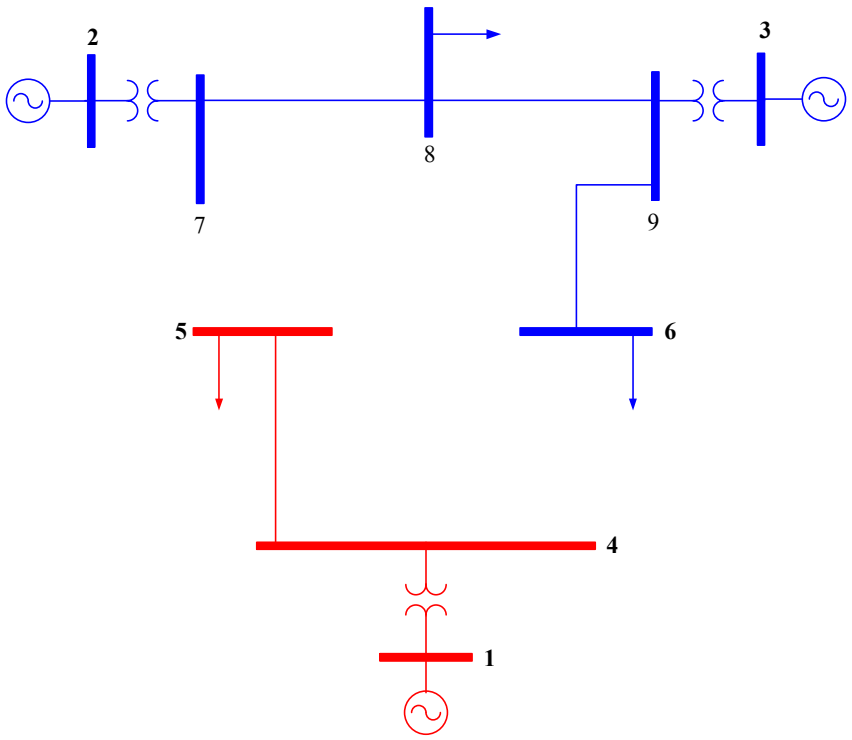

Figure 6.7: 9 Bus – 3 Generators Test System after Islanding

Table 6.1 summarizes the results obtained by using Differential Evolution. Due to the reduced number of control variables the optimization process takes 0.002 sec. The value of the objective function resulting of the optimization process was 6,215.6 MW^2

TABLE 6.1
OPTIMIZATION RESULTS

Group	P_G	P_L (MW)	Difference	Q_G	Q_L (MVAR)	Difference
1	71.6	125.0	-53.4	27.0	50.0	-23.0
2	248.0	190.0	58.0	-4.2	65.0	-69.2

6.4 SPECIAL PROTECTION SCHEMES AND PROTECTION COORDINATION

Because of the large fluctuations in machine electrical output quantities (power, voltage and current) during power swings and out-of-step conditions, the protection performance and power system stability are closely related. Power system protection uses system electrical and mechanical parameters to detect abnormal conditions in a power system. During power swings and out-of-step conditions, the protection performance of protection types that monitor power flows, voltages and currents may be affected by the behavior of these system parameters. These protection types include overcurrent, overvoltage, distance, pilot and loss of excitation protection [96].

The proper coordination with the protection schemes used conventionally in a power system is essential to achieve the main objective of the controlled islanding mechanism. The islanding mechanism will be deployed only if the disturbance potentially affects the synchronism of the generators connected to the system. Hence, some additional protection actions are necessary to avoid incorrect performance of the abovementioned types of protections during power swings and out-of-step conditions. The protection type used for this purpose is known as *out-of-step blocking protection.*

However, while solving the problem of incorrect protection performance, some protection schemes can still operate to separate the unstable generator stations without unnecessary loss of supply to loads or damage to equipments. The protection type used for this purpose is known as *out-of-step tripping protection.*

For both out-of-step protection types (blocking and tripping) the most common method of detecting power swings and out-of-step conditions is based on the fact that the

change in voltage and current during rotor angle unstable conditions is slow, unlike that in short-circuit conditions [96].

From the point of view of design, it is necessary to carefully select the quantities that have to be monitored to initiate the triggering sequence in our controlled islanding approach. After numerous dynamics simulations with different operational conditions, the quantities selected for monitoring were the apparent resistance of the weak tie lines and the frequency of generators. The conditions for controlled islanding would be reached if:

- The rate of change of the apparent resistance of several monitored lines is small when they enter into the operating characteristic of the distance relays.
- The frequency of various generators exceeds 62 Hz.

6.4.1 Out of Step Protection

The out-of-step (OOS) relays are the basic mechanism that supports our islanding strategy. The philosophy of out-of-step relaying is simple and straightforward: avoid tripping of any power system element during stable swings. Protect the power system during unstable or out-of-step conditions.

When two areas of a power system, or two interconnected systems, lose synchronism, the areas must be separated from each other quickly and automatically in order to avoid equipment damage and shutdown of major portions of the power system. Uncontrolled tripping of circuit breakers during an OOS condition could cause equipment damage and pose a safety concern for utility personnel. Therefore, a controlled tripping of certain power system elements is necessary in order to prevent equipment damage, and widespread power outages, and minimize the effects of the disturbance [97].

Out-of-step protection functions detect stable power swings and out-of-step conditions by using the fact that the voltage/current variation during a power swing is gradual while it is virtually a step change during a fault. Both faults and power swings may cause the measured apparent positive-sequence impedance to enter into the operating characteristic of a distance relay element. The fundamental method for discriminating between faults and power swings is to track the rate of change of measured apparent impedance, which is a function of the real and reactive power that flows through a line, as expressed as follows [96].

$$Z_{app} = \left[\frac{P_{ij}}{P_{ij}^2 + Q_{ij}^2} + j \frac{Q_{ij}}{P_{ij}^2 + Q_{ij}^2} \right] |V_i|^2 \tag{6.17}$$

Clearly, swings are severe when P_{ij} and/or Q_{ij} are large and $|V_i|$ small. Under such circumstances Z_{app} is small. If the rate of change of the measured apparent impedance is also small, then the out-of-step protection relays would operate.

Figure 6.8 shows a typical swing trajectory for an out-of-step condition. It is shown in the figure, that this particular fault would activate the primary and remote backup protection for this line and the adjacent ones.

Figure 6.9 shows the plot of apparent resistance for the given condition. As shown in the figure, at approximately 1 sec., the rate of change of the apparent impedance is small, which is the basis for the operation of the out-of-step relays.

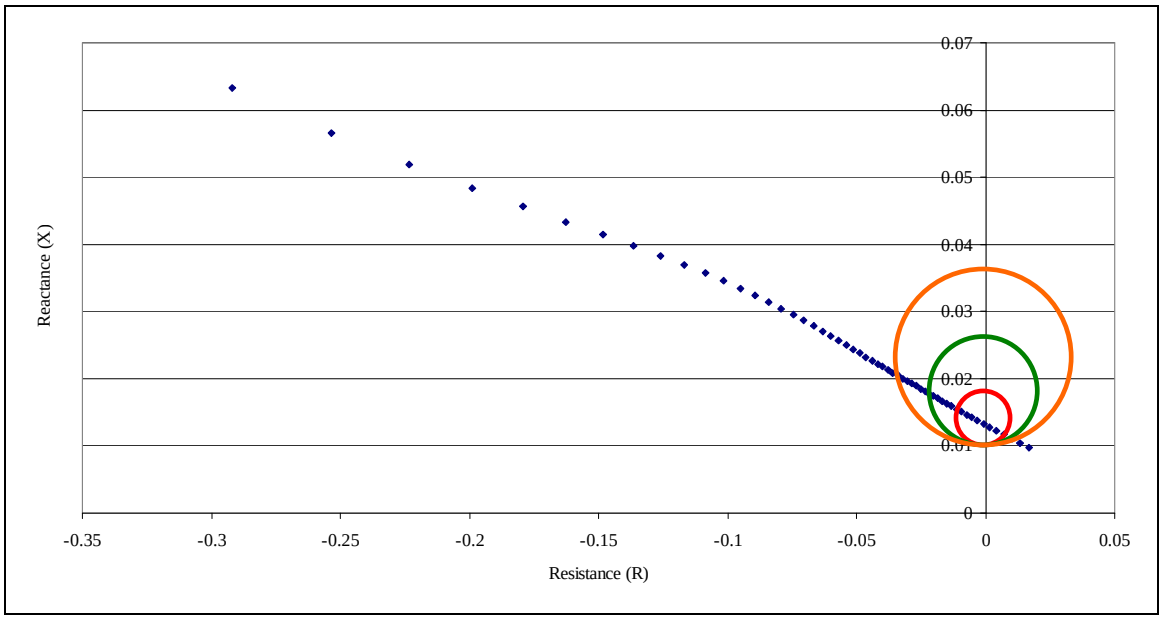

Figure 6.8: Swing Locus for an Out-of-Step Fault

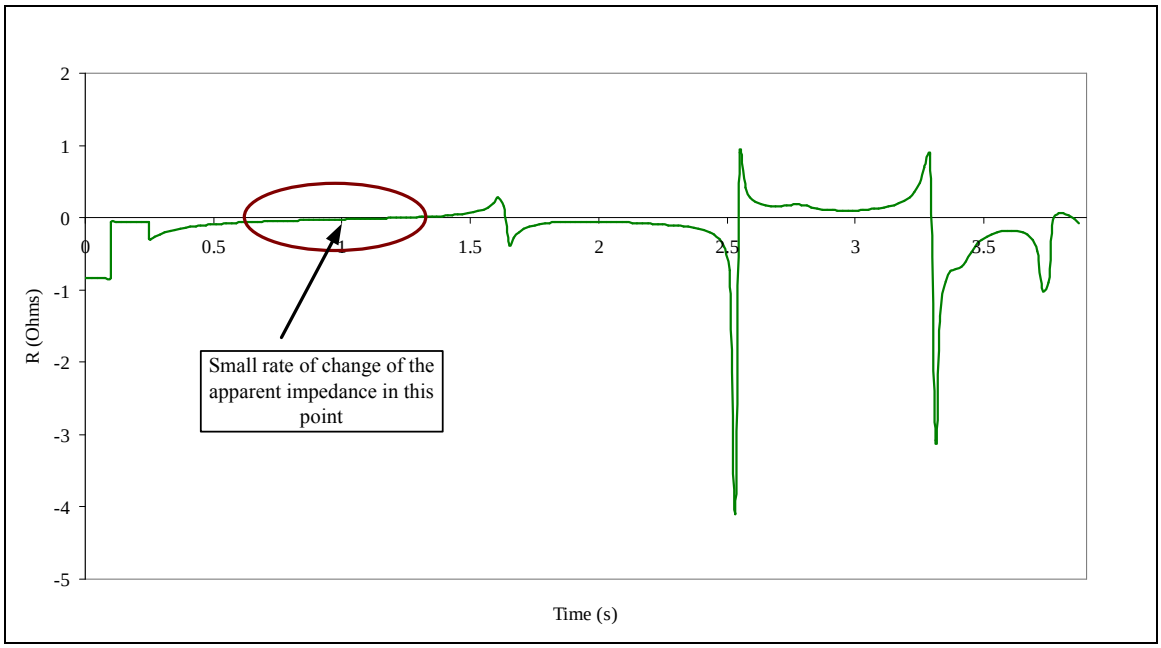

Figure 6.9: Apparent Resistance Plot for the Out-of-Step Fault

Actual implementations of measuring the rate of change of the apparent impedance are normally performed though the use of two impedance measurement elements together with a timing device. If the measured impedance stays between the two impedance measurement elements for a predetermined time, then an out-of-step condition is declared and an out-of-step blocking signal is issued to block the distance relay elements operation [97].

Impedance measurement elements with different shapes have used over the time for out-of-step protection. The most common applications include double blinders, concentric polygons, and concentric circles as shown in Figure 6.10 A, B and C respectively [98].

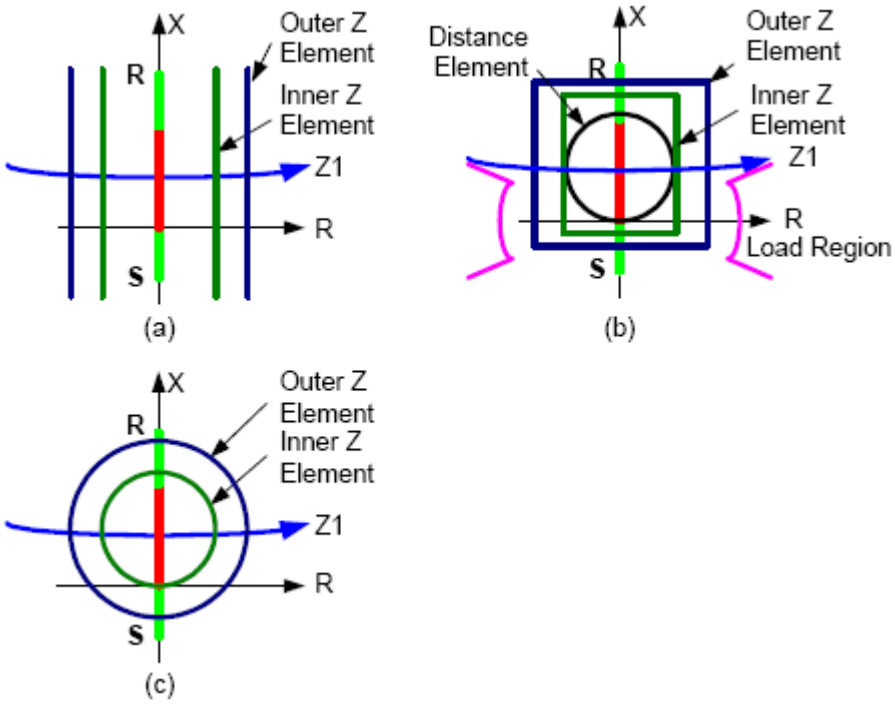

Figure 6.10: Out-of-Step Protection Schemes [98]

As mentioned before, there are basically two functions related to out-of-step protection. One is the out-of-step tripping protection function that discriminates between

stable and unstable power swings and initiates network sectionalizing or islanding during loss of synchronism. The other function, called out-of-step blocking protection function, discriminates between faults and stable or unstable power swings, blocking the action of relay elements prone to operate during unstable power swings, avoiding, therefore, cascading failures.

This blocking action could be used as input signal to intelligent agents, in our case the IPRs, in conjunction with overfrequency signal of the generators to deploy the proposed controlled islanding mechanism. The IPRs control actions will be complemented with both frequency and voltage load shedding and underfrequency/overfrequency protection for generators. The main idea is to fully consider the protection schemes used conventionally in a power system.

6.4.2 Underfrequency Load Shedding

Any part of a power system will begin to deteriorate if there is an excess of load over available generation. The prime movers and their associated generators begin to decelerate as they attempt to carry the excess of the load. Tie lines to other parts of the system, or to other power systems, attempt to supply the deficiency of generation. This combination of events could provoke that the tie lines open due to overload, or the separation of various parts of the systems due to power swings, which results in an instability condition.

To prevent the complete collapse of the system, underfrequency relays are used to automatically drop loads, by following a predetermined scheme, to reduce the imbalance between the available generation and the remnant load in the affected area. To avoid damages in parts of the power system due to abnormal frequency conditions, such actions

must be taken promptly and must be of sufficient magnitude to preserve critical loads, while enabling the remainder of the system to recover from the underfrequency condition.

The main objective of an underfrequency load shedding scheme is to quickly recognize generation deficiency within any system and automatically load shed, such that the generation-load balance is achieved and nominal system frequency is restored. To accomplish this underfrequency relays are used throughout the system to drop increments of load at specific frequencies. A properly designed scheme will prevent a major system outage under various abnormal operating conditions [99].

The traditional load-shedding scheme consists of underfrequency relays located at critical feeder locations. When the frequency drops below a preset value, the critical feeders are disconnected from the system. If the frequency continues to drop, other load-shedding stages are activated. Some underfrequency load-shedding schemes have as many as five underfrequency stages set at, for example, 59.5, 59.3, 58.8, 58.6, and 58.3 Hz [100]-[101]. Ideally, all underfrequency load shedding schemes should have the same operating characteristic so that the schemes act simultaneously across the power system when the frequency drops below the predefined set point.

The amount of load shed is an important issue in the design of any load shedding scheme. The load shed should be sufficient to restore system frequency to normal or close to normal (above 59 Hz). To accomplish this, it would mean the load that is shed should nearly equal the amount of overload.

It is not essential that the frequency be restored exactly to 60 Hz. If the frequency is restored above 59 Hz, the remaining system generators may pick-up the remaining

overload through speed-governor action and restore the frequency to normal condition. If the generation does not have spinning reserve capability, operation above 59 Hz will not be detrimental and the system operator will have sufficient time to drop additional load or to add new generation [100].

In our approach, a typical load shedding scheme in five steps was applied, as shown in Table 6.2. This scheme provides the capability to drop up to 50% of the load. In this case, large amounts of load are shed in the first three stages to restore the system frequency rapidly.

TABLE 6.2
UNDERFREQUENCY LOAD SHEDDING SCHEME PROPOSED

Frequency Hz	Time Delay Cycles	Tripping Delay Cycles	% Load Shed
59.5	3	2	15
59.3	3	2	10
58.8	3	2	10
58.6	3	2	8
58.3	3	2	7

Other more complex schemes of load shedding, based on the rate of frequency decline, have been developed and applied in several utilities. Detailed discussion of such approaches could be found on [93] and [101].

6.4.3 Undervoltage Load Shedding

Voltage has always been considered as an integral part of the power system response and is an important aspect of system stability and security. Thus, voltage stability and collapse cannot be separated from the general problem of system stability. However, in the recent years, the analysis of voltage stability has assumed importance, mainly due to several documents of voltage collapse in France, Japan, Belgium and Florida. There are

several factors which contribute to voltage collapse as increasing load on transmission lines, reactive power constraints, under-load tap changing transformers and load characteristics [93],[102]-[103].

System protection against voltage collapse consists of automatic control actions based on local or wide-area measurements that aim at avoiding voltage instability. The system protection has to be designed in coordination with generators and transmission lines protections.

Several fast undervoltage load shedding schemes have been designed similarly to existing, widely used underfrequency ones [104]-[105]. In our approach, this type of load shedding was applied in conjunction with other protection schemes to prevent system instability. The scheme proposed includes shedding up to 15% of load, in stages, with proper time delay, as shown in Table 6.3.

TABLE 6.3
UNDERVOLTAGE LOAD SHEDDING SCHEME PROPOSED

Voltage p.u.	Time Delay Cycles	Tripping Delay Cycles	% Load Shed
0.89	660	2	5
0.87	540	2	5
0.85	360	2	5

6.4.4 Generators Under/Overfrequency Protection

Generators and their auxiliaries are provides with under/overfrequency relays to prevent damages due to emergency abnormal frequency conditions.

As discussed Section 9.2.3 of [93], there are two main problems with the operation of generating units at low frequency:

1. The first problem is concerned with the vibratory stress on the high-low pressure turbine blades. Since the effects of vibratory stress are cumulative with time, the operation of steam turbine below 58.5 Hz is severely restricted.

2. The second problem is associated with the performance of plant auxiliaries driven by inductions motors, such as boiler feed pumps or fans supplying combustion air. At frequencies below 57 Hz, the plant capability may be severely reduced because of the reduced output of these plant auxiliaries.

Overfrequency conditions, in some instances, would result in reduced excitation of the generating units, due to high voltages derived of a sudden lost of load. If the excitation is greatly reduced, the generator might be tripped by loss-of-excitation protection. Furthermore, as a result of instability conditions, generators tend to accelerate, which, if not controlled promptly, would cause severe damages on the shafts and other rotating components of the units [106].

Generators tripping actions, as a result of severe under/overfrequency conditions, were considered in our approach, as shown in Table 6.4. These tripping actions are based in the steam turbine off-frequency limits shown in Figure 6.11 [99].

TABLE 6.4
GENERATORS OVER/UNDERFREQUENCY TRIPPING SCHEME

Frequency Hz	Time Delay Cycles	Tripping Delay Cycles
62	360	2
63	0	2
57	0	2

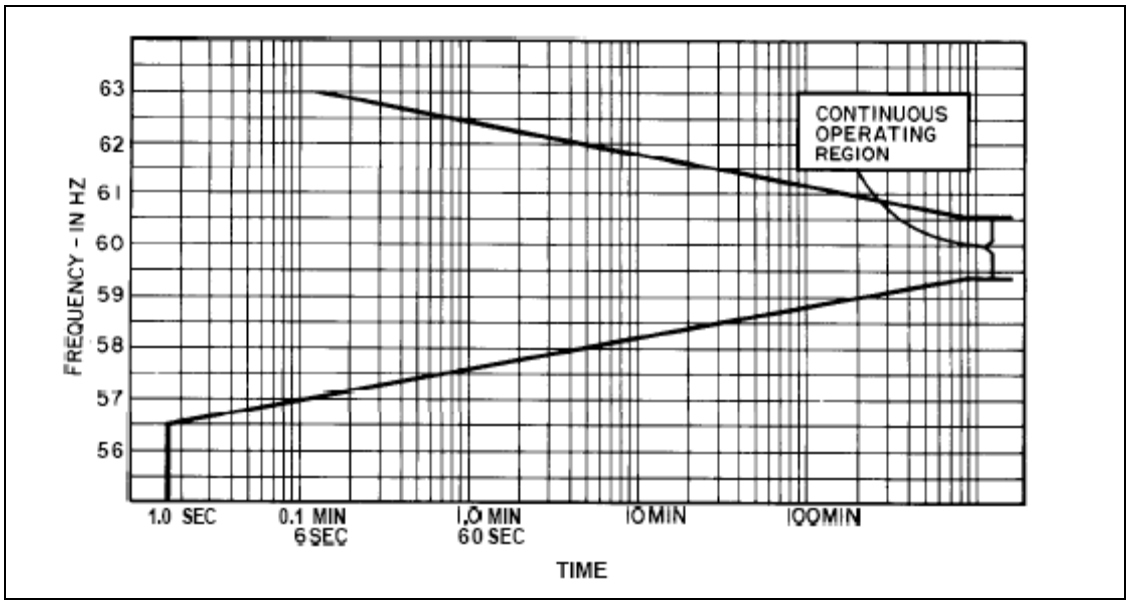

Figure 6.11: Steam Turbine Off-Frequency Limits [99]

6.4.5 Wide Area Control Based on Intelligent Power Routers (WAC-IPRs)

Large interconnected power systems are usually decomposed into areas or zones based on various criteria, such as legislative, historical, geographical, organizational, technical, etc. Therefore also the control of the whole interconnection is shared by network operators responsible for their respective areas.

In many cases, each operator has only a limited access to the data (system state, system dynamics, planned control actions and strategies, etc.) from other areas. Interactions, such as contractual conditions for the energy delivery between energy traders, load-generation balance, inter-area oscillations, etc, are often present between different parts of power systems [107].

To keep security on the desired level, a higher degree of coordination among existing independent system operators (ISOs) is probably required. Obstacles in this effort may arise due to technical (insufficient communication infrastructure, different data formats

etc.) and non-technical constraints (conflicts in commercial and social interests or in regulatory frames).

In this context, researches at University of Puerto Rico - Mayaguez are currently developing technologies for a next generation of electric power distribution networks (EPDN) based on a distributed, de-centralized framework for control and communication between system components. In our framework, the intelligence that can be used for control and coordination operations is embedded into a series of computing devices called the Intelligent Power Routers (IPRs).

The information exchange capability of the routers provides coordination among themselves to reconfigure the network, even when the designated principal control center of the system has collapsed due to a natural or man-made disaster. The IPRs may achieve their task using direct monitoring, area-limited on-line security assessment and adaptive controls to establish a coordinated and local set of control actions to either apply preventive countermeasures prior to a potential disturbance or corrective countermeasures following a disturbance [108].

However, to perform wide area control, it is necessary that the control areas share information about the state of the system at a certain time. For that reason, we propose a new control scheme, based on the IPRs, for collecting and sharing the information necessary to asses the security of the entire system.

The main idea is that these IPRs have a database of all credible contingencies as well as the corresponding control actions in their area. When a disturbance occurs in one area, the IPRs would send an alert message to the contiguous areas. If one of the conditions for

islanding is reached, the affected area would send an emergency message to the other areas to initiate the triggering events, everyone in it area.

Figure 6.12 gives an illustration of the proposed scheme. The local IPRs are capable to perform local control actions such as line tripping, capacitor switching, local load shedding and restoration process, among others. Wide Area Control IPRs (WAC-IPRs) are responsible for the information exchange between areas and the coordination of local control actions through local IPRs when a disturbance affects the integrity of the system.

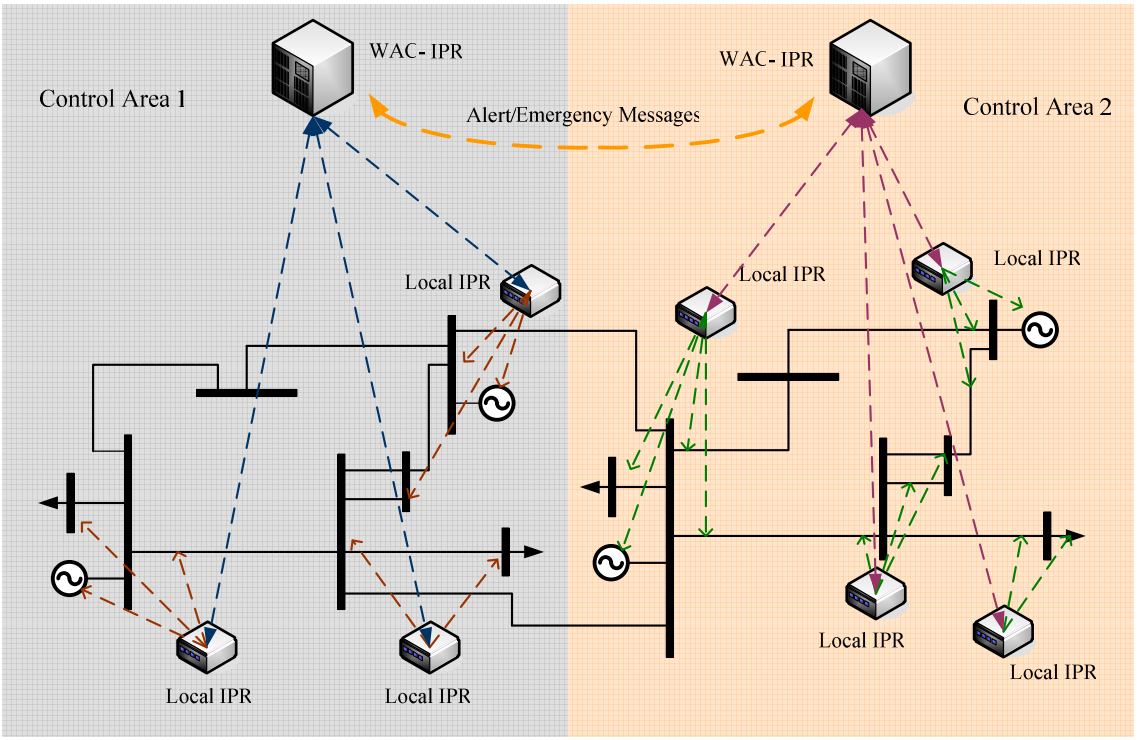

Figure 6.12: IPRs Based Local and Wide Area Control

We will demonstrate through simulations that the inclusion of these intelligent controls minimizes the adverse effects of large disturbances over the system.

6.5 CASE STUDIES AND RESULTS

The effectiveness of the IPRs as defense mechanism against extreme contingencies will be demonstrated through dynamics simulations on the New England 39-bus and the WSCC 179-bus test systems. The main characteristics of these systems are:

TABLE 6.5
MAIN CHARACTERISTICS OF THE NEW ENGLAND 39-BUS TEST SYSTEM

Buses	39
Transmission Lines	38
Transformers	12
Generators	10
Base Demand	6,097.1 MW
Base Generation	6,140.8 MW

TABLE 6.6
MAIN CHARACTERISTICS OF THE WSCC 179-BUS TEST SYSTEM

Buses	179
Transmission Lines	203
Transformers	60
Generators	29
Base Demand	60,785 MW
Base Generation	61, 412 MW

The simulations are made using a detailed generator model with governors, exciters and, for the WSCC 179-bus test system, power system stabilizers (PSS). In those cases, underfrequency/undervoltage load shedding, generators under/overfrequency tripping, as well as out of step protection were also considered. The loads were modeled as constant impedances.

The Dynamic Reduction Program (DYNRED) of the Power System Analysis Package (PSAPAC) was chosen for forming groups of coherent generators. The Differential

Evolution algorithm was employed for solving the system splitting problem for the case studies.

6.5.1 New England 39-Bus Test System

The proposed controlled islanding scheme was originally tested in the New England 39 bus – 10 generator test system with satisfactory results. Several cases with different fault locations were analyzed, as shown as follows:

6.5.1 A: Fault on Buses 4 and 29

In this case the response of the system to simultaneous three phase faults were examined. The sequence of events was:

- At 0.1 seconds a three phase fault occurred in bus 29. The fault is cleared at 0.25 seconds by opening the line 28-29.
- At 0.26 seconds another three phase fault occurred in bus 4, the fault is also cleared at 0.41 seconds by removing the line 4-5.

Figure 6.13 shows a schematic of the New England 39-bus test system and the location of the faults. In this case, if no other emergency control is executed, generators at buses 38 and 39 lost their synchronism, as shown in Figures 6.14 and 6.15.

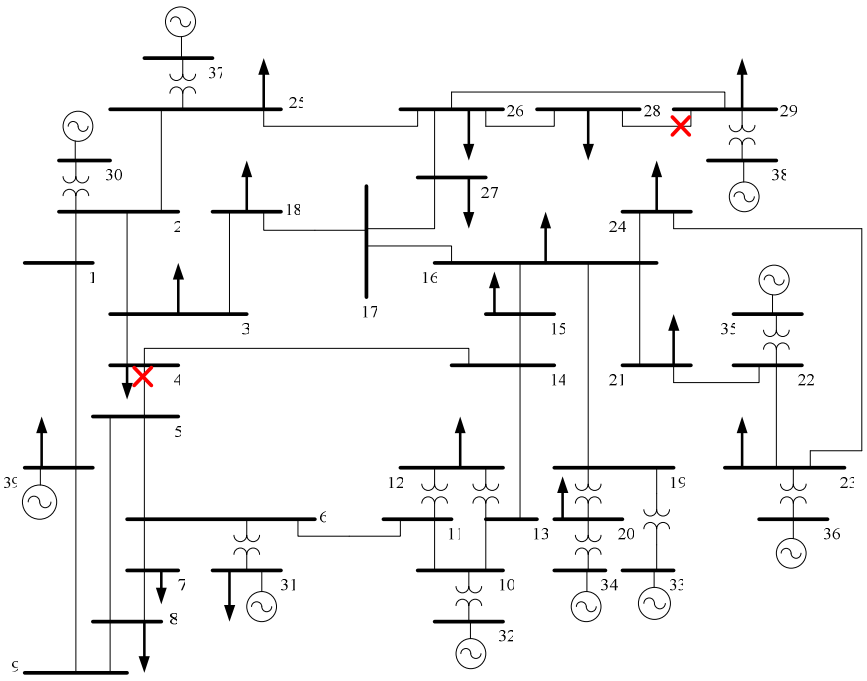

Figure 6.13: New England 39-Bus Test System with Fault Locations

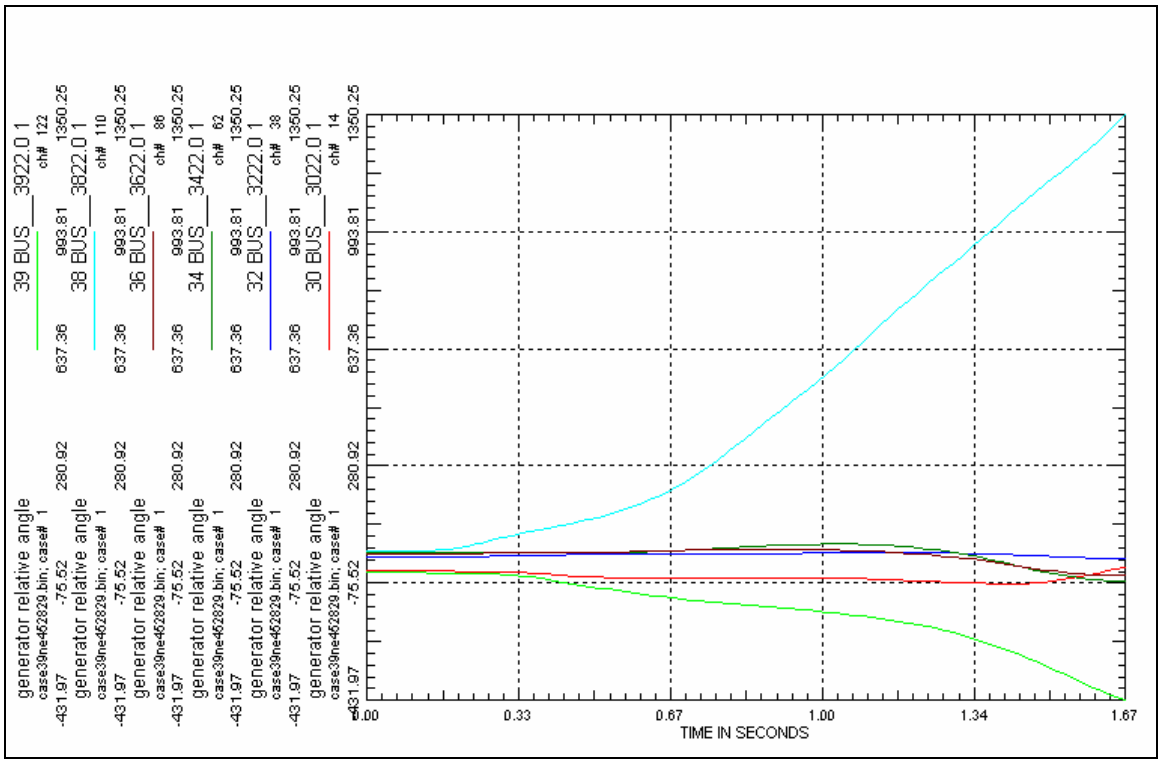

Figure 6.14: Generators Relative Angles

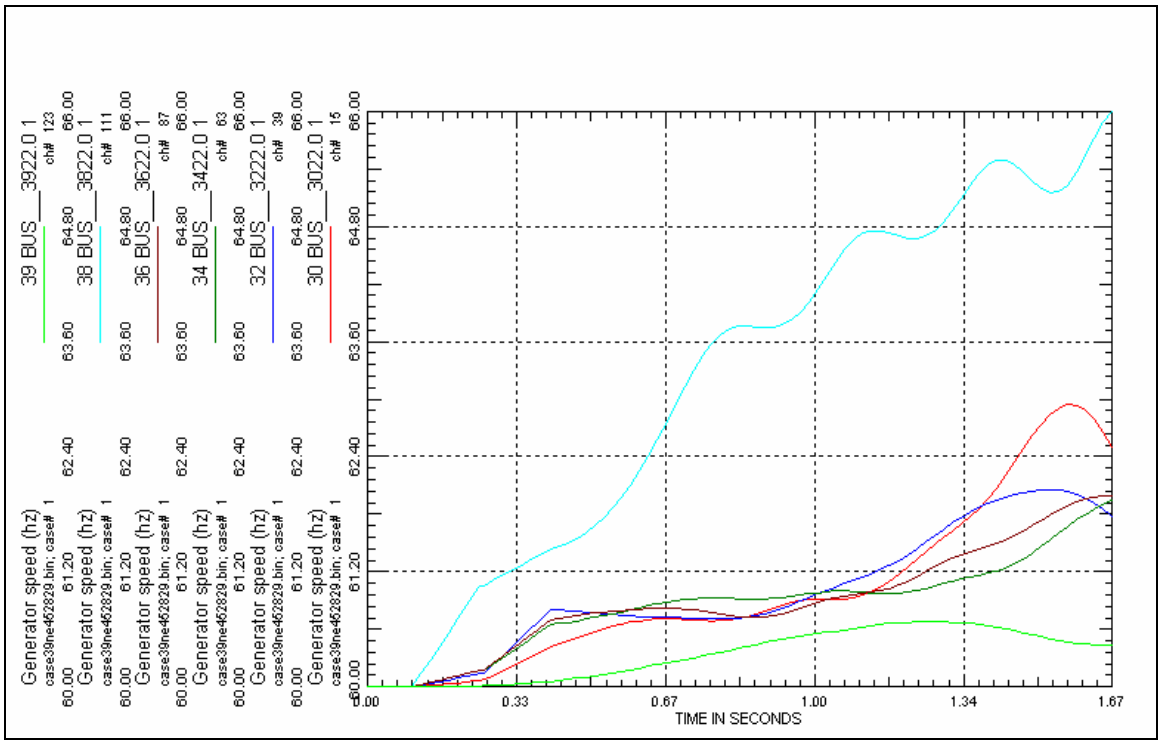

Figure 6.15: Generators Speed (Hz)

The lines 1-2, 8-9, 15-16, 17-27, 17-18 and 25-26 were selected by DYNRED as weak tie lines for this particular case. As mentioned before, the proposed controlled islanding scheme will be deployed by monitoring the rate of change of the apparent resistance and the generators speed. The conditions for controlled islanding would be reached if:

- The rate of change of the apparent resistance of several monitored lines is small when they enter into the operating characteristic of the distance relays.
- The frequency of various generators exceeds 62 Hz.

As shown in the Figure 6.16, after the occurrence of the faults there is a rapid change in the apparent resistance of the monitored lines. However, at approximately 0.57 seconds small changes in the lines apparent resistance are detected and the frequency of

the generator connected at bus 38 surpass the threshold value of 62 Hz. Therefore, the conditions for islanding are reached at this time.

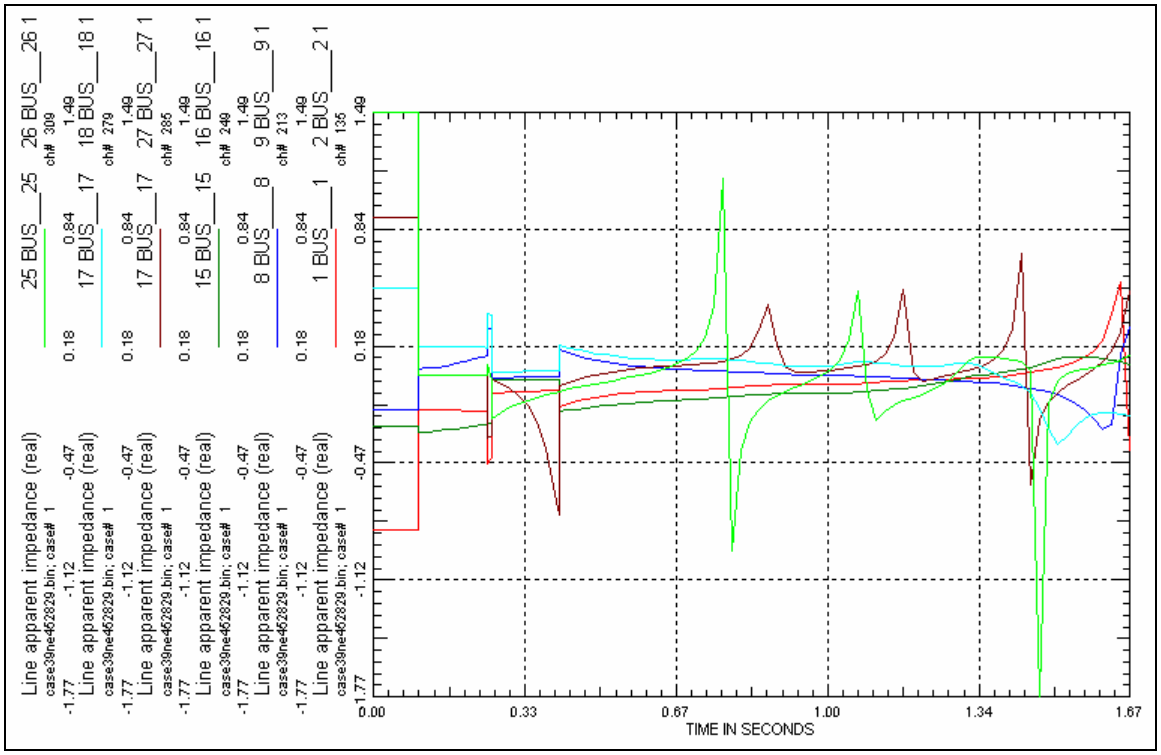

Figure 6.16: Lines Apparent Resistance

Differential Evolution solves effectively the system splitting problem for this particular case. The generator-load imbalance of the islands formed is shown in Table 6.7.

TABLE 6.7
INITIAL GENERATOR-LOAD IMBALANCE

Group	P_G	P_L (MW)	Difference	Q_G	Q_L (MVAR)	Difference
1	830.0	909.5	79.5	22.8	147.0	124.2
2	2350.0	2265.1	84.9	589.2	425.7	163.5
3	1917.1	1818.5	98.6	550.0	586.2	36.2
4	1000.0	1104.0	104.0	88.3	250.0	161.7

The islands are formed by opening the lines 1-39, 8-9, 3-18, 14-15, 25-26 and 17-27 at 0.67 seconds (0.10 seconds after that the condition of islanding is reached). The final configuration of the islands is shown in Figure 6.17

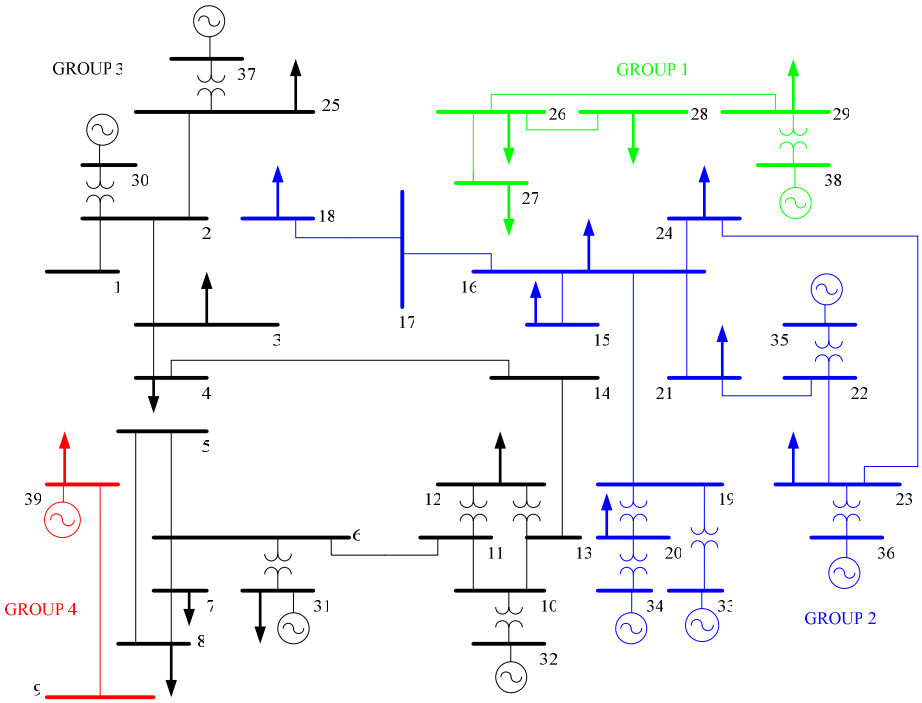

Figure 6.17: Final Configuration of the Islands

Finally, Figure 6.18 shows the generators speed after islanding. By applying the proposed controlled islanding scheme the system remains stable after the occurrence of such disturbances. The proposed underfrequency and undervoltage load shedding schemes drop a total of 213.73 MW and 34.55 MVAR of the load.

It is interesting to note that the generators do not return to nominal frequency after islanding. Therefore, it is necessary to perform some other control actions, such as adjusting the governor's set point, activate non-spinning and contingency reserves or selective load shedding, to restore the system to the nominal frequency.

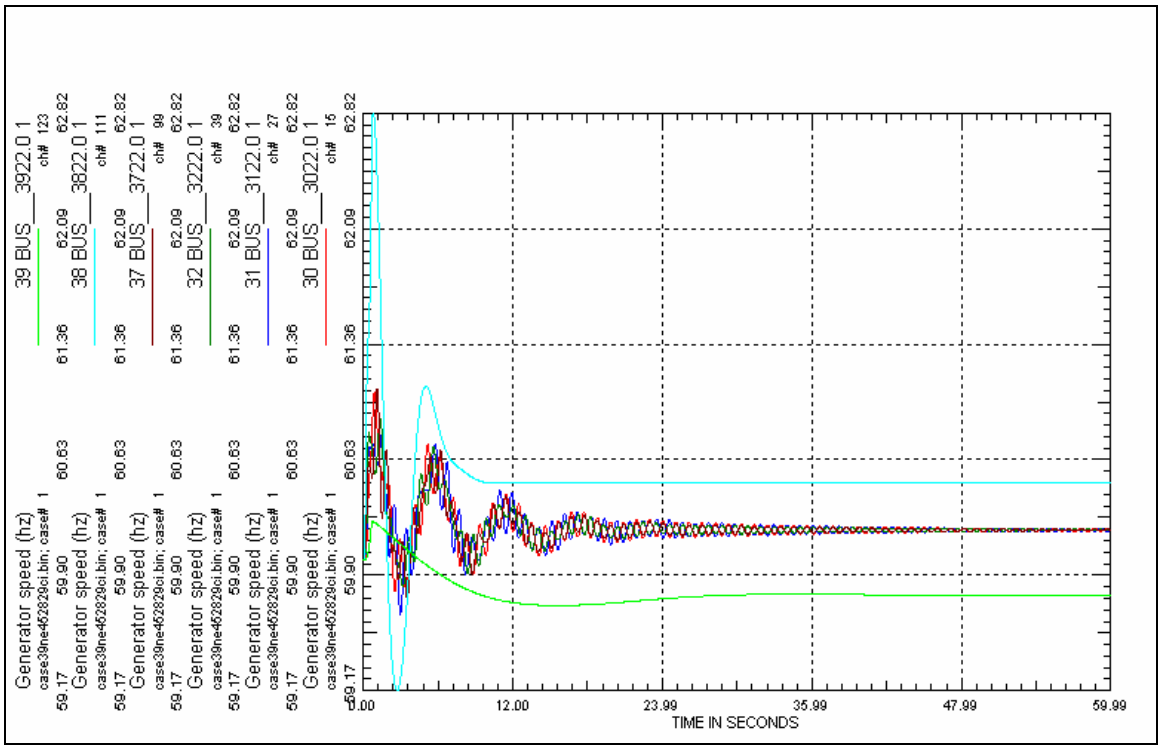

Figure 6.18: Generators Speed after Islanding

6.5.1 B: Fault on Buses 5 and 16

For the second case, simultaneous faults on buses 5 and 16 are considered. The sequence of events used in the analysis was:

- At 0.1 seconds a three phase fault occurred in bus 16. The fault is cleared at 0.25 seconds by opening the line 16-21.
- At 0.26 seconds another three phase fault occurred in bus 5, the fault is also cleared at 0.41 seconds by removing the line 5-6.

Figure 6.19 shows the schematic of the New England 39-bus test system and the location of the faults. The result of these faults, if no other emergency control is executed, is that the generators at buses 30, 34, 38 and 39 lose their synchronism, as shown in Figures 6.20 and 6.21.

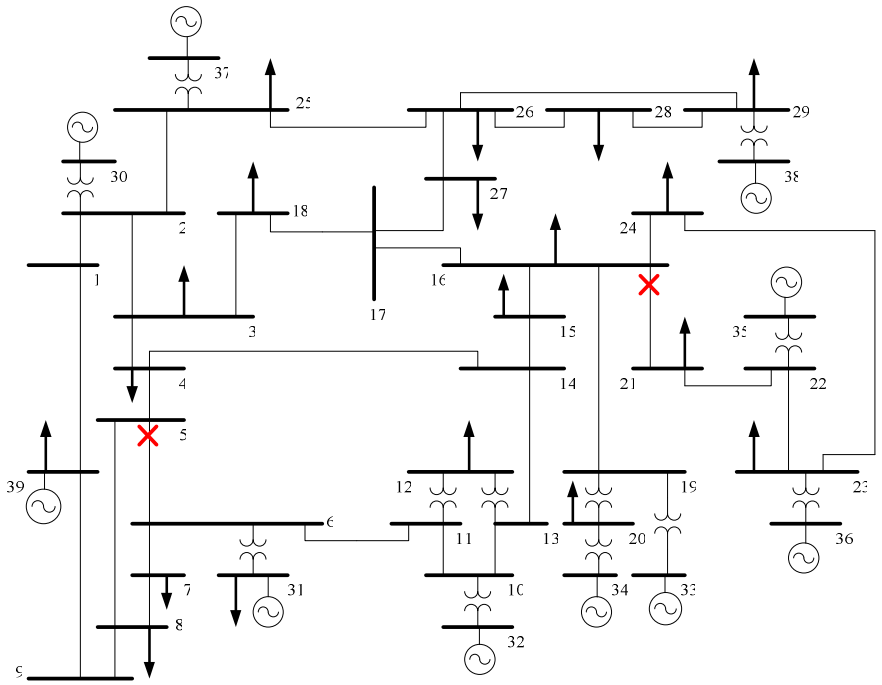

Figure 6.19: New England 39-Bus Test System with Fault Locations

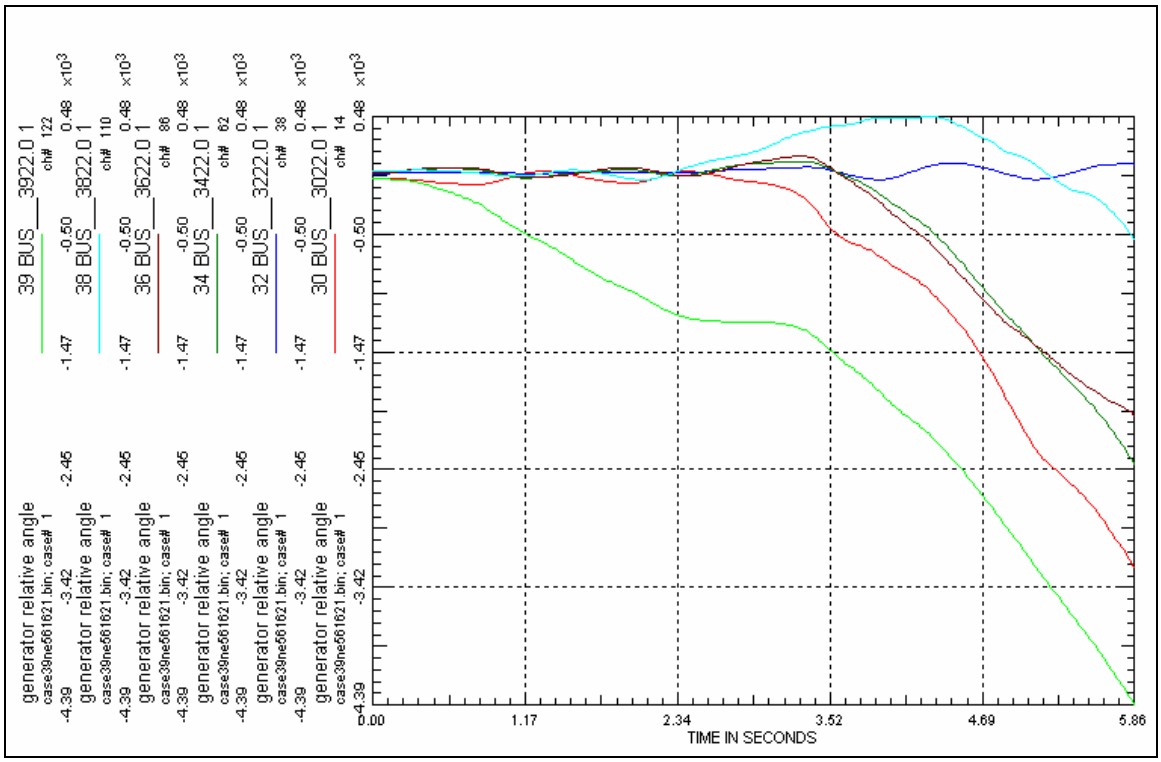

Figure 6.20: Generators Relative Angles

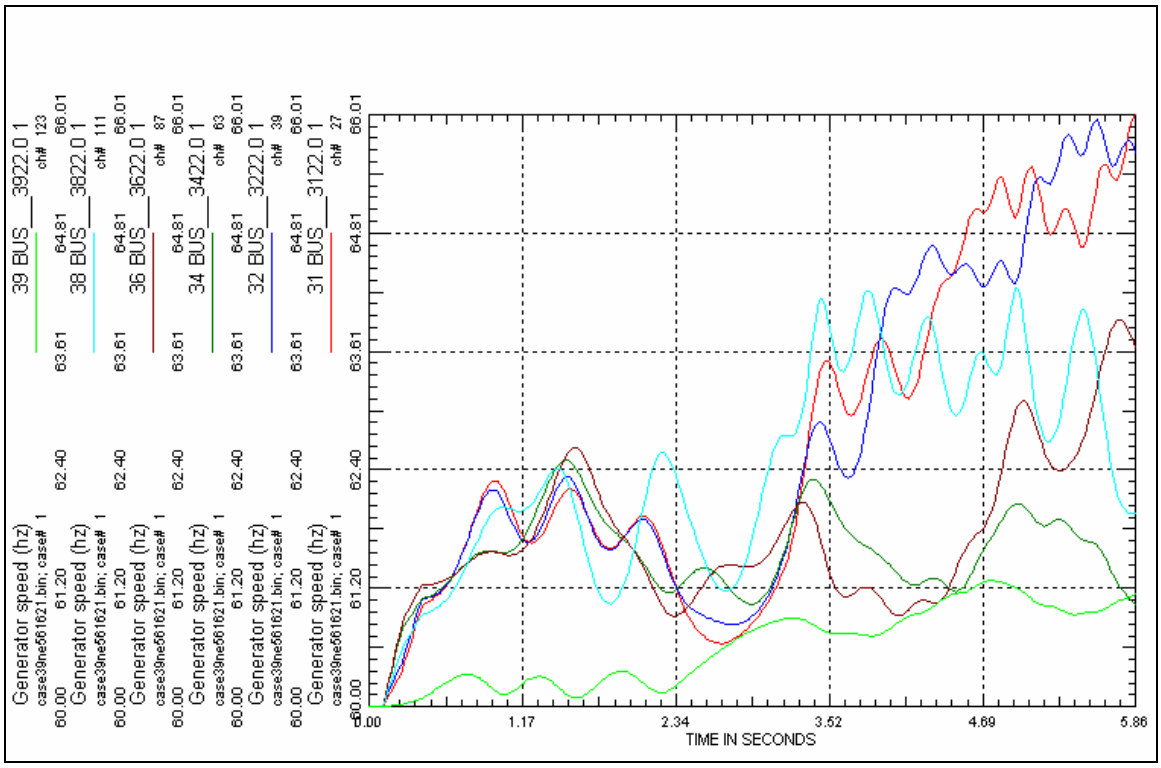

Figure 6.21: Generators Speed

Figure 6.22 shows the plot of the apparent resistance for the tie-lines 1-2, 3-18, 4-14, 5-8, 16-19 and 17-27. By monitoring the rate of change of the apparent resistance of these tie-lines the controlled islanding strategy could be deployed by the IPRs.

Initially, due to the three phase fault at bus 16, the rate of change of the apparent resistance of almost all lines monitored is small. However, at this particular point the magnitude of the line's apparent impedance is still large; hence the out-of-step blocking and tripping functions are not active. This condition of islanding is obtained a few milliseconds later (at approximately 0.78 seconds), as shown in Figure 6.21. Consequently, the islands are formed by opening the lines 1-2, 9-39, 13-14, 16-24, 17-18 and 17-27 at 0.88 seconds. Table 6.8 shows the initial generator-load imbalance obtained through the DE optimization process for the case. Figure 6.23 shows the final configuration of the islands.

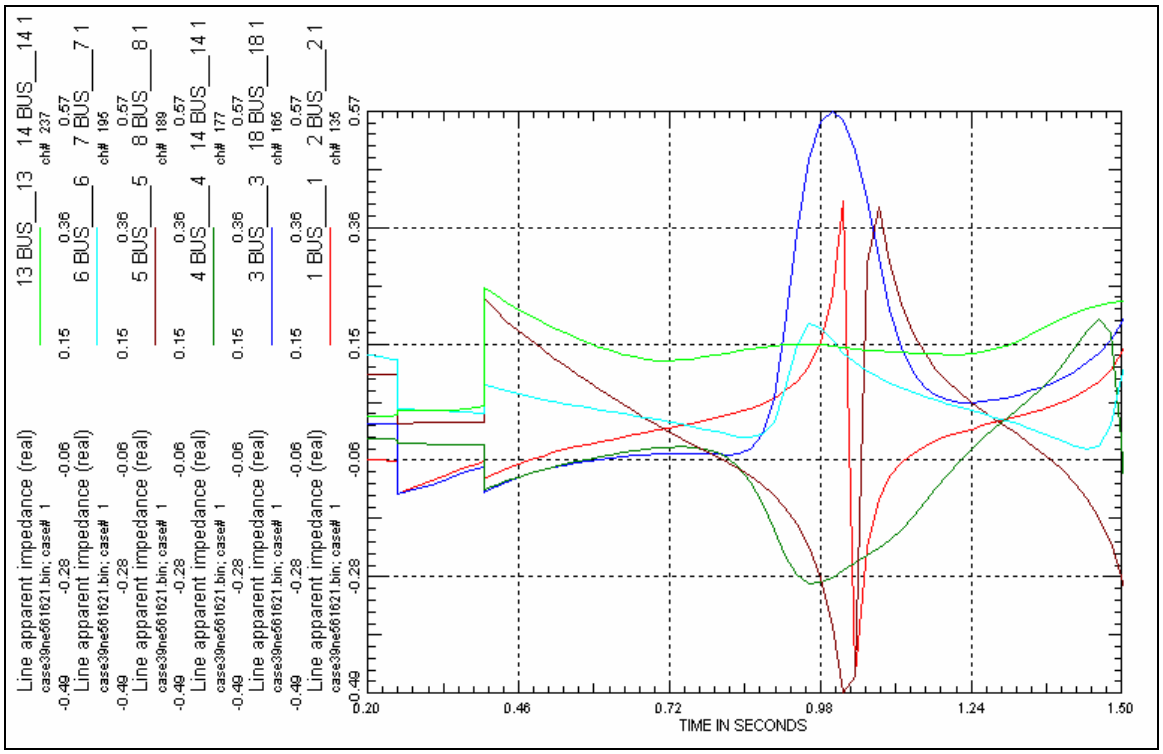

Figure 6.22: Lines Apparent Resistance

TABLE 6.8
INITIAL GENERATOR-LOAD IMBALANCE

Group	P_G	P_L (MW)	Difference	Q_G	Q_L (MVAR)	Difference
1	1140.0	1277.0	137.0	275.7	288.3	12.6
2	2747.1	2886.0	138.9	572.8	763.2	190.4
3	1210.0	830.1	379.9	313.6	107.4	206.2
4	1000.0	1104.0	104.0	88.3	250.0	161.7

Figure 6.24 shows the generators speed after islanding. By applying the proposed controlled islanding scheme the system remains stable after the occurrence of the disturbances. The proposed undefrequency and undervoltage load shedding schemes drop a total of 870.14 MW and 201.49 MVAR of the load. As the previous case, none of the generators returns to nominal speed after islanding, hence some other control actions must be necessary to restore the nominal frequency of the islands.

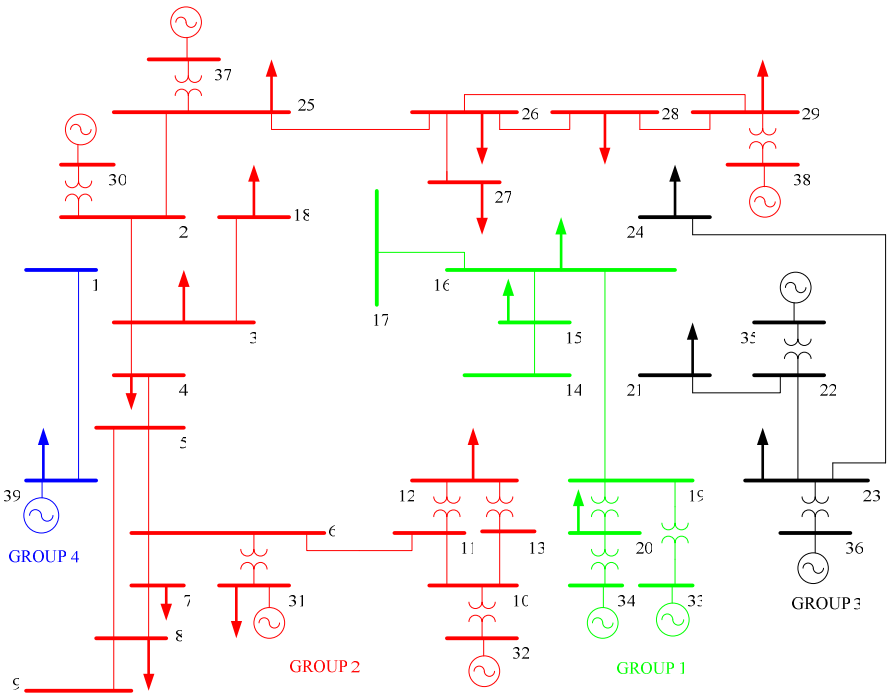

Figure 6.23: Final Configuration of the Islands

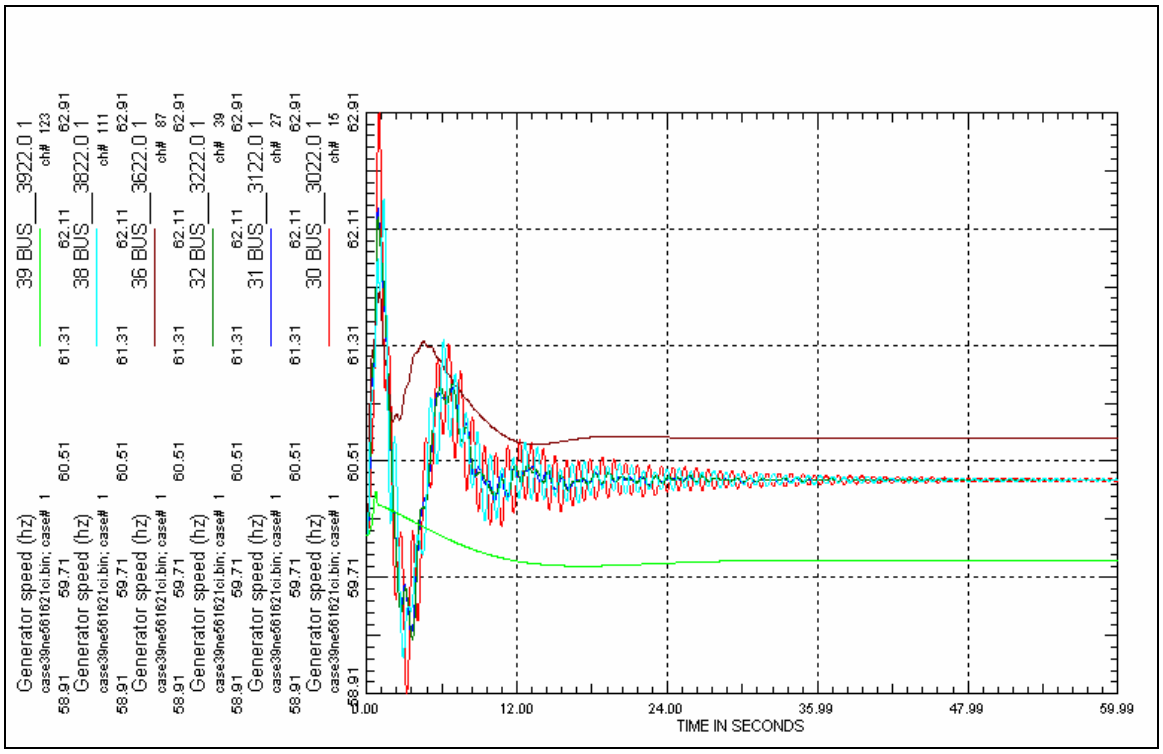

Figure 6.24: Generators Speed after Islanding

6.5.1 C: Summary of Results New England 39-Bus Test System

Table 6.9 gives the summary of results of the simulation performed in the New England 39 Bus – 10 Generators test system. The proposed controlled islanding scheme helps to the system to remain stable in a degraded mode after the occurrence of the disturbances.

TABLE 6.9
REAL AND REACTIVE POWER SHED FOR THE NEW ENGLAND 39-BUS TEST SYSTEM

Fault on lines	Real Power Shed (MW)	Reactive Power Shed (MVAR)	%P Total	%Q Total
16 - 21	978.3	247.1	16.05%	17.54%
16 - 21 / 17 - 18	1003.35	259.26	16.46%	18.40%
5 - 6 / 16 - 21	870.14	201.49	14.27%	14.30%
28 - 29	604.26	110.23	9.91%	7.82%
4 - 5 / 28 - 29	213.73	34.54	3.51%	2.45%
2 - 25 / 19 - 33	1216.02	237.46	19.94%	16.85%

As shown in the table, the most severe contingency was in which simultaneous faults on lines 2-25 and 19-33 occur. Due to unbalances within the islands, 19.94% of the real power demanded has to be shed in order to avoid the complete collapse of the system.

6.5.2 WSCC 179-Bus Test System

To test the capability of the proposed controlled islanding scheme in more realistic scenarios, the WSCC 179-Bus test system was used as a test case system. Figure 6.25 presents the schematic of the test system.

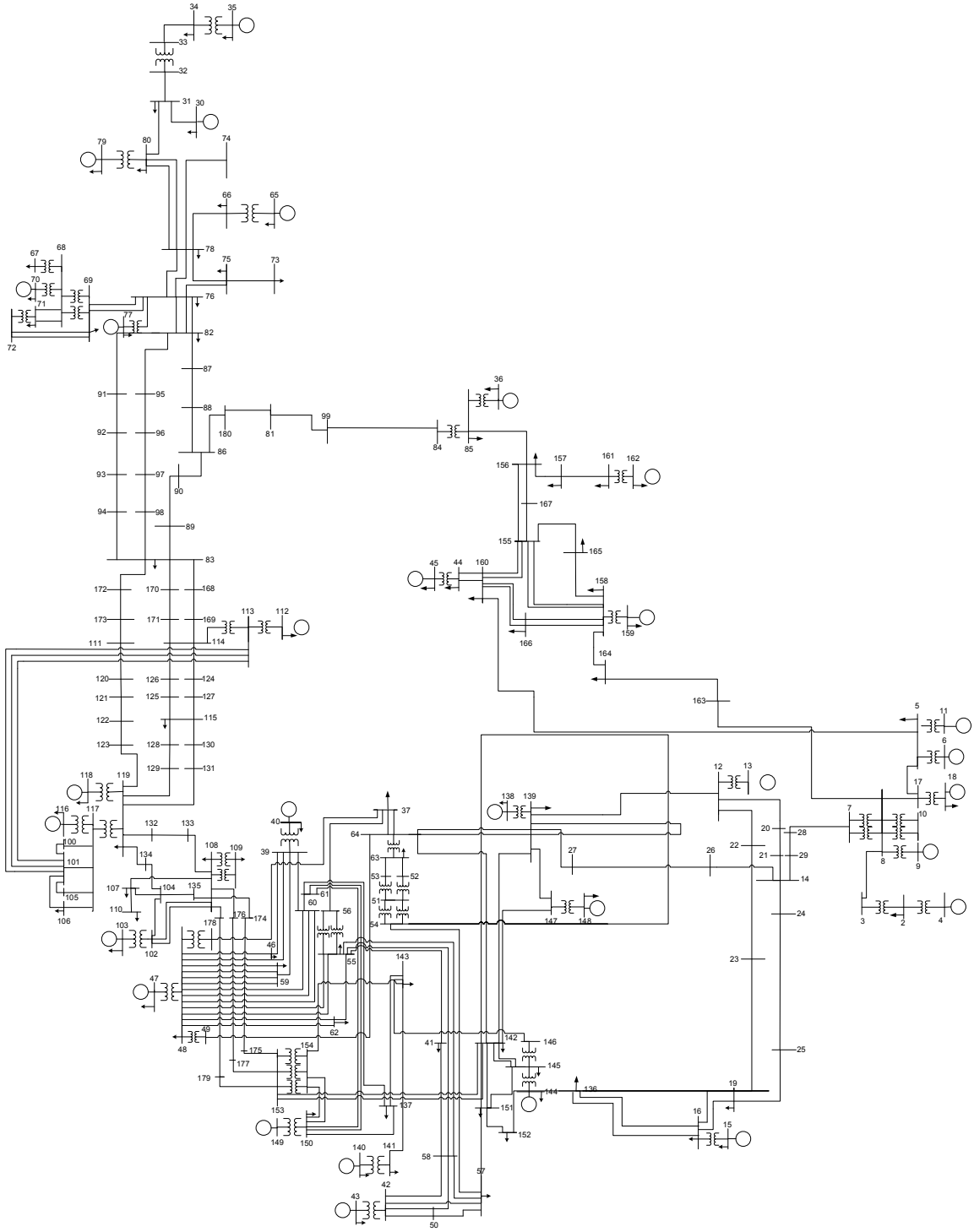

Figure 6.25: WSCC 179-Bus Test System

6.5.2 A: Fault on Buses 83, 170 and 172.

In the first case, three 500-kV transmission lines placed in the west part of the system are tripped simultaneously. The sequence of the events used in simulations was:

- At 0.1 seconds a three phase fault occurred in bus 83. The fault is cleared at 0.25 seconds by opening the line 83-168.
- At 0.26 seconds another three phase fault and a double line to ground fault occurred in buses 170 and 172, respectively. These faults are also cleared at 0.41 seconds by removing the lines 83-170 and 83-172.

Figure 6.26 presents a snapshot of the system in the area of the analysis. Simulations conducted on the system indicate that this disturbance will result in the system being unstable. In this case, generators at buses 36, 65 and 162 lose their synchronism, as shown in Figure 6.27 (generators relative angles) y Figure 6.28 (generators speed) for this particular disturbance.

At 0.55 seconds the lines apparent impedance enter into the operating characteristic of the distance relays, as shown in Figure 6.29, and the speed of generator connected at bus 36 exceed 62 Hz. Hence, the conditions for islanding are reached at this point.

In this case, based on the slow coherency generators grouping, the system was separated into 5 different islands by removing the lines 12-20, 12-22, 16-19 I, 16-19 II, 27-139, 31-32, 66-78 and 85-156 at 0.65 seconds, as shown in Figure 6.30. Table 6.10 shows the initial generation-load imbalance for the islands, obtained by solving the system splitting problem with the Differential Evolution algorithm.

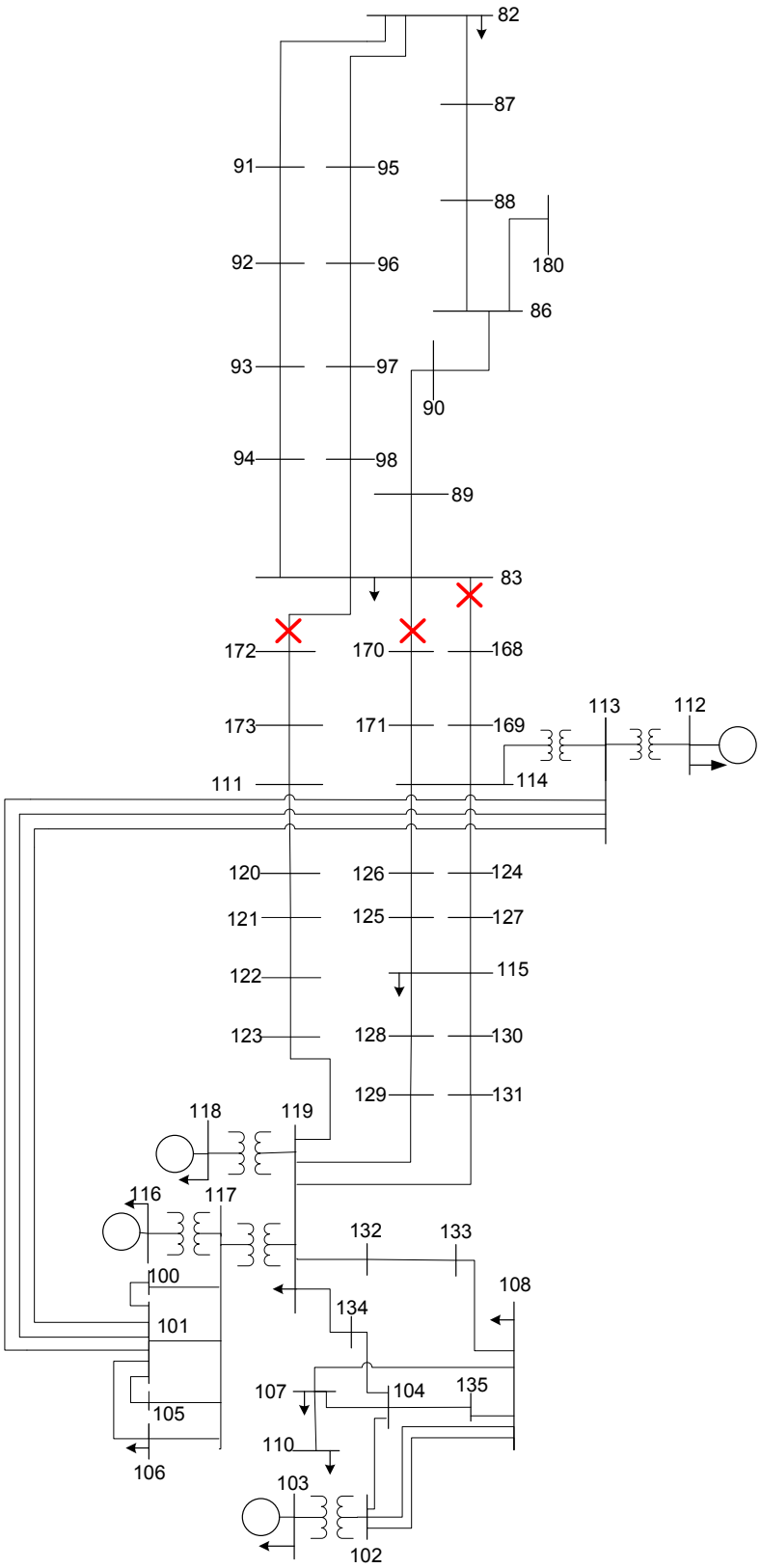

Figure 6.26: Fault Locations in the WSCC 179-Bus Test System

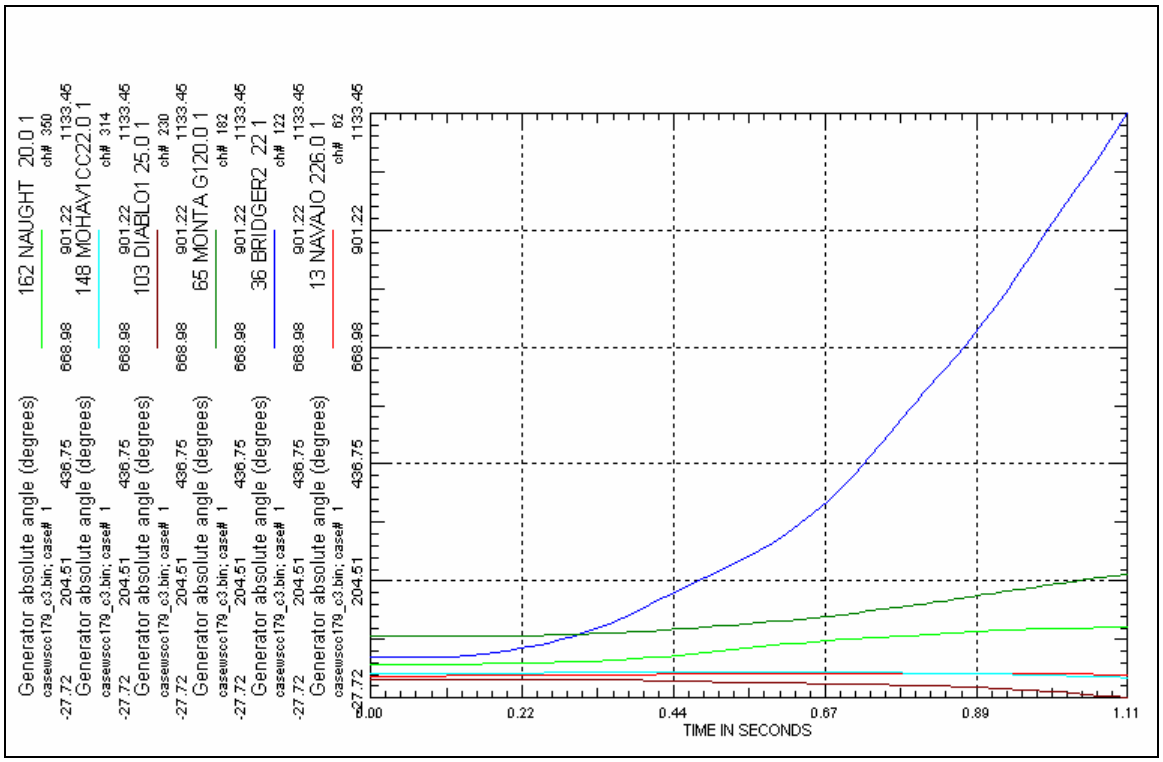

Figure 6.27: Generators Relative Angles

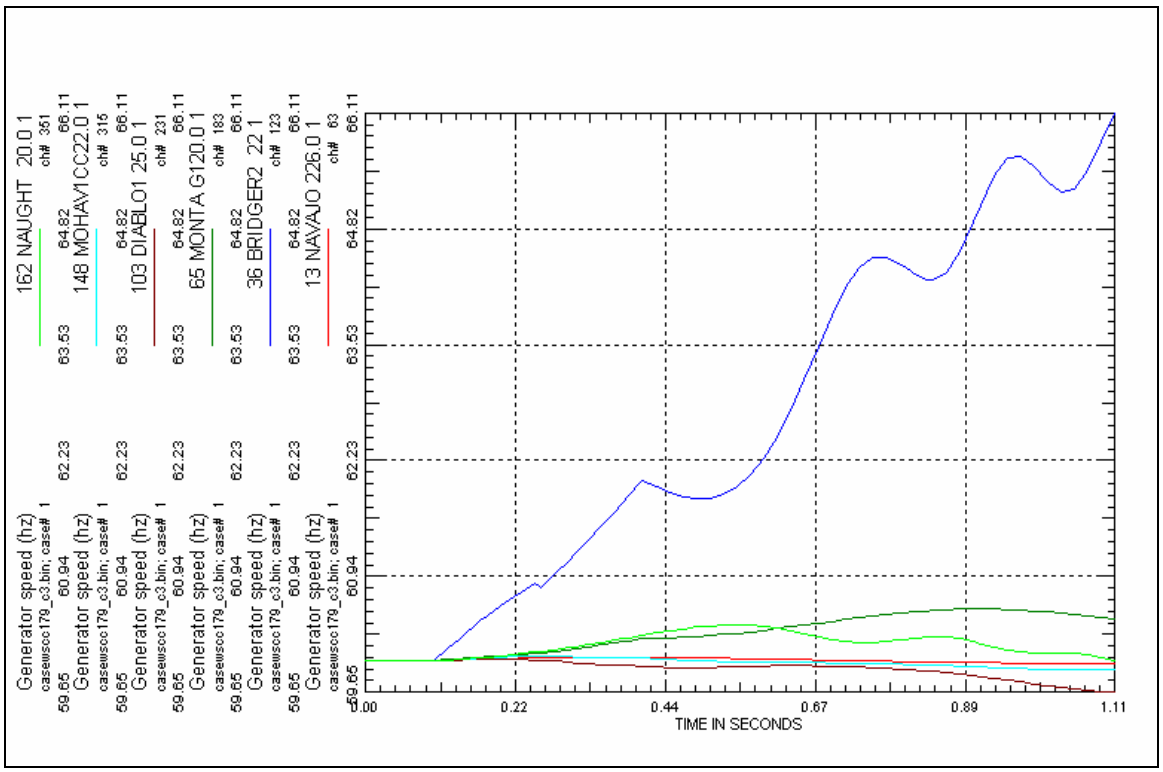

Figure 6.28: Generators Speed

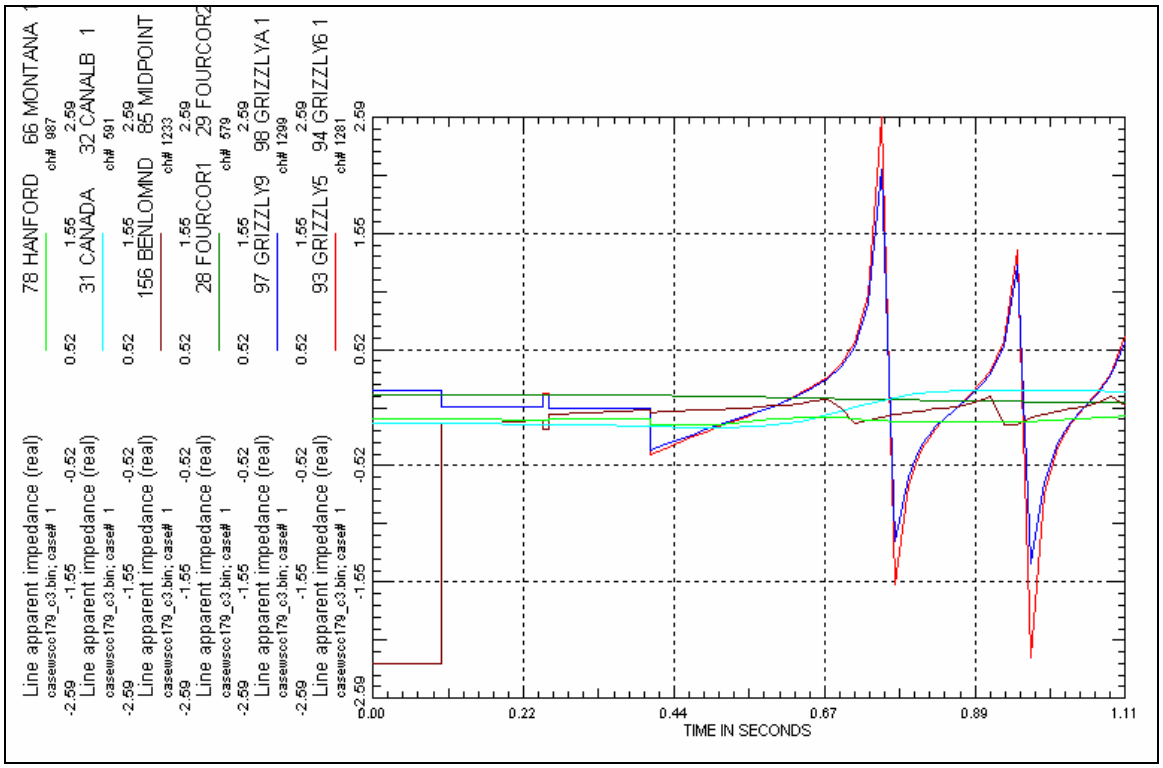

Figure 6.29: Lines Apparent Resistance

TABLE 6.10
INITIAL GENERATOR-LOAD IMBALANCE

Group	P_G	P_L (MW)	Difference	Q_G	Q_L (MVAR)	Difference
1	4480.0	3700.0	780.0	1150.1	700.0	450.1
2	2910.0	1800.0	1110.0	952.7	300.0	652.7
3	22515.0	21049.0	1465.9	4433.1	4608.3	175.2
4	10910.0	10474.0	435.8	1168.1	983.2	184.9
5	20596.0	23763.0	3166.8	4621.5	8759.8	4138.3

Figure 6.31 shows the generators speed after islanding. By applying the proposed controlled islanding scheme the system remains stable after the occurrence of this set of disturbances. The underfrequency and undervoltage load shedding schemes drop a total of 4,611.95 MW and 5,286.81 MVAR of the load.

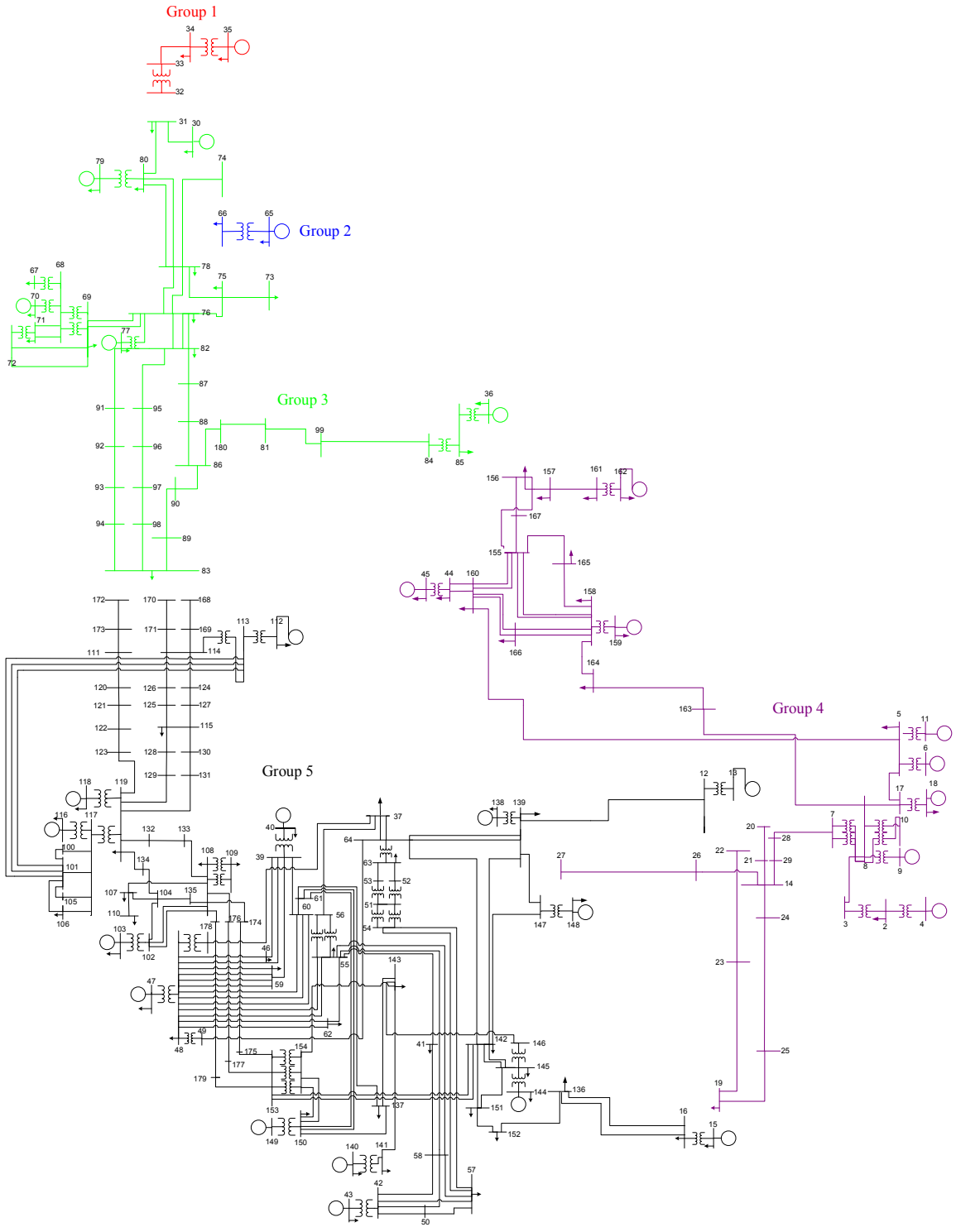

Figure 6.30: Final Configuration of the Islands

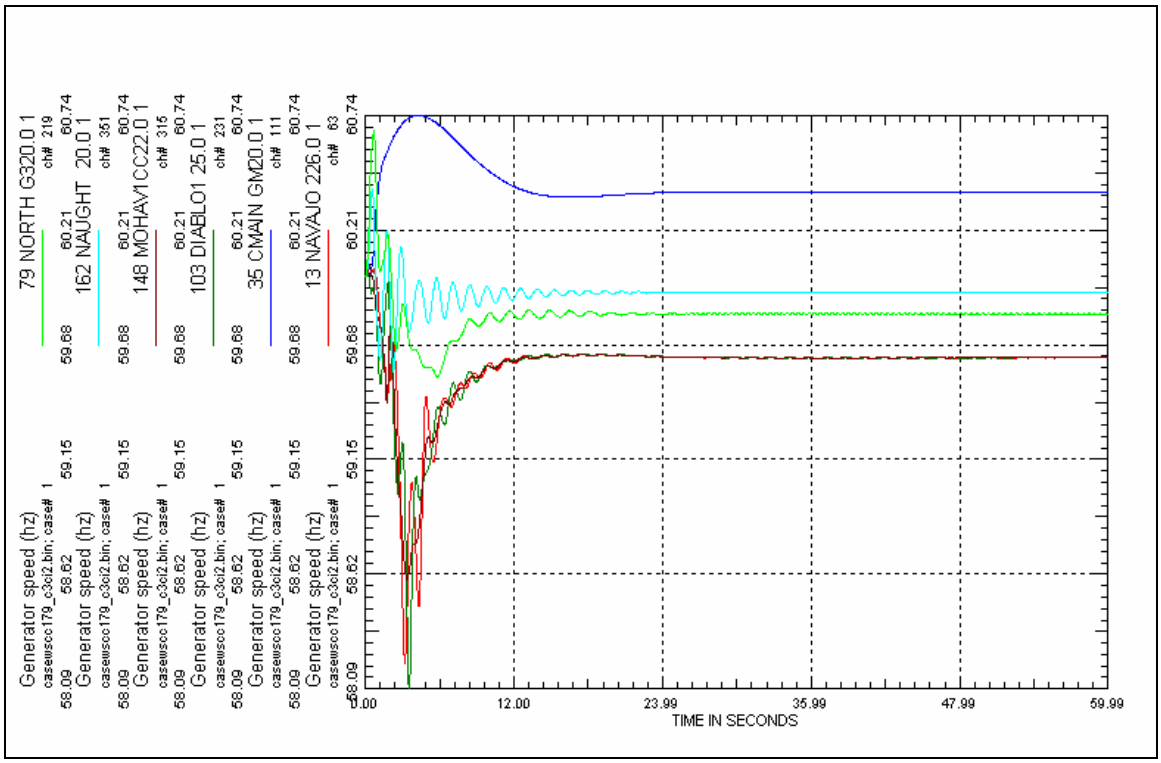

Figure 6.31: Generators Speed after Islanding

6.5.2 B: Fault on Buses 83, 170 and 172.

Finally, an extreme severe contingency was analyzed. In this case, four lines of the eastern part of the system are tripped simultaneously. The sequence of the events used in simulations was:

- At 0.10 seconds a three phase and a double ground to fault occur in buses 12 and 136, respectively, as shown in Figure 6.32. These faults are cleared 0.15 seconds later by removing the lines 12-139, 16-136 I and 16-136 II.
- At 0.26 seconds another three phase fault occurs, in this case in bus 27. The fault is cleared at 0.41 seconds by removing the lines 27-139.

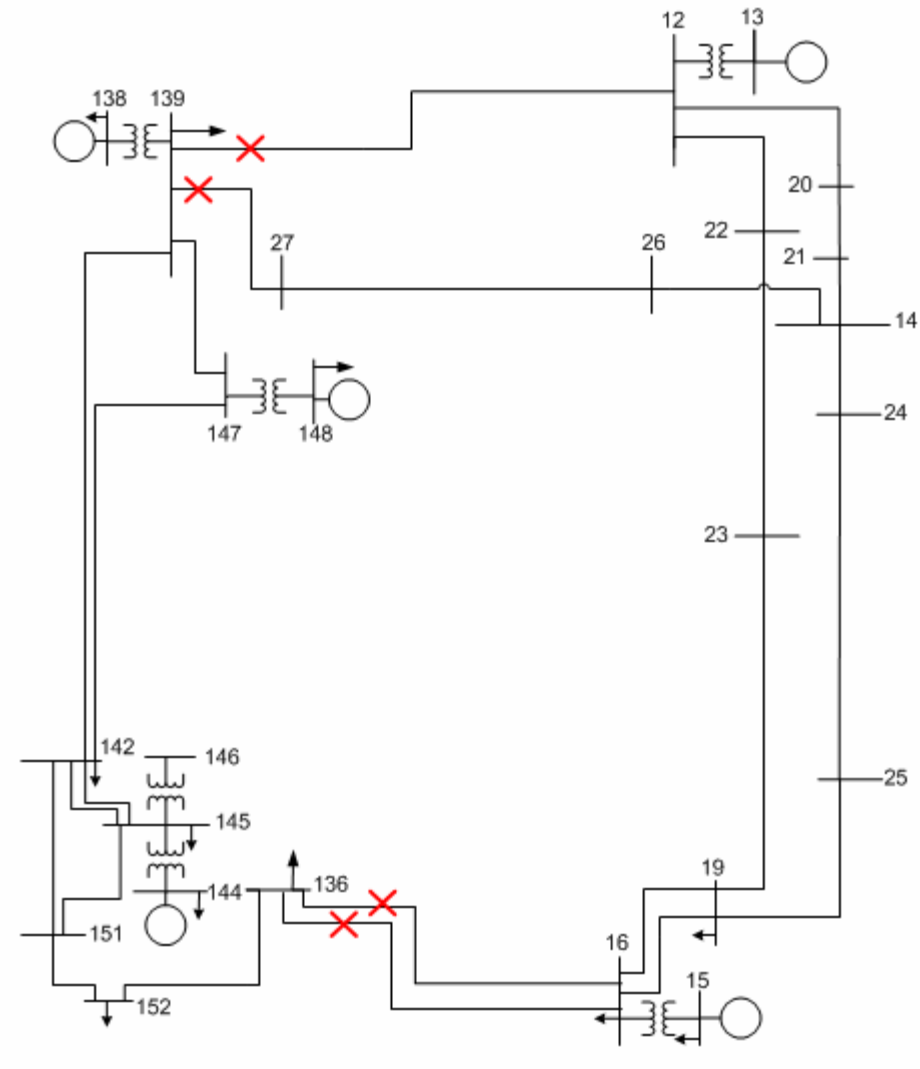

Figure 6.32: Fault Locations in the WSCC 179-Bus Test System

Simulations conducted demonstrated that, after the occurrence of these disturbances, generators at buses 4, 36, 112 and 162 lose their synchronism, as shown in Figures 6.33 and 6.34. As a result of these disturbances, large oscillations in the frequency of generators are observed; even in those generators placed the western part of the system (generators at buses 65, 103 and 112).

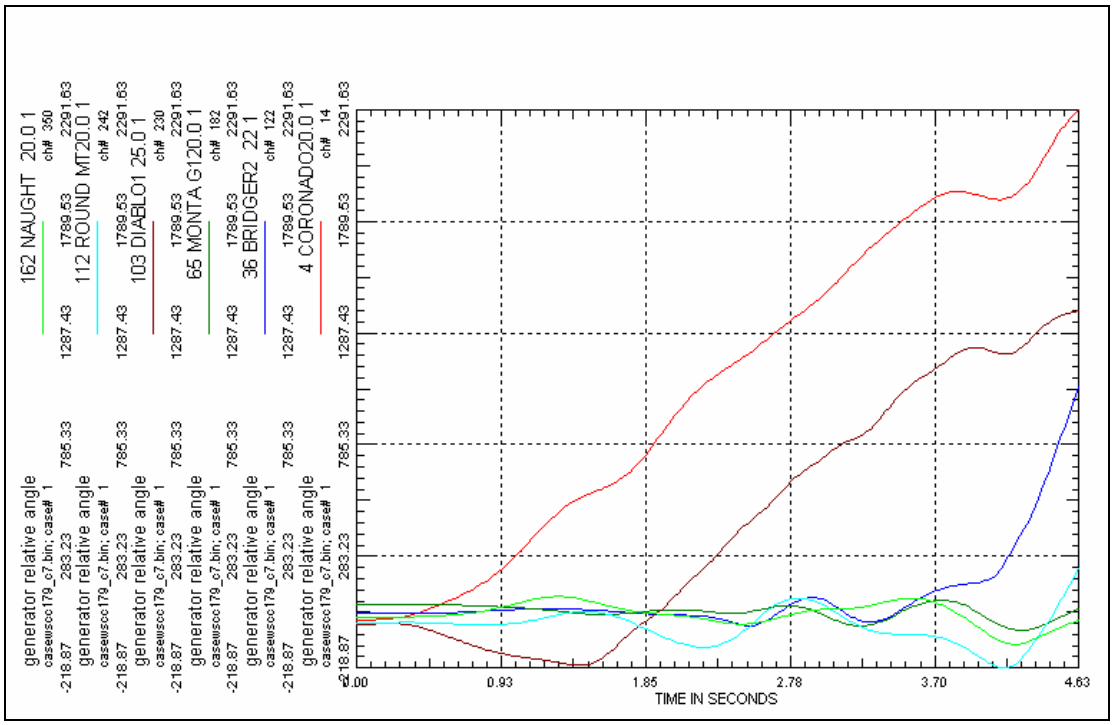

Figure 6.33: Generators Relative Angles

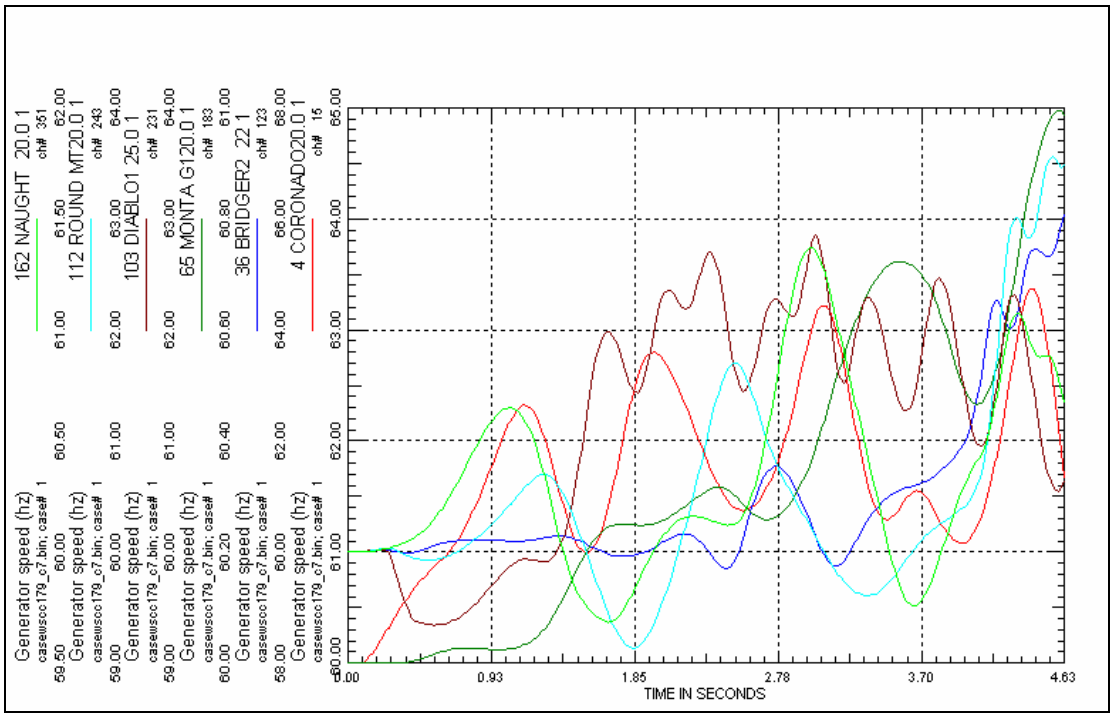

Figure 6.34: Generators Speed

As shown in the Figure 6.35, after the occurrence of the faults there is a rapid change in the apparent resistance of the monitored lines. However, at approximately 0.52 seconds small changes apparent resistance of the lines 5-17 and 158-164 are detected. When the apparent impedance of those lines enters in the operating characteristic of the distance relays, the conditions of islanding are reached at this point.

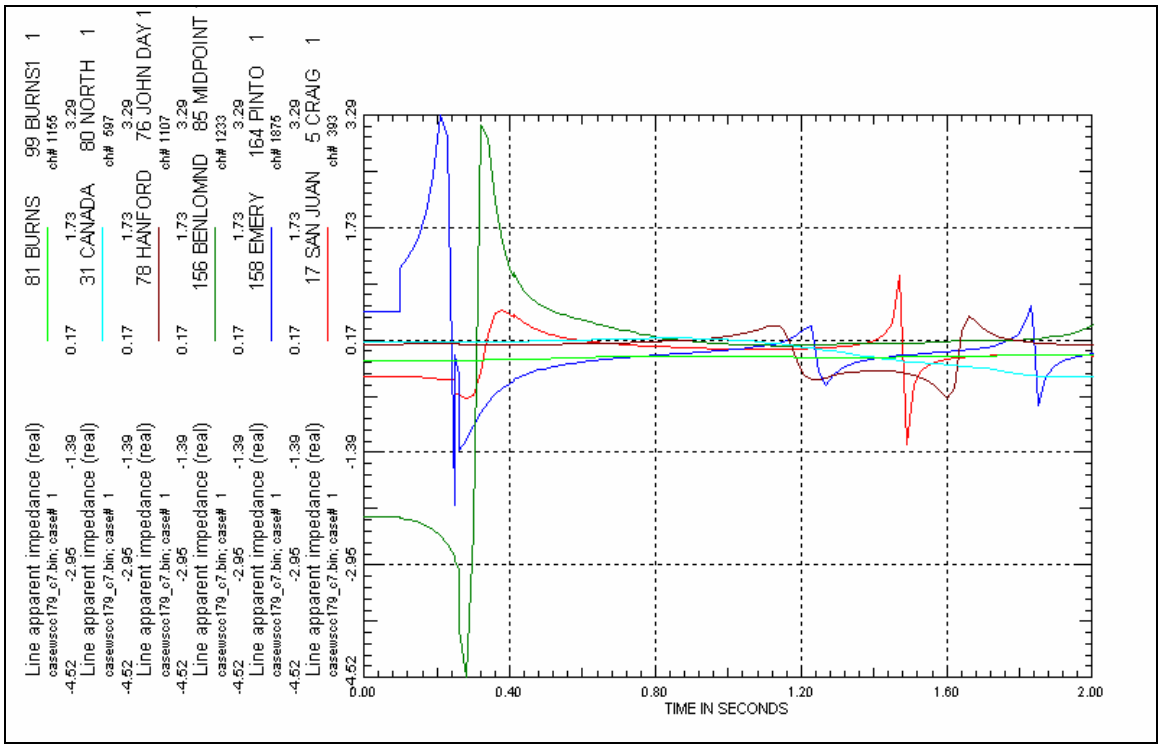

Figure 6.35: Lines Apparent Resistance

Based in the slow coherency generators grouping algorithm, the system was divided in six different islands. The Differential Evolution algorithm solves effectively the system splitting problem for this particular case. The generator-load imbalance of the groups formed is shown in Table 6.11. The islands are formed at 0.62 seconds by tripping the lines 5-17, 31-80, 76-82 (I, II and III), 85-156, 108-133, 119-134 and 158-164, as shown in Figure 6.36.

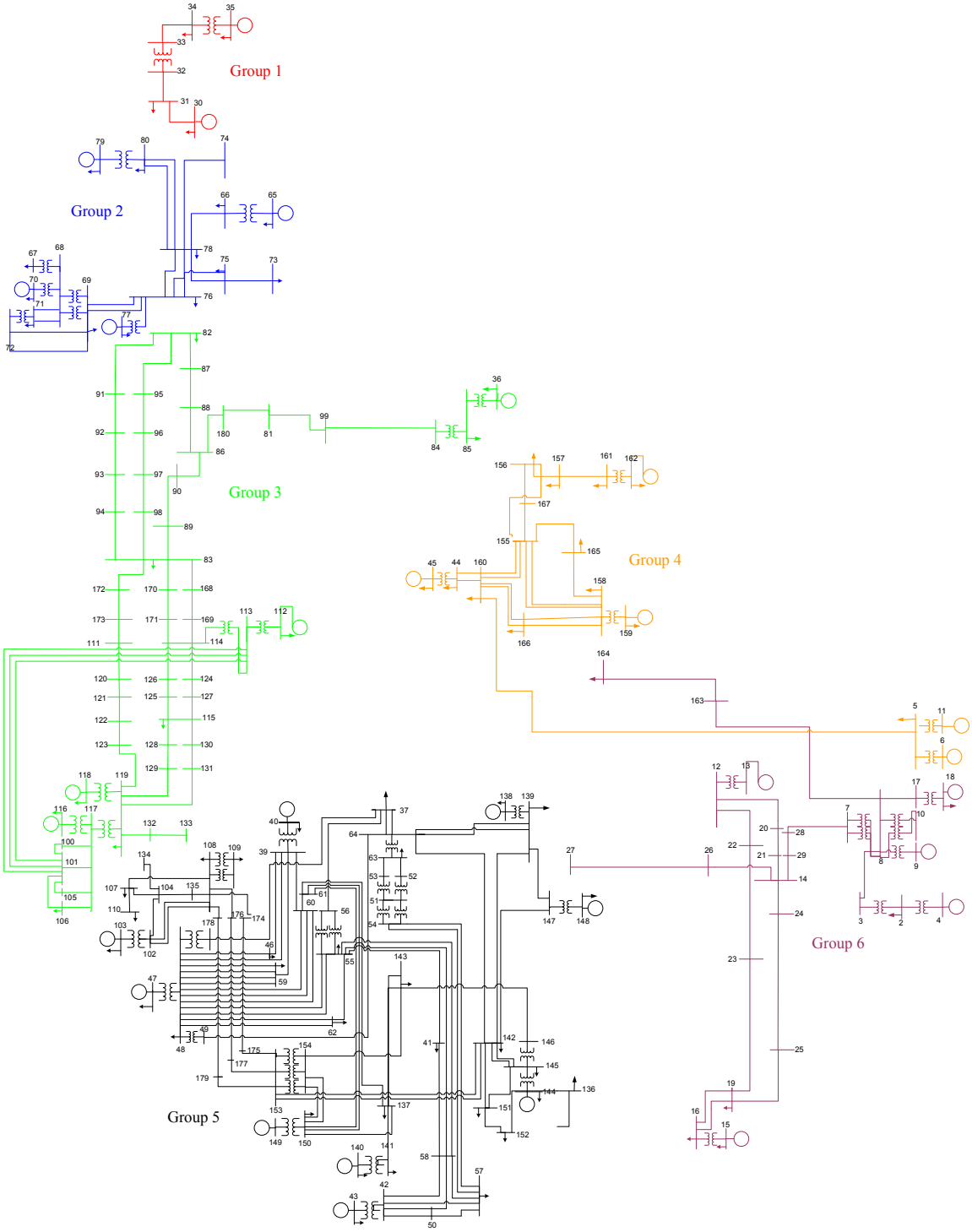

Figure 6.36: Final Configuration of the Islands

TABLE 6.11
INITIAL GENERATOR-LOAD IMBALANCE

Group	P_G	P_L (MW)	Difference	Q_G	Q_L (MVAR)	Difference
1	8930.0	8200.0	730.0	2161.0	1700.0	461.0
2	19335.0	18044.0	1290.3	4089.4	4538.3	448.9
3	6758.0	7615.3	857.3	2156.5	3031.1	874.6
4	6988.0	6556.9	431.1	926.9	1123.9	197.0
5	11148.0	15368.0	4220.5	2176.4	4821.7	2645.3
6	8252.0	5000.7	3251.3	815.3	136.3	679.0

Figure 6.37 shows the generators speed after islanding. By applying the proposed controlled islanding scheme the system remains stable after the occurrence of the disturbances. The proposed undefrequency and undervoltage load shedding schemes drop a total of 4,752.09 MW and 4,323.79 MVAR of the load. As the previous cases, none of the generators returns to nominal speed after islanding, hence some other control actions must be necessary to restore the nominal frequency of the islands.

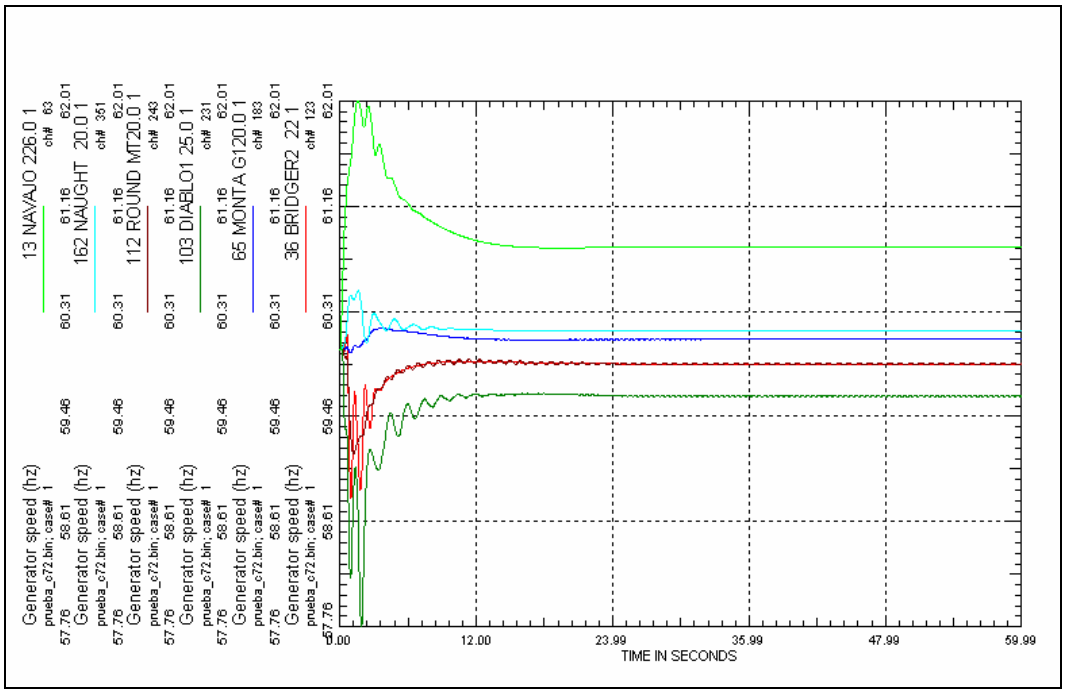

Figure 6.37: Generators Speed after Islanding

6.5.2 C: Summary of WSCC 179-Bus Test System

Table 6.12 gives the summary of results of the simulation performed in the WSCC 179 Bus - 29 Generators test system. The proposed controlled islanding scheme avoids the complete collapse of the system in all case studies, even in those that involve simultaneous faults in multiple locations.

TABLE 6.12
REAL AND REACTIVE POWER SHED FOR THE WSCC 179-BUS TEST SYSTEM

Fault on lines	Real Power Shed (MW)	Reactive Power Shed (MVAR)	%P Total	%Q Total
83 - 168 / 83 - 170	2663.56	4671.26	4.38%	30.43%
83 - 178 / 83 - 170 / 83 – 172	4611.95	5286.81	7.59%	34.44%
12 – 139	2218.8	4107.24	3.65%	26.76%
12 - 139 / 27 - 139	3177.12	4160.49	5.23%	27.10%
13 - 139 / 27 - 139 / 16 - 136 (I)	3083.36	4132.45	5.07%	26.92%
14 - 139 / 27 - 139 / 16 - 136 (I and II)	4752.09	4323.79	7.82%	28.17%

6.6 MODIFICATION OF THE ORIGINAL SIMULATIONS

In order to demonstrate the effectiveness of the proposed controlled islanding scheme in more extreme conditions, the following simulation parameters were modified:

- The underfrequency load shedding scheme.
- The time delay associated to the communication and data processing by the IPRs.
- The load model.

6.6.1: Effect of the Underfrequency Load Shedding Scheme

As explained before, the amount of load shed should be sufficient to restore system frequency to nominal or close to nominal (above 59 Hz). To accomplish this, it would mean the load that is shed should nearly equal the amount of overload.

In the original load shedding scheme applied, in order to restore the system frequency rapidly, large amounts of load are shed in the first three stages. This scheme was modified by changing the percentage of load shed in each stage, as shown in Table 6.13. In all cases the underfrequency load shedding scheme provides the capability to drop up to 50% of the load.

TABLE 6.13
MODIFICATIONS OF THE UNDERFREQUENCY LOAD SHEDDING SCHEME

Frequency Hz	Base Case % Load Shed	LS2 % Load Shed	LS3 % Load Shed	LS4 % Load Shed	LS5 % Load Shed
59.5	15	10	5	0	0
59.3	10	15	15	15	10
58.8	10	10	10	10	10
58.6	8	7.5	7.5	10	15
58.3	7	7.5	7.5	15	15

6.6.1 A: Results on the New England 39-Bus Test System

Table 6.14 and Figure 6.38 show the effect of these modifications on the real and reactive power shed of the New England 39-bus test system.

TABLE 6.14
EFFECT OF THE LOAD SHEDDING SCHEME ON THE NEW ENGLAND 39-BUS TEST SYSTEM

Lines Opened	Base		LS2		LS3		LS4		LS5	
	P_{shed}	Q_{shed}	P_{shed}	Q_{shed}	P_{shed}	Q_{shed}	P_{shed}	Q_{shed}	P_{shed}	Q_{shed}
16 - 21	978.3	247.1	978.3	247.1	904.5	225.7	733.0	182.2	531.2	131.1
16 - 21 / 17 - 18	1003.4	259.3	1002.6	259.1	962.1	242.3	1015.8	261.9	901.0	224.8
5 - 6 / 16 - 21	870.1	201.5	806.5	174.7	620.1	126.0	508.6	104.8	454.0	95.8
28 - 29	604.3	110.2	549.0	97.7	494.3	85.3	608.4	110.9	553.2	98.4
4 - 5 / 28 - 29	213.7	34.5	213.7	34.6	175.1	28.3	136.4	22.1	91.0	14.7
2 - 25 / 19 - 33	1216.0	237.5	1002.3	185.2	814.4	141.1	913.1	157.9	831.8	136.6

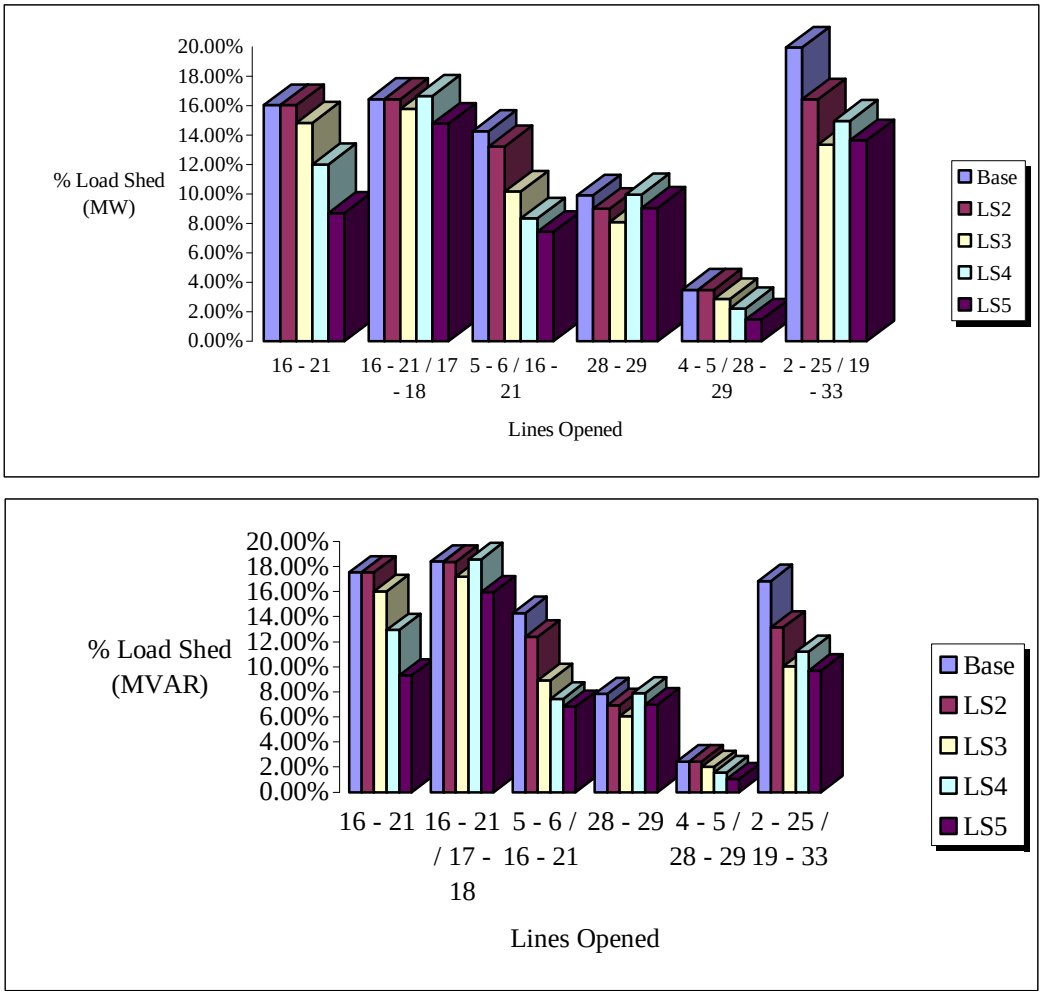

Figure 6.38: Real and Reactive Power Shed by the New Load Shedding Schemes

6.6.1 B: Results on the WSCC 179-Bus Test System

Table 6.15 and Figure 6.39 show the effect of the modifications of the load shedding scheme on the real and reactive power shed of the WSCC 179-bus test system.

Is interesting to observe from the graphics that, in general, the amount of load shedding decreases when reduces the percentage of load shedding in the first stages. In some cases, the percentage of load shedding increases, due to the complex interactions between the generators and their controls.

TABLE 6.15
EFFECT OF THE LOAD SHEDDING SCHEME ON THE WSCC 179-BUS TEST SYSTEM

Lines Opened	Base		LS2		LS3		LS4		LS5	
	P_{shed}	Q_{shed}	P_{shed}	Q_{shed}	P_{shed}	Q_{shed}	P_{shed}	Q_{shed}	P_{shed}	Q_{shed}
83 - 168 / 83 - 170	2663.6	4671.3	3647.6	4784.7	3152.9	4703.9	2192.7	4519.7	3394.1	4658.5
83 - 178 / 83 - 170 / 83 - 172	4612.0	5286.8	4145.6	5146.6	3308.3	4929.7	3546.7	4806.7	3690.0	4782.3
12 - 139	2218.8	4107.2	2209.4	4106.4	2262.0	4010.8	1309.3	3810.5	945.3	3619.1
12 - 139 / 27 - 139	3177.1	4160.5	3050.9	4131.1	2645.7	4039.0	1466.8	3823.3	2462.1	3766.2
13 - 139 / 27 - 139 / 16 - 136 (I)	3083.4	4132.5	3067.6	4131.2	3058.0	4049.9	2104.0	3846.0	1712.3	3652.4
14 - 139 / 27 - 139 / 16 - 136 (I and II)	4752.1	4323.8	4749.5	4323.5	4433.6	4197.3	4190.6	4038.5	3870.5	3832.0

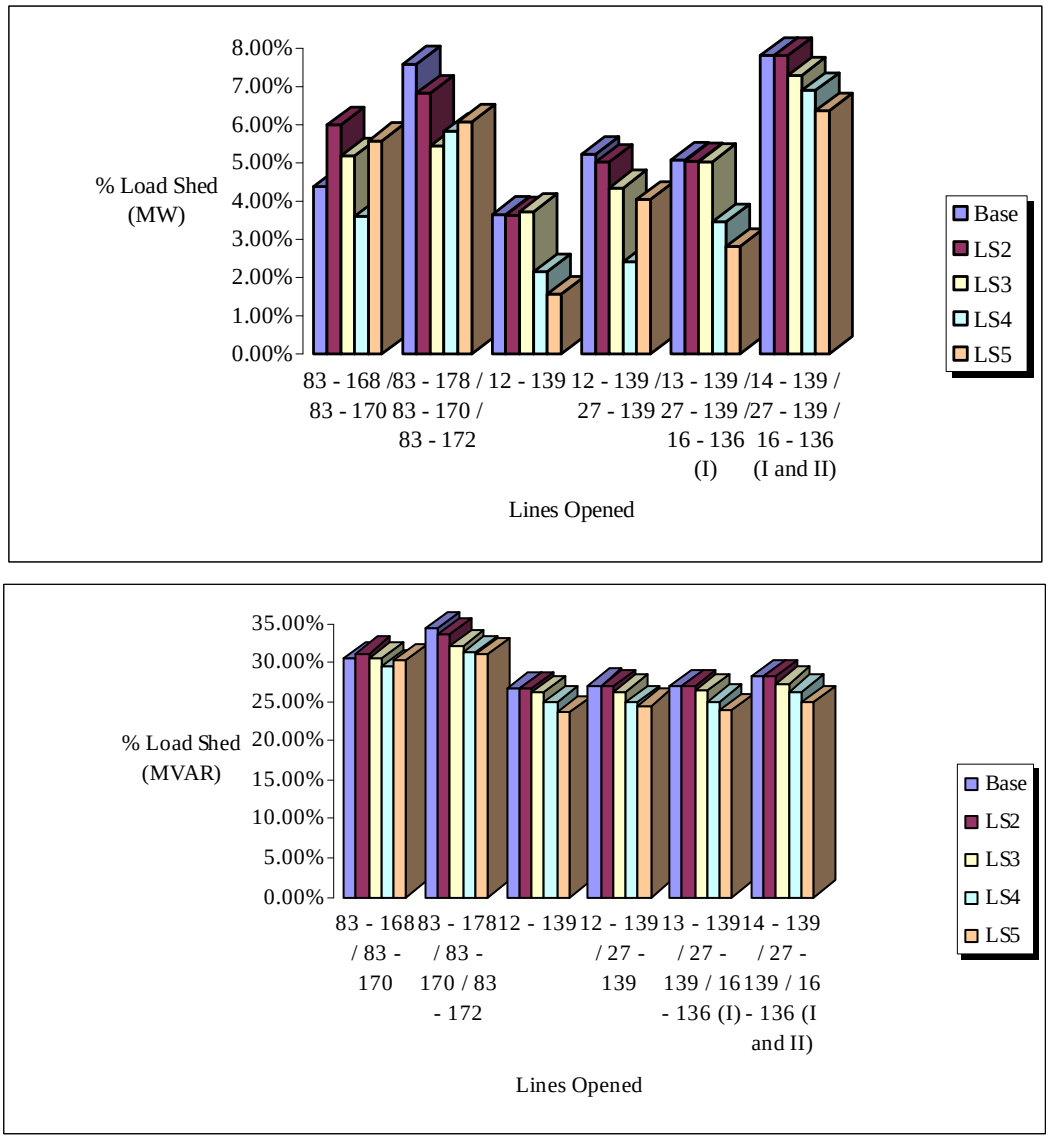

Figure 6.39: Real and Reactive Power Shed by the New Load Shedding Schemes

6.6.2: Effect of the Delay Associated with the Communications and Data Processing

The effectiveness of the controlled islanding scheme depends principally of speed of communication devices and the data processing by the IPRs. The communication delays estimated to various communication links in wide area measurement systems are [109]:

TABLE 6.16
COMMUNICATION DELAYS IN WIDE AREA MEASUREMENT SYSTEMS

Communication Link	Associated Delay (ms)
Fiber optic cables	100-150
Digital microwaves links	100-150
Power line carriers (PLC)	150-350
Telephone lines	200-300
Satellite links	500-700

In the previous simulations, a fixed delay of 100 ms was used for considering the speed of communication devices and the data processing by the IPRs. In order to account more realistic scenarios, this delay was increased in steps of 100 ms, from 100 ms to 500 ms.

6.6.2 A: Results on the New England 39-Bus Test System

Table 6.17 and Figure 6.40 show the effect of the modifications of the delay associated to the communication links and data processing, on the real and reactive power shed of the New England 39-bus test system.

TABLE 6.17
EFFECT OF THE COMMUNICATION DELAYS ON THE NEW ENGLAND 39-BUS TEST SYSTEM

Lines Opened	Base		CTD2		CTD3		CTD4		CTD5	
	P_{shed}	Q_{shed}	P_{shed}	Q_{shed}	P_{shed}	Q_{shed}	P_{shed}	Q_{shed}	P_{shed}	Q_{shed}
16 - 21	531.2	131.1	531.2	131.1	556.7	133.5	633.2	148.6	780.4	186.5
16 - 21 / 17 - 18	901.0	224.8	1059.5	255.5	1296.8	327.5	1195.1	237.9	1594.8	406.4
5 - 6 / 16 - 21	454.0	95.8	242.6	54.8	242.6	54.8	271.0	57.5	333.6	69.5
28 - 29	553.2	98.4	442.9	80.1	553.2	98.4	553.2	98.4	553.2	98.4
4 - 5 / 28 - 29	91.0	14.7	91.0	14.7	91.0	14.7	91.0	14.7	91.0	14.7
2 - 25 / 19 - 33	831.8	136.6	1117.6	224.4	1171.5	242.6	1171.5	242.6	1171.5	242.6

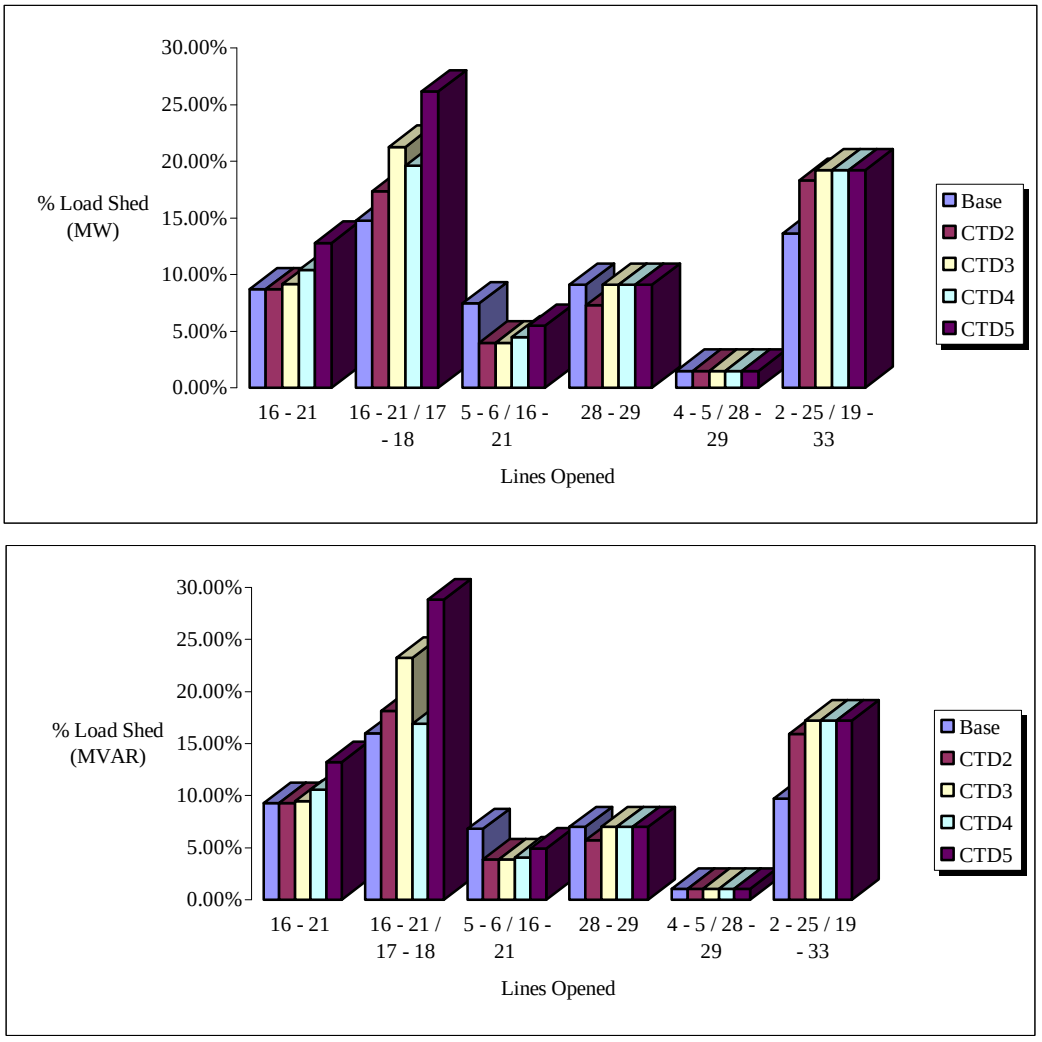

Figure 6.40: Real and Reactive Power Shed by Different Communication Delays

6.6.2 B: Results on the WSCC 179-Bus Test System

Table 6.18 and Figure 6.41 show the effect of the modifications of the delay associated to the communication links and data processing, on the real and reactive power shed of the WSCC 179-bus test system.

TABLE 6.18
EFFECT OF THE COMMUNICATION DELAYS ON THE WSCC 179-BUS TEST SYSTEM

Lines Opened	Base		CTD2		CTD3		CTD4		CTD5	
	P_{shed}	Q_{shed}	P_{shed}	Q_{shed}	P_{shed}	Q_{shed}	P_{shed}	Q_{shed}	P_{shed}	Q_{shed}
83 - 168 / 83 - 170	2663.6	4671.3	3996.5	4808.9	4733.8	5167.2	4733.8	5167.2	4733.8	5167.2
83 - 178 / 83 - 170 / 83 - 172	4612.0	5286.8	3770.8	4788.2	3663.7	4776.1	4100.4	4853.3	3674.6	4779.8
12 - 139	2218.8	4107.2	945.3	3619.1	945.3	3619.1	945.3	3619.1	1517.3	3657.9
12 - 139 / 27 - 139	3177.1	4160.5	2474.3	3766.2	2548.4	3715.9	1574.0	3649.2	4255.9	4676.4
13 - 139 / 27 - 139 / 16 - 136 (I)	3083.4	4132.5	3147.4	3735.3	3229.5	3737.7	2454.5	3787.5	4683.1	4732.6
14 - 139 / 27 - 139 / 16 - 136 (I and II)	4752.1	4323.8	3870.5	3832.0	3852.5	3832.0	3718.9	3782.1	3704.6	3775.7

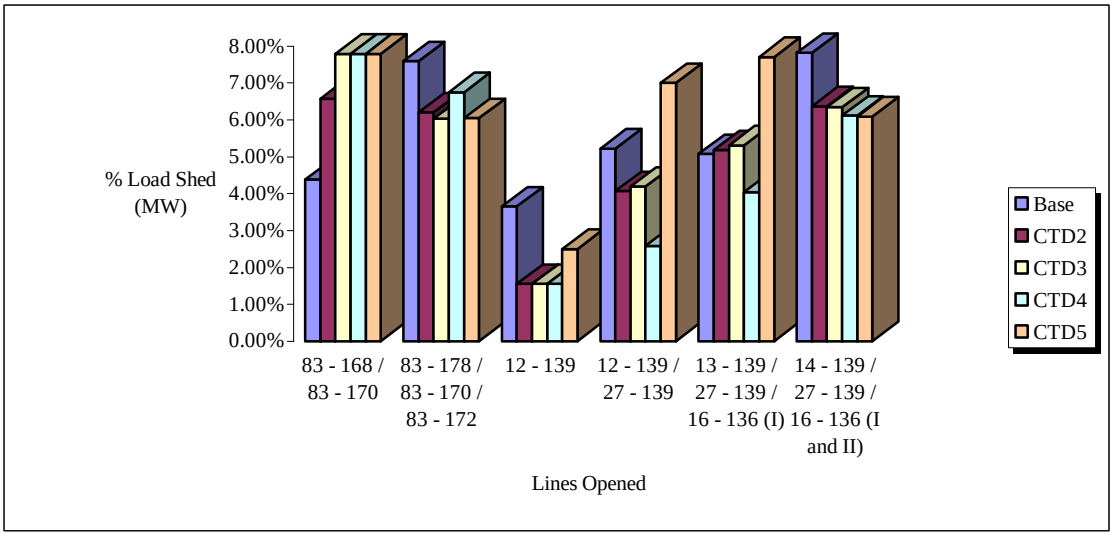

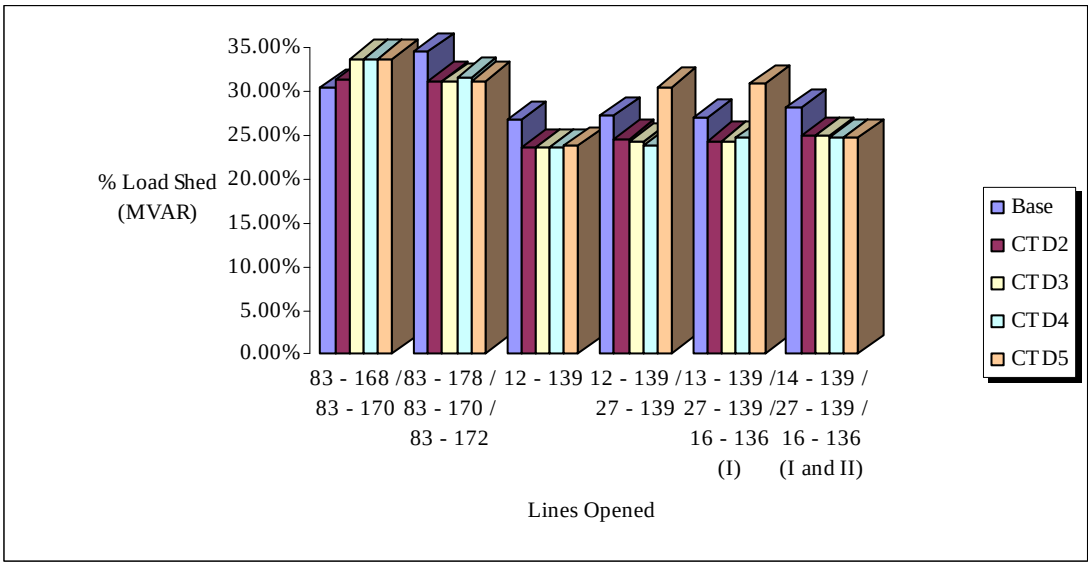

Figure 6.41: Real and Reactive Power Shed by Different Communication Delays

In general, the result of an increased communication delay is an increased amount of real and reactive power shed. However, it is evident that a fast response of the controls and communication devices to major disturbances improves the stability performance of the system.

6.6.3: Effect of the Load Model

Electric loads characteristics play an important role in the power system dynamics. Traditionally, polynomial (ZIP) load models are considered in dynamic simulations. In these models the load could be classified as constant power, constant current, constant impedance or a combination of them depends on the voltage sensitivity of the loads, as shown in (6.18) [110]:

$$P = P_0\left[a_1\left(\frac{V}{V_0}\right)^2 + a_2\left(\frac{V}{V_0}\right) + a_3\right]$$
$$Q = Q_0\left[a_4\left(\frac{V}{V_0}\right)^2 + a_5\left(\frac{V}{V_0}\right) + a_6\right] \qquad (6.18)$$

Where V_0, P_0 and Q_0 are normally taken values at the initial operating conditions. The parameters of this polynomial model are the coefficients a_1 to a_6 and the power factor of the load.

Originally, the constant impedance load model was used in simulations. Other three additional load models were also analyzed in our work, as given in Table 6.19.

TABLE 6.19
MODIFICATIONS OF THE LOAD MODEL

Case Studies	Constant Impedance (Z)		Constant Current (I)		Constant Power (P)	
	P	Q	P	Q	P	Q
Base	100%	100%	-	-	-	-
Model 1	-	100%	100%	-	-	-
Model 2	-	-	100%	100%	-	-
Model 3	30%	30%	40%	40%	30%	30%

6.6.3 A: Results on the New England 39-Bus Test System

Table 6.20 and Figure 6.42 show the effect of the modifications of load model on the real and reactive power shed of the New England 39-bus test system.

TABLE 6.20
EFFECT OF THE LOAD MODEL ON THE NEW ENGLAND 39-BUS TEST SYSTEM

Lines Opened	Base		Model 1		Model 2		Model 3	
	P_{shed}	Q_{shed}	P_{shed}	Q_{shed}	P_{shed}	Q_{shed}	P_{shed}	Q_{shed}
16 - 21	531.2	131.1	517.0	153.3	1223.0	278.9	1431.0	341.9
16 - 21 / 17 - 18	1059.5	255.5	1349.4	333.3	1229.3	314.5	1355.2	329.4
5 - 6 / 16 - 21	242.6	54.8	455.7	105.1	1084.1	247.0	1527.2	409.3
28 - 29	442.9	80.1	553.2	98.4	553.2	98.4	553.2	98.4
4 - 5 / 28 - 29	91.0	14.7	91.0	14.7	91.0	14.7	909.5	147.0
2 - 25 / 19 - 33	1117.6	224.4	1647.9	376.7	1556.1	357.9	1959.3	419.9

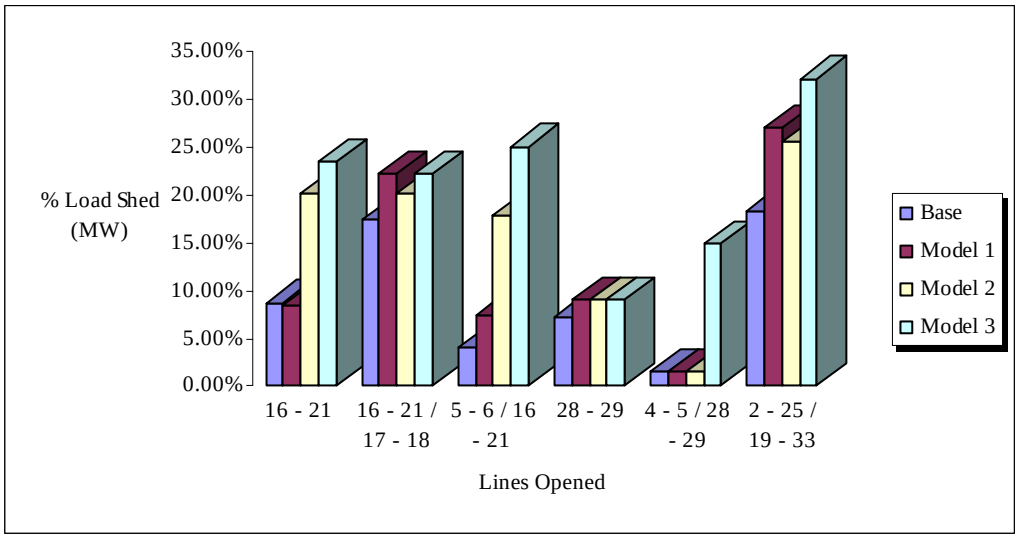

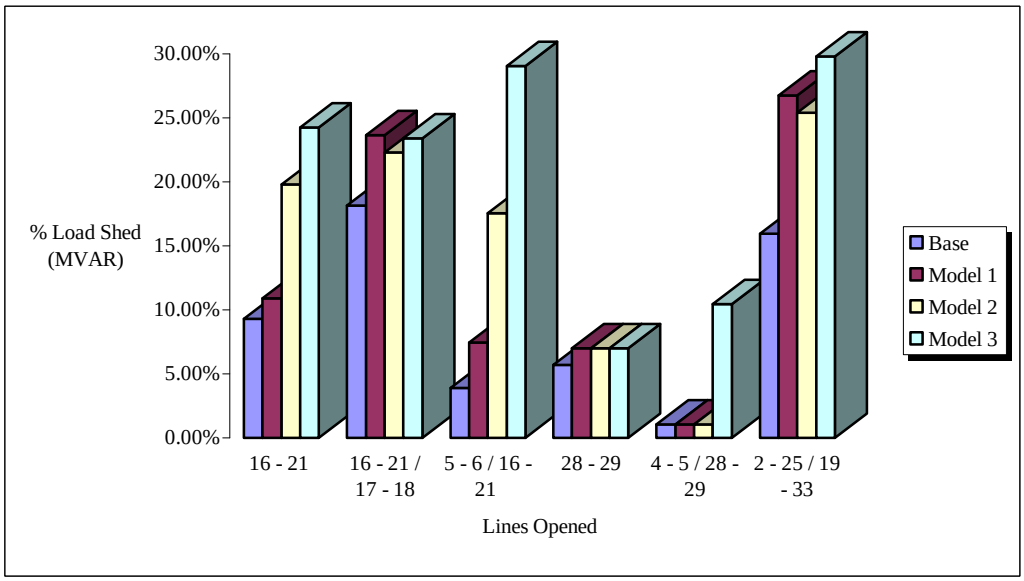

Figure 6.42: Real and Reactive Power Shed by Different Load Models

6.6.3 B: Results on the WSCC 179-Bus Test System

Table 6.21 and Figure 6.43 show the effect of the modifications of load model on the real and reactive power shed of the WSCC 179-bus test system.

TABLE 6.20
EFFECT OF THE LOAD MODEL ON THE WSCC 179-BUS TEST SYSTEM

Lines Opened	Base		Model 1		Model 2		Model 3	
	P_{shed}	Q_{shed}	P_{shed}	Q_{shed}	P_{shed}	Q_{shed}	P_{shed}	Q_{shed}
83 - 168 / 83 - 170	2663.6	4671.3	3209.0	4736.2	3780.8	4835.3	4787.5	4933.4
83 - 178 / 83 - 170 / 83 - 172	4612.0	5286.8	1941.4	4564.7	2049.3	4596.0	2369.3	4718.8
12 - 139	2218.8	4107.2	1507.0	3657.9	1533.7	3657.9	4095.3	3968.2
12 - 139 / 27 - 139	3177.1	4160.5	3852.5	3832.0	4013.9	3839.5	3781.4	3836.3
13 - 139 / 27 - 139 / 16 - 136 (I)	3083.4	4132.5	4592.3	4598.4	4183.0	4260.1	4097.6	4329.7
14 - 139 / 27 - 139 / 16 - 136 (I and II)	4752.1	4323.8	5445.9	4474.5	5077.4	4402.8	5067.0	4402.8

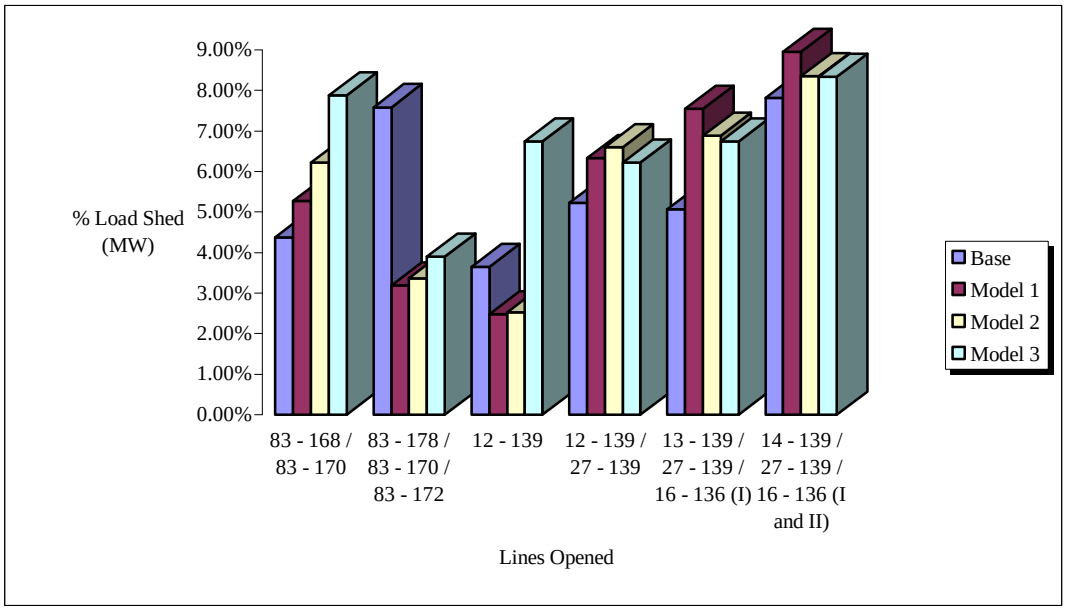

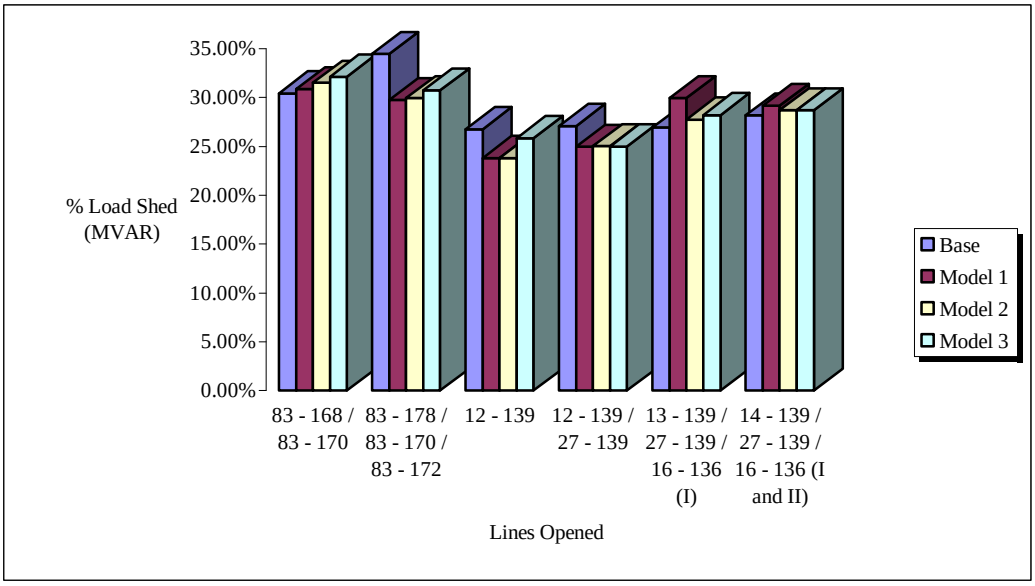

Figure 6.43: Real and Reactive Power Shed by Different Load Models

It is evident that complex load models increase the possibility of collapse of the system in response to major disturbances. In general, composed load models raise the amount of real and reactive power shed through simulations.

6.7 CONCLUSION

Traditionally, power systems have been operated and controlled in a centralized way, and with a considerable amount of human intervention. Under such circumstances, cascading outages may result extremely difficult to prevent or control. In this context, researchers of the University of Puerto Rico at Mayagüez have proposed a distributed and "intelligent" control scheme, the so-called Intelligent Power Routers (IPRs), aimed at minimizing the potential damaging effects that a major disturbance may cause on a power system. One of the potential applications of these intelligent controls is to support a controlled islanding scheme to prevent cascade failures in power systems.

The main objective of the controlled islanding scheme is to properly separate the system into several subsystems of reduced capacity to avoid passive collapse or blackout over the entire system. The basis for forming the islands is to minimize the load–generation imbalance in each island, thereby facilitating the restoration process.

To reduce the amount of inter-area oscillations, asynchronous generators must be separated into different groups or islands. In this case, the slow coherency based generators grouping allows coherency to be examined in terms of the eigenvector matrix of the electromechanical modes.

In the proposed controlled islanding scheme, the selection of the quantities that must be monitored to assess the vulnerability of the system and the coordination with the protection schemes used conventionally are essential to achieve the main objective of the islanding strategy. The islanding mechanism is deployed only if the disturbance potentially affects the synchronism of the generators connected to the system. Hence, some additional protection actions are necessary to avoid incorrect performance of the conventional protection schemes during power swings and out-of-step conditions.

The information exchange capability of the Intelligent Power Routers gives the flexibility to develop an adaptive controlled islanding scheme, which guarantees a better response of the system to large disturbances.

CHAPTER 7

CONCLUSIONS, RECOMMENDATION AND FUTURE WORK

7.1 GENERAL CONCLUSIONS

This thesis has presented a novel optimization technique, the Differential Evolution algorithm, with the intention of solving various complex optimization problems in power systems. In particular, the problems analyzed in our work were the Optimal Reactive Power Planning, Congestion Management in Restructured Power Systems, State Estimation with Phasor Measurement Units, State Estimation with Equality and Inequality Constraints, and the System Splitting Problem for Controlled Islanding.

The DE models developed for solving these problems were successful in finding optimal solutions while providing a good convergence rate. The proposed models were tested in several case studies and the results obtained were compared with those obtained by using other traditional and evolutionary optimization algorithms.

The main features of the developed models for the power optimization problems addressed in this research are highlighted as follows:

1. *Optimal Reactive Power Planning*

DE was capable of solving successfully the Reactive Power Planning problem, which is inherently a mixed discrete optimization problem; providing a considerable reduction in the system losses and an improvement on the voltage profile over the system for all case studies.

Mathematically, the problem was formulated as both single and multiobjective optimization problem with several equality and inequality constraints. The results obtained proved that the DE algorithm is appropriate for solving highly nonlinear mixed-integer optimization problems.

2. Congestion Management in Restructured Power Systems

In this case, the DE algorithm was used for solving various congested scenarios in restructured power systems. The problem was formulated as an optimal power flow function, aimed at minimizing the amount of the pool, bilateral and multilateral transactions that has to be rescheduled in order to avoid system congestion.

The results obtained showed that the willingness to pay and the curtailment strategy selected by market participants are two factors that will significantly affect the constrained dispatch. Obviously, while higher the willingness to pay, less the curtailment of the transaction requested, but the complex interactions among market participants underline the need for careful design of the dispatch strategies.

3. Power Systems State Estimation

In this chapter, the integration of the new technology of phasor measurement units (PMUs), the incorporation of operational constraints to the traditional state estimation formulation, and the way that these features could be used to improve the estimation of the real state of the system in the new emerging electricity markets, have been analyzed. The DE state estimation model developed shows its effectiveness and flexibility for solving larger systems with few available and noised measurements.

The results obtained through the case studies show that the angle measurements could effectively enhance the performance of the WLS estate estimation algorithm. However, these measurements can degrade the performance if they are not accurate enough.

On the other hand, the operational constraints can be utilized effectively in enhancing the reliability of the state estimators. The results obtained through the case studies demonstrated that the constrained WLS estimator, even in the presence of bad data in parts of the system, could perform a reliable estimation of the real state of the system.

4. IPRs Based Controlled Islanding Scheme

Traditionally, power systems have been operated and controlled in a centralized way, and with a considerable amount of human intervention. Under such circumstances, cascading outages may result extremely difficult to prevent or control. In this context, researchers of the University of Puerto Rico at Mayagüez have proposed a distributed and "intelligent" control scheme, the so-called Intelligent Power Routers (IPRs), aimed at minimizing the potential damaging effects that a major disturbance may cause on a power system. One of the potential applications of these intelligent controls is to support a controlled islanding scheme to prevent cascade failures in power systems.

The main objective of the controlled islanding scheme is to properly separate the system into several subsystems of reduced capacity to avoid passive collapse or blackout over the entire system. The basis for forming the islands is to minimize the load–generation imbalance in each island, thereby facilitating the restoration process. In this case, DE was used as optimization tool for solving this complex optimization problem.

Based on the results obtained by DE, a flexible and efficient controlled islanding scheme has been proposed, which guarantees a better response of the system to large disturbances.

According with the successful implementation of the developed models in the addressed problems, we can summarize that these models represents a valuable contribution to the field of the evolutionary computation techniques and their applications for the solution of power systems optimization problems.

7.2 RECOMMENDATIONS

Differential Evolution, as well as other evolutionary algorithms, is based on stochastic methods to determine the solution and therefore do not guarantee to obtain an optimal solution at all times. However, an adequate perturbation strategy along with a correct set of control parameters such as the scaling factor, crossover constant and population size may lead to very successful results in complex and large scale optimization problems, in a reasonable computation time.

The two strategies that perform better were the DE/rand/1/bin and the DE/best/2/bin. The first one creates generations by perturbing a randomly selected vector with the difference vector. The other one creates generations by perturbing the best solution found so far with two difference vectors. The DE/best/2/bin has good convergence property on unimodal functions, but this strategy could confront possible stagnations in local minima in multimodal function, when the population diversity diminished. The classic DE formulation (DE/rand/1/bin) has slower convergence rate, but is more reliable than the DE/best/2/bin. Since this strategy perturbs randomly selected vectors over the solution space, the algorithm has the capability to escape from local minima more easily.

The scaling factor is an important parameter that controls the rate at which population evolves. In general, to avoid premature convergence of the DE algorithm, it is crucial that F be of sufficient magnitude to counteract this selection pressure. On the other hand, the scaling factor F should not be chosen too large, since the number of function evaluations increases as F increases. While there is no upper limit on F, effective values lie in the range of [0, 1+]. However, the classical DE approach (DE/rand/1/bin) performs better with scaling factors in the range [0.5 0.7].

The crossover constant (C_R) controls the diversity of the population. Relatively high values of C_R result in higher diversity and improved convergence speed. However, beyond a certain threshold value, the convergence rate may decrease or the population may converge prematurely. On the other hand, small values of C_R increase the possibility that the algorithm stagnates in local minima. Based on the case studies, as suitable range of the crossover constant for the classical DE approach (DE/rand/1/bin) was [0.75 1.0]. A more succinct range could be [0.85 0.95], since in this range a better performance of the algorithm is observed.

The population size plays an important role in the algorithm convergence rate. Small population may cause a poor searching performance and stagnations in local minima. Large populations increase the possibility for finding optimal solutions at the expense of a large number of function evaluations. The optimal selection of this parameter is that is offers good searching performance with a minimum number of individuals. According to our experience a reasonable choice for the population size is between three to eight times to the number of variables involved in the optimization process. This population size provides to the algorithm enough members for searching the solution space, with a minimum computational requirement.

In constrained optimization problems the penalty parameters for constraint evaluation are very important in the success and performance of the DE algorithm. Large penalty factors typically the convergence speed to a feasible solution, but offer the risk of premature convergence in a suboptimal one, especially during the early stages of the optimization process. Small penalty factors typically slow the convergence toward, or fail to find, feasible solutions.

7.3 FUTURE WORK

This thesis provides an insight in the new heuristic tools capable for complex power systems problems that were difficult to solve with the traditional optimization techniques due to their non-continuous, non-differentiable and highly non-linear nature. A general recommendation for future work is to analyze the applicability of the Differential Evolution optimization algorithm, as well as other evolutionary computation techniques, to other power systems optimization problems. It is recommended to adjust the canonical DE optimization algorithm to include an adaptive and self-adaptive control parameter tuning, which ensure that the population diversity is maintained through the optimization process. Finally, it is also desirable to improve the program code in order to reduce the execution time and computational requirements.

For the power systems problems addressed in this thesis work, the recommendations for future work are the following:

1. *Optimal Reactive Power Planning*

   - To propose a methodology for optimal placement of reactive power sources in both transmission and distribution systems.
   - To incorporate some voltage stability indices in the problem formulation.

- To estimate the impact of the solution obtained in the improvement of the steady state stability margin.

2. *Congestion Management in Restructured Power Systems*
    - To evaluate the influence of the financial instruments such as Firm Transmission Rights (FTRs) in the market dispatch and congestion management.
    - To incorporate new schemes of loss allocation in the problem formulation.
    - To evaluate the impact of FACTS devices and SVCs on enhancing the transactions proposed and minimizing line congestions.
3. *State Estimation in Electric Power Systems*
    - To develop a methodology of optimal placement of phasor measurement units in electric power systems.
    - To develop an integrated methodology that mixes the constrained state estimation with phasor measurement units for multi-area state estimation in large scale power systems.
4. *IPRs Based Controlled Islanding Scheme*
    - To develop an approach for the system splitting problem that considers minimum line tripping, while reducing the generation-load imbalance within the islands.
    - To develop and test an adaptive, semi-adaptive and selective load shedding schemes.
    - To analyze the effect of the control logic of the IPRs in the dynamic performance of the system.

- To develop an optimal power flow function to reduce the amount of the constraints violations (bus voltages magnitude, real and reactive power flows) after forming the islands.
- To develop a methodology for the restoration process following the islands formation.

REFERENCES

[1] Z. Michalewicz, "A Perspective on Evolutionary Computation," *Proceedings of the Workshop on Evolutionary Computation*, New England, Australia, pp. 77-93, November 1994.

[2] T. Bäck, *Evolutionary Algorithms in Theory and Practice*, New York: Oxford University Press, 1996.

[3] R. Storn and K. Price, "Differential Evolution - A Simple and Efficient Heuristic for Global Optimization over Continuous Spaces," *Journal of Global Optimization*, vol. 11, pp. 341-359, 1997.

[4] D. Srinivasan, F. Wen, C. S. Chang, and A. C. Liew, "A Survey of Evolutionary Computing to Power Systems," *Proceedings of the 1996 International Conference on Intelligent Systems Applications to Power Systems*, pp. 35-41, 1996.

[5] V. Miranda, D. Srinivasan, L. M. Proenca, "Evolutionary Computation in Power Systems," *Electrical Power & Energy Systems*, vol. 20, no. 2, pp. 89-98, 1988.

[6] A. P. Alves da Silva, P. J. Abrao, "Applications of Evolutionary Computation in Electric Power Systems," *Proceedings of the 2002 Congress on Evolutionary Computation*, Honolulu, pp. 1057-1062, May 2002.

[7] K. V. Price, "Differential Evolution and the Functions of the 2nd ICEO," *Proceedings of the 1997 IEEE International Conference on Evolutionary Computation*, pp. 153-157, 1997.

[8] Z. Michalewicz, "A Survey of Constraint Handling Techniques in Evolutionary Computation Methods," *Proceedings of the 4th Annual Conference on Evolutionary Programming*, pp. 135-155, 1995. Document available at: www.cs.adelaide.edu.au.

[9] J. Lampinen, "\Multi-Constrained Nonlinear Optimization by the Differential Evolution Algorithm," *Proceedings of the 2001 IASTED International Conference on Artificial Intelligence and Applications*, pp. 177-184, September 2001.

[10] Y. C. Lin, F. S. Wang, and K. S. Hwang, "A Hybrid Method of Evolutionary Algorithm for Mixed-Integer Nonlinear Optimization Problems," *Proceedings of the 1999 Congress on Evolutionary Computation*, pp. 2159-2166, May 1999.

[11] J. Lampinen and I. Zelinka, "Mixed Variable Non-Linear Optimization by Differential Evolution," *Proceedings of 2nd International Prediction Conference (Nostradamus'99)*, pp. 1-10, October 1999. Document available at: http://www.lut.fi/~jlampine/NOSTRA99.ps.

[12] T. Gómez, I. J. Pérez-Arriaga, J. Lumbreras, and V. M. Parra, "A Security-Constrained Decomposition Approach to Optimal Reactive Power Planning," *IEEE Transactions on Power Systems*, vol. 6, no. 3, pp. 1069-1076, August 1991.

[13] A. Venkataramana, J. Carr, and R. S. Ramshaw, "Optimal reactive power allocation," *IEEE Transactions on Power Apparatus and Systems*, vol. PWRS-2, no.1, pp. 138–144, February 1987.

[14] K. Iba, H. Suzuki, K. I. Suzuki, and K. Suzuki, "Practical reactive power allocation/operation planning using successive linear programming, " *IEEE Transactions on Power Systems*, vol. 3, no. 2 , pp.558–566, May 1988.

[15] K. Aoki, M. Fan, and A. Nishikori, “Optimal VAr planning by approximation method for recursive mixed-integer linear programming,” *IEEE Transactions on Power Systems*, vol. 3, no. 4, pp. 1741–1747, November1988.

[16] G Opoku, “Optimal Power Systems VAR Planning,” *IEEE Transactions on Power Systems*, vol. 15, no. 1, pp. 53-60, February 1990.

[17] J. A. Momoh and J. Zhu, “A New Approach to VAr Pricing and Control in the Competitive Environment,” *IEEE Transactions on Power Systems*, vol. 13, no. 1, pp. 541-548, February 1998.

[18] D. Chattopadhyay, K. Bhattacharya, and J. Parikh, “Optimal Reactive Power Planning and Its Spot Pricing: An Integrated Approach,” *IEEE Transactions on Power Systems*, vol. 10, no. 4, pp. 2014-2020, November 1995.

[19] J. T. Ma and L. L. Lai, “Evolutionary Programming Approach to Reactive Power Planning,” *IEE Proceeding on Generation, Transmission and Distribution*, vol. 143, no. 4, pp. 365-370, July 1996.

[20] L. L. Lai and J. T. Ma, “Application of Evolutionary Programming to Reactive Power Planning - Comparison with Nonlinear Programming Approach,” *IEEE Transactions on Power Systems*, vol. 12, no. 1, pp. 198-206, February 1997.

[21] L. L. Lai and J. T. Ma, “Practical Application of Evolutionary Computing to Reactive Power Planning,” *IEE Proceeding on Generation, Transmission and Distribution*, vol. 145, no. 6, pp. 753-758, November 1998.

[22] K. Y. Lee and Y. M. Park, “Optimization Method for Reactive Power Planning by Using a Modified Simple Genetic Algorithm,” *IEEE Transactions on Power Systems*, vol. 10, no. 4, pp. 1843-1850, November 1995.

[23] K. Y. Lee and F. Yang, “Optimal Reactive Power Planning Using Evolutionary Algorithms: A Comparative Study for Evolutionary Programming, Evolution Strategies, Genetic Algorithms and Linear Programming,” *IEEE Transactions on Power Systems*, vol. 13, no. 1, pp. 101-108, February 1998.

[24] J. Z. Zhu, C. S. Chang, W. Yang, and G. Y. Xu, “Reactive Power Optimization Using an Analytic Hierarchical Process and Nonlinear Optimization Neural Network Approach,” *IEE Proceeding on Generation, Transmission and Distribution*, vol. 145, no. 1, pp. 89-97, 1998.

[25] J. R. Mantovani, S. A. Modesto, and A. V. García, “VAr Planning Using Genetic Algorithm and Linear Programming,” *IEE Proceeding on Generation, Transmission and Distribution*, vol. 148, no. 3, pp. 257-262, May 2001.

[26] K. Nara and H. Hu, “A Reactive Power Resource Planning Method by Tabu Search in Competitive Markets,” *Proceedings of the 2000 International Conference on Power Systems Technology*, pp. 1089-1094, December 2000.

[27] Y. L. Chen and Y. L. Ke, “Multi-Objective VAr Planning for Large-Scale Power Systems Using Projection-Based Two-Layer Simulated Annealing Algorithms,” *IEE Proceeding on Generation, Transmission and Distribution*, vol. 151, no. 4, pp. 555-560, July 2004.

[28] F. Li, J. D. Pilgrim, C. Dabeedin, A. Chebbo, et al., “Genetic Algorithms for Optimal Reactive Power Compensation on the National Grid System,” *IEEE Transactions on Power Systems*, vol. 20, no. 1, pp. 493-499, February 2005.

[29] B. Barán, J. Vallejos, R. Ramos, and U. Fernández, "Reactive Power Compensation using a Multi-objective Evolutionary Algorithm," *Proceedings of the 2001 IEEE Power Tech Conference*, Porto, Portugal, pp. 1-6, September 2001.

[30] M. M. Begovic, B. Radibratovic, and F. C. Lambert, "On Multiobjective Volt-VAR Optimization", *Proceedings of the 37th Annual Hawaii Conference on System Sciences*, Hawaii, pp. 59-64, January 2004.

[31] K. Deb, *Multi-Objective Optimization Using Evolutionary Algorithms*. New York: Wiley, 2001.

[32] K. Y. LEE, J. M. Park, and J. L. Ortiz, "A United Approach to Optimal Real and Reactive Power Dispatch," *IEEE Transactions on Power Apparatus and Systems*, Vol. PAS 104, no. 5, pp. 1147-1153, May 1987.

[33] A. S. Nayak and M. Pai, "Congestion Management in Restructured Power System Using an Optimal Power Flow Framework," *PSERC Publication 02-23*, June 2002. Document available at: www.pserc.wisc.edu.

[34] J. G. Waight, A. Bose, and G. B. Sheble, "Generation dispatch with reserve margin constraints using linear programming," *IEEE Transactions on Power Apparatus and Systems*, vol. 100, no. 1, pp. 252-258, January 1981.

[35] G. A. Maria and J. A. Findlay, "A Newton optimal power flow program for Ontario Hydro EMS," *IEEE Transactions on Power Systems*, vol. 2, no. 3, pp. 576-584, August 1987.

[36] R. C. Burchett and H. H. Happ, "Large scale security dispatching: An exact model," *IEEE Transactions on Power Apparatus and Systems*, vol. 102, no. 9, pp. 2995-2999, September 1983.

[37] R. D. Christie, B. F. Wollenberg, and I. Wangensteen, "Transmission Management in the Deregulated Environments," *IEEE Transactions on Power Systems*, vol. 88, no. 2, pp. 170-195, February 2000.

[38] J. Nanda, D. P. Kothari, and S. C. Srivastava, "New optimal power dispatch algorithm using fletcher's quadratic programming method," *IEE Proceedings*, vol. 136, Pt. C, no. 3, pp. 153-161, May 1989. 46

[39] R. C. Burchett, H. H. Happ, and D. R. Vierath, "Quadratically convergent optimal power flow," *IEEE Transactions on Power Apparatus and Systems*, vol. 103, no. 11, pp. 3267-3276, November 1984.

[40] L. S. Vargas, V. H. Quintana, and A. Vannelli, "A tutorial description of an interior point method and its application to security-constrained economic dispatch," *IEEE Transactions on Power Systems*, vol. 8, no. 3, pp. 1315-1324, August 1993.

[41] J. A Momoh, S. X. Guo, E. C. Ogboubiri, and R. Adapa, "Quadratic interior point method for solving power system optimization problems," *IEEE Transactions on Power Systems*, vol. 9, no. 3, pp. 1327-1336, August 1994.

[42] D. Shirmohammadi, B. Wollenberg, A. Vojdani, P.Sandrin, M.Pereira, F.Rahimi, T. Schneider and B. Scott, "Transmission Dispatch and Congestion Management in the Emerging Energy Markets Structures", *IEEE Transactions on Power Systems*, vol. 13, no. 4, November 1998, pp. 1466 – 1474.

[43] C. A. Cañizares, H. Chen, F. Milano, and A. Singh, "Transmission Congestion Management and Pricing in Simple Auction Electricity Markets," *International Journal of Emerging Power Systems*, vol. 1, no. 1, pp. 1-28 2004. Document available at: www.bepress.com/ijeeps.

[44] K. Y. Lee, M. Choi, and M. Shin, "Network Congestion Assessment for Short-term Transmission Planning under Deregulated Environments," *IEEE Transactions on Power Systems*, vol. 16, no. 2, May 2001.

[45] P. Wei, Y. Ni, and F. F. Wu, "Decentralized Approach for Congestion Management and Congestion Price Discovering," *IEE Proceedings of Generation, Transmission and Distribution*, vol. 149, no. 6, pp. 645-651, November 2002.

[46] H. Glatvitsch and F. Alvarado, "Management of multiple congested conditions in unbundled operation of a power system," *IEEE Transactions on Power Systems*, vol. 13, no. 3, pp. 1013-1019, August 1998.

[47] R. S. Fang and A. K. David, "Transmission Congestion Management in an Electricity Market," *IEEE Transactions on Power Systems*, vol. 14, no. 3, pp. 877-883, August 1999.

[48] A. K. David, "Dispatch Methodologies for Open Access Transmission System," *IEEE Transactions on Power Systems*, vol. 13, no. 1, pp. 46-53, February 1998.

[49] R. S. Fang and A. K. David, "Optimal Dispatch Under Transmission Contracts," *IEEE Transactions on Power Systems*, vol. 14, no. 2, pp. 732-737, May 1999.

[50] S. C. Srivastava and P. Kumar, "Optimal Power Dispatch in Deregulated Market Considering Congestion Management," *Proceedings of the Electric Utility Deregulation and Restructuring and Power Technologies Conference*, City University, London, pp. 53-59, April 2000.

[51] F. D. Galiana, I. Kockar, and P. Cuervo-Franco, "Combined Pool/Bilateral Dispatch - Part I: Performance of Trading Strategies," *IEEE Transactions on Power Systems*, vol. 17, no. 1, pp. 92-99, February 2002.

[52] F. D. Galiana, I. Kockar, and P. Cuervo-Franco, “Combined Pool/Bilateral Dispatch - Part II: Curtailment of Firm and Nonfirm Contracts,” *IEEE Transactions on Power Systems*, vol. 17, no. 4, pp. 1184-1190, November 2002.

[53] F. D. Galiana, I. Kockar, and P. Cuervo-Franco, “Combined Pool/Bilateral Operation - Part III: Unbundling Costs of Trading Services,” *IEEE Transactions on Power Systems,* vol. 17, no. 4, pp. 1191-1198, November 2002.

[54] M. Shahidehpour, H. Yamin, and Z. Li, *Market Operation in Electric Power Systems: Forecasting, Scheduling and Risk Management*. New York: Wiley, 2002.

[55] J. Grainger and W. D. Stevenson, *Power System Analysis*. New York: Mc-Graw-Hill, 1994.

[56] M. Crow, *Computational Methods for Electric Power Systems*, Boca Ratón, Florida: CRC Press, 2002.

[57] R. F. Nuqui and A. G. Phadke, “Phasor Measurement Unit Placement Techniques for Complete and Incomplete Observability,” *IEEE Transactions on Power Delivery*, vol. 20, no. 4, pp. 2381-2388, October 2005.

[58] A. Abur and M. K. Celik, "Least Absolute Value State Estimation with Equality and Inequality Constraints," *IEEE Transactions on Power Systems*, vol. 8, no. 2, pp. 680-686, May 1993.

[59] A. J. Wood and B. F. Wollenberg, *Power Generation, Operation and Control*, New York: Wiley, 1996.

[60] A. Monticelli, "Electric Power System State Estimation," *Proceedings of the IEEE*, vol. 88, no. 2, pp. 262-282, February 2000.

[61] A. Abur and A. Gómez-Expósito, *Power Systems State Estimation: Theory and Implementation*, New York: Marcel Decker, Inc., 2004.

[62] A. Monticelli, *State Estimation in Electric Power Systems: A Generalized Approach*, Norwell, Massachusetts: Kluwer Academic Publishers, 1999.

[63] Depablos, J., V. Centeno, et al.. "Comparative Testing of Synchronized Phasor Measurement Units," *IEEE Power Engineering Society General Meeting*, Virginia, pp. 948-954, June 2004.

[64] R. O. Burnett, M. M. Butts, and P. S. Sterlina, "Power Systems Applications of Phasor Measurement Units," *IEEE Computer Applications in Power*, vol. 7, no. 1, January 1994.

[65] R. P. Schulz, L. S. VanSlyck, and S. H. Horowitz, "Application of Fast Phasor Measurements on Utility Systems," *Power Industry Computer Application Conference (PICA)*, Seattle, pp. 49-55, January 1989.

[66] G. Benmouval, E. O. Schweitzer, A. García, "Synchronized Phasor Measurement in Protective Relays for Protection, Control, and Analysis of Electric Power Systems," *57th Annual Conference for Protective Relay Engineers*, Washington, pp. 1-32, April 2004.

[67] R. Zivanovic and C. Cairns, "Implementation of PMU Technology in State Estimation: An Overiview," *Proceedings of the 4th IEEE AFRICON*, pp. 1006-1011, September 1996.

[68] M. Rice and G. Heydt, "Phasor Measurement Unit Data in Power System State Estimation," *PSERC Publication 05-02*, January 2005. Document available at: www.pserc.org.

[69] I. W. Slutsker, J. M. González-Provost, J. B. Sierra, S. Mokhtari, M. Baena-Pérez, et al., "Implementation of Phasor Measurements in State Estimator at Sevillana de Electricidad," *Proceedings of the 1995 Power Industry Computer Application Conference*, pp. 392-398, May 1995.

[70] L. Zhao and A. Abur, "Multiarea State Estimation Using Synchronized Phasor Measurements," *IEEE Transactions on Power Systems*, vol. 20, no. 2, pp. 611-617, May 2005.

[71] B. Xu and A. Abur, "Observability Analysis and Measurement Placement in Systems with PMUs," *Proceedings of the 2004 Power System Conference and Exposition*, pp. 943-946, October 2004.

[72] X, Dongjie, H. Renmu, W. Peng, and X. Tao, "Comparison of Several PMU Placement Algorithms for State Estimation," *8th International Conference on Developments in Power System Protection*," Beijing, China, pp. 32-35, April 2004.

[73] K. A. Clements, G. W. Woodzell, R. C Burchett, "A Mew Method for Solving Equality-Constrained Power System Static-State Estimation, " *IEEE Transactions on Power Systems*, vol. 5, no. 4, pp. 1460-1466, November 1990.

[74] G. N. Korres, "A Robust Method for Equality Constrained State Estimation," *IEEE Transactions on Power Systems*, vol. 17, no. 2, pp. 305-314, May 2002.

[75] H. Singh, F. L. Alvarado, and W. E. Liu, "Constrained LAV State Estimation Using Penalty Functions," *IEEE Transactions on Power Systems*, vol. 12, no. 1, pp. 383-388, February 1997.

[76] A. Abur and M. K. Celik, "Least Absolute Value State Estimation with Equality and Inequality Constraints," *IEEE Transactions on Power Systems*, vol. 8, no. 2, pp. 680-686, May 1993.

[77] K. A. Clements, P. W. Davis, and K. D. Frey, "Treatment of Inequality Constraints in Power System State Estimation," *IEEE Transactions on Power Systems*, vol. 10, no. 2, pp. 567-574, May 1995.

[78] K. Chitte, and K. S. Swarup, "Power System State Estimation using IP Barrier Method," 2*003 Conference on Convergent Technologies for Asia-Pacific Region (TENCON)*, Madras, India, pp. 460-465, October 2003.

[79] L. Holten, A. Gjelsvik, S. Aam, F. Wu, and W. H. E. Liu, "Comparison of Different Methods for State Estimation," *IEEE Transactions on Power Systems*, vol. 3, no. 4, pp. 1798-1806, November 1988.

[80] G.J. Battaglia, "Mean Square Error," *AMP Journal of Technology*, vol. 5, no. 1, pp. 31-36, 1996.

[81] H. You and V. Vittal, "Slow Coherency-Based Islanding," *IEEE Transactions on Power Systems*, vol. 19, no. 1, pp. 483-491, February 2004.

[82] H. You and V. Vittal, "Self-Healing in Power Systems: An Approach Using Islanding and Rate of Frequency Decline-Based Load Shedding," *IEEE Transactions on Power Systems*, vol. 18, no. 1, pp. 174-181, February 2003.

[83] X. Wang and V. Vittal, "System Islanding Using Minimal Cutsets with Minimun Net Flow," *IEEE Transactions on Power Systems*, vol. 19, no. 2, pp. 1-6, May 2004.

[84] Q. Zhao, K. Sun, D. Zheng, J. Ma, and Q. Lu, "A Study of System Splitting Strategies for Island Operation of Power System: A Two-Phase Method Based on

OBDDs," *IEEE Transactions on Power Systems*, vol. 18, no. 4, pp. 1556-1565, November 2003.

[85] K. Sun, D. Zheng, and Q. Lu, "Splitting Strategies fro Islanding Operation of Large-Scale Power Systems Using OBDD-Based Methods," *IEEE Transactions on Power Systems*, vol. 18, no. 4, pp. 1556-1565, November 2003.

[86] K. Sun, D. Zheng, and Q. Lu, "A Simulation Study of OBDD-Based Proper Splitting Strategies for Power Systems Under Consideration of Transient Stability," *IEEE Transactions on Power Systems*, vol. 20, no. 1, pp. 389-399, February 2005.

[87] S. B. Yusof, G. J. Rogers, and R. T. H. Alden, "Slow Coherency Based Network Partitioning Including Load Buses," *IEEE Transactions on Power Systems*, vol. 8, no. 3, pp. 1375--1382, August 1993.

[88] G. Rogers, "Power Systems Structure and Oscillations," *IEEE Computer Application in Power Systems*, vol. 12, no. 2, pp. 14-21, April 1999.

[89] M. Y. Hussain and V. G. Rau, "Coherency Identification and Construction of Dynamic Equivalents for Large Power Systems," *Proceedings of the 2nd IEE International Conference on Advances in Power Systems Controls*, Hong Kong, pp. 887-892, December 1993.

[90] E. J. Pires-D.Souza and A. M. Leite-D.Silva, "An Efficient Methodology for Coherency-Based Dynamic Equivalents," *IEE Proceedings on Power Systems*, vol. 139, no. 5, pp. 371-382, September 1992.

[91] J. E. Chow, P. V. Kokotovic, R. J. Thomas, *Systems and Control Theory for Power Systems*, New York: Springer-Verlag, 1995.

[92] P. M. Anderson and A. A. Fouad, *Power System Control and Stability*. New Jersey: IEEE Press, 1994.

[93] P. Kundur, *Power System Stability and Control*, San Francisco: McGraw-Hill, 1994.

[94] R. K. Ahuja, J. B. Orlin, and T. L. Magnanti, *Network Flows: Theory, Algorithms and Applications*, New Jersey: Prentice Hall, 1993.

[95] H. Wang, and J. S. Thorp, "Computer Simulation of Cascading Disturbances in Electric Power Systems: Impact of Protection Systems on Transmission System Reliability," *PSERC Publication 01-01*, May 2001. Document available at: www.pserc.wisc.edu

[96] J. van Eyssen, "Introducing a New Application Philosophy for Out-of-Step Protection," *Proceedings of the 6th International Conference on Developments in Power System Protection*, pp. 214-217, March 1997.

[97] D. A. Tziouvaras and D. Hou, "Out-of-Step Protection Fundamentals and Advancements," *Proceedings of the 57th Annual Conference for Protective Relay Engineering*, pp. 282-307, March 2004.

[98] G. Benmouyal, D. Hou, and D. Tziouvaras, "Zero-Setting Power-Swing Blocking Protection." Document available at: www.selinc.com/techpprs

[99] M. Etezadi-Amoli, "On Underfrequency Load Shedding Schemes," *Proceedings of the 22th North American Power Symposium (NAPS)*, Auburn, pp. 172-180, October 1990.

[100] W. C. New, "Load Conservation by Means Underfrequency Relays." Document available at: www.geindustrial.com

[101] B. Delfino, S. Massucco, A. Morini, P. Scalera, and F. Silvestro, "Implementation and Comparison of Different Under Frequency Load-Shedding Schemes," *Proceedings of the 2001 IEEE Power Engineering Society Summer Meeting*, pp. 307-312, July 2001.

[102] T. Van Custem and C. Vournas, *Voltage Stability of Electric Power Systems*, Boston: Kluwer Academic Publishers, 1998.

[103] C. W. Taylor, *Power System Voltage Stability*, New York: McGraw-Hill, 1993.

[104] M. Larson and D. Karlsson, "Coordinated System Protection Scheme Against Voltage Collapse Using Heuristic Search and Predictive Control," *IEEE Transactions on Power Systems*, vol. 18, no. 3, pp. 1001-1006 , August 2003.

[105] D. Lefebvre, S. Bernard, and T. Van-Custem, "Undervoltage Load Shedding Scheme for the Hydro-Québec System," *Proceedings of the 2004 Power Engineering Society General Meeting*, pp. 1619-1624, June 2004.

[106] P. M. Anderson, *Power System Protection*, New York: Wiley, 1998.

[107] M. Zima and D. Ernst, "On Multi-Area Control in Electric Power Systems," *Proceedings of the 15th Power System Computation Conference*, Liege, Belgium, pp. 1-8, August 2005.

[108] M Vélez-Reyes, J. Cedeño-Maldonado, E. O'neill-Carrillo, A. Ramírez, and A. Irizarry-Rivera, "Intelligent Power Routers for Distributed Coordination in Electric Energy Processing Networks," *2003 EPNES Workshop*, October 2003. Document available at: www.ece.uprm.edu/~agustin

[109] B. Naduvathuparambil, M. C. Valenti, and A. Feliachi, "Communication Delays in Wide Area Measurement Systems," *Proceedings of the 34th Southern Symposium on System Theory*, West Virginia, pp. 118-122, March 2002.

[110] J. Machowski, J. Bialek, and J. R. Bumby, *Power System Dynamics and Stability*, New York: Wiley, 1997.